UNIVERSITÉ DE SHERBROOKE

Faculté de génie
Département de génie civil

ÉTUDE DE LA DURABILITÉ DES BÉTONS DE MATÉRIAUX ALCALI-ACTIVÉS

STUDY OF THE DURABILITY OF ALKALI-ACTIVATED CONCRETES

Thèse de doctorat / PhD thèse
Spécialité/Speciality : Génie civil / Civil engineering

Jury : Josée Duchesne
Ammar Yahia
Rachid Hakkou
Arezki Tagnit-Hamou

JOSEP ALIQUES GRANERO

12 avril, 2018, à Sherbrooke (Québec) Canada

RÉSUMÉ

Les matériaux alcali-activés (MAA) sont considérés comme une alternative pour réduire l'utilisation du ciment Portland. Ces matériaux, développés il y plus de quarante ans, présentent des propriétés mécaniques similaires ou supérieures à certains bétons de ciment Portland. De plus ces matériaux semblent avoir une bonne durabilité face aux environnements agressifs tels que les acides, les sulfates.... Les MAA sont le résultat de l'activation par une solution alcaline (ex. : NaOH, silicate de sodium,) de matériaux siliceux ou silico-alumineux, qui sont le plus souvent des déchets industriels (laitier, cendre volante, poudre de verre, etc) ou des matériaux naturels qui subissent un léger traitement thermique (calcination du kaolin autour de 700 °C pour avoir du métakaolin) à des températures inférieures ou égales à 100°C. Les émissions de gaz à effet de serre et le coût énergétique liés à la production des MAA sont plus faibles par rapport à ceux des bétons de ciment Portland, ce qui constitue un avantage écologique.

Cependant, même si les propriétés très bénéfiques des MAA alcali-activés sont assez connues, leur mise en œuvre à l'échelle industrielle reste problématique pour diverses raisons :

- Mêmes si ces matériaux ont été développés depuis plus de 40 ans, ce n'est que durant les dix dernières années que leur utilisation comme matériaux de construction a eu un regain d'intérêt. De plus, les propriétés physico-chimiques des produits finaux dépendent fortement des matières premières utilisées conduisant à des résultats souvent divergents.

- Il n'existe pas de normes pour la mise en œuvre et la caractérisation des MAA. Celles actuellement utilisées sont les normes conçues pour le ciment Portland et les ajouts cimentaires. De plus, la durabilité est un facteur très important pour les matériaux utilisés dans le domaine de la construction. La caractérisation actuelle de la durabilité des MAA est basée sur les normes déjà existantes utilisées pour la chimie du ciment Portland. Ceci reste problématique puisque la composition chimique des MAA diffère de celle du ciment portland. À l'état actuel, il n'existe aucune norme qui porte sur l'analyse de la durabilité des matériaux alcali-activés.

Ce projet constitue la dernière phase d'un programme de recherche mené à l'Université de Sherbrooke. Ce programme portait sur le développement de nouveaux liants basés sur les matériaux silico-alumineux. L'objectif principal de cette étude est d'analyser la durabilité des bétons incorporant les nouveaux liants qui ont été développés dans les premières phases du programme de recherche. Ces phases se rapportaient à l'optimisation de la formulation de nouveaux liants obtenus par activation alcaline de déchets industriels locaux (poudre de verre). Pour cela, une étude expérimentale préalable (première partie du projet) basée sur les méthodes de caractérisation de la durabilité existantes pour les bétons de ciment Portland a été réalisée. Dans cette étude, des formulations alcali-activés basés sur la cendre volante et le laitier, deux précurseurs hautement étudiés par la communauté scientifique, ont été utilisés. Pour une application au MAA, les résultats ont montré les lacunes des méthodes décrites dans les normes, telles que les conditions de murissement, et des recommandations sont donnés dans chaque essai évalué dans le projet.

Enfin, les recommandations obtenues dans cette phase préliminaire ont été utilisées pour déterminer les propriétés de durabilité des nouveaux liants activés à base de poudre de verre et de métakaolin. Plus spécifiquement, trois formulations ont été étudiées, avec différentes teneurs de poudre de verre et de métakaolin à savoir : 95% massique poudre de verre + 5% massique métakaolin, 85% massique poudre de verre + 15% massique metakaolin et 70% massique poudre de verre + 30t% massique métakaolin. Les résultats sont très prometteurs, avec des très bonnes propriétés de durabilité, surtout quand la combinaison 70% massique poudre de verre + 30% massique metakaolin est utilisée.

ABSTRACT

Alkali-activated materials (AAM) are considered as an alternative to reduce the use of Portland cement in concrete. These materials, developed more than 40 years ago, have similar mechanical properties and in some cases superior to those of Portland cement concrete. Furthermore, these materials seem to possess very good durability properties against aggressive environments like acids, sulfates, etc. AAM are the results of the alkali dissolution of some siliceous or alumino-siliceous materials by means of NaOH, sodium silicate, and similar dissolutions. These siliceous or alumino-siliceous materials are in most cases industrial wastes such as fly ash, slags, glass powder… In other cases, natural materials with some previous treatment are used as well, such as metakaolin. Greenhouse gas emissions and the production cost associated to AAM are considered lowers in comparison to those of Portland cement.

Despite of the benefits that AAM are showing good mechanical and durability and environmental friendly behavior, its industrial implantation is hindered by some facts such as:

- Although these materials have been developed more than 40 years ago, it's growing interest as a building material just started during the last decade. Also, their physico-chemical properties are highly influenced by the raw materials used that may lead to diversified results.
- No specification/standards yet exists for its industrial uses neither for their characterization. The ones that it can be found have been developed for Portland cement or blended Portland cement concrete. In the case of the durability properties, most of the studies dealing with AAM have been performed following methods described on those standards, standards that have been developed for the cement Portland chemistry. This point is critic since AAM chemistry is indeed different to those of Portland cement.

The project shown in this thesis forms part in a research program conducted in the civil engineering department of the University de Sherbrooke. The aim of this research program is to develop new binders based on siliceous and silico-aluminous materials. This thesis is in fact the last part of this program, and the principal aim is to characterize the durability of concretes based on the new binders developed in the former parts of the research program. More specifically, in these former parts it has been developed new binders based on the alkali-activation of glass powder, and industrial waste of the province of Quebec.

The work of these thesis have been divided into two phases: first phase consist in a preliminary study of the applicability of the existing durability test methods to AAM (secondary objective of this study). For this purpose, well known formulations obtained from literature have been used, such as alkali-activated slag and fly ash, together with a cement Portland formulation. Results of this phase has demonstrated some lacks of the standards in order to be applied to AAM, such as the curing conditions of samples, and some recommendations for future standards are given.

In the second phase, conclusions obtained in the first phase will be applied to characterize the durability of the novel binders, based on a mix of glass powder and metakaolin. Three formulations based on this system has been analyzed: 95 wt.% glass powder + 5 wt.% metakaolin, 85 wt.% glass powder + 15 wt.% metakaolin and 70 wt.% glass powder + 30 wt.% of metakaolin. Results of this second phase have revealed promising results in terms of very good durability properties, especially for the mix 70 wt.% glass powder + 30 wt.% of metakaolin.

RESUMEN

Los materiales activados alcalinamente (MAA) son considerados una alternativa para reducir la utilización del cemento Portland. Estos materiales, desarrollados hace más de 40 años, poseen propiedades mecánicas similares o superiores en ciertos casos a las del cemento Portland. Además, estos materiales parecen tener una buena durabilidad frente a ambientes agresivos tales como la presencia de ácidos, sulfatos… Los MAA son el resultado de la activación mediante disoluciones alcalinas (tales como el NaOH, silicato sódico,…) de materiales silíceos o silico-aluminosos. Estos materiales son a menudo desechos industriales tales como las cenizas volantes, escorias de altos hornos, polvo de vidrio, etc…, o de materiales naturales que pueden tener algún tratamiento térmico tales como el metacaolin (procedente de la calcinación del caolín). Las emisiones de gases de efecto invernadero y el coste ligado a la producción de los MAA son menores a los asociados a la producción del cemento Portlnad, por lo que constituye una ventaja ecológica.

Sin embargo, a pesar de las propiedades beneficiosas que poseen estos materiales son bien conocidas a día de hoy (buena durabilidad, medioambiental), su implantación a nivel industrial está siendo dificultada por diversas razones:

- Todo y que estos materiales han sido desarrollados hace más de 40 años, no es sino en los últimos 10 años cuando han recibido un particular interés como material de construcción. Además, las propiedades físico-químicas de los productos finales dependen fuertemente de los materiales de partida utilizadas, lo que genera una gran diversidad.

- No existen normas ni especificaciones para su colocación/utilización en obras ni para su caracterización, ya que las existentes han sido desarrolladas para el cemento Portland y sus adiciones. Este es el caso de la caracterización de la durabilidad. Los estudios actuales de durabilidad sobre los MAA se están realizando a partir de las normas existentes, normas que han sido desarrolladas para la química del cemento Portland. Utilizar los procedimientos descritos en estas normas es un parámetro crítico, ya que la química de los MAA difiere a la del cemento Portland. Actualmente, no existe ninguna norma de durabilidad específica para los MAA.

El proyecto presentado en esta tesis forma parte de un proyecto general más amplio llevado a cabo en el departamento de ingeniería civil de la Universidad de Sherbrooke. Este proyecto general trata sobre el desarrollo de nuevos conglomerantes basados en materiales aluminio-silicios. El objetivo principal de la parte específica que se presenta en esta tesis, y que además es la última parte, es analizar la durabilidad de hormigones con conglomerantes desarrollados en fases anteriores de este proyecto general. Más específicamente, estas fases anteriores han consistido en la optimización de conglomerantes obtenidos mediante la activación alcalina de desechos de la industria local de la provincia de Quebec, en especial el polvo de vidrio.

El trabajo de esta tesis ha sido dividido en dos fases, un estudio preliminar sobre el efecto de los actuales ensayos de durabilidad en los MAA (objetivo secundario del proyecto) y una segunda parte donde se aplican los conocimientos obtenidos en la primera fase para caracterizar la durabilidad de los nuevos conglomerantes (objetivo principal). Para la primera fase se han empleado formulaciones altamente estudiadas por la comunidad científica, como las escorias de altos hornos y las cenizas volantes procedentes de las centrales térmicas de carbón. Los resultados de esta primera fase han mostrado ciertas carencias en las actuales normas para caracterizar la durabilidad, como las condiciones de curado, y de estos resultados se han podido extraer recomendaciones para la realización de los ensayos de durabilidad analizados.

En la segunda fase del proyecto se han utilizado por lo tanto los conocimientos obtenidos en la primera fase del proyecto para caracterizar la durabilidad de los nuevos conglomerantes basados en el polvo de

vidrio y el metacaolin. Tres formulaciones basadas en este sistema han sido caracterizadas: 95% polvo de vidrio + 5% metacaolin, 85% polvo de vidrio + 15% metacaolin y 70% polvo de vidrio + 30% metacaolin. Los resultados de esta segunda fase han sido muy prometedores, mostrando muy buenas propiedades de durabilidad a la combinación de 70% polvo de vidrio + 30% metacaolin.

REMERCIEMENTS / ACKNOLEDGEMENTS / AGRADECIMIENTOS

Il ne faut pas finir cette étape de ma vie sans des bons mots pour toutes les personnes qui m'ont aidé pendant la durée de mon doctorat au Québec.

Toute commence quand le professeur Arezki Tagnit-Hamou m'a offert l'opportunité de réaliser des études de doctorat dans le sein du groupe de béton en 2011. Merci beaucoup au professeur Arezki pour cette opportunité, sa supervision et ses conseils.

N'était pas facile pour moi de prendre la décision de quitter l'Espagne pour aller au Canada, non seulement pour changer le climat méditerranéen pour les froids hivers de Canada (pas facile), mais aussi pour la distance avec ma famille et surtout avec ma copine Sara. Quelques décisions difficiles après, et mon aventure au Canada a commencé.

Cette aventure n'a pas été facile pour moi, mais heureusement, je me suis faitdes amis au sein du groupe du béton, ce qui m'a aidé à être bien accompagné. Ces amis que je n'oublierai jamais : Ana, Behrouz, Daddy, Manu, Jorge, Yolanda, Tatiana, Massoud, et en général, à toute l'équipe du béton.

Je ne voudrais pas aussi oublier une personne qui m'a aidé beaucoup pour durant mon parcours au doctorat, Monique. Merci beaucoup pour ton aide contant et tes encouragement.

D'ailleurs, je voudrais remercier tous les techniciens du laboratoires du groupe de bétons, des personnes très amaibles qui sans leur contribution, mon travail de recherche n'aurait pas été possible.

En terminant, je vais écrire les prochains mots dans ma belle langue maternelle :

En aquest punt canvie al Valencià per poder expresar tot el que senc pel suport que he obtingut durant aquesta etapa de la meua vida, en especial a la meva mare i al amor de la meua vida Sara. Sense el vostre suport no hagués sigut posible aguantar els 4 anys a Canadá. A la meua Sara que et vull moltíssim i que en tots els anys que ens queden per davant seran dedicats per a fer-te feliç al meua costat, i viure moltes aventures junts. A la meva mare, gracies per tots els bons consells i l'amor incondicional que sempre m'has demostrat. Vos estime.

INDEX

RÉSUMÉ iii

ABSTRACT v

RESUMEN vii

REMERCIEMENTS / ACKNOLEDGEMENTS / AGRADECIMIENTOS ix

INDEX xi

LIST OF FIGURES xix

LIST OF TABLES xxv

ABRÉVIATIONS / ABBREVIATIONS xxvii

CHAPTER 1. Introduction 1

1.1 Contextualization 1

1.2 Research project definition 3

1.3 Objectives of the research project 4

1.4 Original contributions 4

1.5 Document plan 5

CHAPTER 2. State of the art 6

2.1 History of alkali-activated materials 6

2.2 Why alkali-activated materials? 7

2.3 Alkali-activated materials chemistry 12

2.3.1 Classification of alkali-activated materials 12

2.3.2 Reaction mechanisms and hydration products 13

2.3.2.1 High-calcium systems 14

2.3.2.2 Low-calcium systems 15

2.3.3 Types of activators 16

2.4 Durability concerns using existing standards in AAMs 17

2.5 Review of the AAM durability 18

2.5.1 Sulfate resistance 19
2.5.2 Acid resistance 25
2.5.3 Alkali-aggregate reaction 30
2.5.4 Freeze-thaw resistance 35
2.5.5 Permeability 38
2.6 Glass 42
2.6.1 Production of glass 42
2.6.2 Glass recycling: an environmental benefit? 43
2.6.3 Market outlets of recycled glass 44
2.6.4 Recycled glass as a Portland cement replacement 45
2.6.5 Glass powder as an AAM precursor 46
CHAPTER 3. Experimental plan, methods and materials 51
3.1 Experimental plan 51
3.2 Characterization of materials 52
3.2.1 Raw materials 52
3.2.1.1 General use Portland cement 52
3.2.1.2 Blast furnace slag 54
3.2.1.3 Class F fly ash 55
3.2.1.4 Metakaolin 56
3.2.1.5 Glass Powder 57
3.2.2 Activating Solutions and chemical admixtures 57
3.2.2.1 Sodium silicate solution 57
3.2.2.2 Sodium hydroxide solution 58
3.2.2.3 Calcium hydroxide solution 58
3.2.2.4 Air-entraining agent 58
3.2.2.5 Water reducing admixture 58
3.2.3 Aggregates 59

3.3 Sample preparation 60
3.3.1 Mix design 60
3.3.2 Mixing, casting and curing 62
3.3.2.1 Mortars 62
3.3.2.2 Concretes 66
3.4 Compressive strength test 66
3.5 Durability tests methods 67
3.5.1 Dimensional stability in water 67
3.5.2 Sulfate resistance test 67
3.5.3 Acid resistance test 68
3.5.4 Alkali-aggregate reaction 69
3.5.5 Freeze-Thaw (F-T) resistance 70
3.5.6 Permeability 71
3.5.8 Sodium leaching in distilled water 73
3.6 Characterization methods 74
3.6.1 Density 74
3.6.2 Blaine fineness 74
3.6.3 Laser diffraction particle size distribution 75
3.6.4 Chemical composition by means of X-ray fluorescence spectrometry (XRF) 76
3.6.5 Mineralogical characterization by means of X-ray diffraction (XRD) 77
3.6.6 Microstructural analysis by means of Scanning electron microscope (SEM) 77
3.6.7 Inductively coupled plasma – Mass spectroscopy (ICP-MS) 78
CHAPTER 4. Applicability of the durability test methods to traditional alkali-activated materials 81
4.1 Compressive strength 81
4.2 Dimensional stability in water 84
4.3 Sulfate resistance 85
4.3.1 Expansion results 85

4.3.2 Mineralogical characterization by means of X-ray diffraction 88
4.3.3 Microstructural analysis by means of SEM-BSE 93
4.3.4 Discussion 98
4.3.5 Conclusions 102
4.3.6 Applicability of the ASTM C1012 test method to AAM 103
4.4 Acid resistance 104
4.4.1 Mass change 104
4.4.2 Cross-sectional dimension change 106
4.4.3 Visual appearance 107
4.4.4 Compressive strength 108
4.4.5 Mineralogical characterization by means of X-ray diffraction 110
4.4.6 Microstructural analysis by means of SEM-BSE 112
4.4.7 Discussion 115
4.4.8 Conclusions 119
4.4.9 Applicability of the test method to AAM 120
4.5 Alkali-Silica Reaction 121
4.5.1 Adaptation of the formulations according to the standards 121
4.5.2 ASTM C1260 (Accelerated mortar-bar test method) 123
4.5.2.1 Length change 123
4.5.2.2 Microstructural analysis by means of SEM-BSE 124
4.5.2.3 Discussion 125
4.5.2.4 Conclusions 127
4.5.3 ASTM C1293 (test method in concrete) 127
4.5.3.1 Length change 127
4.5.3.2 Mass change 129
4.5.3.3 Discussion 131
4.5.3.4 Conclusions 132

4.5.4 Applicability of the ASR test methods to AAM 133
4.6 Freeze-thaw resistance 134
4.6.2 Relative dynamic modulus of elasticity (RDME) 136
4.6.3 Length change 142
4.6.4 Mass change 144
4.6.5 Discussion 147
4.6.6 Conclusion 150
4.7 Permeability 151
4.7.1 Results 151
4.7.2 Relationships between RCPT, BR and compressive strength 152
4.7.3 Discussion 155
4.7.4 Conclusion 158
4.7.5 Applicability of test methods to AAMs 158
4.8 Alkali leaching 159
4.8.1 Results 159
4.8.2 Discussion 160
4.8.3 Conclusion 162
CHAPTER 5. Durability of a novel alkali-activated material based on glass powder/metakaolin 165
5.1 Compressive strength 165
5.2 Stability in water 166
5.2.1 Description of the test 166
5.2.2 Results 166
5.2.3 Discussion 167
5.2.4 Conclusion 169
5.3 Leaching test: Sodium ions 169
5.3.1 Results 169
5.3.2 Discussion 170

5.3.3 Conclusion 172
5.4 Sulfate resistance 172
5.4.1 Expansion results 172
5.4.2 Mineralogical characterization by means of X-ray diffraction 174
5.4.3 Microstructural analysis by means of SEM-BSE 175
5.4.4 Discussion 176
5.4.5 Conclusions 179
5.5 Acid resistance 179
5.5.1 Mass and cross-sectional dimension change 180
5.5.2 Visual appearance 181
5.5.3 Compressive strength 182
5.5.4 Mineralogical characterization by means of X-ray diffraction 185
5.5.5 Microstructural analysis by means of SEM-BSE 188
5.5.6 Discussion 194
5.5.7 Conclusions 199
5.6 Alkali-silica reaction (ASR) 200
5.6.1 Adaptation of the formulations according to the standards 200
5.6.2 Length change 201
5.6.3 Mass change 202
5.6.4 Mineralogical characterization by means of X-ray diffraction 202
5.6.5 Microstructural analysis by means of SEM-BSE 203
5.6.6 Discussion 208
5.6.7 Conclusions 212
CHAPTER 6. General conclusions and Future research lines 213
6.1 General conclusion 213
6.1.1 Conclusions/recommendations of existing durability test methods for AAMs 213
6.1.2 Conclusions of AAS and AAFA durability properties 214

6.1.3 Conclusions of AAGP durability properties 216
6.2 General conclusion 217
6.3 Future research lines 218
References 219

LIST OF FIGURES

Figure 2.1 Number of publications related to the alkali-activated technology in the last 24 years (source: Scopus) using as a keywords “alkali-activated” and “geopolymer” 8

Figure 2.2 Classification of AAM with comparison to calcium-based binders. Shading indicate approximate alkali content; darker shading corresponds to higher concentration of alkalis (Provis & van Deventer 2013). 13

Figure 2.3 Descriptive model for alkali activation of aluminosilicates (Shi et al. 2011) 16

Figure 3.1 Methodology schedule of the project 52

Figure 3.2 Particle size distribution of the raw materials measured by laser diffraction. a) Between particles sizes, b) Above particles sizes 53

Figure 3.3 Mineralogical composition of the General use Portland cement. A: C_3S, C: C_3A, F: C_4AF 54

Figure 3.4 Mineralogical composition of the blast furnace slag. 55

Figure 3.5 Mineralogical composition of the fly ash. 56

Figure 3.6 Mineralogical composition of the Metakaolin. 57

Figure 3.7 Mineralogical composition of the Glass Powder. 58

Figure 3.8 Example of preconditioning of the molds with tape 64

Figure 3.9 Curing procedure of AAFA mortars 65

Figure 3.10 RCPT cell assembly with specimen 72

Figure 3.11 Bulk resistivity assembly with specimen 73

Figure 3.12 Helium pycnometer 74

Figure 3.13 Blaine permeabilimeter 75

Figure 3.14 Laser diffractometer 76

Figure 3.15 X-ray difractometer 77

Figure 3.16 Scanning Electron microscope 78

Figure 4.1 Compressive strength for OPC (a), AAS (b) and AAFA (c) mortars at 1, 7 and 28 days for different curing temperatures during the first 24h: 23, 35 and 80ºC, followed with a normal temperature of 23ºC until test. 82

Figure 4.2 Dimensional stability of OPC, AAS and AAFA mortar bars submerged in water during time: a) Curing procedure 35ºC (24h) + 23ºC, b) 80ºC (24h) + 23ºC, c) Comparison of OPC and AAS cured at 35ºC with FA cured at 80ºC. 84

Figure 4.3 Sulfate resistance for OPC bars (ASTM C1012) at 2, 5 and 8% of sulfate concentrations. a) Curing temperature for first 24h of 23ºC. b) 35ºC. c) 80ºC, followed by a normal temperature conditioning at 23ºC. 86

Figure 4.4 Sulfate resistance for AAS bars (ASTM C1012) at 2, 5 and 8% of sulfate concentrations. a) Curing temperature for first 24h of 23ºC. b) 35ºC. c) 80ºC. 87

Figure 4.5 Sulfate resistance for AAFA bars (ASTM C1012) at 2, 5 and 8% of sulfate concentrations. a) Curing temperature for first 24h of 23ºC. b) 35ºC. c) 80ºC. 89

Figure 4.6 XRD patterns for OPC mortar bars exposed at different sodium sulfates dissolutions (2, 5, and 8wt%) after 1 year of exposition. a) curing temperature during the first 24h: 23ºC; b) 35ºC; c) 80ºC. Peaks: E, ettringite; G, gypsum; P, portlandite; Q, quartz; X, C-S-H gel 91

Figure 4.7 XRD patterns for AAS mortar bars exposed at different sulfates dissolutions (2, 5, and 8wt%) after 1 year of exposition. a) curing temperature during the first 24h: 23ºC; b) 35ºC; c) 80ºC. Peaks: Q, quartz; X, C-(A)-S-H gel; HT, hydrotalcite; C, calcite. 92

Figure 4.8 XRD patterns for AAFA mortar bars exposed at different sulfates dissolutions (2, 5, and 8wt%) after 1 year of exposition. a) curing temperature during the first 24h: 23ºC; b) 35ºC; c) 80ºC. Peaks: Q, quartz; M, mullite; N, magnetite. 93

Figure 4.9 SEM-BSE images for OPC mortar bars exposed to 5% of sulfate concentration after 1 year of exposition. a) Curing temperature during the first 24h: 23ºC; b) 35ºC; c) 80ºC. 95

Figure 4.10. SEM-BSE images for AAS mortar bars exposed to 5% of sulfate concentration after 1 year of exposition. a) Curing temperature during the first 24h: 23ºC; b) 35ºC; c) 80ºC. 96

Figure 4.11. SEM-BSE images for AAFA mortar bars exposed to 5% of sulfate concentration after 1 year of exposition. a) Curing temperature during the first 24h: 23ºC; b) 35ºC; c) 80ºC. 97

Figure 4.12. Mass change of mortar cubes exposed to acid solutions with different concentration (1, 3 and 5wt%) and different curing time before exposure to acid (7 and 28 days). a) OPC, b) AAS, c) AAFA. 105

Figure 4.13. Cross-sectional dimension change of mortar cubes exposed to acid solutions with different concentration (1, 3 and 5wt%) and different curing time before exposure to acid (7 and 28 days). a) OPC, b) BFS, c) FA. 106

Figure 4.14 Visual appearance of mortars cured during 7 days after 28 and 196 days of exposure to sulfuric acid. In all the photos, first cube was immersed in 1wt% sulfuric acid solution, second cube was immersed in 3wt% and the third cube in 5wt%..... 108

Figure 4.15 Compressive strength evolution of AAFA mortar cubes exposed to acid solutions with different concentration (1, 3 and 5wt%) and different curing time before exposure to acid, a) 7 and b) 28 days. 109

Figure 4.16 Split mortar cubes after 56 days of exposure to acid attack: a) half cube exposed at 1wt% of acid concentration; b) 3wt%; c) 5wt% 110

Figure 4.17 XRD patterns of the specimens after 28 days of exposure in the different acid solutions: a) OPC, b) AAS, c) AAFA. INT: unreacted core; EXT: corroded layer. Pics: Q, quartz; P, portlandite; E, ettringite; G, gypsum; X, C-S-H gel; M, mullite; N, magnetite. 111

Figure 4.18 Microstructural analysis of OPC mortar after 28 days of exposure to 5% acid solution: a) SEM (BSE) image and b) EDX analysis (line scan) 113

Figure 4.19 Microstructural analysis of AAS mortar after 28 days of exposure to 5% acid solution: a) SEM (BSE) image and b) EDX analysis (line scan) 114

Figure 4.20 SEM (BSE) images and EDX analysis after 28 days of exposure to 5% acid solution for AAFA. a) internal region; b) external region. 115

Figure 4.21 SEM (BSE) images and EDX analysis after 28 days of exposure to 5% acid solution for AAFA showing gypsum crystals in a pore..... 116

Figure 4.22 Proposed mechanism of sulfuric acid attack in OPC mortars..... 117

Figure. 4.23 Proposed mechanism of sulfuric acid attack in AAS mortars 118

Figure 4.24 Expansion results for the OPC, AAS and AAFA systems with a reactive aggregate Spratt 123

Figure 4.25 SEM-BSE images for OPC (A) and AAS (B) confectioned with the reactive aggregates after 28 days of exposure to 1M NaOH at 80ºC 124

Figure 4.26 Expansion of OPC (a), AAS (b) and AAFA (c) concrete prisms exposed at different conditions: at 23ºC/100% RH all the time; at 38ºC/100%RH (ASTM C1293) after demolding, after 28 days and after 90 days at 23ºC/100% RH. 129

Figure 4.27 Mass change of OPC (a), AAS (b) and AAFA (c) concrete prisms exposed at different conditions: at 23ºC/100% RH the whole time; at 38ºC/100%RH (ASTM C1293) after demolding, after 28 days and after 90 days at 23ºC/100% RH. 130

Figure 4.28 Compressive strength evolution in function of the AEA agent added 136

Figure 4.29 Relative dynamic modulus of elasticity of OPC concretes exposed to F-T cycles at different curing times: A, without AEA; B, with 60mL of AEA/100kg of binder 138

Figure 4.30 Relative dynamic modulus of elasticity of AAS concretes exposed to F-T cycles at different curing times: A, without AEA; B, with 60mL of AEA/100kg of binder; C, with 120mL of AEA/100kg of binder 140

Figure 4.31 Relative dynamic modulus of elasticity of AAFA concretes exposed to F-T cycles at different curing times: A, without AEA; B, with 60mL of AEA/100kg of binder; C, with 120mL of AEA/100kg of binder 141

Figure 4.32 Length change of OPC concretes exposed to F-T cycles at different curing times: A, without AEA; B, with 60mL of AEA/100kg of binder 143

Figure 4.33 Length change of AAS concretes exposed to F-T cycles at different curing times: A, without AEA; B, with 60mL of AEA/100kg of binder; C, with 120mL of AEA/100kg of binder 144

Figure 4.34 Mass change of OPC concretes exposed to F-T cycles at different curing times: A, without AEA; B, with 60mL of AEA/100kg of binder 145

Figure 4.35 Mass change of AAS concretes exposed to F-T cycles at different curing times: A, without AEA; B, with 60mL of AEA/100kg of binder; C, with 120mL of AEA/100kg of binder 146

Figure 4.36 Relationship between RCPT and bulk resistivity measurements 153

Figure 4.37 Relationship between RCPT and compressive strength 154

Figure 4.38 Relationship between bulk resistivity and compressive strength 155

Figure 4.39 Sodium leaching of AAS (a) and AAFA (b) mortars when submerged in distilled water 159

Figure 4.40 Sodium leaching accumulate of AAS (a) and AAFA (b) mortars when submerged in distilled water 160

Figure 4.41 Degree of sodium leached regarding the initial sodium content in the mix.(a) AAS, and (b) AAFA 161

Figure 5.1 Compressive strength of AAGP mortar cubes 166

Figure 5.2. Dimensional stability (a) and mass change (b) of AAGP mortars bars submerged in tap water during time 167

Figure 5.3. “Na” leaching of bars exposed in distilled water during 4 weeks 170

Figure 5.4 Sulfate resistance for AAGP bars exposed at 5% of sulfate concentration during 1 year .. 173

Figure 5.5 Visual aspect of AAGP bars after 28 days of exposure to 5% sodium sulfate solution. a) 95GP, b) 85GP, and c) 70GP. 173

Figure 5.6 X-ray diffraction spectra for AAGP systems after 12 months of exposure to 5wt% sulfate solution 174

Figure 5.7 SEM-BSE images for AAGP mortars bars exposed to 5% of sulfate concentration after 1 year of exposition. A) 95GP; B) 85GP; C) 70GP. 177

Figure 5.8 Mass and cross-sectional dimension change of AAGP mortar cubes exposed to sulfuric acid at 3 and 5% of concentration during 196 days 181

Figure 5.9 Visual appearance of AAGP mortars cured during 7 days after 28 and 196 days of exposure to sulfuric acid. In 95GP photos, first cube was immersed in 1wt% sulfuric acid solution, second cube was immersed in 3wt% and the third cube in 5wt%. For 85GP and 70GP photos, first cube was immersed in 3wt% sulfuric acid solution and the second cube was immersed in 5wt%. 182

Figure 5.10 White gel formed at the surface of 95GP cubes after 1 week of exposure to 1% of sulfuric acid solution 182

Figure 5.11 Compressive strength of AAGP mortar cubes at different exposure conditions: 56% RH, tap water (TW), and 3 and 5% acid solution. Temperature during test was always 23ºC. 184

Figure 5.12 Split mortar cubes after 28 days of exposure to tap water and acid solutions (1, 3 and 5%). One half is shown just after splitting (above half) and the other was sprayed with phenolphthalein solution (below half). a) 95GP mortar cubes, b) 85GP and c) 70GP. 185

Figure 5.13 X-ray patterns of 95GP specimens after 28 days of exposure to acid solutions and tap water. INT: inner core; EXT: outer layer. Pics: Q, quartz; I, illite; G, gypsum. 186

Figure 5.14 X-ray patterns of 85GP specimens after 28 days of exposure to acid solutions and tap water. INT: inner core; EXT: outer layer. Pics: Q, quartz; I, illite; G, gypsum; Z, zeolite type A. 187

Figure 5.15 X-ray patterns of 70GP specimens after 28 days of exposure to acid solutions and tap water. INT: inner core; EXT: outer layer. Pics: Q, quartz; I, illite; G, gypsum; Z, zeolite type A. 188

Figure 5.16a SEM (BSE) images and EDX analysis of 95GP mortar cubes after 28 days of exposure to tap water and 5% acid solution. a) Tap water, b) Face-exposed to acid solution (EXT) 189

Figure 5.16b SEM (BSE) images and EDX analysis of 95GP mortar cubes after 28 days of exposure to tap water and 5% acid solution. c) Inner part not exposed to acid solution (INT), d) Gypsum formed in the face-exposed to acid solution 190

Figure 5.17a SEM (BSE) images and EDX analysis of 85GP mortar cubes after 28 days of exposure to tap water and 5% acid solution. a) Tap water, b) Face-exposed to acid solution (EXT) 192

Figure 5.17b SEM (BSE) images and EDX analysis of 85GP mortar cubes after 28 days of exposure to tap water and 5% acid solution. c) inner part not exposed to acid solution (INT), d) Gypsum formed in the face-exposed to acid solution 193

Figure 5.18a SEM (BSE) images and EDX analysis of 70GP mortar cubes after 28 days of exposure to tap water and 5% acid solution. a) Tap water, b) Face-exposed to acid solution (EXT) 194

Figure 5.18b SEM (BSE) images and EDX analysis of 70GP mortar cubes after 28 days of exposure to tap water and 5% acid solution. c) Inner part not exposed to acid solution (INT), d) Gypsum formed in the face-exposed to acid solution 195

Figure 5.19 Expansion results for the AAGP systems with Spratt aggregate 202

Figure 5.20 Mass change for the AAGP systems with Spratt aggregate..... 203

Figure 5.21 X-ray patterns of 85GP and 70GP specimens with Spratt aggregate after 28 days of exposition to 1M NaOH solution at 80ºC. Q, quartz; C, calcite; V, vaterite; K, kaolinite; N, Ankerite. 204

Figure 5.22 SEM (BSE) images and EDX analysis of 95GP specimens after 28 days of exposition to 1M NaOH solution at 80ºC. a) Fissured gel; b) Reactive aggregate with internal fissures filled with a gel; c) Rosette-like product in air voids. 205

Figure 5.23 SEM (BSE) images and EDX analysis of 85GP specimens after 28 days of exposition to 1M NaOH solution at 80ºC. a) Cracked calcareous aggregate; b) Air-void filled with a gel; c) Attacked reactive aggregate at the top right 206

Figure 5.24 SEM (BSE) images and EDX analysis of 70GP specimens after 28 days of exposition to 1M NaOH solution at 80ºC. a) Paste; b) Gel inside a crack; c) Gel in small air-voids 209

LIST OF TABLES

Table 2.1a Summary of the sulfate resistance test conditions used in several works 23

Table 2.1b Summary of the sulfate resistance test conditions used in several works 24

Table 2.2a Summary of the acid resistance test conditions used in several works 28

Table 2.2b Summary of the acid resistance test conditions used in several works 29

Table 2.3 Summary of the AAR test conditions used in several works 34

Table 2.4 Summary of the F-T test conditions used in several works 37

Table 3.1 Physical properties of the raw materials 53

Table 3.2 Chemical composition of the raw materials 54

Table 3.3 Grading of the Sand 0-5 59

Table 3.4 Grading of the aggregates 5-14 and 10-20 59

Table 3.5 Main parameters of the AAFA and AAS formulations 61

Table 3.6 Mix proportions of OPC, AAS and AAFA mortars and concretes 61

Table 3.7 Main parameters of the AAGP formulations 62

Table 3.8 Mix proportions of AAGP mortars 62

Table 3.9 Grading requirements 69

Table 4.1. Expansion of OPC mortar bars at 6 and 12 months 87

Table 4.2 Atomic ratios obtained by the EDX analysis of the AAFA mortars exposed during 12 months to 5wt% sodium sulfate solution. A) Curing temperature during the first 24 hours of 23ºC, b) 35ºC, c) 80ºC. 98

Table 4.3 Mortar formulations according to ASTM C1260 122

Table 4.4 Concrete formulations according to ASTM C1293 122

Table 4.5 Fresh properties of the concretes with and without AEA 134

Table 4.6 Hardened properties of the concretes with and without AEA 135

Table 4.7 Durability factors of OPC, AAS and AAFA concrete prisms whit different curing times .. 142

Table 4.8 Charge passed and BR with time 152

Table 4.9 Classification of permeability results by means of ASTM C1202 and bulk resistivity (bulk resistivity based on literature review)..... 153

Table 5.1 Atomic ratios for AAGP mortars bars exposed to 5% of sulfate concentration after 1 year of exposition 176

Table 5.2 Average elemental ratios obtained by EDX analysis of 95GP, 85GP and 70GP samples ... 195

Table 5.3 Mix proportions of AAGP mortars for the AAR test 201

Table 5.4 Summary of the atomic percentages of the EDX analysis of the AAGP systems..... 207

ABRÉVIATIONS / ABBREVIATIONS

Al	Aluminum
AA	Alkali-activation
AAFA	Alkali-activated class F fly ash
AAMk	Alkali-activated metakaolin
AAMs	Alkali-activated materials
AAR	Alkali-aggregate reaction
AAS	Alkali-activated blast furnace slag
AC	Alternative current
ACR	Alkali-carbonate reaction
AEA	Air entrainer agent
ASR	Alkali-silica reaction
BFS	Blast furnace slag
BR	Bulk resistivity
BSE	Back scattering electron
Ca	Calcium
C-A-S-H	Calcium aluminosilicate hydrate
C-S-H	Calcium silicate hydrate
DC	Direct current
DEF	Delayed ettringite formation
DF	Durability factor
EDX	Energy dispersive X-ray
ESA	External sulfate attack
FA	Class F fly ash
F-T	Freeze-thaw
GHG	Greenhouse gas
GP	Glass powder
HL	Hydrated lime
ISA	Internal sulfate attack
K	Potassium
Na	Sodium
N-A-S-H	Sodium aluminosilicate hydrate
OPC	Ordinary portland cement
RCPT	Rapid chloride penetrability test
RDME	Relative dynamic modulus of elasticity
SEM	Scanning electron microscope
SH	Sodium hydroxide solution
Si	Silicon
SS	Sodium silicate solution
XRD	X-ray diffraction
WRA	Water reducing admixture

CHAPTER 1. Introduction

1.1 Context

Portland cement (OPC) remains one of the materials that contribute most to the development of societies. However, it is responsible for the negative environmental impact of the concrete industry. Indeed, the production of the OPC generates significant greenhouse gas emissions (GHG). It is well known that 1 ton of OPC emits approximately 0.9 tons of carbon dioxide (CO_2) related firstly to the decarbonation of limestone (0.5 tons) and secondly, to the use of fossil fuels as an energy source (0.4 tons) (Gartner 2004; Damtoft et al. 2008). This CO_2 emissions have been estimated on 7-10% of the total global CO_2 emissions (Ali et al. 2011).

Cement industry will have to find solutions to reduce GHG emissions associated with its production in order to meet the environmental requirements defined by the Kyoto Protocol to control and minimize emissions due to human activity. CO_2 emissions are still elevated despite the actions that the cement industry has already adopted, as the use of alternative sources of energy, the reduction of the clinker/cement ratio, the use of non-carbonated raw materials, etc.

Therefore, societies needs to find alternatives to OPC. The materials which have received a special attention by the scientific community as an alternative to OPC are the so-called "Alkali-activated materials" (AAMs). AAMs are OPC-free materials obtained through the activation of a solid aluminosilicate precursor by means of an alkaline source (normally in a liquid state, as alkaline hydroxides, silicates, etc.). The precursors typically used are the materials with good pozzolanic properties used in blended OPC. Thus, these materials are generally either industrial wastes – such as blast furnace slag (BFS) and fly ash from pulverized coal combustion (FA) -, or natural materials such as calcined kaolinite clays (metakaolin (Mk)). However, other potential materials could be used as precursors and are nevertheless receiving less attention from the scientific community. This lack of studies about other precursors may affect considerably the use and the implementation of AAMs at the industrial scale, as its use will be restricted only to the regions with access to typical precursors (BFS, FA, Mk). Furthermore, the low variability of precursors could hinder the interest of governments in adopting these materials in the regulations. The most important requirement of a precursor, to be used in AAMs, is it content on reactive silica and alumina soluble under alkaline conditions.

Due to its composition and physical properties, glass powder (GP) is one of the wastes that is starting to receive attention by the scientific community as a material for the concrete production. GP is produced by grinding recycled glass.. Despite that our society is more aware of the everyday recycling, reusing glass is

being problematic by the lack of market outlets. As a consequence, part of the glass -specially mixed color waste glass- is being landfilled, with subsequent economic and environmental costs. Therefore, the usage of glass as a fine powder for concrete production would largely contribute to solve this problem.

GP was first introduced as an OPC replacement, providing some mechanical (Jani & Hogland 2014) and durability (Zidol 2009; Mafalda Matos & Sousa-Coutinho 2012) benefits. Another possibility was to use the glass as aggregate to replace the conventional ones in concrete, with the environmental benefit of restricting the natural sources. However, this possibility was restricted in OPC concretes due to Alkali Silica Reaction (ASR) (Federico & Chidiac 2009). Another use of GP is as an alternative for the conventional alkaline activators -like waterglass- that are responsible of the major environmental impact of the production of AAMs-based concretes. Thus, GP is used in this effect to obtain an emulation of waterglass by dissolving the silica and alkalis into a solution (Torres-Carrasco et al. 2015; Torres-Carrasco & Puertas 2015).

Moreover, due to its composition, rich in reactive silica, GP can be used as well as precursor of AAMs to produce sustainable and durable concretes. A few studies have been done on this subject showing good mechanical properties (Cyr et al. 2012; Redden & Neithalath 2014; Balaguer-Pascual et al. 2014; Tashima, Soriano, et al. 2012; Bobirică et al. 2015; Zhang 2015). However, it seems that the resulting reaction product (a sodium silicate gel) has low durability, associated to its instability in humid conditions (Cyr et al. 2012; Redden & Neithalath 2014). Therefore, more research is needed in order to obtain durable concretes when using GP as a precursor.

Another issue affecting OPC-based concretes is its durability. Experience in last decades showed that OPC-based concretes had some problems when exposed to certain service situations reducing its service life: for instance, presence of chloride ions; corrosion of reinforced concrete; presence of sulfate ions; presence of acids when concretes are mixed with reactive aggregates (alkali-aggregate reaction); frost environments; etc. This has entailed elevated cost due to reparation of the structures, hence a negative impact for the society. Instead, research on AAMs is showing that durability of AAMs mortars and concretes is in most cases superior to those of OPC. Nevertheless, there is a drawback on the validity and/or reliability of AAMs durability results. Indeed, existing characterizations methods are based on standards developed and adapted for OPC chemistry. Since the chemistry of hydration of OPC is very different from those of AAMs, there is a concern on the applicability of these durability tests methods on AAMs. Therefore, it is necessary to evaluate if the existing durability test methods are applicable to them.

Moreover, most standards/codes/regulations do not take into account these new materials, making it difficult to implement them on an industrial scale. Only two non-prescriptive standards allow the use of any

material (and not only OPC and OPC blends): CSA A3004: E1 and ASTM C1157. The only requirement of these standards is that the material has to achieve mechanical and durability properties high enough to face the environment in which the concrete will be exposed. However, these kind of standards are still not adopted by the industry.

The distrust felt by society implementing AAMs on an industrial scale is due to the ignorance of the behavior of these materials including long-term sustainability and the lack of specific standards for its characterization. It is therefore imperative to conduct more research in this area in order to establish specific standards for AAMs and thus promote their production on an industrial scale, hence the interest of this research project.

1.2 Research project definition

This project is part of a *general program* conducted at the Concrete group of the civil engineering department of the faculty of engineering at the University of Sherbrooke. This *general program* is called "*Development of new binders based on aluminosilicate materials*", which is divided into several phases. The early phases of this *general program* deal with the development of an optimum AAMs formulation based on Quebec local industrial byproducts such as glass powder (Balaguer Pascual 2014).

The last phase of the *general program*, which is the subject of this study, treats the "*Durability study of AAMs-based concretes*", explained in detail next.

Several problems associated with AAMs have been addressed in this project. The first one is associated to the applicability of the durability test methods to AAMs. Existing standards for assessing the durability of mortars and concretes have been designed and adapted during last decades to OPC and blended OPC chemistry, thus there is a concern about how these methods will affect (negatively or positively) the interpretation of the AAMs durability results. Therefore, in a **first phase** of this project, the most used durability test methods described by American standards (ASTM) have been evaluated to see their applicability to AAMs. For this purpose, two precursors which have received a lot of attention by the scientific community have been used: the blast furnace slag and the class F fly ash (from coal combustion). As a comparative purpose, a conventional OPC formulation has been used in this part. Results of the first phase will provide a more detailed comprehension of the applicability of these standards to AAMs, and will therefore be applied in the second phase, described next.

The second problem associated with AAMs is the lack of studies dealing with new precursors other than the conventional ones already in use, as BFS, FA, and Mk. In this project, a local industrial byproduct of the province of Quebec (Canada), the glass powder (GP), has been validated as AAM precursor. The GP

used in this project comes from the glass recycling industry, specifically the mixed colored glass. This mixed colored glass has difficulties to be reused due to different problems (as the presence of contaminants and the difficulty to separate the glass by colors). Therefore, it is normally being landfilled. The glass is a weaklybiodegradable material. The stock in landfills is therefore environmentally negative and generates associated costs. Therefore, it is necessary to find new market opportunities to valorize it. This will be done in the **second phase** of the project, where the durability of the novel AAMs formulation based on GP and Mk developed in former phases of the *program* will be assessed. (Balaguer Pascual 2014).

In each phase of the project, we attempted to answer the following questions:

- Phase 1: Are the existing durability tests suited to AAMs chemistry? Or, do they need some modifications?
- Phase 2: Does this new kind of binders, based on GP and Mk, possess good durability properties?

1.3 Objectives of the research project

This research project was conducted following two general objectives. The **first objective** was to study the durability of the novel AAMs developed at the University of Sherbrooke from local industrial byproducts available in the province of Quebec (Canada), specifically the GP. In this project, GP has been mixed together with Mk as AAM precursor. Therefore, by using the GP in AAM concrete, it is expected to find a new market for the mixed colored glass. This objective has been addressed in the second phase of the project, following the considered adaptations of the durability test methods under the recommendations given in the first phase of the project.

As explained before, in order to assess the durability of this novel formulation, a study of the applicability of some standardized durability test methods to AAMs has been performed. This has been the **second objective** of the project, assessed in the first phase of the project.

1.4 Original contributions

The contributions of this project are several. In the first phase, new information has been obtained regarding the use of the existing durability test methods described in the standards to AAMs. Aspects as curing regimes, test conditions and indicators of the degree of attack have been shown to be critical on the AAMs performance against aggressive environments. Thus, recommendations are given for future standards describing durability test methods for AAMs.

The second phase of this study showed the durability results of the AAM system glass powder/metakaolin for the first time. In the study, the influence of the metakaolin content in the binder on the durability properties has been evaluated, providing worth information about the type of gel formed and its influence

on the durability properties. Therefore, it has been demonstrated that the replacement of a 30wt% of the glass powder in the binder by metakaolin leads to the formation of a sodium aluminosilicate gel that improves considerably the durability of the system, becoming a promising material for the production of a sustainable and environmental friendly concrete.

1.5 Document plan

The memory of this thesis is divided into 6 chapters. The **first chapter** is an introduction to place our project in context: detailing the problems; researching project definition; explaining the motivation and objectives of this research; and a brief summary of the original contributions of this project. The **second chapter** is focused on understanding better the AAMs and the related works found in literature that will put in evidence the necessity of this research project. In the **third chapter** the experimental methods used in the project, the characterization techniques and the physical/chemical characterization of the materials used are presented.

The next two chapters show the results. The **fourth chapter** shows the results of the first phase of the project. The durability performances of two AAMs formulations, one with BFS and the other with class F FA are presented. These two formulations have been used to analyze the applicability of the OPC durability test methods. Following the obtained results, this chapter gives a critical view of the standards, giving some recommendations that contribute to adapt the standards for AAMs for future application in the field. The **chapter 5** shows the durability test results of several mixes of GP/Mk (95%, 85% and 70% of GP being the rest Mk). The durability test methods have been adapted according to recommendations done in chapter 4. The influence of replacing the GP by Mk was also analyzed.

General conclusions are presented in the third part. They have been divided in two chapters, 6 and 7. Thus, **chapter 6** is addressed to summarize all the conclusions obtained in each phase of the project, and some recommendations for future lines of investigation in order to improve the knowledge provided in this project.

Cited references are shown at the end of the memory.

CHAPTER 2. State of the art

This chapteraboard all the aspects of the alkali-activated materials (AAMs), know its origins, the importance of using them to produce sustainable concretes, their chemistry, what has been studied about their durability and what are the problems that hinder their utilization at industrial scale. At the end of this chapter we will see some aspects about the glass powder. Therefore, we will know all the steps that the glass follows from its origins to its conception as a construction material. Finally, we will see the state-of-the-art about the use of glass powder (GP) in concretes by means of alkali-activation technology (AAT).

2.1 History of alkali-activated materials

Although AAMs, as we understand them nowadays, were not used until the last century, it is believed that ancient Egyptians and Romans could make use of a similar technology in their constructions, using alkaline cements. Some studies carried out by Davidovits (Davidovits 1987; Davidovits & Davidovits 2001), state that the Egyptian pyramids could have been built with a concrete casted in place, and not as the traditionally theory states (carve-and-hoist). This concrete is suggested to have been prepared by mixing the soft, marly, kaolinitic, nummulitic limestone of Giza with Nile river water, lime, and locally available natron [$Na_2CO_3.10H_2O$]. The reaction of the lime with natron produces sodium hydroxide, responsible of the dissociation of the aluminosilicate species of the kaolinitic limestone to produce the geopolymeric binder.

On the other hand we have the Roman constructions, which are still in service after 2000 years. Although some Roman structures have been degraded over centuries, there are still some of them that are kept in good service conditions (as the Pantheon of Rome). Roman concrete were produced by mixing lime and volcanic ash (from the region of Pozzuoli). The elevated pH of the reaction of the lime initiated the reaction of the volcanic ash. Examinations of the Roman concretes after 2000 years revealed the presence of some zeolitic compounds, as analcime ($NaAlSi_2O_6 \cdot H_2O$).

After the decay of Roman Empire, there is no evidence of the use of alkaline cements, so the Roman concrete technology was forgotten for the next centuries.

The firsts contemporary studies found with the use of alkali-activation technology are the patents of the engineers J. Whiting in 1985 (Whiting 1895) and H. Khül in 1908 (Kühl 1908). Whiting patented a new cement produced by adding a caustic soda, potash, sodium chloride or equivalents, or any substance of which the latter are ingredients, in form of aqueous solution or dried state, of blast furnace slag (Whiting 1895). The performance of this cement described by the author was: "*shall be equal in quality to the best Portland or other similar cement, and which shall at the same time be more economical to manufacture*". Few years later, Khül patented a cement composed by a basic blast furnace slag mixed with sodium sulfate,

sodium carbonate, or suitable mixtures of the same, with or without added alkaline earth oxides or hydroxides (Kühl 1908). The author described the performance of the cement as: "*to be fully equal to the best Portland cement*". Nevertheless, it was not until 1940 when the scientific bases of AAMs were developed by Purdon (Purdon 1940). In his work, the author studied different blast furnace slags mixed with sodium hydroxide and combinations of calcium hydroxide with different salts. Purdon also identified the difficulties of using this technology for ready-mixed and precast applications that are still unsolved nowadays. For example, sensitivity of the activation conditions and the handling of concentrated caustic solutions hinder the use of AAM.

Few works were published afterwards. The most important works done in that period was reported by Roy (1999). One work to be mentioned from that report is Glukhowsky's (1959), who introduced the theoretical bases and development of the alkaline cements, being the first to later introduce the term of *alkaline cements* (Glukhowsky 1965). A few years later, Davidovits (1979) was the first one to introduce the term geopolymer cement, widely used today to name a specific group of AAMs with very low calcium content.

After the nineties, the works published relating the AAMs increased considerably, showing the high interest of the scientific community to prove the benefits of these materials as an alternative to portland cement (see **Figure 2.1**). Most of these works have been reported in several books published in last years, as:

- Alkali-activated cements and concretes (Shi et al. 2006)
- Geopolymer chemistry and their applications (Davidovits 2008)
- Geopolymer, structure, processing, properties and industrial applications (Provis & van Deventer 2009)
- Alkali-activated materials: State of the art report (Provis & van Deventer 2013)
- Handbook of alkali-activated cements, mortars and concretes (Pacheco-Torgal et al. 2015)

2.2 Why alkali-activated materials?

The necessity to replace OPC as a binder for mortars and concretes due to its environmental problems associated to its production initiated researches on alternative binders.

OPC is one of the most consumed products due to its use in concrete, which is the most widely used construction material (Gartner 2004). The production of OPC is being increased every year. Worldwide, production of cement has passed from 1.7 billion of tons in 2000 to 4.1 billion of tons in 2017 (USGS 2017). In the last few years, this increment in the production of cement is mainly due to the high demand of developing countries. For instance, China's production in 2013 itself accounted for 59% of the world

total output for the year. This huge production of cement involves serious environmental problems, and it contributes in about 7-10% of the total worldwide CO_2 emissions (Ali et al. 2011).

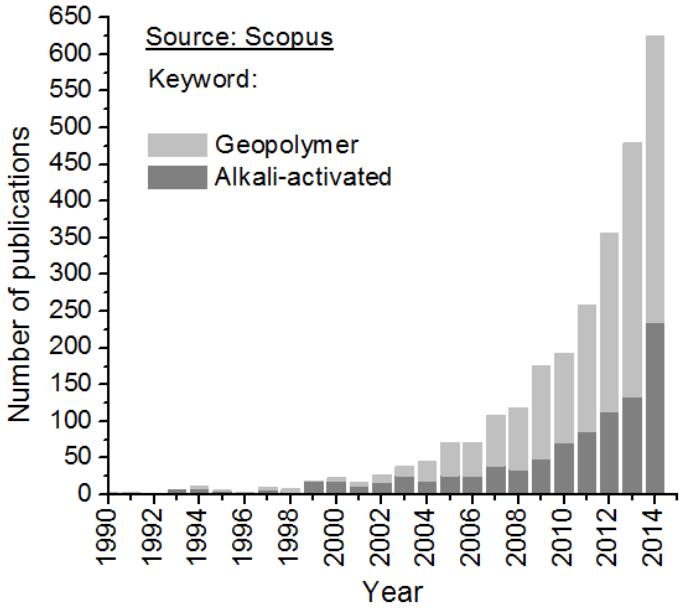

Figure 2.1 Number of publications related to the alkali-activated technology in the last 24 years (source: Scopus) using as a keywords "alkali-activated" and "geopolymer"

The environmental problems of OPC production are associated to CO_2 emitted during the decomposition of limestone (mostly $CaCO_3$), at elevated temperatures (around 1450ºC) to produce reactive products (clinker). The clinker is mainly composed by calcium silicate compounds, as alite ($3CaO{\cdot}SiO_2$) and belite ($2CaO{\cdot}SiO_2$), and other minor but also important phases as aluminate-rich compounds, tricalcium aluminate ($CaO{\cdot}3Al_2O_3$) and aluminoferrite phases ($4CaO{\cdot}Al_2O_3{\cdot}Fe_2O$). The reaction in which CO_2 is released is described in **equation 2.1**:

$$CaCO_3 \xrightarrow{\Delta} CaO + CO_2 \uparrow \qquad (2.1)$$

According to Gartner (2004), CO_2 emissions by the decomposition of the carbonates compounds (**equation 2.1**) are around 0.5 tons of CO_2 per ton of clinker. Else, a high demand of energy is required in the kiln to reach the elevated temperatures, normally obtained by burning combustible fuels that also increase CO_2 emissions. According to Damtoft et al. (2008), CO_2 emissions derived from burning traditional carbon based fuels (coal, oil or petroleum coke) are around 0.31-0.60 tons per ton of clinker produced, depending on the efficiency of the kiln and the fuel used. In the case of raw materials, the same authors estimated CO_2 emissions around 0.53 tons per ton of clinker, similarly to the estimations of Gartner. Therefore, total CO_2

emissions due to the energy consumption in the kilns and the raw materials range from 0.84 to 1.15 tons per ton of clinker.

In order to reduce this high CO_2 emissions, cement industry is implementing several techniques, as the use of alternative sources of energy (alternative fuels), the reduction of the clinker/cement ratio (blended cements), the use of non-carbonated raw materials, the optimization of the production process, the implantation of CO_2 capture and storage technologies, and others (Ali et al. 2011). These techniques are estimated to reduce CO_2 by 20%. In the case of CO_2 capture and storage technologies, the reduction can achieve around 65-70%, but the implementation and operating costs associated to these techniques are high.

One of the main advantages of using AAMs is the reduction of CO_2 emissions, which is used as one of the inherent characteristics to promote these materials as an alternative to OPC, among other probed advantages. Otherwise, other alternatives to OPC are proposed, and some of them already used, as calcium aluminate cements, calcium sulfoaluminate cements and supersulfated cements. In the case of AAMs, while still under discussion, extent of the reduction of CO_2 emissions has been considered to be between 55 to 80% (Duxson, Provis, et al. 2007; Yang et al. 2013; McLellan et al. 2011; Habert et al. 2011). Contrary to these estimations, another study argues that some factors could have not been taken into consideration, and estimates that CO_2 emissions reduction by a geopolymer concrete are 9% less than comparable concrete containing 100% OPC binder (Turner & Collins 2013). These estimations are based on the use of a geopolymer concrete made with fly ash. In this estimation, half of CO_2 emissions are due to the activators production (the sodium silicate and sodium hydroxide, which are the most used activators); and another important quantity is due to the curing process, in this case 60ºC during first 24 hours. Looking at the new efforts done in the research for alternative alkaline activators (Torres-Carrasco & Puertas 2015; Kim et al. 2013; Passuello et al. 2017), not all AAMs need elevated temperatures. It is thus expected that CO_2 emissions reduction may be higher than 9%.

Other environmental advantages of using AAMs instead of OPC are the natural resources used. To obtain clinker, we add natural compounds to the kiln, like limestone, clay, bauxite and other minor compounds, with the consequent landscape destruction by quarries. In the case of the concrete aggregates, quarries are required for AAMs in the same manner as for OPC. On the contrary, typical raw materials in AAMs are industrial wastes as fly ash (FA) and blast furnace slag (BFS). However, these materials are not the only wastes that can be used in AAMs. Other wastes such as glass powder (Balaguer Pascual 2014; Redden & Neithalath 2014; Cyr et al. 2012), magnesia-iron slags (Zosin et al. 1998), ferronickel slags (Komnitsas et al. 2007; Maragkos et al. 2009; Komnitsas et al. 2009), tungsten mine waste (Pacheco-Torgal et al. 2008b; Pacheco-Torgal et al. 2009), fluid catalytic cracking catalyst residue (Tashima et al. 2012; Rodríguez et al. 2013), and others (Provis et al. 2015) are proving to be valuable for its use in AAM concretes. In addition,

there is an added benefit, the valorization of some wastes in these case is highly beneficial for the environment, since these wastes will not be landfilled. Natural resources, such as kaolin, are also used from which after heating at around 700ºC yields metakaolin, a very reactive powder. Using industrial wastes to produce AAMs based concretes will furthermore eliminate the environmental problems associated with the quarrying of raw materials, as well landfilling of high-volume wastes.

Even though the proven environmental benefits that AAMs offer comparing to OPC binder, it is not sufficient to implement this technology in the market, due to some technical and commercial drivers. Historically, the driver competition to the choice of the construction material by the industry has been the lowest price (Van Deventer et al. 2012). Thus, for years, engineers have optimized formulation to obtain a concrete at the lowest price, being OPC their choice as a binder due to its high availability, its low cost and good performance that it offers. However, in the last years, a new driver is appearing to have more importance in the selection of materials due to the changes of the world regulations to control the climate change (Kyoto protocol, Paris Agreement): CO_2 emissions. Hence, these changing trends in the selection of materials are promoting the use of alternative binder systems. Therefore, the short-term adoption of AAMs seems to be an opportunity.

Another driver is the availability of raw materials normally used in AAMs. Traditional raw materials, as BFS and FA, are not available everywhere, so it should be an interesting market in terms of low cost shipping to get this materials everywhere. Nevertheless, the technology of AAM offers a viable solution to valorize a wide range of industrial wastes different than traditional ones, so different regions could make use of this technology with different wastes. E.g., a region that generates a non-recoverable waste, and without easy access to OPC, could profit this waste by means of AAT to make concrete.

Some of the major barriers that hinder the use of AAMs by the construction industry nowadays are related to the regulations and lack of long-term data. Most of the construction codes, standards and instructions prohibit the use of materials different than portland-based cements, bringing difficulties to the adoption of AAMs by the industry. A non-prescriptive standard that allows the use of no matter which material while it achieves a required level of performance, i.e. ASTM C1157, nevertheless exists. Other standards, as CSA 3004:E1 and ASTM C1709, are based on material science approach, and could be used for AAMs too. Furthermore, most of the existing standards to analyze the mechanical and durability properties of the concretes have been based on OPC chemistry, as it has been for the traditional binder. Nowadays, the differences in chemistry between OPC-based binders and AAMs binders are well known, hence, there is a mistrust on the results obtained using prescriptive standards. This point will be discussed in more detail in **section 2.4**. Therefore, some of the criteria to pass the test could be the misinterpretation of the behavior of

AAMs in real service. To face this problem, there is actually a RILEM technical committee dealing with it, the TC 247-DTA "*Durability testing of alkali activated materials*".

The lack of long-term data is another fact that hinders the use of AAMs by the construction industry. As all the constructions are designed for a service life of decades, it would be valuable to have available long-term data of the performance of the materials. Most of the existing investigations have been done for OPC, as it was traditionally the construction material by excellence. Thus, construction industry has a historical base in order to design an OPC-based concrete for future structures. On the contrary, AAMs data is relatively low compared to OPC, and is rare to find long-term data, and consequently, there is a mistrust on how these materials will behave some decades later. To solve this problem, efforts in the development of new standards that could predict in a more realistic manner the long-term properties of the material, and consequently accelerate the industrial scale implementation of new materials need to be developed.

Several studies showing the performance of AAMs can be found, but this will be analyzed in more detail in **section 2.5**. A summary of the properties has been already reported elsewhere (Duxson et al. 2007):

- high compressive strength gain
- good abrasion resistance
- rapid controllable setting and hardening
- fire resistance (up to 1000 °C) and no emission of toxic fumes when heated — either in the form of a carbon fiber/geopolymer composite or as a pure geopolymer (e.g. a geopolymeric coating on an exposed surface)
- high level of resistance to a range of different acids and salt solutions
- not subject to deleterious alkali–aggregate reactions
- low shrinkage and low thermal conductivity
- adhesion to fresh and old concrete substrates, steel, glass, ceramics
- high surface definition that replicates mold patterns
- inherent protection of steel reinforcing due to high residual pH and low chloride diffusion rates

Not every single one of these properties will be present on all AAMs. It will depend on the mix design. Thus, formulations have to be designed taking in account the required specifications.

As observed in this section, there are a lot of benefits of using AAMs instead of OPC as a construction material. The most important benefit at this moment may be CO_2 emissions reduction, in which construction industry may put its attention for a short-term adoption, because of the environmental regulations pressure. Moreover, the excellent durability properties that most of these materials offer will play a significant role

for the future adoption of them. The factors that actually hinder the adoption of AAM technology by the construction industry seem to be more regulatory rather than technical. Therefore, more performance standards should appear instead of the actual prescriptive standards with a minimum required content of clinker.

2.3 Alkali-activated materials chemistry

In order to understand the factors affecting the durability properties of AAMs that will be discussed in later sections, it is important to know the chemistry of these materials.

Firstly, some clarifications about the different terminologies used to describe these materials are necessary. During the last years, different names have been used in publications to refer to them, including mineral polymers, inorganic polymers, inorganic polymer glasses, alkali-bonded ceramics, alkali ash material, soil cements, soil silicates, SKJ-binder, F-concrete, hydroceramics, zeocements, zeoceramics, geopolymer and others (Provis & van Deventer 2013). Hereafter, alkali-activated materials (AAMs) will be used as the term embracing any binder system resulting of the reaction of an alkali metal source (activator) with a solid silicate powder (precursor). Else, the widely used term "geopolymer cement" will be a minor part of the AAMs, normally applicable to low-calcium precursors where the binding phase is almost an sodium aluminosilicate highly coordinated.

2.3.1 Classification of alkali-activated materials

AAMs binders are obtained by the reaction of materials with high content of alumina (Al) and silica (Si) (aluminosilicate precursor) with an alkaline metal (normally sodium (Na) or potassium (K)) in an aqueous media (water may act only as a media or as a participant of the reactions). Other compounds such as calcium (Ca) that play an important role in the products and reactions mechanisms can be found in the precursors (as detailed later).

Figure 2.2 shows a basic classification of AAMs compared to other calcium-based binders. It servesas a comparative tool to see the differences in regard to the Ca, Al and alkali metal content. It can be observed that AAMs have much lower Ca content than OPC, with a wide range of Al content. Else, geopolymer cement is only a minor part of AAMs, corresponding with the lower Ca and high Al contents. Regarding the alkali content, **Figure 2.2** shows a darker color when the alkali content is higher. Thus, AAMs have more alkali content than the other materials, and among AAMs, geopolymer cement type has the most content.

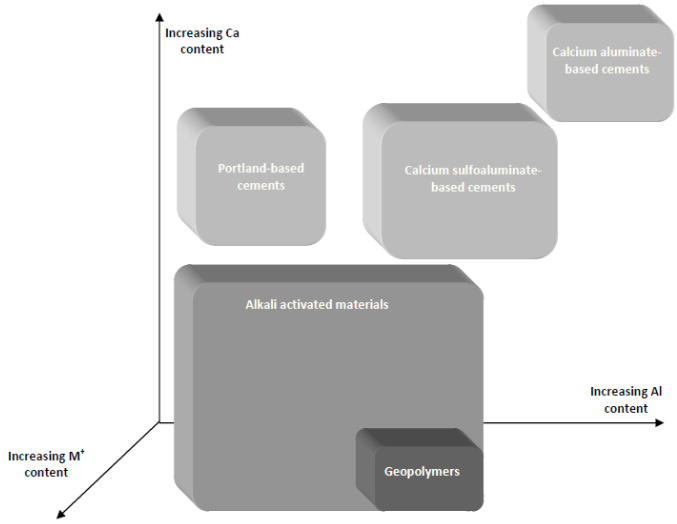

Figure 2.2 Classification of AAM with comparison to calcium-based binders. Shading indicate approximate alkali content; darker shading corresponds to higher concentration of alkalis (Provis & van Deventer 2013).

AAMs can be classified according to their composition, falling in the Me_2O-MeO-Me_2O_3-SiO_2-H_2O system (Me = divalent cation; Me_2 = monovalent cation). This system is different to OPC-based materials, based on the composition in the MeO-Me_2O_3-SiO_2 system. Glukhovsky was the first one that separated them into two systems: Me_2O–CaO–Al_2O_3–SiO_2–H_2O and Me_2O–Al_2O_3–SiO_2–H_2O. The main difference between these two systems lies in the calcium content, being high-Ca materials the first group, and low-Ca materials the second group. Thus, depending on the calcium content of the precursor, the corresponding products will be different, although these can no doubt overlap.

Therefore, AAMs can be classified into two groups:

1. Group 1 Me_2O–CaO–Al_2O_3–SiO_2–H_2O: this system corresponds to materials with high-Ca content such as blast furnace slag. The main reaction product is a calcium silicate hydrate gel that normally uptakes aluminum in its structure (C-A-S-H).
2. Group 2 Me_2O–Al_2O_3–SiO_2–H_2O: this system corresponds to materials with low-Ca content such as class F fly ash. The main reaction product is an alkaline aluminosilicate binder highly coordinated (Me-A-S-H).

2.3.2 Reaction mechanisms and hydration products

The reaction mechanisms and hydration products of AAMs depend on the chemistry of the aluminosilicate precursor used, specifically on their Ca content, and also on the nature of the source of alkalis. Therefore,

two different reaction mechanisms can be divided according to the Ca content, as observed in former section: low-Ca systems and high-Ca systems.

2.3.2.1 High-calcium systems

The reaction mechanisms and hydration products of this system was based on BFS as an aluminosilicate precursor.

The hydration products are the result of a complex reaction consisting in several stages: destruction of the structure of the starting material (BFS) followed by polycondensation-crystallization of the reaction products (Fernández-Jiménez & Puertas 1997). This reaction has also been proposed to occur in five stages by Huanhai et al. (1993), namely: initial, induction, acceleration, deceleration and decay. In their study, the authors used a BFS activated with a mix of waterglass and a sodium hydroxide solution. Although the stages found for BFS were similar to those found with OPC based binders, the authors specified that the reaction mechanisms are different. Therefore, the first step is associated to the reaction of the silicate ions present in the waterglass solution (used as a source of alkalis) with the Ca ions from the BFS to form calcium silicate hydrate (C-S-H). Afterwards, the new C-S-H formed coat around the slag grains suppressing further hydration and hence starting the induction period. This induction period is shorter when increasing the pH of the activation solution. The end of the induction phase coincides with the start of the acceleration phase and the hydration of the slag. At this point the reaction occurs between the aluminates and silicates with metal ions (Na, Ca, Mg, etc.) to form a "secondary C-S-H" and other more complex nature hydration products. The transition of the induction stage to the acceleration stage could be explained by the delayed nucleation theory, as for OPC. Thus, the concentration of Ca ions and Si, from the dissolution of the slag, may exceed the saturation concentration of the hydrated calcium silicate, and the nucleation, growth and precipitation of hydrate could occur. The hydration process continues, but the reaction rate gradually decreases. Slower reaction would be attributed to a massive precipitation of the reaction products around the slag grains, and a reduction of free water, which inhibits or impedes the diffusion processes resulting in the gradual reduction of the hydration reactions. These steps thus correspond to the deceleration and decline stages.

The role of alkalis in the process of hydration is difficult to identify. However, it seems that alkalis act as catalysts to accelerate the reaction at an early age rather than be part of the hydration products (Krivenko 1994). Conversely, as the reactions advance, alkalis could be incorporated to the hydration product (see **equations 2.2** to **2.4**), resulting in the formation of zeolites such products.

$$Si - O^{-} + R^{+} = Si - O - R \tag{2.2}$$

$$Si-O-R+OH^- = Si-O-R-OH^- \quad (2.3)$$

$$Si-O-R-OH^- + Ca^{2+} = Si-O-Ca-OH+R^+ \quad (2.4)$$

where R is the alkaline ion.

The main reaction product is, as mentioned before, a calcium silicate hydrate (Wang & Scrivener 1995), similar to those produced in the hydration of the OPC. This gel, commonly named as C-A-S-H, incorporate a non-negligible Al content and is characterized to have a low Ca/Si ratio (0.8-1.2).

Other secondary products are formed depending on the starting material, activator type and concentration, curing conditions and pH (Wang & Scrivener 1995; Puertas 1995; Puertas et al. 2004; Ben Haha et al. 2011; Fernández Jiménez 2000). Among the secondary products, it has been found hydrotalcite ($Mg_6Al_2CO_3(OH)_{16}\cdot 4H_2O$) (Wang & Scrivener 1995; Ben Haha, et al. 2011; Fernández Jiménez 2000), as well as C_4AH_{13} (Wang & Scrivener 1995), some zeolites as gismondine (Bernal et al. 2011) and carbonated phases.

2.3.2.2 Low-calcium systems

The classical low-Ca precursors in AAMs are the class F fly ash and metakaolin (Mk-750), hence most of the theory about reaction mechanisms and products are based on these aluminosilicate precursors.

In the 1950s, Glukhovsky proposed a general reaction mechanism which was based in three stages: (a) destruction - coagulation; (b) coagulation - condensation; (c) condensation - crystallization (Duxson et al. 2007). As research in alkali activation of fly ashes has advanced in last decades, a new mechanism for low-Ca systems was proposed by A. Palomo et al. (2004), consisting in two stages: (a) nucleation and (b) growth. The first stage, nucleation (englobing stage *a* and *b* of the mechanism proposed by Glukhovsky), consist in the dissolution of the aluminosilicates present in the ash and the formation, via polymerization, of complex ionic species. The second stage, growth, starts when the nuclei reach a critical size and the crystal begins to grow.

This model was later revised by the same authors (Shi et al. 2011; Fernández-Jiménez et al. 2005; Duxson et al. 2007). The new model is summarized in **Figure 2.3**. In a first step, there is a dissolution of the aluminosilicate source by alkaline hydrolysis (consuming water) producing aluminate and silicate monomers. This monomers will react afterwards between them to form larger molecules that precipitate to form a gel under saturation conditions. This first gel, represented as Gel 1 in the figure (step 3), is rich in Al (Palomo et al. 2004; Fernández-Jiménez et al. 2006), and it is a metastable intermediate gel. The high-Al content in the gel can be explained by a higher concentration of Al ions in the alkaline medium at early hours, attributed to the fast dissolution of the Al-O bonds that are weaker than the Si-O ones. As the reaction

progresses, more silica species from the original source are dissolved in the alkaline medium and the Gel 1 evolves to a more Si-rich gel, represented as Gel 2 in the figure (step 4). This alkaline aluminosilicate gel has been called as N-A-S-H gel ("N" represent the sodium ion if this cation is used as source of alkalis). Both gels formation processes release the water that was consumed during the dissolution stage. Water, therefore, plays a role of a reaction medium. However, it resides within the pores in the gel. When the gel is formed, the system continues to rearrange and reorganize, resulting in a three-dimensional aluminosilicate network.

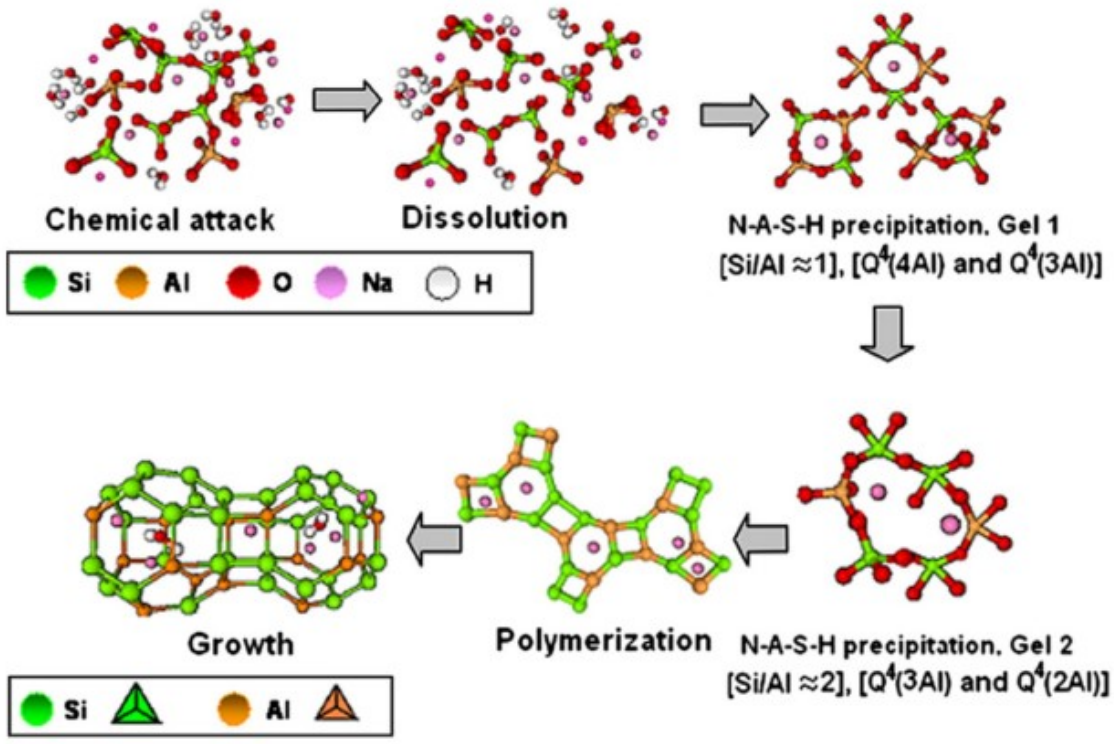

Figure 2.3 Descriptive model for alkali activation of aluminosilicates (Shi et al. 2011)

In these systems, the main reaction product is an alkaline aluminosilicate gel, commonly named as N-A-S-H (if the source of alkalis is the sodium) (Palomo et al. 2004).

There have been found some zeolites such as hydroxysodalite, Na-chabazite, zeolite-Y, zeolite-P and faujasite (Palomo et al. 2014; Duxson et al. 2007) as secondary reaction products in these systems.

2.3.3 Types of activators

Alkaline activating solutions (activators) are the second component in AAM technology. Thus, the aluminosilicate precursor (slag, fly ash, metakaolin, others) is combined with the alkaline activating solutions to generate novel cementitious materials.

The alkaline activating solutions are used to generate high basicity in the system, necessary for the dissolution of the ionic species of the aluminosilicate precursors. Depending on the aluminate precursor, the basicity of these solutions could differ from strong to weak.

A strong variability of the activators used can be found in literature. However, the most used activators are (Provis & van Deventer 2013):

- Alkaline hydroxides: mostly sodium and potassium hydroxide.
- Alkaline silicates: mostly sodium and potassium silicate.
- Alkaline carbonate: sodium carbonate
- Alkaline sulfates: sodium sulfate and gypsum

Although a great variety of alkaline activating solutions can be used, the performance of the final product varies considerably. The most used activators, providing the best mechanical and durability results, are sodium hydroxide, sodium silicate, sodium carbonate or a mix of them.

Moreover, the use of a sodium silicate solution is being under discussion in the literature because of its CO_2 emissions during their production. However, due to its low content of this activator in AAMs, CO_2 emissions associated to an AAM concrete are still lower than an OPC concrete.

2.4 Durability concerns using existing standards in AAMs

As mentioned in previous sections, one of the factors that is hindering the implementation of AAMs on an industrial scale is the existing prescriptive standards and specifications. Standards and specifications have evolved at the same time than OPC knowledge, the construction material of the 20th century. Basically, most of them have been adapted to the chemistry of OPC cement, or OPC-blended cements, and thus, not including the latest materials.

In that sense, AAMs have a barrier to be accepted as a construction material, as these prescriptive standards have not yet been adapted to them. It is well known that a new product that wants to be brought to the market must be able to meet the standards required by national and international authorities.

In order to meet the objectives for a sustainable society, it is necessary to move towards performance-based tests and limits rather than the traditional prescriptive requirements. Hence, new developed materials will have an opportunity to play their role in a sustainable society. Therefore, to evolve to performance-based standards, it will be necessary to obtain the consensus from producers, users of the standard and general and governmental agencies interests (Hooton 2008).

Nowadays, several performance based standards such as ASTM C1157 and CSA 3004 can be found. ASTMC 1157 is a pure performance specification for any hydraulic cement (either blended or Portland) and has no restrictions on composition or raw materials. However, since its development, it has not been widely used due to the lack of an historical record supporting the performance requirements as it does for the prescriptive standards, such as ASTM C595 and C150 (Hooton 2008). Instead, CSA A3004-E1 and later ASTM C1709 were developed to evaluate new materials where field experience is limited and where a more rigorous evaluation is warranted (Hooton 2015). Both standards CSA A3004-E1 and ASTM C1709 are based on the concept of "material science approach". In this concept, fundamental material science issues need to be understood to explain the material behavior: for instance, chemical reactions, kinetic reactions, phase stability and phase evolution during time, pore structure evolution, sensitivity to changes in temperature, humidity, etc. and changes when exposed to common environmental exposures (Hooton 2015). In that sense, AAMs science is quite advanced at this moment and numerous studies can be found providing all this information.

It is of general knowledge that when there is an existing necessity, as the creation of a new test method or materials standard, and a person or group of persons are eager to champion, then standards will be developed relatively quickly. In line with this concept, the RILEM TC224-AAM "*Alkali-activated materials: State-of-the-Art Report*" was established in 2007. This technical committee did a compilation and summary of all the works related the AAM technology done up to that moment. The aim was threefold: to analyze the state-of-the art in alkali-activation technology; to develop recommendations for national Standards bodies based on the current state of understanding of alkali-activated materials; and to develop appropriate testing methods to be incorporated into the recommended Standards (Provis & van Deventer 2013). This technical committee was later continued by the RILEM TC 247-DTA "*Durability testing of alkali-activated materials*", on progress nowadays, with this aim: to provide recommendations regarding appropriate test methodologies and protocols for the analysis of the durability of alkali-activated binders, mortars and concretes. Therefore, efforts in order to create standards (or adapt the existing ones) including AAMs are being done.

Moreover, it is an important aspect to show the benefits of AAMs as a construction material, then their utilization will proceed regardless of the standards and their use will positively influence the eventual standards development.

2.5 Review of the AAM durability

In this section, a brief compilation of the most important works in different durability test methods has been done. A more extensive compilation of them can be found in the RILEM TC 224-AAM report (Provis &

van Deventer 2013), and the "Handbook of alkali-activated cements, mortars and concretes" (Pacheco-Torgal et al. 2015).

The aim of this review will be to discuss the test methods used to assess different durability properties as well as the results. As explained in **section 2.4**, existing prescriptive standards for assessing durability properties have been based on the OPC chemistry, and therefore do not include AAMs as a binder. In order to get more realistic durability results of AAMs, multitude of test methods based on the existing standards have appeared. This fact does difficult to compare results between different studies because the conditions of the tests are not the same. The stronger and weaker points of these new test methods will then be discussed.

2.5.1 Sulfate resistance

External sulfate attack is an important durability aspect in concretes. Several service applications can subject concrete to external sulfate attack that may deteriorate it. Thus, it has been a classic point to study in OPC-based binders.

The major part of the test methods used to evaluate chemical resistance to sulfate ions are conducted under accelerated conditions to reduce the testing time. Therefore, sulfate ions penetration in the samples is accelerated by immersing the samples in a high sulfate concentration solution. The sulfate concentration in the solution usually is ten times higher than that accepted in practice (Mielich & Ötll 2004).

For this test, several American standards can be found:

- ASTM C 452/452M-10 : Standard test method for potential expansion of Portland-cement mortars exposed to sulfate
- ASTM C1012/1012M-10 : Standard test method for length change of hydraulic cement mortars exposed to a sulfate solution

ASTM C452 standard is very prescriptive and it can be only applicable to OPC as the sole binder. However, ASTM C1012 standard can also be applied to blends of OPC with pozzolans or slags, and blended hydraulic cements. Neither of them contemplate the possibility of using other materials than these.

Other methods used in the literature are described below:

- Kock-Steinegger (Mielich & Ötll 2004): Measures of bending strength over time of samples immersed in sulphate solution (4.4%, 29.8 g/L)
- Wittekindt (Mielich & Ötll 2004): Measurement of the sample expansion (1x4x16 cm) immersed in a sulphate solution (4.4%, 29.8 g/L) for 56 days.

- Committee of Experts (SVA) of the German Institute of Civil Engineering (Mielich & Ötll 2004): Measurement of the sample expansion (1x4x16cm) immersed in a sulphate solution (4.4%, 29.8 g / L) for 91 days. In this method there are special curing conditions, as the demolding after 2 days, followed by immersion of the samples in a saturated solution of $Ca(OH)_2$ for 12 days and then their immersion in the sulphate solution.

All these cited methods have been developed for OPC, but can also be used for blended cements.

Very little work has been done to characterize the sulfate resistance of AAMs. A summary of these works are reported next, cited according to the aluminosilicate precursor used.

Palomo et al. (1999) subjected 10x10x60mm AAMk pastes to 4.4% sodium sulfate solution and sea water (ASTM D1141-90) during 270 days. The authors did analytical characterization along the test by the following techniques: XRD, FTIR and TGA. Samples were immersed in the aggressive solutions after demolding. Results showed good stability of AAMk samples for up to 270 days when submerged in aggressive liquids of various types.

Škvára et al. (2005) conducted sulphate resistance tests on alkali-activated fly ash (AAFA). They used a different procedure from that described in ASTM C1012. This procedure consisted in immersing the mortar samples after 28 days of curing in laboratory conditions in sodium sulphate and magnesium solutions (44 g/dm^3 and 5 g/dm^3 respectively). Compressive strength, weight loss and sulphate ions penetration were followed. In all cases, the authors found a good sulfate resistance without deterioration. In the formulations used, compressive strength increases slightly after 2 years of exposure in both solutions, with a mass loss less than 2%.

Bakharev (2005a) also studied sulphate resistance of AAFA. In this work, the author studied the influence of the activator and the source of sulphate used. The procedure was also different from ASTM C1012, however, the author used the concentration of sulfates similar to those specified in the standard. This procedure consisted in immersing the samples (pastes) at the age of 2 months after a special curing conditions (based on heating at different temperatures and times) in sodium and magnesium sulfate solutions (5% concentration) and a mixed of both (5% sodium sulfate - 5% magnesium sulfate). Compressive strength and XRD were performed. The author concluded that the stability of all the AAM studied depended on the type of activator used, which demonstrates the importance of using an optimized formulation, and the concentration and nature of the cation used for sulphate solution. The formulation with sodium hydroxide as activating solution gave the best results.

Wallah & Rangan (2006) also characterized the sulphate resistance of AAFA. The test method used was a modification of ASTM C1012. The authors used a sodium sulphate solution (5% concentration) and analyzed the compressive strength, the mass loss and the dimensions change. Results showed that AAFA had good resistance to sulphates after 1 year of exposure, with negligible variations of weight and compressive strength.

Fernandez-Jimenez et al. (2007) analyzed the sulfate resistance of 40x40x160mm AAFA mortar samples. Samples were immersed after demolding in 4.4% sodium sulfate solution and sea water (ASTM D1141-90) during 365 days. Along the test, compressive strength and analytical characterization were conducted. The authors found that AAFA mortars performed satisfactorily when exposed to sulphates and seawater, better than OPC samples.

Sata et al. (2012) studied the sulfate resistance of another type of ash, lignite bottom ash (AABA) by means of ASTM C1012. Thus, samples were immersed after demolding in 5% sodium sulphate solution. Results showed that AABA mortars were less susceptible to sulfate attack compared to the OPC-based system.

Recently, a work conducted by Sukmak et al. (2015) analyzed the sulphate resistance of a clay high-calcium fly ash geopolymer by means of modified ASTM C1012. After 28 days of curing, the samples were immersed in 5% sodium sulfate and magnesium sulfate solutions. Compressive strength of 75x90x230mm samples and SEM and XRD was performed. The authors found that clay-FA geopolymer was susceptible to sulphate attack, having the worst results when magnesium sulphate was used as a source of sulphates.

Sulfate resistance of a mix of alkali-activated slag/fly ash (AASFA) was conducted in cylindrical 25x25mm pastes by Ismail et al. (2012). Curing time in this case was 28 days at ambient conditions (25ºC). The authors used sodium and magnesium sulfate solutions (5% concentration) and did analytical characterization after 3 months by the following techniques: XRD, FTIR, SEM-EDX and TGA. The results showed a great dependence of the sulphate resistance depending on the cation used. $MgSO_4$ was found more aggressive to the alkali-activated binder pastes than Na_2SO_4 solution.

Sulphate resistance of alkali-activated blast furnace slag (AAS) has also been the subject of several studies. Bakharev et al. (2002) used a procedure based on ASTM C1012 but in cylindrical concrete specimens instead of mortars. In this case, as observed in the study of Škvára et al. (2005), the authors changed the curing time before immersion of samples in the sulphate solution to 28 days. Two sulphate solutions were used, a sodium sulphate and a magnesium sulfate solution (5% concentration each). They found a strength loss after one year of 17% for the AAS samples immersed in the sodium sulfate solution in comparison with 25% of OPC. In the case of the magnesium sulfate solution, they found a strength loss of 23 and 37% for the AAS and OPC samples respectively. In both solutions, AAS performed better than OPC.

Puertas et al. (2002), based on ASTM C1012 and the Kock-Steinegger method, also characterized sulphate resistance of AAS mortars. Else, compressive strength was measured in 50.8x50.8mm specimens. In the case of ASTM C1012, curing time prior to exposure to sulphate was 28 days while for the other method was 21 days. They used two solutions, a sodium sulphate solution (4.4%) and artificial sea water solution (ASTM D1141-86), and different activating solutions. In both methods they found that AAS was highly resistant to sulphate ions as well as seawater after 200 days. The best results were observed in AAS activated with a sodium silicate solution, giving the higher compressive strengths.

A more recent study, conducted by Komljenović et al. (2013), analyzed AAS mortar samples immersed in 5% Na_2SO_4 solution for up to 90 days. Sulphate solution was renewed every 30 days. Mortars were cured in humidity chamber in order to avoid premature leaching during 27 days after demolding. Sulphate resistance were measure by compressive strength test. The results showed a decrease in strength of control mixture (CEM II), but not in AAS.

This literature review of AAMs sulfate resistance showed a great variability of procedures, as summarized in **table 2.1a and b**, in terms of curing conditions, time and conditions of exposure, type of samples used (paste, mortar or concrete) and indicator used (expansion, compressive and flexural strength, mass change or analytical characterization). Therefore, there is an evident necessity to establish standardized procedures to better compare the results of different works. However, the new procedures should have some flexibility in the mix design and curing conditions, as AAMs performance is highly dependent on the formulation and sometimes requires a short special curing at elevated temperatures. Else, there are few works focusing on concretes, as there are not standards test methods for evaluating the sulfate resistance in concretes.

Regarding the sulfate resistance of AAMs (AAFA, AAMk, AAS and AABA), practically all proved to perform very good in sulfate conditions. AAS showed the worst results, however, it performed better than OPC system. This is mostly due to the high-Ca content of this AAS systems. Instead, the low-Ca systems showed practically no damage by sulfates.

Table 2.1a Summary of the sulfate resistance test conditions used in several works

Work	Material	Standard*	Type	Indicator	Specimen (mm)	Sulfate source	$[SO_4]^{2-}$	Curing time (days)	Test duration (days)	Renew fresh solution
(Bakharev et al., 2002)	AAS	ASTM C1012**	Concrete	Comp. strength	Ø100x200	Na_2SO_4 $MgSO_4$	5%	28 (hum. Chamber)	365	Every 2 weeks first 3 months, and 4, 6, 9 and 12 months
(Puertas et al., 2002)	AAS	ASTM C1012	Mortar	Expansion Comp. strength	25x25x285 50.8x50.8	Na_2SO_4 Sea water	4.4%	28 (hum. Chamber)	200	At 1, 2, 3, 4, 8, 13, 15 weeks, and 4, 6, 9 and 12 months
		Kock-Steinegger		Expansion	10x10x60		--	21(hum. Chamber)	180	--
(Komljenović et al. 2013)	AAS	--	Mortar	Expansion Comp. strength	40x40x160	Na_2SO_4	5%	28 (hum. Chamber)	90	Every 30 days
(Ismail et al., 2012)	AA-S/FA	--	Paste	XRD/FTIR/TGA SEM-EDX	Ø25x25	Na_2SO_4 $MgSO_4$	5%	28 (lab. Cond.)	90	--
(Skvára et al., 2005)	AAFA	CNS EN 206-1**	Slurries Mortar	Comp. strength Mass change	20x20x20 40x40x160	Na_2SO_4 $MgSO_4$	4.4% 0.5%	28 (lab. Cond.)	720	Every month

Table 2.1b Summary of the sulfate resistance test conditions used in several works

Work	Material	Standard*	Type	Indicator	Specimen (mm)	Sulfate source	$[SO_4]^{2-}$	Curing time (days)	Test duration (days)	Renew fresh solution
(Fernandez-Jimenez et al., 2007)	AAFA	--	Mortar	Comp. strength	40x40x160	Na_2SO_4 Sea water	4.4%	After demold	365	--
(Sukmak et al., 2015)	AAFA (high Ca)	ASTM C1012*	Mortar	Comp. Strength SEM-EDX, XRD	75x90x230	Na_2SO_4 $MgSO_4$	5%	28	365	At 30, 60, 90, 120,150, 180, and 210 days
(Sata et al., 2012)	AABA	ASTM C1012	Mortar	Expansion	25x25x285	Na_2SO_4	5%	After demold	365	At 7, 14, 28, 56, 84, 120 and 240 days
(Palomo, Blanco-Varela, et al. 1999)	AAMk	--	Paste	XRD/FTIR/TGA Flex. strength	10x10x60	Na_2SO_4 Sea water	4.4%	After demold	270	--

* Standard followed if the case.

** Test procedure modified

2.5.2 Acid resistance

Acid resistance has become an important durability aspect in concretes, especially in OPC-based binders. Even if acidic conditions are rare to found, applications in which concrete is exposed to them can severely damage it. Thus, acid resistance is usually an important aspect to study.

Due to the diversity of acidic conditions (in terms of types and concentration of acids, exposure conditions), there are not specific standardized test methods, even for OPC. However, there is a standard for analyzing chemical resistance that has been conventionally used for this purpose, ASTM C267-01: *Standard test methods for chemical resistance of mortars, grouts, and monolithic surfacings and polymer concrete*. This standard provides guidelines and allows analysis of samples exposed in a given chemical environment by means of mass and cross-sectional dimension change, visual inspection and compressive strength. Most test methods found in literature to evaluate acid resistance of portland cement-based binders are based on mass loss measurements. Fewer are based on the corrosion depth and others measure the extent of loss of compressive strength.

As in the case of sulfate resistance, very few studies have been addressed for characterizing the AAMs acid resistance. Some of these studies are described next.

Shi & Stegemann (2000) analyzed the AAS acid resistance of pastes. The procedure used herein was to measure the corrosion depth during time of samples immersed in three different acidic solutions (pH 3 nitric acid, pH 3 and pH 5 acetic acid). Samples were immersed after a curing time of 1 year. All samples, before immersion, were covered with a polystyrene mold so that only one face was in contact with the acid. PH was constantly controlled throughout the tests. Results showed that AAS exhibited very good resistance to all acids, being the most aggressive solution the pH 3 acetic acid.

Acid resistance of AAS concretes was also conducted by Bakharev et al. (2003). The authors analyzed the compressive strength and the microstructural changes of the samples immersed in a pH 4 acetic acid solution during 12 months. Samples were immersed after a curing time of 28 days. The results showed that AAS concrete of Grade 40 (40 MPa) had a superior durability to OPC concrete of similar grade under acetic acid attack.

Bernal et al. (2012) studied the influence of several acids in AAS pastes (HNO with pH 3, H_2SO_4 and HCl and CH_3COOH with pH 4.5). Sample pastes were cured during 60 days, and then immersed in the acid solutions during 150 days. Compressive strength as well as XRD and FTIR tests were conducted. The authors found that compressive strength of AAS samples were not degraded in all the acidic solutions except for the CH_3COOH acid, where samples lost 25% of the original strength after 150 days.

Allahverdi & Škvára (2001a, 2001b, 2005a, 2005b) did a series of works analyzing the nitric and sulfuric acid resistance of a 1:1 alkali-activated slag/fly ash mix. In both acids, concentration was

maintained constant at pH 1, 2 and 3 and renewed monthly. The authors analyzed the corroded depth by means of XRD, FTIR, NMR and SEM techniques. Paste samples were immersed in acid solutions after 28 days of dry curing (40-50% RH) during 60 days. For acid nitric attack, when pH was 1 and 2, they found fine shrinkage cracks and relatively hard and brittle corroded layers; whereas for pH 3, nitric acid led to no changes in color and appearance of the samples, with a formation of relatively soft and easily removable surface layer. The authors also suggested a corrosion mechanism based on the structural characterization: leaching of sodium and calcium ions that are depleted and exchanged by H^+ or H_3O^+ ions from the solution and an electrophilic attack by acidic protons on polymeric Si-O-Al bonds resulting in the formation of a partially dealkalized and decalcified Si, Al-rich residue. For acid sulfuric attack, when pH was 1 and 2, they found no recognizable change in color, significant expansion, no visually observable crack and a very hard and difficult to remove corroded layer; whereas for pH 3, sulfuric acid led to a soft and easily removable surface layer. The corrosion mechanism found was the same one than for nitric acid, but in this case, gypsum was also formed.

Bakharev (2005b) studied the acid resistance of AAFA paste samples. Compressive strength of the samples immersed in two 5% acid solutions (pH 0.8 sulfuric acid, pH 2.4 acetic acid) as well as the analytical characterization was followed during 150 days. The authors studied the influence of the activator type as well. Immersion of samples was made after a special curing time, at the age of 4 days. Results showed a dependence on the nature of the activator and of the acid used. In both acids, AAFA pastes performed better than OPC samples and OPC samples with 20% FA replacement. Analytical characterization showed a dealumination and dealkalinization of the alkaline aluminosilicate gel.

Wallah & Rangan (2006) used sulfuric acid solutions with different concentrations (0.5, 1 and 2%) to examine the acid resistance of AAFA mortars and concretes. Samples were tested during 1 year. The results showed a mass loss about 3% after 1 year and they found that degradation of the compressive strength varied in function of the acid concentration (up to 65% loss at 2% acid solution).

In the work of Fernandez-Jimenez et al. (2007), acid resistance by means of hydrochloric acid (0.1 N, pH 1) was analyzed. 30x30x30mm specimens were placed in acidic solution after demolding during 90 days. The authors found that AAFA samples underwent dealumination in highly acidic media with a loss of mass and a decline in mechanical strength. Performance was still better, however, than observed in OPC mortars.

Sata et al. (2012), meanwhile, have studied the acid resistance of another type of AAM, in this case, bottom ash geopolymer mortar (AABA). The bottom ash is a by-product of coal combustion in power plants. The authors used the procedure based on ASTM C267. Mortars samples immersed in a 3% sulfuric acid solution during 120 days, experimented a weight loss less than 4% indicating good acid resistance. AABA samples performed better than OPC samples.

Lloyd et al. (2012) analyzed the acid resistance of three different types of fly ash with slag replacements. Paste samples were immersed after 28 days of curing time in sulfuric and nitric acids (pH 1) during 100 days. The authors analyzed the influence of several factors on the sample corroded depth. They found that the replacement of fly ash by slag and the increase of the alkali content in the binder had a positive effect on the acid resistance.

Burciaga-Díaz & Escalante-García (2012) analyzed the acid resistance of Mk paste samples in 0.5N hydrochloric acid during 10 days. In this case, the authors performed exposure conditions at 60ºC, in order to induce the chemical aggressive conditions. The authors found that degradation of the pastes in HCl media was due to the destruction of the geopolymeric structure and the release of Na and Al, as it occurred in AAFA, with a reduction of the strength. The highest reduction was found when the SiO_2/Al_2O_3 ratio was higher, with a 31.3% reduction at the end of the test.

Other study related to AAMk acid resistance was conducted by Gao et al. (2013). AAMk pastes were immersed in 0.01N hydrochloric acid (pH 2) during 28 days. Three methods were used, in order to study several factors: M1, effect of the immersion time; M2, refresh the acid solution every 7 days to ensure a continuous attack; and M3, samples were removed from the solution to determine the mass and then re-immersed in the solution. Analytical characterization was also performed. The results showed that the immersion time had a little influence on the acid attack of AAMk after 28 days (M1). Successive immersion in HCl (M2) appeared to lead to surface changes. Else, the authors found that the geopolymer network was intact after 28 days of attack by XRD and SEM characterization.

The literature review of acid attack on AAMs showed, as for sulfate resistance, a great variability of test methods used. This can be probably due to the lack of standardized test methods for acid resistance. Because of the great variability of service conditions in which acid attack may take place, it has been difficult to assess a unique test method for laboratory analysis. In **table 2.2 a and b** a summary of the test methods used by the former works described can be found. The variability of indicators used (compressive strength, mass change, corroded depth, and visual appearance) and the different test conditions applied (nature and concentration of acid used, curing time, exposition time, temperature of exposition) can be seen. The most predominant indicator used is based on the measurement of the corroded depth, as several authors are already recommending to be more realistic (Lloyd et al. 2012). On the contrary, mass change may not be appropriate due to degradation processes of AAMs, since some products can be deposited inside the binder at the same time that the leaching or dissolution of binder. Moreover, compressive strength can be difficult due to the different strength of the affected and unnaffected regions.

Table 2.2a Summary of the acid resistance test conditions used in several works

Work	Material	Standard*	Type	Indicator	Specimen (mm)	Acid source	pH/ Concentration	Curing time (days)	Test duration (days)	Renew fresh solution
(Shi & Stegemann 2000)	AAS	--	Paste	Corroded depth	Ø45x75	HNO_3	pH 3	365	580	pH constant
						CH_3COOH	pH 3 and 5			
(Bakharev et al., 2003)	AAS	--	Concrete	Comp. strength XRD/SEM	Ø100x200	CH_3COOH	pH 4	28	365	At 1, 2, 3, 4, 6 and 9 months
(Bernal et al., 2012)	AAS	--	Paste	Comp. strength XRD/FTIR	Ø30x60	HCl / HNO_3 H_2SO_4 CH_3COOH	pH 3 pH 4.5	60	150	pH constant
(Allahverdi et al., 2001a, 2001b)	AAS/FA	--	Paste	Corroded depth XRD/MAS-NMR/FTIR7SEM	20x20x20	HNO_3	pH 1, 2, 3	28 (dry conditions)	60	pH constant Monthly
(Allahverdi et al., 2005a, 2005b)	AAS/FA	--	Paste	Corroded depth XRD/MAS-NMR/FTIR7SEM	20x20x20	H_2SO_4	pH 1, 2, 3	28 (dry conditions)	60	pH constant Monthly
(Bakharev 2005c)	AAFA	--	Paste	Comp. strength XRD/FTIR/SEM	Ø25x50	CH_3COOH H_2SO_4	5% pH 2.4 5% pH 0.8	4 (after special curing)	150	Monthly

* Standard followed if the case.

** Test procedure modified

Table 2.2b Summary of the acid resistance test conditions used in several works

Work	Material	Standard*	Type	Indicator	Specimen (mm)	Acid source	pH/ Concentration	Curing time (days)	Test duration (days)	Renew fresh solution
(Wallah et al., 2006)	AAFA	--	Mortar Concrete	Mass change Visual appearance Comp. strength	75x75x75 Ø100x200	H_2SO_4	0.25, 0.5 and 1% 0.5, 1 and 2%	After special during	365	Monthly
(Fernandez-Jimenez et al., 2007)	AAFA	ANS 16.1	Mortar	Mass change Comp. strength	30x30x30	HCl	0.1N, pH 1	After demolding	365	At 1, 2, 3, 7, 28, 56 and 90
(Sata et al., 2012)	AABA	ASTM C267**	Mortar	Mass change	50x50x50	H_2SO_4	3%	28	120	At 7, 14, 28, 56, 84 and 120
(Lloyd et al., 2012)	AAFA/S	--	Paste	Corroded depth	Ø25x50	HNO_3 H_2SO_4	pH 1	28	100	pH constant
(Burciaga-Díaz et al-, 2012)	AAMk	--	Paste	Comp. strength FTIR/ SEM/ICP-AES	25x25x140	HCl	0.5 N	28	10 (at 60ºC)	No renewed
(Gao et al., 2013)	AAMk	--	Paste	Comp. strength FTIR/XRD/SEM	Ø15x30	HCl	0.01N, pH 2	After demolding	28	Every week

* Standard followed if the case.

** Test procedure modified

Despite the great variability of test methods found, all of them used aggressive conditions that do not represent the real service conditions. Else, any works of biogenic sulfuric acid attack have been found to date on AAMs.

Finally, these works show the very good acid resistance of AAMs in several aggressive acidic media. The best results are found, as in sulfate conditions, for low-Ca content AAMs.

2.5.3 Alkali-aggregate reaction

The alkali-aggregate reaction (AAR) is a dangerous reaction that usually occurs in OPC-based binders. This reaction can be divided in two: alkali-silica reaction (ASR) and alkali-carbonate reaction (ACR). Although both may occur, the first one is the most common and thus the subject of almost all studies related to AAR.

To analyze the susceptibility of AAR in mortars and concretes, several international standardized test methods have been developed worldwide. Among the American standards it can be found the followings:

- ASTM C1260-14: Standard test method for potential alkali reactivity of aggregates (Mortar-Bar Method) (similar we found CAN/CSA A23.2-25A-09 and NBRI Accelerated mortar-bar test)
- ASTM C1567-13: Standard test method for determining the potential alkali-silica reactivity of combinations of cementitious materials and aggregate (Accelerated Mortar-Bar Method)
- ASTM C227-10: Standard test method for potential alkali reactivity of cement-aggregate combinations (Mortar-Bar Method)
- ASTM C1293-08b: Standard test method for determination of length change of concrete due to alkali-silica reaction (similar we found CAN/CSA A23.2-14A-09)
- ASTM C1778-14: Standard guide for reducing the risk of deleterious alkali-aggregate reaction in concrete
- CAN/CSA A23.2-27A-09: Standard practice to identify potential for alkali-reactivity of aggregates and measures to avoid deleterious expansion in concrete
- CAN/CSA A23.2-28A: Standard practice for laboratory testing to demonstrate the effectiveness of supplementary cementing materials and lithium-based admixtures to prevent alkali-silica reaction in concrete

Some of these standards propose accelerated tests methods, such as ASTM C1260, CSA A23.2-25A and ASTM C1567, in which the duration of the test is relatively short, i.e. less than one month. In these tests, the conditions are more aggressive in order to accelerate the alkali-aggregate

reactions. All standards use 1M NaOH solution for the attack, regardless the alkali content of the binder, and temperatures of 80ºC. These standards are not addressed for evaluating mixtures of aggregates with cement materials but the reactivity of the aggregate. Although these standards are widely used and accepted, test conditions do not represent real service. ASTM C1567 is a modified version of ASTM C1260 exclusively to evaluate pozzolans and slags.

In the other standards, the testing period is longer: between 6 to 12 months. These test methods are thus considered to be more representative of the service life. Regarding ASTM C227, carried out in mortar specimens, is designed to determinate the susceptibility of cement-aggregate combinations to expansive reactions. The standard requires to have an alkali content more than 0.6% Na_2O_{eq}, which is the case of almost all the AAMs. However, this standard is being in disuse because of the failure to correctly identify both alkali-silica and alkali-carbonate reactions in slowly reactive rocks. This is mainly due to a leaching of alkalis from mortar specimens that will not be able to react with the aggregate and thus giving better results (Thomas et al. 2006). Therefore, this standard is not recommended.

ASTM C1293 and CSA 23.2-14A are exclusive for OPC concretes of OPC with SCMs. In these tests, concrete prisms are exposed to 38ºC in humidity sealed conditions. Else, NaOH is added to the cement mixture in order to boost alkali content to 1.25% Na_2O_{eq} by mass of cement. This was found effective to balance the possible alkali leaching during test. Although this test is accelerated by temperature and extra alkalis, it is better reproducing the real service conditions.

In the case of CSA A23.2-27A (prescriptive based-risk mitigation) and CSA A23.2-28A (performance testing option), recommendations are given for determining the aggregate reactivity, and also for prevent AAR. Recently, standard ASTM C1778 was approved similar to the CSA A23-2-27A.

The studies found in the literature to evaluate the AAR of AAMs are summarized next.

Gifford & Gillott (1996) studied the influence of using different activators and aggregates on the AAR of AAS concrete following the test method described in CSA A23.2-14A standard (38ºC and 100% RH). For their tests, they used six different types of aggregates: one as a control, four aggregates to induce ASR (mostly siliceous limestone with reactive quartz and gravels with small chert particles amount) and one aggregate to induce ACR (dolomitic limestone). The authors found that AAS concretes were less susceptible to ASR than OPC concretes, but more susceptible to ACR.

Bakharev et al. (2001) also studied the AAR of AAS concrete but following the ASTM C1293 standard (similar to CSA A23.2-14A). In this case, the authors found that the AAS concrete was more susceptible to deterioration from AAR than OPC concrete of similar grade after 2 years, contrary to the results of Gifford & Gillott (1996).

The work of Fernández-Jiménez & Puertas (2002) focused on the AAR of AAS mortars using an accelerated test method, ASTM C1260 (80ºC and 1M NaOH solution). In this case, the duration of the test was prolonged from 16 to 160 days. For the test a potentially reactive aggregate (opal) with a reactive silica content of 21% was used. The results showed that AAS was less susceptible to AAR than OPC that is in good agreement with the results found by Gifford & Gillott (1996). However, the authors warn that the test duration, 16 days, may not be sufficient to detect the AAR of AAS with an aggregate because the reaction rate is slower than OPC, then much longer time is needed.

You-zhi et al. (2002) also studied the AAR of AAS mortars with a method similar to ASTM C227 (38ºC and 100% RH). The authors analyzed the influence of various parameters such as type of activator, alkali content, size and aggregate content (quartz glass), and type of slag. They reached the conclusion that, when the amount of active aggregate was below 15 % and the mass fraction of alkali was not more than 5% (Na_2O), the expansion due to AAR would not lead to dangerous destruction. In addition, depending on the nature of the activator, different behaviors were observed under the conditions of their studies, with NaOH giving the best results. In general, AAS mortar was found less susceptible to AAR than OPC mortars under the same conditions.

Based on the British standard BS DD 218 (*Testing aggregates. Method for determination of alkali-silica reactivity. Concrete prism method*), Al-Otaibi (2008) studied ASR on AAS concretes (60ºC and 100% RH). The author studied the effect of the activator and the alkali content. After 1 year of measurements, the author concluded that an alkali content of 4% gave no dangerous expansion, with higher expansion when alkali content was higher. These results agree with those obtained by You-Zhi et al. (2002).

Puertas et al. (2009) studied the effect of the aggregate type on the ASR with AAS mortars by means of ASTM C1260 (80ºC and 100% RH). For their tests, a reactive sand from Greywacke type rock source was used. After the first period of 24 hours in water at 80ºC, two exposure conditions were followed: in water at 21ºC and in 1N NaOH solution at 80ºC (as standard). Else, test duration was enlarged to 4 months according to the recommendations of Fernandez-Jimenez et al. (2002). The authors found that at the standard conditions (80ºC at 1M NaOH solution) the expansion was 4 times lower for AAS mortars than OPC mortars when a reactive siliceous aggregate was used. In general, AAS mortars performed better than OPC mortars. Else, AAS mortars were more susceptible to AAR with a siliceous aggregate than with a calcareous aggregate.

In a recent work, Z. Shi et al. (2015) conducted ASR on AAS mortars by means of ASTM C1260 standard with modified curing and exposure conditions. Thus, the authors conducted the test in three conditions at 80ºC: in 1N NaOH solution, in water and in steam. The authors found that AAS mortars suffered less expansion than OPC mortars when exposed in 1N NaOH solution. On the

contrary, when AAS mortars were exposed in water or in steam, expansion was higher than OPC mortars, but still meeting the limit expansion criteria of the ASTM C1260 (0.1% at 14 days).

Other works can be found in literature concerning the AAR in AAS mortars and concretes. As the aim of this review is not to show all the existing works but to focus on the methodologies used, some of the works will not be discussed in this section. A review of some other works in AAR of AAS can be found in the work of C. Shi et al. (2015).

Regarding studies about ASR of AAFA, the work of García-Lodeiro et al. (2007) can be found. The authors assessed the ASR of AAFA mortars with a modified ASTM C1260 test method using different aggregates (siliceous and opal). In this case, temperature was changed to 85 ºC (instead of 80ºC) as well as the aggregate grain size distribution. Else, AAFA mortars were immersed in 1N NaOH solution after their special curing of 20 hours at 85ºC, thus eliminating the 24 hours period in water at 80ºC. They concluded that AAFA mortars were less susceptible to generate expansion by ASR than OPC mortars.

Kupwade-Patil et al. (2013) analyzed the ASR in two types of FA, class F and class C, using different types of aggregates (quartz, limestone and sandstone from different regions). The authors found higher average expansion in OPC concrete than in AAFA concretes, by a factor of 6, after 90 days of exposure to 1M NaOH solution at 80ºC.

Regarding the AAMk, few studies have been found. Pouhet & Cyr (2015) conducted a recent study assessing the ASR of AAMk, using six different aggregates (marble sand, siliceous sand, quartzite sand, sedimentary siliceous limestone, alluvial sand and glass sand from the crushing of glass bottles). The test method used was based on the NF P 18-454 standard (60ºC and 100% RH). Specimens were placed in the standard conditions after a curing time in humidity chamber of 28 days. The authors found that AAMk did not lead to the ASR swelling characteristic of OPC mortars.

In **table 2.3** summarizes the test methods used by the former works. The accelerated test method ASTM C1260 is still by far the most used despite the aggressive exposure conditions. However, authors are beginning to do modifications in this test method such as test duration and curing conditions. As recommended by Fernández-Jiménez & Puertas (2002), test duration should be longer than 14 days due to the slow rate reaction of AAS comparing to OPC, and it has been adopted by other authors in their studies (Z. Shi et al. 2015; Puertas et al. 2009). Nevertheless, these authors do not specify if the 14 days expansion criteria of ASTM C1260 should be maintained to 0.1% at longer time. Else, some authors have changed the curing conditions prior to place specimens in 1M NaOH solution, i.e. to steam cure specimens at 80ºC instead of in water as specified in the standard, in order to avoid alkali leaching (Z. Shi et al. 2015). Others, instead, prefer to start the test after demolding (García-Lodeiro, a. Palomo, et al. 2007). These modifications of the conditions of the

Table 2.3 Summary of the AAR test conditions used in several works

Work	Material	Standard*	Type	Specimen (mm)	Curing time (days)	T and RH	Test duration
(Gifford & Gillott 1996a)	AAS	CSA A23.2-14A	Concrete	75x75x305	After demolding	38ºC 100%	1 year
(Bakharev et al., 2001)	AAS	ASTM C1293	Concrete	75x75x285	After demolding	38ºC 100%	2 year
(Fernández-Jiménez et al., 2002)	AAS	ASTM C1260**	Mortar	25x25x285	After demolding	80ºC 1M NaOH	140 days
(You-zhi et al., 2002)	AAS	--	Mortar	10x10x60	After demolding	38ºC 100%	180 days
(Al-Otaibi 2008)	AAS	BSI Draft DD218: (1995)	Concrete	75x75x280	After demolding	60ºC 100% RH	1 year
(Puertas et al, 2009)	AAS	ASTM C1260**	Mortar	25x25x285	After demolding	80ºC in 1N NaOH 21ºC in water	4 months
(Shi et al., 2015)	AAS	ASTM C1260**	Mortar	25x25x285	After demolding	80ºC 1M NaOH / water / steam	56 days
(García-Lodeiro et al, 2007)	AAFA	ASTM C1260**	Mortar	25x25x285	After demolding	85ºC 1M NaOH	90 days
(Kupwade-Patil et al., 2013)	AAFA (class F and C)	ASTM C1260**	Mortar	51x51x254	After demolding	80ºC 1M NaOH	90 days
(Pouhet & Cyr 2015)	AAMk	NF P 18-454	Mortar	20x20x160	28 (20ºC/95%RH)	60ºC 100% RH	250 days

* Standard followed if the case. ** Test procedure modified

ASTM C1260 put in evidence that more research is needed in that sense in order to establish standardized test methods for AAMs.

Regarding the susceptibility of AAMs to AAR, it can be concluded as seen in this review that:

- For AAS, in general trends, is less susceptible to ASR than OPC. Even the better results, in some studies expansion results exceed the limit expansion criteria of 0.1% (ASTM C1260). Else, some authors found AAS more susceptible than OPC (Bakharev et al. 2001).
- For AAFA, the few works found show low susceptibility to ASR, observing in most cases negligible expansion.

For AAMk, the only work found shows promising results too, although more research must be done to confirm the results.

2.5.4 Freeze-thaw resistance

Frost resistance has been an important aspect to consider when designing concretes in the regions subjected to low temperatures. Thus, although it is not a concern worldwide, it has been an important study aspect. Two types of frost damage can occur: internal cracking and external surface scaling. In this section, internal cracking will be addressed.

Several international standards have been conceived for analyzing the internal frost damage. The American standards that can be found are the following:

- ASTM C666/666M-03: Standard test method for resistance of concrete to rapid freezing and thawing
- ASTM C1645/1645M-11: Standard test method for freeze-thaw and de-icing salt durability of solid concrete interlocking paving units
- CAN/CSA-A23.2-9B-09: Freeze/Thaw resistance
- CAN/CSA-A23.2-16C-09: Resistance to de-icings salts
- CAN/CSA-A23.2-24A-09: Method of test for resistance of unconfined coarse aggregate to freezing and thawing

Among ASTM standards, ASTM C666 is the most used to measure the resistance to freeze-thaw cycles (F-T). The principle of this standard is to subject the materials to very large variations in temperature, allowing freezing and thawing of the water within the concrete.

Very few studies on AAMs resistance to F-T cycles have been conducted. Some of these tests encountered in the literature are described below.

Douglas et al. (1992) performed the F-T resistance of AAS concrete following ASTM C666 standard by means of measuring the relative dynamic modulus of elasticity (RDME) during 500 cycles in aqueous environment. In all concretes AEA was added to increase the air content. The authors found very good resistance to F-T cycles in all the different mixes analyzed. Else, the authors pointed that the air-void spacing factor in all mixtures was higher than the usual recommended limit of 0.220 mm for concrete resistant to F-T cycles. Even though, all concretes experimented a good resistance.

Gifford & Gillott (1996b) also analyzed the F-T resistance of AAS concrete by means of ASTM C666 standard, during 300 cycles in aqueous environment. In this case, RDME and mass change were followed along the test. A commercial AEA normally used in OPC was added to all concretes. The authors analyzed the effect of activator type, the dosage of AEA and the curing procedure (heat curing at 60ºC during 6 hours or moist curing). They found that F-T durability of sodium-silicate AAS concrete was at least as good as OPC, which gives adequate air-void parameters. Else, F-T durability of AAS was found to be slightly inferior when heated at 60ºC during 6 hours than that of the moist cured AAS.

Fu et al. (2011) conducted the F-T resistance of AAS concrete according to ASTM C666 and GB/T 50082-2009 by means of measuring RDME and mass change. In this study, no addition of AEA was notified. The authors found excellent F-T resistance with a relative dynamic elasticity modulus of 90% at 300 cycles.

Škvára et al. (2005) presented their work on resistance of AAFA to F-T cycles, using the Czech standard CSN 72 2452. AAFA mortar samples were subjected after 28 days curing time period to 150 freeze-thaw cycles in an aqueous environment. Different formulations were studied, with and without air-entraining agent (AEA), measuring variations in mass and in compressive strength. The authors found that, for mortars without AEA, the mass did not change significantly after 150 cycles and had 70% less compressive strength compared with mortars at the same age in normal conditions, i.e. with a curing at 23ºC and 100% RH. For mortars with AEA, the decrease in strength was lower, although the total resistance was lower because of air bubbles. They concluded that the AAFA mortars had excellent resistance to F-T cycles.

Rostami et al. (2003) have also studied the behavior of AAFA to F-T cycles following the procedure described in ASTM C666 standard. Concrete samples were subjected to F-T cycles in an aqueous environment. The authors measured the dynamic modulus, compressive and flexural strength and mass change. The effect of adding an AEA to the formulations was also analyzed. The results showed that the concrete had a good F-T resistance. Else, it was found that the AEA added to the concrete did not improve the F-T resistance, contrary to the results obtained by Škvára et al. (2005).

Table 2.4 Summary of the F-T test conditions used in several works

Work	Material	Standard*	Type	Indicators	Specimen (mm)	Curing time (days)	Freeze-thaw environment	Cycles
(Douglas et al., 1992)	AAS	ASTM C666	Concrete	RDME Mass change Length change	76x102x390	14 (moist curing)	Aqueous	500
(Gifford et al., 1996)	AAS	ASTM C666	Concrete	RDME Mass change	75x75x350	14 (moist curing)	Aqueous	300
(Fu et al., 2011)	AAS	ASTM C666 GB/T 50082-2009	Concrete	RDME Mass change	100x100x400	14 (moist curing)	Aqueous	300
(Škvára et al., 2005)	AAFA	CSN 72 2452	Mortar	Comp. strength	40x40x160	28 (lab. temp. and 40% RH)	Aqueous	150
(Rostami & Brendley 2003)	AAFA	ASTM C666	Concrete	Mass change	75x75x355	14 (moist curing)	Aqueous	300
(Sun & Wu 2013)	AAFA	ASTM C666	Mortar	RDME Mass change Comp. strength	23.5x23.5x50.8	14 (moist curing)	Aqueous	300
(Steinerova 2011)	AAMk	--	Mortar	Comp. strength Young's modulus Flex. strength	40x40x160	28 (ambient temp.)	Aqueous	25

In a recent study, Sun & Wu (2013) analyzed the F-T of AAFA but in this case in mortars. The authors followed the ASTM C666 standard as well. The effect of the AEA was study on RDME, compressive strength and mass change. Results showed that the AAFA mortars with AEA did not experiment any change in terms of RDME, showing very good F-T resistance. AAFA without AEA rather showed very good results, with a final RDME after 300 cycles of 95%.

Steinerova (2011) conducted the F-T resistance on AAMk samples. The author analyzed the effect of the sand content on the F-T resistance by means of measuring compressive and flexural strength and Young's modulus. In this work, AEA was not used. The results showed that specimens were frost resistant from 34 wt.% or more of sand.

In **table 2.4** a summary of the works presented in this review can be found. A few other works can be found in the book of Pacheco-Torgal et al. (2015). It can be seen that the most test method used is ASTM C666 standard, with RDME, mass and length change as indicators of the degree of attack. Moreover, compressive strength is often used by some authors as the main indicator (Škvára et al. 2005; Steinerova 2011).

Although little work has been done, results show very good resistance of different AAMs to freeze-thaw cycles. In general, the addition of AEA to OPC-based concrete increases the resistance to freeze-thaw cycles. Conversely, the addition of them to AAMs concrete seems to have the opposite effect (Rostami & Brendley 2003). It appears that the uniform and stable pore structure which increases the durability is not formed. However, there are works that mention a small improvement with air included (Škvára et al. 2005; Gifford & Gillott 1996b). Else, as shown by the works without AEA, it seems that AEA is not required in AAM systems in order to get a binder with frost resistance.

2.5.5 Permeability

Pore structure is one of the most important aspects of concrete as it plays an important role in all the chemical and physical attacks. In chemical attacks, external agents can penetrate from outside into the concrete pore structure, and hence the attacks can occur. Therefore, measuring permeability of concrete will give information of how concrete can be exposed to further chemical attacks in service conditions. Permeability is then the ability of concrete to allow water pass through the pore structure of concrete under a pressure gradient.

Nevertheless, it cannot be found any American standard allowing the measure of permeability by a pressure gradient. Instead, standardized test methods exist by indirectly measuring permeability. Among these standards it can be found the followings:

- ASTM C1202-12: Standard test method for electrical indication of concrete's ability to resist chloride ion penetration
- AASHTO T277-07: Standard method of test for electrical indication of concrete's ability to resist chloride ion penetration
- MTO LS-433: Method of test for electrical indication of concrete's ability to resist chloride ion penetration
- ASTM C1760-12: Standard test method for bulk electrical conductivity of hardened concrete
- AASHTO TP95-14: Method of test for surface resistivity indication of concrete's ability to resist chloride ion penetration
- MTO LS-444: Method of test for determining the electrical resistivity of concrete

ASTM C1202, AASHTO T 277 and MTO LS-433 standards are also called RCPT (Rapid chloride permeability test) because they are accelerated test methods in which the penetration of chloride ions into the pore structure of concrete is measured in order to predict the permeability. The acceleration is produced through the application of an electric current (60V) during 6 hours which increases the movement of chloride ions into the porous material.

Contrary to these standards, ASTM C1760, MTO LS-444 and AASHTO TP95-14 propose a different test method (electrical resistivity) based on the ability of the water filled pores of concrete to conduct electrical current, thus giving an indirect measure of the permeability too. During recent years, the electrical resistivity is receiving more interest to predict the possibility of corrosion of concretes rather than RCPT method, and it serves as an indirect measure to predict the permeability as well. However, RCPT is still the most accepted and demanded test for quality criteria. These standard use different methods to assess electrical resistivity: ASTM C1760 and MTO LS-444 use bulk resistivity (two electrode method) and AASHTO TP95 uses surface resistivity (four electrode method). ASTM C1760 is similar to RCPT but the time is shortened to 1 min. MTO LS-444 uses another equipment, based on MERLIN test. And AASHTO TP95 is based on the Wenner method.

Other test methods exist to directly measure the permeability of concretes, such as pressurized water or air permeability. Although these test methods are more reliable of service conditions, since they are based on pressure gradients, there are not American standards for them. For example, for pressurized water permeability exists the European standard "*EN 12390-8: Testing hardened concrete. Part 8. Water penetration depth under pressure*". In the case of air permeability, it can be found the *Torrent method* (Torrent 1992). This method has been standardized as part of *SIA 262/1* standard.

The works regarding the AAMs permeability, by means of indirect or direct measure, are summarized next.

Shi (1996) measured the chloride ions penetrability in AAS mortars following ASTM C1202 standard and did a water permeability test. The author studied the effect of age and the type of activator used. The results of ASTM C1202 showed that AAS concretes were less permeable than the OPC concrete. In addition, NaOH appeared to be the best activator which led to lowest permeability. The results of the water permeability test also showed less permeability of AAS samples than OPC ones. The author concluded that, aside from the pore structure, chemistry of the pore-solution had a significant effect on the permeability of the concretes.

Bernal et al. (2011) also determined the chloride ions penetrability in AAS but in concretes according to ASTM C1202. Samples were tested after 28 days of curing time. The results indicated that AAS had low penetration of chloride ions according to ASTM C1202 classification, and also lower than that of OPC samples. However, the authors also highlighted the effect of the pore solution chemistry. These results are in good agreement with those observed by Shi (1996). Thus, they stated that alkalis in the pore solution could influence the test results increasing the values of electric conductivity and therefore overestimating the results.

Chi (2012) also studied the chloride ions penetrability in AAS concretes according to ASTM C1202. The author studied the effect of Na_2O dosage and the curing conditions on the mechanical and durability properties. The results showed the same penetration class (moderate class according standard) of chloride ions of AAS concrete compared with OPC concrete. The author found an increase of the measured charge when the initial alkali content was higher. This behavior is consistent with previous observations (Bernal et al., 2011) that showed the possibility of alkalis to increase the electrical conductivity of the porous solution.

Z. Zhang et al (2010) used the Darcy method to measure the permeability of a BFS/Mk geopolymer. The authors developed a system in which water under pressure (20.1 MPa) was applied to a confined surface of paste samples. Samples were analyzed after 3 days of curing. They studied the effect of liquid/solid ratio, BFS content and curing condition on permeability. The results showed that increasing the liquid/solid ratio, the permeability was increased due to a higher pore connectivity. Else, it was found beneficial the addition of BFS at higher liquid/solid ratios. The different curing conditions used in this work showed slight variations on the permeability. The authors concluded that this geopolymers had low permeability and excellent anticorrosion property.

Ma et al. (2013) also studied the water permeability but in this case of AAFA specimens. The hydrostatic pressure was 0.7 MPa, much lower than those applied in the experiments of Z. Zhang et al. (2010). The effect of silica and alkali content and the continuous heat curing on pore structure development on water permeability were analyzed. The authors found that prolonged heat curing could significantly decrease the AAFA permeability. Else, higher silica contents resulted in lower water permeability, and higher alkali content showed a slight effect at early ages but a more pronounced effect at later ages (decreasing permeability as well).

Oxygen permeability and RCPT of alkali-activated natural pozzolans (AANP) were analyzed by Bondar et al. (2012). In this work, oxygen under pressure was forced to flow through the sample. Else, RCPT (followed as per ASTM C1202) was modified by reducing the voltage from 60V to 20V to avoid heating of the samples. The authors studied the effect of the w/b ratio and curing temperature on permeability in several natural pozzolans. The results showed that AANP had 10 to 35% lower O_2 permeability at 90 days in normal curing conditions than OPC. Increasing curing temperature and reducing the w/b ratio the permeability was reduced. According to the RCPT results, the authors found higher permeability for all AANP studied than of OPC at 90 days. Thus, authors confirm the negative effect of the chemistry of AANP pore solution in the measured passed charge, overestimating the results.

In another study, Nasvi et al. (2014) conducted the CO_2 permeability of BFS/FA geopolymers. The addition of different proportions of BFS to FA as well as the confining and injection pressures were analyzed. It was found that the addition of slag improved the microstructure and reduced the apparent CO_2 permeability of geopolymer. Else, the apparent CO_2 permeability of geopolymer was 100-1000 times lower than that of the control mixtures (with G cement). The same authors, in other study (Nasvi, P.G. Ranjith, et al. 2014) found that increasing temperature, the permeability of geopolymer increased. Also at a given temperature, the permeability of geopolymer decreased with increasing the inlet pressure.

As seen in this review, very few works can be found assessing the permeability with test methods based on pressure gradient. Some of them are based in pressurized water and some others use gas permeability (O_2 and CO_2). In other works, permeability has been measured with indirect measurements, such as RCPT. This test, widely used with OPC concretes for quality control, has been criticized because of the high voltage used (60V) that can rise the temperature which increases the mobility of all ions (not only chlorides). The increased mobility of ions by elevated temperatures will therefore increase the charge passed. As it is based on electrical conductivity measurements, measures are highly affected by the chemical composition of the pore solution as well as the pore structure. Therefore, in binders where

pore solution has a high concentration of ionic species (such as AAMs), it is expected to influence the results. Some works have been adopted to reduce the voltage to 20V (Bondar et al. 2012), yet it may be not sufficient as shown by the authors.

In conclusion, it seems that the chloride ion permeability values of AAMs, which have a high concentration of alkalis (Lloyd et al. 2010), are very low. Taking into account that the presence of alkali causes an increase of the measured values, the actual values of AAMs would be even lower. Regarding the pressure gradient permeability tests, AAMs performed better in all cases that the respective control mixtures with OPC.

2.6 Glass

Glass is an important material that forms part of our lives. It is an amorphous solid which has a vast amount applications such as container, flat, fiber, and others, converting the glass in one of the most used materials.

In the next sections we will see some points to understand the technical, environmental and economic aspects which led to consider waste glass as a construction material in concretes. Therefore, we will see the negative environmental aspects in the production of new glass, the associated negative aspects of recycling waste glass, the need to find new high-value added applications and its revalorization as a construction material in concretes.

2.6.1 Production of glass

Glass production consists in several processes: raw materials mixing and preparation, melting, forming and finishing processes. Raw materials are mostly composed of silica (sand) with sodium carbonate (soda ash). Other components as dolomite, lime and aluminum oxide are also added as stabilizers in order to reduce weathering of the glasses (Ecofys 2009). Another component that is taking an important environmental aspect is the use of waste glass (cullet) as raw material. Depending on the final product, the molding and finishing processes will vary. Therefore, the most important point is the melting process.

During the melting process, mixed raw materials are introduced continuously into a furnace and heated to temperatures around 1600ºC. Melted glass is afterwards passed to the forming and finishing processes. This process is energetically expensive, as it is necessary to achieve high temperatures.

Direct CO_2 emissions are attributed to the glass production. These emissions are divided into two categories: a) process emission, derived from the decarbonation of raw materials as sodium carbonate

(Na_2CO_3), limestone (Ca_2CO_3) and dolomite ($CaMg(CO_3)_2$); and b) fuel combustion, used for the energetic requirements in all the processes. Most of these CO_2 emissions are attributed to the energy requirements, e.g. for the container glass sector, direct emissions due to energetic requirements are around 85-90% and direct emissions due to process are 10-15% (Ecofys 2009). It is estimated that each 1 ton of colorless bottles produces 0.5 tons of CO_2, whereas 1 ton of colored bottles emits 0.37 tons of CO_2 (Ecofys 2009). Therefore, glass production has an environmental cost too. The use of recycled glass as raw materials (cullet) will entrain several benefits: decrease of CO_2 emissions associated to decarbonation of some raw materials, energy savings during the melting process (as the melting point of cullet is lower than that of raw materials) and less environmental impact due to quarrying of the earth's natural resources as raw materials. It has been estimated that each 1 kg of sheet glass consumed 1.73 kg of raw materials and 0.15 m^3 of water (Saito & Shukuya 1996).

2.6.2 Glass recycling: an environmental benefit?

Glass is a difficult to biodegrade material because it is a non-biodegradable material so its footprint is high (in terms of space of landfills). Hence, it is importance to recycle it. In the last decades, society is starting to be conscious of the importance of recycling, in order to be more respectful with the environment. Therefore, the quantity of recycled materials is increasing year by year. This is the case of the bottled glass. E.g., in the Province of Québec (Canada), the recycled glass has passed from 34000 tons in 1988 to 128000 tons in 2008 (Gagné 2010).

Recycled glass can have several benefits in terms of the production of new glass, both economic and environmental. Therefore, recycled glass can be used to produce new glass with economic savings by energy reduction during the melting process of raw materials and reducing the use of Earth's new natural resources that would negatively impact the environment. However, not all the recycled glass can be used to this purpose. This option is only limited by the availability of recycled glass with the right quality and right chemical compatibility. Recycled glass may have contamination due to paper and plastic labels, caps and corks, and sugars remaining from the original use and content of the bottles (Federico & Chidiac 2009). Else, it is difficult and costly for the sorting plants to separate the glass by colors (i.e. the bottles). This recycled glass that is not selected by colors is referred as mixed glass. As a result, recycled mixed glass is often discarded to landfills because of a lack of market outlets. The quantity of mixed glass can vary from one sorting to other, depending on the efficiency of its facilities.

Although there already exists applications for the mixed glass (described in next section), some of them are considered as a low-value added. Else, not all the mixed glass is revalorized, and is discarded in landfills. It is necessary therefore to find new market outlets for the mixed glass, i.e. revalue them.

2.6.3 Market outlets of recycled glass

Some applications for the recycled glass can be found, in order to add an extra value after the conceived initial use. Among these applications, it can be found the followings:

- Production of new glass
- Production of wool fiberglass
- Glass aggregate for its use in concretes
- Glass powder as a SCM's
- Others.

Production of new glass has already been detailed in previous sections. As seen before, this option is restricted to the quality and the chemical compatibility of the recycled glass. Thus, colorless recycled glass will be useful to produce new colorless glass, green glass will be useful to produce new green glass, and so on. The introduction of recycled glass as raw material for the production of new glass will be economical and environmental beneficial, as explained before.

Recycled glass can also be introduced as a raw material for the production of new wool fiberglass, as in the case of new glass, reducing the quantity of earth's natural raw materials, and reducing the energy requirements during the melting process.

Early attempts to incorporate waste glass in concrete during the 20th century tended to focus on aggregate replacement. However, they were unsuccessful due to the destructive alkali–silica reaction which takes place in the presence of the amorphous waste glass and concrete pore solution (Federico & Chidiac 2009). Later works, reviewed by the same authors, have demonstrated that by lowering particle sizes, a higher percentage of waste glass can be incorporated as an aggregate in a safety manner. This is practically due to the pozzolanic properties of the glass.

Recycled glass was therefore thought to be used as a SCM's, due to its pozzolanic properties. Thus, it can be useful to replace part of the cement by ground recycled glass. It has been found that it can be replaced up to 30% of cement by ground recycled glass keeping or improving the performance of the concretes (Jani & Hogland 2014).

Other uses of recycled glass, but with a low-value added, is to incorporate them as a daily cover material in the technical landfills. Sometimes, this application is the most used for the recycled glass, i.e., in the Province of Québec, Canada, 94% of recycled glass in 2014 was revalorized, however, 57% of it was used in technical landfills as a daily cover material, which is considered to be a low-value added application (Recyc-Québec 2015).

A life cycle analysis done in the Province of Québec, by Quantis (Quantis 2015), has compared 4 recycled glass applications (production of new glass bottles, aggregates for concrete, wool fiberglass and glass powder as SCM's) with a low-value added application such as incorporation as a daily cover material in the technical landfills. This study has demonstrated that it is preferable, in terms of GHG emissions reduction, to transport the glass for recycling or revalorize it to distances covering several thousands of kilometers rather than use it in local technical landfills. Thus, according to this study, it will be preferable to transport it by truck until 115 km for its use as a glass aggregate, distance from which profitability is questionable. In the case of using it for new glass bottles, it can be transported until 2000 km, for wool fiberglass until 2100 km and for glass powder until 8950 km. As it can be seen, the use of recycled glass as a glass powder could be an interesting option due to the broad region which it could be transported with a positive environmental benefit.

2.6.4 Recycled glass as a Portland cement replacement

As described by Malhotra and Mehta (Malhotra & Mehta 1996), the use of supplementary cementitious materials (SCMs) can have three benefits: functional or engineering benefits, economic benefits and ecological benefits. Due to its chemical composition and physical properties, which are similar to those of cement, mixed glass has been considered to be a potential SCM's. Therefore, recycled glass can contribute to all of the benefits described before.

The waste mixed glass can be finely ground to get a glass powder (GP). The use of GP as a cement replacement has been extendedly studied in the last years. Summary of the works already done can been found in several reviews (Shi & Zheng 2007; Federico & Chidiac 2009; Jani & Hogland 2014). Therefore, the most important aspects will be summarized next.

Due to its high silica content, GP is considered as a good pozzolanic material. However, there are other elements in its composition that have caused problems, as the high alkali content. Thus, the major concern when adding GP as a cement replacement is the stimulation of ASR. This was the case of the use of GP as an aggregate, that caused dangerous ASR (Federico & Chidiac 2009). In that sense, the efforts of using GP as a cement replacement were due to find a way of use it without increasing the susceptibility of concretes to ASR.

One of the treatments done in order to minimize the ASR was to decrease the size particle through grinding, until getting a glass powder. Several studies have shown that reducing size particle and increasing the incorporation rate was beneficious in terms of higher ASR resistance (Shao et al. 2000; Shi et al. 2005; Shayan & Xu 2004; Mafalda Matos & Sousa-Coutinho 2012; Schwarz & Neithalath 2008; Zidol 2009). This was attributed to an increase of the pozzolanic properties. Therefore, there is a

competition between the pozzolanic reaction and the ASR. Since pozzolanic reaction occurs before than ASR, less alkali will be present to induce ASR (Mafalda Matos & Sousa-Coutinho 2012). Compressive strength has been found to decrease at early ages as GP is increased, whereas at later ages seems to improve or at least equalize the control mixtures (100% cement) (Shao et al. 2000). In these works, up to 30% of cement was satisfactory replaced by GP.

Other studies in GP as a SCM's are focusing on other durability properties different to ASR resistance (Laldji & Tagnit-Hamou 2007; Mafalda Matos & Sousa-Coutinho 2012; Schwarz et al. 2008; Zidol 2009). For instance, Zidol (2009), using mixed colored waste glass from bottles, obtained improved freeze-thaw resistance up to 20% of replacement comparing to the control mixtures, scaling resistance meeting the ASTM specification and a low-class chloride ion penetrability. In another study, Mafalda Matos et al. (2012) found higher resistance to chloride penetration increasing with the GP dosage replacement, higher carbonation depths increasing with the GP, and a remarkable resistance to sulphate attack with a 10% replacement.

Moreover, some field trials as the ones reported by Tagnit-Hamou (Tagnit-Hamou & Bengougam 2012) demonstrate the viability of concretes with up to 30% of cement replacement in terms of mechanical and durability properties. The mechanical and durability properties of slabs, sidewalks and a wall were followed by analyzing specimens recollected during the concrete placement. The authors concluded that the use of GP as an innovative SCM is very promising. Concrete mixtures containing GP exhibited good workability during the placement, and improvements in compressive strength after 28 days comparing the control mixtures without GP. Else, the concrete mixture with 20% GP was found to have low and very low chloride ion penetrability at 56 and 91 days respectively. All concretes with GP showed very good freeze-thaw resistance with durability factors ranging from 98 to 102%, and tested specimens also showed only a slight scaling in the salt scaling test. This study therefore put in evidence the applicability at an industrial scale of concretes based on OPC with GP.

As shown in this section, the viability of the use of GP from different waste sources as a cement replacement is well proved.

2.6.5 Glass powder as an AAM precursor

As the basis of AAM technology (reaction mechanisms, reaction products, and mechanical and durability properties) have evolved during the last decade by means of BFS and FA as precursors, new trends are focusing on new precursors, mostly industrial wastes (Provis et al. 2015). This is the case of the recycled glass which, if finely ground, can be used as a powder (GP). As detailed in previous sections, an AAMs precursor is a source of Si and Al. Although most GPs have a low content in Al,

they have a high-Si content. Else, they have high alkali content with a moderate-Ca content. According to the classification shown in **section 2.3.1**, GP would not meet any of the two systems but a mix of both.

Limited studies have been conducted using the GP as an AAM precursor. Some of these studies use the glass powder as 100% of the binder (Redden & Neithalath 2014; Cyr et al. 2012; Tashima, Soriano, et al. 2012) while others have tested to mix with another classical AAMs precursor such as BFS, FA (Bobirică et al. 2015) and Mk (Balaguer Pascual 2014), or a mix of them (Zhang 2015; Redden & Neithalath 2014; Bobirică et al. 2015).

Cyr et al. (2012) studied the use of glass cullet from soda-glass to get a geopolymer cement. The authors analyzed the fineness of the glass (from 100 to 4000 cm^2/g), the temperature of synthesis (20, 40 and 60ºC) and the nature and concentration of the activation solution (NaOH and KOH). They concluded that the soda-glass cullet can be used for the production of geopolymer cement, with the best compressive strength when finer was the glass cullet, using KOH as activating solution (although NaOH was good too), and an optimal curing temperature of 60ºC. Regarding the durability, the authors found that it was affected by the water conservation probably due to a lack of aluminum.

Tashima et al. (Tashima et al. 2013a; Tashima et al. 2013b; Tashima et al. 2012) conducted several studies using a waste from glass fiber manufacturing: the vitreous calcium aluminosilicate (VCAS). The authors studied the influence of curing time on the strength and microstructures, and different activators (NaOH, KOH). They developed mixtures, which can achieve up to 77 MPa in compressive strength after 3 days of curing at 65ºC and proposed a mathematical model for the strength development in the range of 4-72 hours of curing time. They also found an influence of the cation of the activating system, getting the best compressive strength when using NaOH. Else, they were able to get high compressive strength (78.5 and 89.55 MPa after 91 and 360 days of curing respectively) cured at room temperature.

Balaguer Pascual (2014) studied the use of alkali-activated glass powder with metakaolin. In this case, Mk was added to increase Al content. Therefore, the author studied the influence of Mk content as a replacement of GP (0, 3, 5 and 8wt%), the influence of the concentration of the activation solution (3M, 5M, 8M and 10M NaOH), and the influence of curing temperature, time and storage conditions. She concluded that the best activation conditions were to use a 5M NaOH solution with a curing temperature of 60ºC during the first 2 days. After this period, the storage conditions giving the optimal compressive strength were dry conditions at 56% of relative humidity (RH) at 23ºC. As observed by Cyr et al. (2012), there was a negative influence on the compressive strength development in moisture

conditions. Else, increasing the Mk up to 5 and 8% decreased the compressive strengths at early ages, but practically achieve similar ones after 91 days for all the cases.

Other study using GP as the solely material was presented by Redden & Neithalath (2014). This GP was a by-product of industrial and highway safety glass bead manufacturing. The authors analyzed the NaOH concentration (4, 6 and 8M), the curing temperature (50 and 75ºC) and the time (24, 48 and 72 hours). Else, the authors studied the influence of adding other materials to glass powder such as BFS and FA on the durability properties. They concluded that higher curing temperatures and durations affected adversely the compressive strength when higher alkalinity activator is used. Else, the sodium silicate gel produced, due to its lack of hydrolytic stability, had a drastic strength loss in moisture conditions, as found by Balaguer Pascual (2014). They explained that this was probably due to a silica depolymerization of the sodium silicate gel. The doping of this system with Al and Ca, by adding FA and BFS respectively, allowed a better stability of the strength loss in moisture conditions, as predicted by Cyr et al. (2012).

Bobirică et al. (2015) studied the addition of waste glass, derived from spent fluorescent lamps, on inorganic polymers based on FA and BFS. They found that increasing the amount of glass to the mixture led to a decrease of the strength attributed to an increase of the SiO_2/Al_2O_3 ratio. The decrease on the Al content would retard the Si incorporation to the gel at later reaction ages, and thus it would result in an increased defect density because of the unreacted raw materials. It was also found that the addition of BFS to the synthesis mixtures improved the strength, most likely due to the formation of Ca-based reaction products that increased the overall degree of polymerization. In this work, the authors found necessary to control the SiO_2/Al_2O_3 ratio in order to get good compressive strength.

In the work of S. Zhang (2015), the influence of waste glass powder as a partial replacement of FA (0, 10, 20 and 30%) in alkali-activated slag/fly ash binder was analyzed. The author found that the replacement of GP for FA in alkali activated slag/fly ash binder generally leads to an increase in compressive strength at 7 and 28 days with 20% and 30% GP replacement. This was attributed to more available silica introduced by GP replacement and finally a higher amount of gel products in the structure.

Although most of the studies with GP in AAM technology are focused on its use as an aluminosilicate precursor. There is however another way to valorize it. It has been also used as a source of silica and alkalis for alternative activators (Torres-Carrasco et al. 2015; Torres-Carrasco & Puertas 2015). This alternative activator could be used to replace the sodium silicate-based activators which have a bad environmental footprint due to their CO_2 emissions during its production.

In this section, some studies related to the use of GP from different waste sources in AAM technology for the concrete and mortar production has been seen. Although almost all the studies seen before showed good results in terms of mechanical properties, there is a lack of studies dealing with the durability properties. As found by Cyr et al. (2012) and later by Redden & Neithalath (2014), there is an incompatibility with moisture curing of binders made with low-Al content. Hence, low-Al GP needs to be accompanied by another source of Al, such as Mk, FA or BFS. More works are needed in terms of durability of GP binders in AAM technology.

Moreover, although the use of recycled glass as a GP has shown to be beneficial as cement replacement (**section 2.6.5**), its use is limited to a 30% of replacement. The use of GP as an AAM precursor can elevate this percentage up to 100%, which means to revalorize higher quantities of waste glass and therefore eliminate the environmental problems associated to landfills.

CHAPTER 3. Experimental plan, methods and materials

The research program of this project is presented in this chapter. In the first part, we will see a detailed experimental plan. Then, we will see the materials used during the project, as well as their characterization (physical and chemical properties). The mortars/concretes formulations, and the experimental test methods that have been used for the achievement of phase 1 and 2 of the project are also presented. Finally, a description of the characterization techniques used for physical and chemical analysis will be described.

This chapter will be referred during the next chapters of this thesis.

3.1 Experimental plan

The experimental plan is divided in 2 phases, as described in **figure 3.1**. The phase 1 is addressed to understand the associated problems of using durability test methods, as described at the standards, with AAMs. For this phase, two traditional alkali-activated (AA) formulations widely studied in the literature have been used, such as AAS and AAFA. Else, as comparative purposes, a conventional formulation with OPC has also been used. The durability tests that have been analyzed are the following: stability in water, permeability, sulfate resistance, acid resistance, alkali-silica reaction, freeze-thaw resistance, and alkali ion leaching. Moreover, compressive strength has been conducted. In order to detect possible problems, durability of the former AA formulations have been analyzed using the test methods as described at the standards and with the modified test methods. Changing the most important parameters of each test (in terms of curing time and conditions, temperature, concentrations, etc.) as well as the indicators of the degree of attack (expansion, mass, compressive strength, etc.) will give valuable information about the influence of the test method conditions on the results. Moreover, characterization of samples at the end of each test by means of X-ray diffraction (XRD) and Scanning electron microscope (SEM), have been done in some tests to identify the degradation mechanisms. In every test, the results of AAMs durability will be compared to OPC results, the binder in which most of the test methods have been based. At the end of this phase, recommendations and future practices to assess AAMs durability are given.

In the phase 2, recommendations obtained in the phase 1 are applied in order to evaluate the durability of a novel formulation based on alkali-activated glass powder/metakaolin mix. Three formulations of this system have been analyzed, by replacing glass powder with metakaolin (5, 15 and 30 wt%). The following durability tests are analyzed: stability in water, alkali ion leaching, sulfate resistance, acid

resistance and alkali-silica reaction. Furthermore, compressive strength in mortars has been conducted. In this phase, we will for the first time get information about the durability behavior of these novel AA formulations when exposed to different damaging conditions, i.e. degradation mechanism and reaction products.

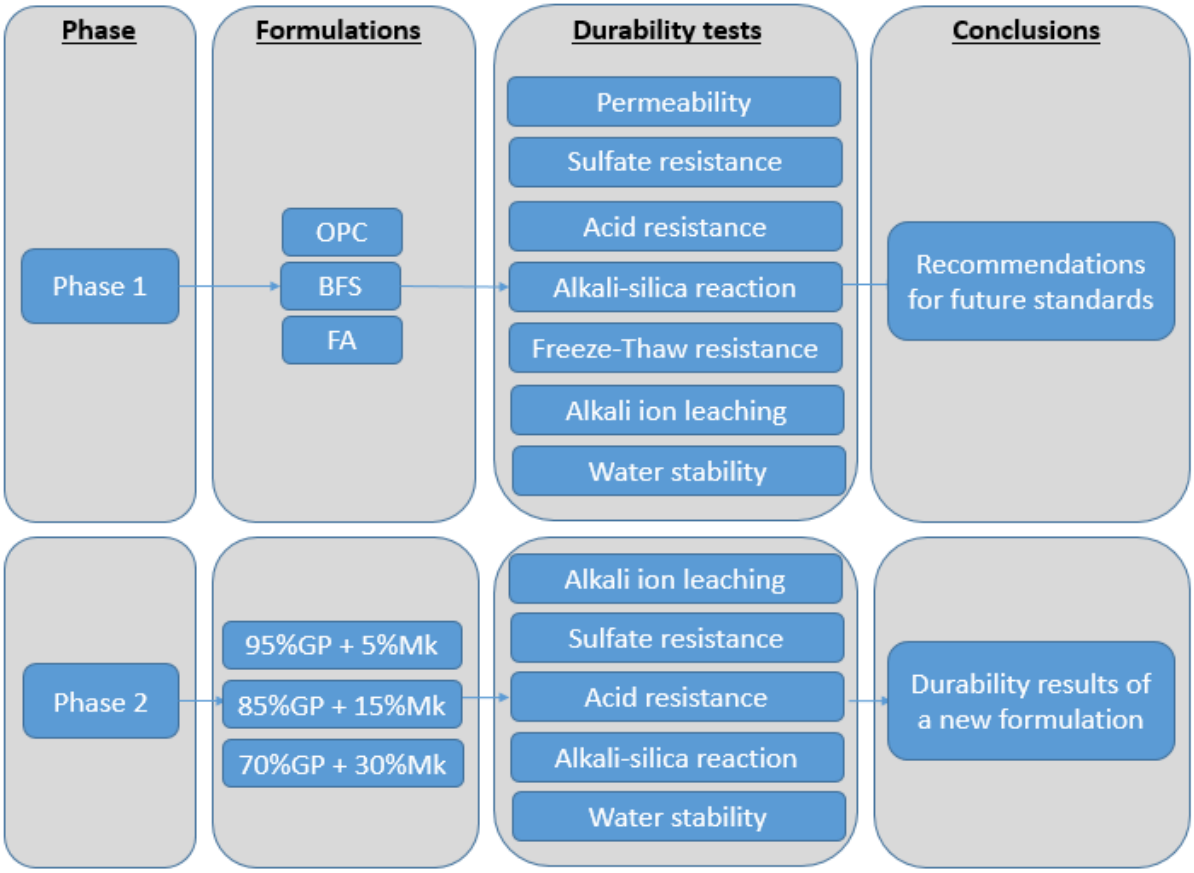

Figure 3.1 Methodology schedule of the project

3.2 Characterization of materials

In this part we will see all the materials used during this project. It has been divided into three groups: raw materials; activating solutions and chemical admixtures; and aggregates.

3.2.1 Raw materials

The raw materials used in this project have been the following: general use portland cement, blast furnace slag, class F fly ash from coal combustion, metakaolin and glass powder.

3.2.1.1 General Use Portland cement

General Use portland cement (OPC) is the most classical cement, without additions, usually used in ordinary mortars and concretes. OPC has been chosen in this project for comparative purposes in phase 1, in order to establish a direct relationship between test methods and results.

The OPC used in this project was supplied by the company "CRH", in the Province of Québec, Canada. The physical properties of the cement are shown in **table 3.1** and **figure 3.2**, as well as the other raw materials used in this project. The density of all materials was measured by means of a Helium pycnometer (**chapter 3.6.1**), the fineness by means of the Blaine method (**chapter 3.6.2**) and the granulometry by means of laser diffraction technique (**chapter 3.6.3**).

Table 3.1 Physical properties of the raw materials

	Density (kg/m^3)	Blaine (cm^2/g)
General use portland Cement	3.15 ± 0.00	3820 ± 15
Blast furnace slag	2.97 ± 0.01	6422 ± 56
Class F Fly Ash	2.59 ± 0.00	3723 ± 39
Metakaolin	2.75 ± 0.01	18898 ± 32
Glass Powder	2.57 ± 0.01	5124 ± 97

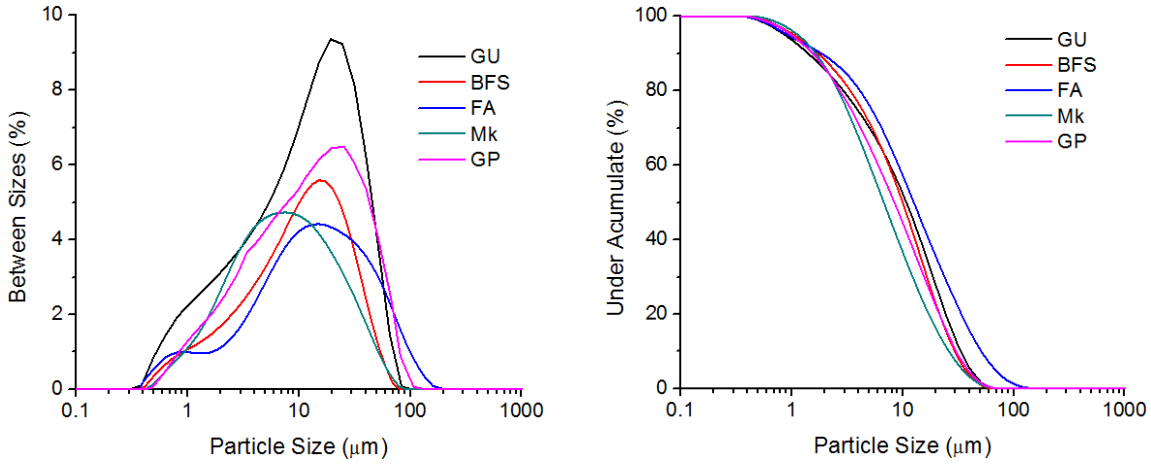

a) Between b) Above

Figure 3.2 Particle size distribution of the raw materials measured by laser diffraction. a) Between particles sizes, b) Above particles sizes

The chemical composition of the cement was measured by X-ray fluorescence (**chapter 3.6.4**), and the results are shown in the **table 3.2**:

Table 3.2 Chemical composition of the raw materials

	SiO_2	Al_2O_3	Fe_2O_3	CaO	Na_2O	K_2O	MgO	SO_3	LOI [1]
General use portland Cement	19.5	4.6	2.3	62.5	0.2	0.8	2.0	3.0	5.2
Blast furnace slag	35.1	10.8	0.4	42.0	0.2	0.3	7.9	1.1	1.7
Class F Fly ash	45.9	23.2	16.9	4.5	1.3	1.9	1.0	0.1	4.2
Metakaolin	55.2	41.5	0.4	0.0	0.2	0.1	0.0	0.0	0.5
Glass Powder	71.8	1.4	0.4	12.0	12.3	0.5	1.1	0.1	0.0

1. LOI: Lost on ignition

The mineralogical composition of the cement, obtained by X-ray diffraction (**chapter 3.6.5**), is shown in the **figure 3.3**. It can be seen that the cement is composed by crystal phases of alite (A), ferrite (F) and aluminate (C). The Bogue composition of this cement has been found to be: 65.9% C_3S, 6.3% C_2S, 7.4% C_3A and 7.1% C_4AF.

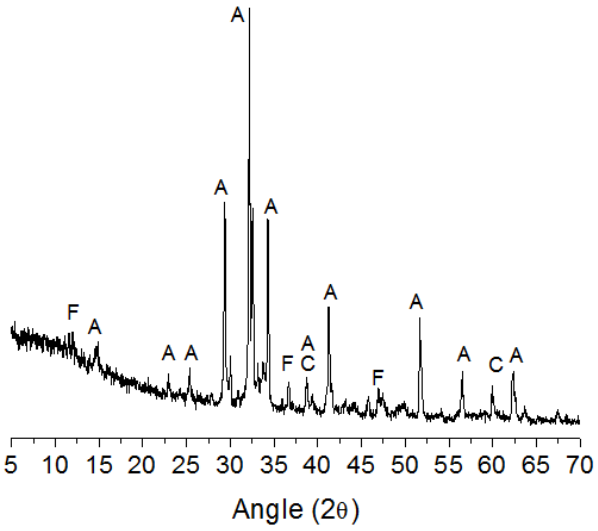

Figure 3.3 Mineralogical composition of the General use Portland cement. A: C_3S, C: C_3A, F: C_4AF

3.2.1.2 Blast furnace slag

Blast furnace slag is a by-product from iron production process. It is generated in a blast furnace in which, after the melting process of all the raw materials (iron ore, coke, limestone, dolomite...), molten iron slag product is separated by decantation. Thus, steel with higher density is extracted from the bottom, and the rest (slag), is extracted from the top. In order to get a highly reactive slag, the molten slag is rapidly quenched to get a glassy product that is then dried. Depending on the cooling process, different types of slag products can be obtained. When it is cooled by water, a granular slag is obtained. This slag is then grounded to finally get the ground granulated blast furnace slag.

The ground granulated blast furnace slag used in this project was supplied by the company "GRANCEM", in the state of New Jersey, United States. The physical properties of the slag are shown in **table 3.1** and **figure 3.2** and the chemical composition is shown in the **table 3.2**. The slag is mostly composed of CaO (42%) and SiO_2 (35.1%), with an important content in Al_2O_3 (10.2%) and other minor phases. The mineralogical composition (**figure 3.4**) shows that the slag is an amorphous material.

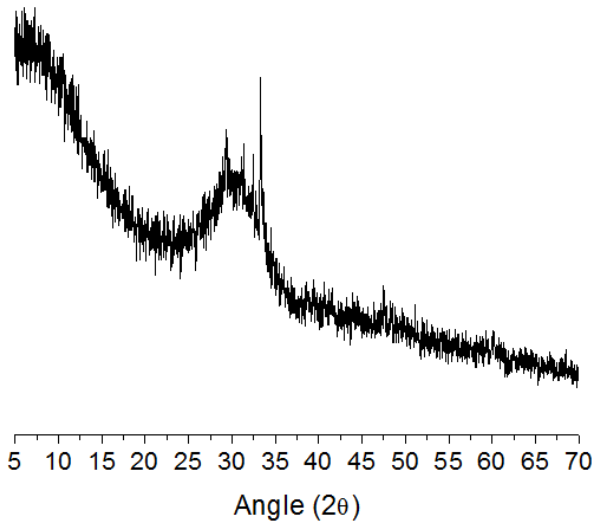

Figure 3.4 Mineralogical composition of the blast furnace slag.

3.2.1.3 Class F fly ash

The fly ash used in this project is a residue from the coal combustion of coal-fired power plants. During this process, coal is burned in a boiler at elevated temperatures. The ash that is driven out of the boiler with the flue gases is recovered in filters (electrostatics, bags or cyclones) in order to clean these gases before they reach the chimneys. This ash is then called fly ash. When the ash is suspended in the flue gasses, it is rapidly cooled and solidifies in spherical shape. Fly ashes are mainly glassy but during the cooling process, some minerals are able to crystallize (mullite, magnetite, etc.), doing fly ash a heterogeneous material. Depending on the coal used for the combustion, the composition of the fly ash will vary. Thus, according to ASTM C618, fly ash is divided in two classes depending on its calcium, silicon and aluminum content:

- Class F fly ash: when $SiO_2 + Al_2O_3 + Fe_2O_3 \geq 70\%$, $SO_3 \leq 5\%$, moisture content $\leq 3\%$ and the loss of ignition (LOI) $\leq 6\%$.
- Class C fly ash: when $SiO_2 + Al_2O_3 + Fe_2O_3 \geq 50\%$, $SO_3 \leq 5\%$, moisture content $\leq 3\%$ and the loss of ignition $\leq 6\%$.

The class F fly ash used in this project was supplied by the company "CRH", located in Montreal, Quebec, Canada. The physical properties of the class F fly ash are shown in **table 3.1** and **figure 3.2**

and the chemical composition is shown in the **table 3.2**. The chemical composition shows that effectively the fly ash is of type F and the summation of SiO_2 +Al_2O_3 + Fe_2O_3 of 85.9% is higher than 70%. Else, SO_3 content is quite below 5% (0.1%) and the LOI of 4.2%, below 6%.

The mineralogical composition of the fly ash is shown in the **figure 3.5**. It can been seen the amorphous characteristic of the fly ash, represented by a broad halo between 15 and 35 degree 2θ, as well as the typical crystalline products of class F fly ashes, such as mullite (M), magnetite (N) and quartz (Q).

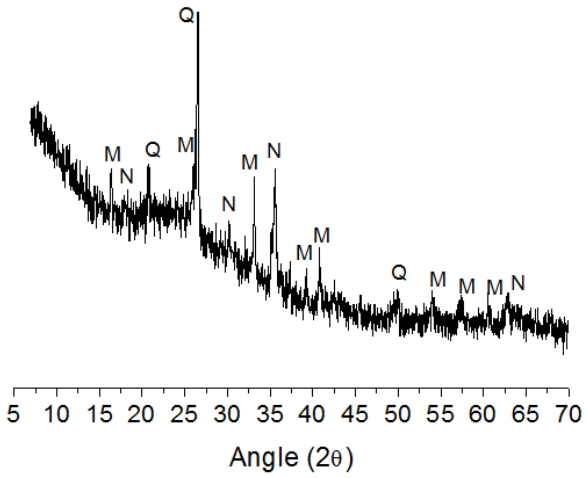

Figure 3.5 Mineralogical composition of the fly ash.

3.2.1.4 Metakaolin

Metakaolin is a product obtained from the calcined kaolin. Kaolin is a hydrated aluminosilicate material ($Al_2Si_2O_5(OH)_4$). It is a layered material, with tetrahedral sheets of SiO_4 linked to octahedral sheets of AlO_6 through the oxygen atoms. When it is heated between a wide ranges of temperatures (normally 550-850ºC) kaolin dehydroxilates to get metakaolin, a disordered amorphous, highly pozzolanic material.

The metakaolin used in this project was supplied by the company UNICAL. In this case, metakaolin was obtained by calcination of kaolin at 700ºC. The physical properties of the metakaolin are shown in **table 3.1** and **figure 3.2** and the chemical composition is shown in the **table 3.2**. It can be seen that it is composed mainly by silica (55.2%) and alumina (41.5%). It is a very fine material, with a Blaine of 18898 cm^2/g. The mineralogical composition (**figure 3.6**) shows that it's an amorphous material with crystalline phases such as illite (I) and quartz (Q).

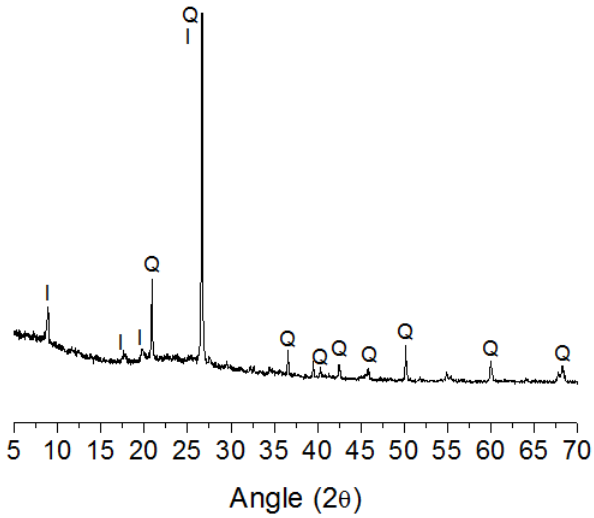

Figure 3.6 Mineralogical composition of the Metakaolin.

3.2.1.5 Glass Powder

Glass powder is an amorphous silica-rich material obtained by grinding the mixed colored glass waste of the sorting plants. The mixed colored glass waste, due to the difficulties of revalorizing it to produce new glass, is ground to obtain a glass powder. This glass powder, due to its composition (silica-rich material), possesses pozzolanic properties and thus can be used as a SCMs.

The glass powder used in this project was supplied by one of the sorting plants of the company "Tricentris", located in the Province of Quebec, Canada. The physical properties of the glass powder are shown in **table 3.1** and **figure 3.2** and the chemical composition is shown in the **table 3.2**. It can be seen that this material possesses a high fineness (higher than OPC and FA). The mineralogical composition of the glass powder (**figure 3.7**) shows an amorphous material without presence of crystalline phases.

3.2.2 Activating Solutions and chemical admixtures

The chemical activators used in this project are the following ones: an industrial sodium silicate solution, a 50 wt.% sodium hydroxide solution and a calcium hydroxide solution.

Two chemical admixtures have been used, one air-entraining agent and one water reducing admixture.

3.2.2.1 Sodium silicate solution

An industrial sodium silicate solution (SS) has been used as the main activator of the alkali-activated precursors. The solution was supplied by the company "Brenntag Canada". The chemical composition

was: 29.3 wt% of SiO_2, 9.1 wt% of Na_2O and 61.6 wt% of H_2O. The silica modulus in molar was of 3.3.

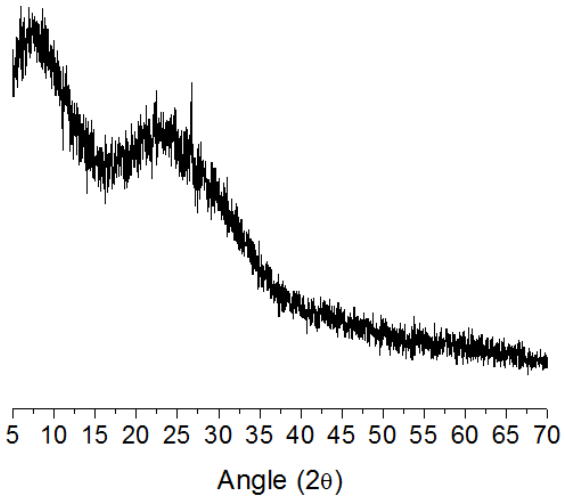

Figure 3.7 Mineralogical composition of the Glass Powder.

3.2.2.2 Sodium hydroxide solution

A 50 wt.% sodium hydroxide solution (SH) was prepared by diluting pure sodium hydroxide (pearl) in distilled water. The pure sodium hydroxide (pearl) was supplied by the company "Brenntag Canada".

3.2.2.3 Calcium hydroxide solution

A 50 wt.% calcium hydroxide solution was prepared by dilution of pure calcium hydroxide in distilled water. The calcium hydroxide was supplied by the company "Brenntag Canada".

3.2.2.4 Air-entraining agent

An air-entraining agent (AEA) was used in this project for the freeze-thaw resistance test, in order to increase the air content of concretes. The AEA used was "Airex-L", and was supplied by "Euclid Chemical Company". Airex-L is a liquid solution of hydrocarbons.

3.2.2.5 Water reducing admixture

A water reducing admixture (WRA) was used in order to improve the workability of the glass powder/metakaolin mixes (see formulations in **chapter 3.3.1**). WRA was the "Eucon WR", and was

supplied by “Euclid Chemical Company”. This WRA is composed by a solution of modified salt of ligno sulfonic acid.

3.2.3 Aggregates

Several aggregates have been used in this project. They have been used to produce the mortars and concretes.

A silica graded sand has been used to produce the mortars. The silica sand meets the specifications of the ASTM C778 standard. This sand was supplied by “GENEQ Inc.”. The provenance of this sand is Ottawa, Illinois (EE.UU). The particle size of this sand ranges between 600 μm (sieve No. 30) and 150 μm (sieve No. 100).

Another silica sand has been used to produce the concretes. The theoretical grading of this sand is 0 to 5 mm. This sand was supplied by DJL Estrie, Quebec (Canada). The particle size distribution of this sand is shown in the **table 3.3**:

Table 3.3 Grading of the Sand 0-5

Size (mm)	0.080	0.160	0.315	0.630	1.25	2.5	5	10
Cumulative passing (%)	0.2	7.5	30.4	54.9	70.7	84.2	96.7	100.0

The saturated surface dry density of the sand 0-5 mm was of 2.68 g/cm^3 and the absorption was of 0.9%.

The mineral characterization of this sand showed to be mostly composed by quartz, with other minor constituents as feldspars (albite), mica (muscovite), calcite, vaterite, kaolinite and chlorite.

For concretes, two different grading coarse aggregates have been used to produce concretes, the aggregate 5-14 mm and the aggregate 10-20 mm. Both types of aggregates were supplied by “Carrière Saint Dominique”, Quebec, Canada. The granulometry of the aggregates is shown in the **table 3.4**:

Table 3.4 Grading of the aggregates 5-14 mm and 10-20 mm

Size (mm)		1.25	2.5	5	10	14	20	28
Cumulative passing (%)	A 5-14	1.0	1.2	3.5	45.6	87.0	100.0	100.0
	A 10-20	0.6	0.7	0.9	3.3	18.9	95.9	100.0

The saturated surface dry density of the aggregates 5-14 mm and 10-20 mm was 2.73 g/cm^3 and 2.75 respectively, and the absorption was 0.41% and 0.46%.

Another type of aggregate has been used specially for the alkali-silica reaction test. This aggregate, named "Spratt", is a siliceous and dolomite limestone that is commonly used in Canada for the alkali-silica reaction test. It is known to be highly reactive with alkalis. The mineralogical analysis showed to be mostly composed by calcite with some traces of ankerite (dolomite) and quartz. The grading curves of this aggregate will be according to the standards followed to do the alkali-silica reaction test, thus, it will be shown in later sections.

3.3 Sample preparation

3.3.1 Mix design

Several formulations of concrete have been used in this project, based on different aluminosilicate precursors. The aluminosilicate precursors used in the first phase of the project were the blast furnace slag (BFS) and the class F fly ash (FA). Also, in this first part of the project, general use Portland cement (OPC) was used as a reference. In the second part of the project, a novel formulation has been used, based on glass powder and metakaolin mixes (GP/Mk) as a source of aluminosilicate.

The formulations used for the first part of the project have been taken from the literature. Therefore, by comparing some studies of the literature an optimized formulation of AAFA have been taken (Fernandez-Jimenez & Palomo 2004; Kovalchuk et al. 2007; Kovalchuk et al. 2008; Temuujin & van Riessen 2009; Wallah & Rangan 2006; Winnefeld et al. 2010) and AAS (Al-Otaibi 2008; Aydın & Baradan 2012; Bakharev et al. 2002; Bernal et al. 2010; Bernal, Provis, et al. 2011; Bernal, de Gutiérrez, et al. 2011; Puertas et al. 2007; Wang et al. 1994; Krizan & Zivanovic 2002; Collins & Sanjayan 1999). These formulations have later been adapted in laboratory in order to adjust the rheology of the mortars and concretes to our materials.

The optimized formulations chosen for AAFA and AAS have been activated by a mix of sodium silicate (SS) and a 50 wt% of sodium hydroxide solution (SH). The SH have been used in order to reduce the silica modulus (M_s) of the SS. Furthermore, in the case of AAS, as setting time was detected 5 minutes after casting the mortar, 2 wt.% of hydrated lime (HL) in form of slurry was added (Douglas et al. 1992; Gifford & Gillott 1996a) to delay the setting timefrom 5 min to 62 min in mortars, measured according to ASTM C807 standard. Therefore, the main parameters of these formulations are shown in the **table 3.5**.

Table 3.5 Main parameters of the AAFA and AAS formulations

	Total molar ratios (binder + activator)				Activator			
	$\frac{SiO_2}{Al_2O_3}$	$\frac{Na_2O}{SiO_2}$	$\frac{Na_2O}{Al_2O_3}$	w/s	Ms	$\frac{wt\%\,Na_2O}{Binder}$	$\frac{Alcaline\ Solution}{Binder}$	$\frac{Sodium\ silicate}{NaOH}$
AAS	6.00	0.12	0.55	0.45	1.42	5.0	0.31	3.2
AAFA	4.00	0.13	0.50	0.25	1.46	7.1	0.37	3.3

* w/s: water to solid ratio (solid = binder plus solid part of the activators)

In the case of the OPC formulation, a general mix has been used. Since it is used for reference purpose, and not to prove its durability, this formulation has not been improved (in terms of w/b ratio, admixtures, additions, etc.).

The mix proportions of the OPC, AAS and AAFA mortars and concretes are shown in **table 3.6**. The mix proportions of the concretes have been designed by the method of the absolute volume, adjusting the sand content in order to constantly keep 1 cubic meter. The mass of the coarse aggregate of 1070 kg/m^3, with 80% of the gravel 5-14 and 20% of the gravel 10-20.

Table 3.6 Mix proportions of OPC, AAS and AAFA mortars and concretes

	Mortar (g)			Concrete (kg/m^3)		
	OPC	**AAS**	**AAFA**	**OPC**	**AAS**	**AAFA**
Binder	400	400	465	400	400	465
w/s	0.49	0.45	0.25	0.49	0.45	0.25
SS	--	93.8	133.2	--	93.8	133.2
SH	--	29.6	40.7	--	29.6	40.7
HL	--	8	--	--	8	--
Sand Ottawa	1100	1100	1279	--	--	--
Sand 0-5	--	--	--	755	648	677
Gravel 5-14	--	--	--	856	856	856
Gravel 10-20	--	--	--	214	214	214

For the second phase of the project, a novel alkali-activated formulation has been used, based on a mix of glass powder and metakaolin (AAGP) as an aluminosilicate precursors. This new formulation has been developed in a related project carried out in the same research group by (Balaguer Pascual 2014) (see **chapter 1.2**). The aim of this project was to develop and optimize a new formulation incorporating

glass powder as a novel precursor by means of the alkali-activated technology (AAT). Hence, three formulations have been adopted in this project, where the proportions of GP and Mk were varied: a) 95GP: 95% of GP and 5% of Mk; b) 85GP: 85% of GP and 15% of Mk, and c) 70GP: 70% of GP and 30% of Mk (percentages in weight). The main parameters of these formulations are shown in the **table 3.7**.

Table 3.7 Main parameters of the AAGP formulations

	Total molar ratios (binder + activator)				**Activator**	
	$\frac{SiO_2}{Al_2O_3}$	$\frac{SiO_2}{Na_2O}$	$\frac{Na_2O}{Al_2O_3}$	w/s	$\frac{wt\%\,Na_2O}{Binder}$	$\frac{Alcaline\ Solution}{Binder}$
95GP	32.58	3.70	8.81	0.45	20.0	0.60
85GP	14.66	3.85	3.82	0.45	18.7	0.60
70GP	7.77	4.17	1.90	0.45	16.8	0.60

The mix proportions of the AAGP mortars are shown in **table 3.8**.

Table 3.8 Mix proportions of AAGP mortars

		Mortar (g)		
		95GP	**85GP**	**70GP**
Binder	GP	380	360	280
	Mk	20	60	120
w/s		0.45	0.45	0.45
SH		240	240	240
% Ad *		0	0	0.5
Sand Ottawa		2035	2035	2035

*%Ad: % of admixture in dry powder: Lignosulfonate (EUCON WR P)

3.3.2 Mixing, casting and curing

3.3.2.1 Mortars

The standard ASTM C305 describes a procedure for the mechanical mixing of hydraulic cement pastes and mortars of plastic consistency. Taking this standard as a basis, different mixing procedures have

been developed for the alkali-activated binders, as these binders do not behave like the hydraulic cement mortars.

So, the mixing procedure described at the standard ASTM C305 is the following:

1. Place all the mixing water in the bowl.
2. Add the cement to the water; then start the mixer and mix at slow speed for 30 seconds.
3. Slowly add the entire quantity of sand over a 30 seconds period, while mixing at slow speed.
4. Stop the mixer, change to medium speed, and mix for 30 seconds.
5. Stop the mixer and let the mortar stand for 90 seconds.
6. Finish by mixing for 60 seconds at medium speed.

In the case of the OPC mortars, the mixing procedure used is exactly as described in the ASTM C305 standard. Upon completion of the mixing period, the flow was measured in accordance with procedure given in standard ASTM C1437. Afterwards, the mortar was properly cast into the desired mould (depending on the test, see **chapter 3.4** and **3.5**). Once the mortar was cast into the molds, the molds were covered by a plastic film, in order to prevent water evaporation, and were placed in a humidity chamber at 23ºC and 100% RH. After 24 hours, the specimens were demolded and kept in the same conditions until tested.

In the case of the AAS mortars, the mixing procedure had some modifications according to procedure described at the ASTM C305. In this manner, the period of 90 seconds where we let the mortar stand was eliminated, and replaced by another 90 seconds of mixing at medium speed. It needs to be pointed out that for all the alkali-activated systems, the chemical activator used was prepared 1 day before the mortar mixing, in order to have a thermally and chemically stable dissolution. The mixing procedure results in:

1. Place all the mixing water (activators plus free water) in the bowl.
2. Add the slag to the liquid; then start the mixer and mix at slow speed for 30 seconds.
3. Add the entire quantity of sand slowly over a 30 seconds period, while mixing at slow speed.
4. Stop the mixer, change to medium speed, and finish by mixing for 180 seconds.

Upon completion of the mixing period, the flow, molding and curing were carried out in the same way as described for OPC mortars.

The mixing procedure of the AAFA mortars was similar to that of the AAS mortars, but with another modification. In this case, the dissolution period (step 2 in all the procedures) was extended from 30 seconds to 60 seconds. Thus, the mixing procedure results in:

1. Place all the mixing water (activators plus free water) in the bowl.
2. Add the fly ash to the liquid; then start the mixer and mix at slow speed for 60 seconds.
3. Slowly add the entire quantity of sand over a 30 seconds period, while mixing at slow speed.
4. Stop the mixer, change to medium speed, and finish by mixing for 180 seconds.

Upon completion of the mixing period, the flow was measured in accordance with procedure given in standard ASTM C1437. Afterwards, the AAFA mortar was cast into the moulds, in the same way as OPC and AAS mortars, as the mortar consistency was similar. Nevertheless, in this case all the mold surface that was in contact with the mortar was covered with a film (tape) prior casting (see **figure 3.8**), especially for metallic molds, due to the stickiness of AAFA mortars. Without the film, the mortars were glued to the surface and was undemoldable. For concretes, it was proceeded in the same manner except for cylindrical concrete specimens (100Øx200mm), where disposable carton molds were used, recovering their internal surface with a plastic film to avoid the concrete to be glued to the carton.

1.- Recovering of the internal faces of the mold to be in contact with the mortar

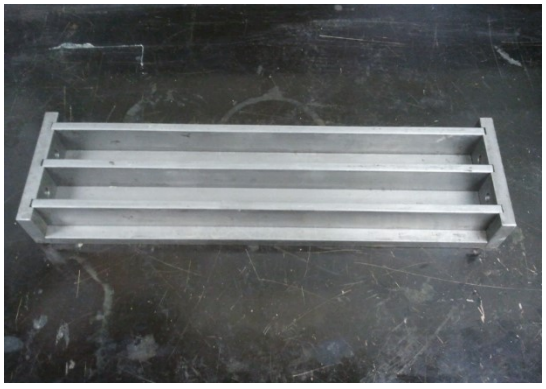

2.- Mold finished and ready to be used

Figure 3.8 Example of preconditioning of the molds with tape

Moreover, the curing for AAFA specimens was different to the others. In this kind of binders, the hardening mechanisms are very slow at normal curing temperature. Hence, once the mortars were cast into the moulds, they were thermally activated putting the moulds in an oven at 80ºC during 24 hours (Palomo, Grutzeck, et al. 1999; Fernandez-Jimenez & Palomo 2007). In order to prevent the high evaporation at this temperature, the moulds were covered first with a plastic film, and then introduced in a well closed bags with enough water inside (see **figure 3.9**). After the first 24 hours at 80ºC, specimens were demoulded and placed into a humidity chamber at 23ºC and 100% RH until test.

a) Moulds covered with plastic film

b) Covered moulds inside the bags with water containers keeping humidity constant

Figure 3.9 Curing procedure of AAFA mortars

For the AAGP mortars, the mixing procedure is practically the same than for AAFA, but with a minor modification. In this case, as the binder is composed of two materials, glass powder and metakaolin, the dissolution period was enlarged to 90 seconds. During the first 60 seconds, the glass powder was added to the activator liquid for a first dissolution, and during the next 30 seconds the metakaolin was added to the already formed glass powder paste. This mixing procedure was according to the recommendations of Balaguer findings (Balaguer Pascual 2014). Thus, the mixing procedure results in:

1. Place all the mixing water (activators plus free water) in the bowl. If it is the case, add to the liquid the admixture.
2. Add the glass powder to the liquid; then start the mixer and mix at slow speed for 60 seconds.
3. Slowly add the metakaolin powder during 15 seconds, and keep mixing another 15 seconds at slow speed.
4. Add the entire quantity of sand slowly over a 30 seconds period, while mixing at slow speed.
5. Stop the mixer, change to medium speed, and finish by mixing for 180 seconds.

Upon completion of the mixing period, the flow was measured in accordance with procedure given in standard ASTM C1437. Afterwards the AAGP mortar was cast into the moulds, in the same way as the other formulations. Like the AAFA mortars, the hardening mechanism is very slow at normal curing temperature. The mortars were thus thermally activated by introducing the molds in an oven at 60ºC during 48 hours, following the recommendations of Balaguer's work (Balaguer Pascual 2014). After the first 48 hours at 60ºC, specimens were demolded and placed into a chamber at 23ºC and 56% RH until test.

3.3.2.2 Concretes

For concretes, the mixing procedure described at the standard ASTM C192 (*Making and curing concrete test specimens in the laboratory*) has been used as a basis:

1. Add the aggregates to the mixer and mix in dry conditions during 30 seconds to homogenize them.
2. Add half the total water to the dry aggregates and mix during for at least 30 seconds.
3. Add the cement powder to the mixer and mix during 30 seconds.
4. Add the rest of the water to the mixer and mix during 120 seconds.
5. Stop the mixer, and let the concrete stand for 180 seconds.
6. Finish with another 120 seconds of mixing.

This procedure has been used as described at the standard for the production of OPC concretes. For AAS and AAFA concretes, similar mixing procedure was used eliminating the stand period. As well as for mortars, the activating solution was prepared one day before the mixing and was added in the step 4, with the second half of the water.

After mixing, the flow was measured according to ASTM C143 and the fresh density and the air content (if required) were measured according to ASTM C231. OPC and AAS concretes were similarly cast according to the requirements of each test. After cast into the molds, the molds were covered with plastics in order to prevent evaporation, and stored at laboratory temperature (23ºC) during 24 hours. Afterwards, specimens were demolded and stored in a moist chamber at 23ºC (100% RH) until used. In the case of AAFA concretes, after cast into the molds, the molds were covered with a plastic film and placed inside a tightly closed bags with water inside, and thermally activated at 80ºC in an oven during 24 hours. After this period, specimens were demolded and stored in a chamber at 23ºC and 100% RH until use.

3.4 Compressive strength test

Compressive strength tests were carried out following the instruction given at the ASTM C109 standard (*Compressive strength of hydraulic cement mortars (using cube specimens)*) for mortars and the ASTM C39 standard (*Compressive strength of cylindrical concrete specimens*) for concretes.

3.5 Durability tests methods

The durability test methods described next are those applied in the first phase of the project (results are shown in **chapter 4**). For the second phase of the project (**chapter 5**), the test methods was slightly modified, thus the modifications will be explained later.

3.5.1 Dimensional stability in water

The goal of this test was to study the behavior of the new formulations in tap water. The test was carried out following a similar procedure to that described at the ASTM C1038 standard. The mixing of the sample was according to **chapter 3.3.2.1** and the molding according to the ASTM C157 standard. The procedure consisted in putting mortars bars of 25x25x285mm of size in tap water after demolding. The expansion and mass of bars were measured at 15, 30, 45, 60, 90, 120, 150 and 180 minutes. Afterward every day until 1 week.

Two set of bars were prepared. The first set was heated during the first 24 hours of curing at 35ºC, applying the conditions of the sulfate resistance test (see **chapter 3.5.2**), and the other set at 80ºC, applying the AAFA curing conditions.

3.5.2 Sulfate resistance test

Sulfate resistance test was carried out by following the procedure described at the ASTM C1012 standard. This procedure consists in mixing the mortars according to **chapter 3.3.2.1** and casting according to ASTM C157 standard. Two types of specimens were prepared: 25x25x285mm specimens for sulfate resistance tests and 50x50cm specimens for compressive strength tests. After molding, molds are put in a curing tank with water at 35ºC for 24 hours. Afterwards, specimens were demolded and checked for compressive strength. According to the standard, if compressive strength is equal or higher than 20 MPa, then specimens are placed in a sulfate solution to start the test. If specimens do not reach that strength, they are stored in a humidity chamber at 23ºC and 100% of RH until 20 MPa is reached. Once the test has started, the expansion and mass of specimens were measured at the following ages: 1, 2, 3 and 4 weeks, then at 2, 3, 4, 6, 9 and 12 months. In every reading, the sulfate solution is renewed by a fresh sulfate solution.

The standard recommends to use sodium sulfate as a source of sulfates, at a concentration of 5 wt%. However, it allows to use other sources of sulfates and other concentrations depending on the real service conditions that we want to reproduce. In this project, as the aim is to evaluate the procedure

rather than a real service conditions, sodium sulfate was used as the sulfate source, whereas sulfate concentration was changed (2, 5 and 8wt%).

In order to evaluate the applicability of this test for AAMs, some parameters of the test method described at the standard were modified. Hence, the influence of the curing temperature (35ºC according to the standard) and the sulfate concentration on the results were analyzed. In this sense, 3 different curing temperatures during the first 24h have been studied: 23ºC (normal curing), 35ºC (according to ASTM C1012), and 80ºC (special curing temperature for AAFA). Specimens subjected to thermal curing were cured according to the procedure described in **chapter 3.3.2.1** (see **figure 3.9**). After the different curing conditions, specimens were placed in 3 different sulfate concentrations: 2, 5 and 8 wt% of sodium sulfate.

The measurement parameters, the expansion and the mass change, have also been evaluated as indicators of the degree of attack for AAMs.

3.5.3 Acid resistance test

This test does not have a specific standard associated to it. For this reason, the ASTM C267 standard, named "*Chemical resistance of mortars, grouts, and monolithic surfacings and polymer concretes*", has been used as a basis for this test. More specifically, the procedure B of this standard has been taken with some modifications.

The procedure B of the standard consists in: Mix the sample according to **chapter 3.3.2.1** and cast into the molds according to the ASTMC109 standard. After demolding, the mortar cubes of 50x50x50 mm size are stored in a humidity chamber at 23ºC and 100% RH during a specific time (standard specifies different curing times depending on the material). Afterwards, the cubes are placed in the acidic solution. The mass, the cross-sectional dimensions, the compressive strength and the visual inspection are measured at the following intervals: 1, 7, 14, 28, 56 and 84 days (more time if desired). After each measurement, the solution is renewed by a fresh acid solution.

Sulfuric acid was used to test the acid resistance of the mortars. This type of acid is considered as that causes more problems in real conditions, e.g. in sewage conductions.

The parameters of the test that have been evaluated are the acid concentration and the curing time. Curing time will give valuable information on the influence of the maturity of the AA binders versus the sulfuric acid resistance. Regarding the acid concentration, 3 different concentrations have been studied: 1, 3 and 5 wt.%. For the curing time, two ages of maturity have been evaluated, 7 and 28 days.

Moreover, in order to see the sulfuric acid resistance beyond the ages specified at the standard, the test was extended. Thus, the new measuring intervals were 7, 14, 21, 28, 56, and 84 days; and 16, 20 and 28 weeks, replacing the media solution in each measurement.

At the same time, this study also evaluates the applicability of the indicators of the degree of attack in the AAM, being in this test the mass and cross-sectional dimension change, the visual inspection, and the compressive strength. This evaluation will be done according to the corrosion mechanisms in each system (OPC, AAS, and AAFA).

3.5.4 Alkali-aggregate reaction

Two standards have been evaluated in this test: ASTM C1260 (*Potential alkali reactivity of aggregates (Mortar-Bar method)*) in mortars and ASTM C1293 (*Determination of length change of concrete due to alkali-silica reaction*) in concretes.

In both tests, a reactive aggregate has been used for this purpose. The reactive aggregate used is named Spratt, and is described in a previous section (**chapter 3.2.3.2**). The Spratt aggregate has been sieved according to the standards requirements, as shown in **table 3.9**.

The ASTM C1260 standard is an accelerated mortar bar test, consisting in mixing the sample according to **chapter 3.3.2.1** and molding according to the ASTMC109 standard. After demolding at 24 hours, the mortar bars of 25x25x285mm of size are placed in water at 80ºC during 24h. After this period, the first reading of the expansion and mass is taken, and then the bars are placed in 1M NaOH at 80ºC during 14 days. The standard specifies to measure the expansion and mass with at least 4 readings in that period.

Table 3.9 Grading requirements

ASTM C1260			ASTM C1293		
Sieve Size		Mass, %	Sieve Size		Mass fraction
Passing	Retained		Passing	Retained	Coarse
4.75 mm	2.36 mm	10	19.0 mm	12.5 mm	1/3
2.36 mm	1.18 mm	25	12.5 mm	9.5 mm	1/3
1.18 mm	600 µm	25	9.5 mm	4.75 mm	1/3
600 µm	300 µm	25			
300 µm	150 µm	15			

In this method, the influence of exposing the AAMs to 80ºC in a solution with a high concentration of alkalis has been evaluated. As AAMs hydration is enhanced by this conditions, the reactive aggregate and the binder could compete for alkalis. Also, the test has been extended to 28 days, to see the evolution after the 14 days period.

On the other hand, the ASTM C1293 standard, for concretes, consists inmixing the concrete according to **Chapter 3.3.2.2**, molding according to the ASTM C192 standard and conditioning the samples according to the ASTM C157 standard. After the conditioning period, the concrete prisms of 75x75x285mm size are placed in a storage container to persue the test. The storage container has enough water to keep a high level of humidity inside, and is sealed to prevent evaporation. The storage container with the bars inside is then placed in a chamber at 38ºC during all the test. At the following ages, the length and mass changes are measured: 7, 28 and 56 days; and 3, 6, 9 and 12 months. If desired, readings at every 6 months may be done after a year. The storage container has to be removed from the chamber set at 38ºC and placed in chamber at 23ºC for 16 hours before each reading.

This standard requires a minimum content of alkalis of 1.25 wt% Na_2O equivalent. Thus, only in the case of OPC formulation, it was necessary to add a specific quantity of NaOH to the mix water to reach that level. In the case of the AAM, as shown in **chapter 3.3.1**, all the alkali contents are higher than 1.25 wt.%, and the addition of NaOH was not necessary.

In this method, the parameter to study was the curing time before putting the bars in the storage containers at 38ºC (1 day according to the standard). Therefore, different curing times have been applied at 1, 28 and 90 days. It is pretended in this manner to observe the influence of allowing more time to the alkali-activated binders to fix the alkalis in the binder structure before accelerating the AAR by increasing the temperature, and thus, allowing less alkalis to participate in the AAR, according to Krivenko (1992).

3.5.5 Freeze-Thaw (F-T) resistance

The test was conducted following the instructions given in the ASTM C666 standard (*Resistance of concrete to rapid freezing and thawing*). More specifically, the procedure A of the standard was adopted, consisting in a rapid freezing and thawing in water. The procedure consisted in: mixing according to the **chapter 3.3.2.2** and molding according to the ASTM C192 standard. The air content was measured according to the ASTM C231 standard. After demolding, the specimens of 75x75x380mm size are stored in humidity chamber at 23ºC and 100% RH during 14 days. After the conditioning period, the specimens are brought to a temperature of 4ºC (thaw temperature) and the fundamental transverse frequency, the mass, the length and the cross-section dimensions are measured.

Subsequently, the specimens are placed in the thawing water and the F-T cycles are started. The temperature ranges between -18ºC in the freeze conditions to 4ºC in the thaw conditions. Every 36 cycles or less, measures are conducted when the specimens are in the thaw conditions, until a maximum of 300 cycles.

In this test, the parameter to study in order to see the effect of the method with AAMs was the conditioning period (14 days according to the test). Thus, three conditioning periods were studied: 7, 14 and 28 days.

Another considered parameter in this study was the effect of the air-entraining agent (AEA) in the stabilization of air voids in AAMs concretes, since its formation is essential in classic concretes to be frost resistant. The AEA used in this project was Airex-L (see **chapter 3.2.2.4**). In this sense, three sets of concrete specimens were confectioned in order to see the influence of the quantity of AEA. The first set of specimens were preparedwithout AEA, the second set with a dosage of 60mL/100kg of binder, typically used in OPC concretes to reach around 5 to 8% of air voids, and the third test with a dosage of 120mL/100kg of binder. This latter dosage is considered to fix a high percentage of air voids in OPC concretes. The air content was measured in fresh conditions according to ASTM C231 and in hardened conditions according to ASTM C457 (modified point count method).

3.5.6 Permeability

In this test, two test methods have been compared in order to see if both give comparable results with AAMs and which one gives more realistic information: the one described at the ASTM C1202 standard (*Electrical indication of concrete's ability to resist chloride ion penetration*) and a bulk resistivity test.

The method described in the ASTM C1202 standard is a method based on the Rapid Chloride Permeability test (RCPT). The procedure consisted in mixing the sample according to **chapter 3.3.2.1** and casting according to the ASTM C192 standard. After demold, cylinders of 100Øx200mm of size are stored in humidity chamber at 23ºC and 100% RH during 28 days. At 21 days in moist conditions, specimens are prepared for the test. For this purpose, it is necessary to cut a slice of 100x50mm of size from the top that will be the test specimen. When the specimen is cut, the longitudinal face has to be sealed and then specially conditioned according to the standard. Once the specimen is ready, it is tested in a RCPT cells (**figure 3.10**). This assembly is composed by two cells containing two solutions, 3 wt.% NaCl solution in one cell and 0.3N NaOH solution in the other. The test specimen is immersed between the cellules, and a 60V direct current is applied from the NaCl cell to the NaOH one. In this way, chloride ions circulate through the pore structure from one cell to the other. The current is applied

for 6 hours, controlling the temperature in each cell all the time to avoid overheating due to the current. After the 6 hours period, the total charge passed through the chloride ions is noted (Coulombs).

The advantage of this test is that it is very rapid, but there are some aspects to take into account. First, the conditioning period is laborious, there are a lot of steps to do in order to have the specimen ready for the test. Second, the applied charge is very high, and thus it could affect the pore structure of AAMs concretes (even for OPC concretes). The high alkali content in the pore structure of AAMs concretes could also overestimate the results, as the alkalis are highly conductive, like the chloride ions, and the total measured charge could be higher than the real. Else, as a consequence of the increase of the charge by the alkalis, the temperature could be raised too much and accelerate the ions movement, increasing the charge passed as well.

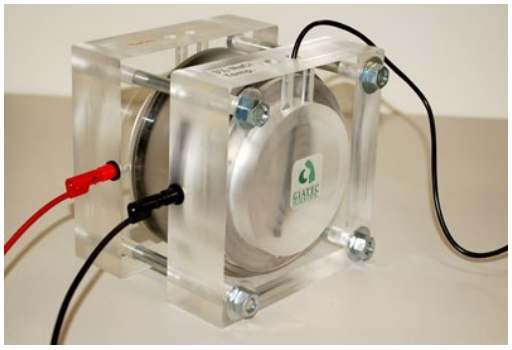

Figure 3.10 RCPT cell assembly with specimen

The surface resistivity test method starts to receive attention for permeability measurements, as most of the disadvantages of the RCPT method are eliminated and it is a non-destructive test. In the case of bulk resistivity (BR), two standards describing a test method can be found, the MTO LS-444 and ASTM C1760. In the case of the MTO LS-444, the described test method is only valid when using a specific equipment, not available at our laboratory. The ASTM C1760 uses the same equipment as the RCPT method with a high voltage (60V DC). However, DC has been found problematic due to inducing electrodes polarization (Polder 2001). Both methods have therefore been discarded. In this project, BR has been measured by means of the concrete resistivity meter Giatec RCON2. The test consisted in mixing the sample according to **Chapter 3.3.2.2** and casting according to the ASTM C192 standard. After demolding, cylinders of Ø100x200mm of size are stored at humidity chamber at 23ºC and 100% RH until desired age. Before the measurement, the specimen is placed in laboratory conditions during 5 min in order to get the longitudinal faces dried, but keeping the specimen saturated. Afterwards, both top and bottom faces are covered with an electrolytic gel that serves to minimize the resistance between the specimen and the wet sponges of the conductive plates (**figure 3.11**). Once the assembly is ready,

an AC current is applied with a frequency of 1 kHz. In few seconds the resistance of the sample is obtained (kΩ). Then, the resistivity is calculated according to a geometric factor to transform in kΩ/cm.

In order to compare if both methods give comparable permeability results, several specimens have been prepared. Permeability was then measured, by means of both test methods, at the following ages: 3, 7, 28 and 90 days. Separated specimens were used for each test at the specified times.

Comparing both test methods will give us fundamental information about the alkali fixation (from pore solution to the binder) that can interfere in the charge passed.

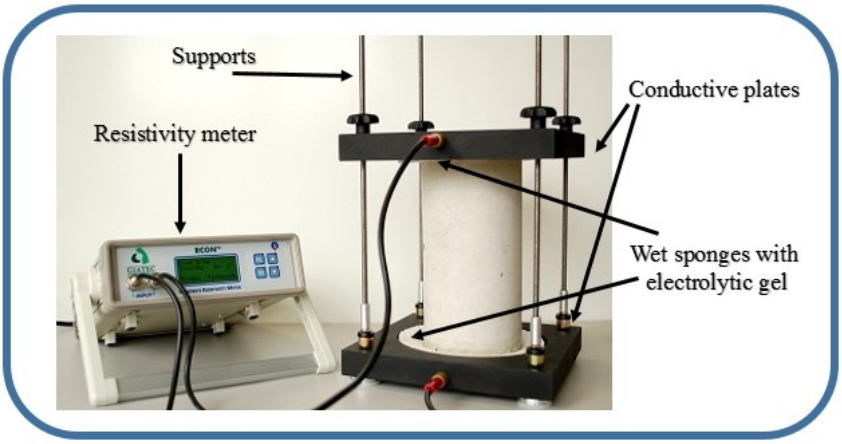

Figure 3.11 Bulk resistivity assembly with specimen

3.5.8 Sodium leaching in distilled water

This test has not been conducted according to standards. In this case, an experimental method has been used. The test consisted in: after mixing and casting according to **chapter 3.3.2.2** and the ASTM C157 standard, the mortar specimens of 25x25x285mm of size are demolded and stored in the humidity chamber at 23ºC and 100%RH. At the desired age, the specimens are put in distilled water, with a ratio of 6 parts of distilled water to 1 part of mortar in volume. Then, a sample of 20mL is taken every day for measuring the sodium content dissolved in the distilled water. The sodium content is analyzed by the inductively coupled plasma technique (ICP-MS) (see **chapter 3.6.7**). The distilled water is renewed every 7 days, until an age of 28 days.

In this test, it is pretended to observe the quantity of alkalis, in this case sodium, that are believed to pass to the distilled water from the pore structure [ref?]. This uptake of alkalis by the surrounding media could affect the performance of the binder. In that sense, the parameter to study in this test will be the curing time before the bars are submerged in the distilled water, such as 1 day, 7 and 28 days after demolding. During the curing time in humidity chamber, bars were stored inside a container, allowing

humidity pass but avoiding a direct contact with the water (or fog) in order to minimize any leaching of ions from the pore solution.

3.6 Characterization methods

3.6.1 Density

The density of each material was measured by a gas displacement Helium pycnometer, shown in **figure 3.12** (from *Quantrachome Instruments*).

Figure 3.12 Helium pycnometer

The measurement principle is to calculate the quantity of Helium gas required to fill the empty space of a weighted quantity of material in a known volume cell. Thus, knowing the volume of Helium gas used to fill the empty space of the cell (with a fixed volume) the volume occupied by the material will be obtained by difference. Knowing the weight of the material introduced in the cell as well as the volume of this material, the density will be obtained:

$$\rho = \frac{\text{mass}}{\text{volume of material}} \tag{3.2}$$

3.6.2 Blaine fineness

The Blaine test method has been traditionally used to determine the fineness of cement. This fineness is measured as specific surface, expressed as the surface of all material particles in a given quantity of material (cm^2/g).

The Blaine test method is an air permeability method. The principle of air permeabilimeters is to measure the time of a fixed quantity of air to flow through a compacted material bed (**figure 3.13**).

Depending on the particle size distribution (number and size of individual pores), the elapsed time of the air to flow through the compacted material bed will vary.

Figure 3.13 Blaine permeabilimeter

As this test method is comparative rather than absolute, the use of a reference sample with known specific surface to calibration purposes is always necessary.

The fineness is measured according to the following equation:

$$S = \frac{K}{\rho} \cdot \frac{\sqrt{e^3}}{(1-e)} \frac{\sqrt{t}}{0.1\eta} \tag{3.1}$$

where:

- K is the apparatus constant, obtained by the reference sample
- e is the porosity of the bed
- t is the measured time
- ρ is the density of the material
- η is the viscosity of the air at the test temperature

Thus, it is necessary to previously know the density and porosity of the material.

3.6.3 Laser diffraction particle size distribution

The laser diffraction technique was used to characterize the particle size distribution of raw materials. The equipment used was the Mastersizer 2000 by Malvern Instruments (**figure 3.14**). This equipment allows to measure particle sizes from 0.02 to 2000 microns in a single measurement, obtaining the particle sizes curve distribution.

This equipment uses the MIE diffraction theory of light scattering to calculate the particle size distribution, assuming an equivalent volume spherical model. The laser diffraction technique is based on the phenomenon that all particles scatter light in all directions with an intensity pattern which depends on the total particle size. This scattered light has different intensities depending on the angle of observation.

The technique consists in impacting a laser beam on a dispersed sample, capturing the resulting scattered light in several detectors. Thus, angular scattering intensity data is used to calculate particle size distribution according to the MIE theory.

Figure 3.14 Laser diffractometer

3.6.4 Chemical composition by means of X-ray fluorescence spectrometry (XRF)

Chemical composition of raw materials was performed by X-ray fluorescence spectrometry by means of dispersive wavelengths, using reference standards guaranteeing traceability of measures. The equipment used in this project was the AXIOS PANALYTICAL spectrometer model equipped with Rh tube and 4kW power.

This technique consists in irradiating a sample with X-ray beam. Then, the excited sample emits X-rays in turn, along a spectrum of wavelengths characteristic of the types of atoms present in the sample. The emission of characteristic X-rays indicates the type of atoms present in the sample. With the help of detectors, the intensity of these emissions are measured. The intensity of the energy measured by these detectors is proportional to the abundance of the element in the sample.

3.6.5 Mineralogical characterization by means of X-ray diffraction (XRD)

This technique is used for determining the mineralogical composition of raw materials. The technique examines the crystal structure of a solid material by means of the diversion that a primary or monochromatic X-ray beam experiment when is passed through a sample. The deflection angles are closely related to the distance between the planes of the crystal lattice of the material, following the so-called Bragg's law (**equation 3.3**), where "n" is a positive integer (order of reflection), "λ" is the wavelength of X-rays, "d" is the interplanar distance between two successive atomic planes in the crystal and "θ" is the scattering angle formed in the atomic plane between the incident and reflected beam. The values of "d" and the number and type of atoms on each plane are unique to each mineral. The reflected beam is therefore measured by a detector.

$$n\lambda = 2d \cdot \sin\theta \qquad \text{Bragg's law} \qquad (3.3)$$

In this project, XRD analyses were performed using an X'pert Pro MPD difractometer from PANalytical in CuKα configuration (**figure 3.15**).

Figure 3.15 X-ray difractometer

Data was obtained by scanning at 0.1° (2θ) with divergence slits degree of 1/4°. Analyses were conducted between 5 to 70 2θ angles. Data was then analysed with the JADE 2010 software in order to identify the peaks of the spectra.

3.6.6 Microstructural analysis by means of Scanning electron microscope (SEM)

SEM is a widely used technique in research that provides useful information about the sample by means of high resolution micrographies.

The principle of this technique is based on the interaction of a beam of electrons with the atoms of the sample. This interaction produces a series of signals that are recorded by several detectors. Thus, depending on the type of signals produced, different information can be obtained (surface topography and composition). The different types of emitted signals are:

- Secondary electrons (SE): Provide high resolution images of sample surface with a three-dimensional appearance.
- Back-scattered electrons (BSE): Images with less resolution, but provide useful information about the distribution of the elements in the sample.
- X-ray (EDX): Provide information about the composition and abundance of each element in the sample.

In this project, Hitachi S-3400N SEM equipped with an energy dispersive X-ray spectroscopy (EDX) was used for microstructural observation (**figure 3.16**).

Figure 3.16 Scanning Electron microscope

All the analyses were performed in BSE mode with polished surfaces. Thus, samples were polished prior the test as follows: a piece of sample was placed into a mold and embedded with an epoxy resin within a hardener. Once hardened, sample was demolded and cut with a diamond saw in order to have part of the sample exposed in the surface. Then, surface was polished with different polishing cloths sizes (15, 3 and 1 μm). Sample surface was polished two times for each polishing cloths sizes (4 min each). After each polishing step, sample was immersed in ethanol and ultrasounds were applied in order to clean it during 4 min.

3.6.7 Inductively coupled plasma – Mass spectroscopy (ICP-MS)

The ICP-MS is a technique based on the coupling of a method for generating ions (inductively coupled plasma) and a method for separating and detecting ions (mass spectrometer). This technique allows

elemental analysis of most of the metallic elements of the periodic table. Using different strategies, elements of a sample are converted into atoms or ions to be analyzed.

In the ICP techniques, an argon (Ar) stream is introduced into a radiofrequency field where the kinetic energy of the Ar^+ ions can generate temperatures of 8000ºC. At this temperature, ionization, excitation and subsequent emission of radiation of the elements (atoms and ions) present in the sample occur. Different techniques can be found in order to measure these atoms and ions. Thus, ICP-AES (atomic emission spectroscopy), ICP-MS (mass spectroscopy) and ICP-RIE (reacting-ion etching), among others can be found. In this project, the technique used was the ICP-MS. ICP-MS separates the ions based on their mass to charge ratio. Then, a detector receives the ion signals proportional to the concentration.

CHAPTER 4. Applicability of the durability test methods to traditional alkali-activated materials

In this chapter, the results of the phase 1 of the project are presented.

4.1 Compressive strength

The compressive strength of OPC, AAS, and AAFA mortar cubes are shown in **figure 4.1**. We can observe the behavior of the mechanical properties of each system depending on the curing temperature during the first 24 hours: 23, 35 or 80ºC. After the first 24 hours, in all the cases the mortar cubes were stored at 23ºC and 100% RH until test. These curing temperatures have been used as the following: 23ºC is the normal curing temperature for laboratory tests, 35ºC have been used in order to reproduce the sulfate resistance test conditions (see **Chapter 3.5.2**), and 80ºC is the curing temperature for the AAFA system (see **Chapter 3.3.2.1**).

In the case of OPC mortars (**figure 4.1a**), it can be observed that the best compressive strength after 28 days is obtained with a normal curing at 23ºC, with 40 MPa. When the specimens are heated during the first day at 35ºC, the compressive strength after the 1st day is increased from 15 MPa in the case of 23ºC, to 21 MPa. However, the evolution of the compressive strength afterwards is not the same as for 23ºC. As it can be observed, the compressive strength at 7 and 28 days is lower than those obtained when the mortar cubes were maintained at 23ºC. The same behavior is observed when the specimens are heated at 80ºC during the first day. In this case, the compressive strength is increased up to 33 MPa, but then decreases to 3 MPa to thereafter raise a little after 28 days.

The lower compressive strength of the OPC mortar cubes at later ages when they are cured at elevated temperatures is related to the total porosity. When a thermal curing is applied, the reaction rate is accelerated and hydration products precipitates near the anhydrous cement particle because at this point the diffusion rate is lower than the reaction rate. Thus, the hydration products do not have time to diffuse correctly to the matrix producing a heterogeneous microstructure. Moreover, CSH gel formed is denser and hinder the further hydration of the unhydrated particle (Kjellsen et al. 1991; Thomas et al. 2003; Lothenbach et al. 2007). Due to this fast formation of CSH gel, it will not diffuse to the capillary pore space with the same efficacy, and consequently the final porosity of the system will be increased. This higher porosity is marked by a lower compressive strength at later ages, as shown in the results. It is also observed that when the curing temperature was 80ºC, after 7 days the compressive strength decreased 3 MPa. Afterwards, the compressive strength increases but with a very slow rate of reaction. As shown by other authors (Al-Dulaijan et al. 1990; Elkhadiri et al. 2009) when OPC mortars are

subjected to elevated temperatures, specifically above 55ºC, the compressive strength continuously decrease because of an increase of the porosity. When we stop applying the elevated temperatures, it is supposed to continue the hydration as normal, with a low reaction rate, and thus corroborating with the slight increase of the compressive strength at 28 days shown in the results.

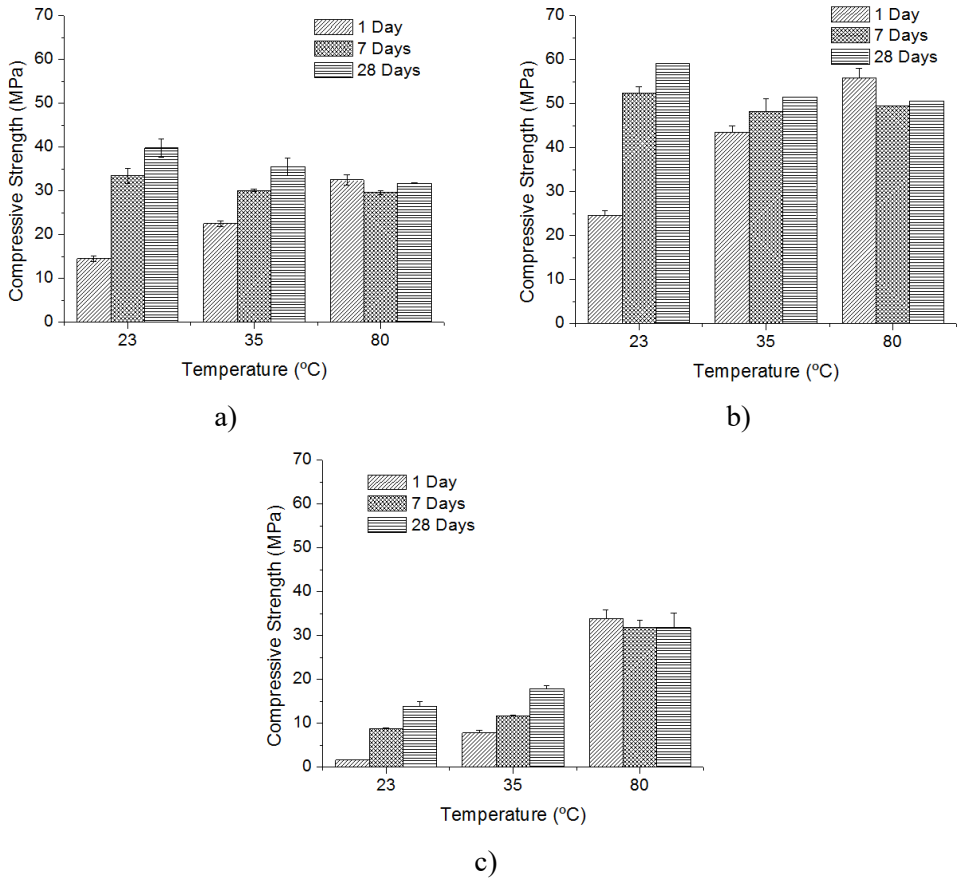

Figure 4.1 Compressive strength for OPC (a), AAS (b) and AAFA (c) mortars at 1, 7 and 28 days for different curing temperatures during the first 24h: 23, 35 and 80ºC, followed with a normal temperature of 23ºC until test.

In the case of AAS (**figure 4.1b**), similar behavior as in OPC is observed. The best compressive strength after 28 days is obtained with a normal curing at 23ºC, with 59 MPa. As for OPC, when we heat during the first day at 35 or 80ºC, the compressive strength after the 1st day is increased from 25 MPa in the case of 23ºC, to 44 and 56 MPa respectively. Afterwards, the compressive strength of the mortar cubes cured at 35ºC the first day continue increasing up to 52 MPa at 28 days (lower than in the case of 23ºC), and for the bars heated at 80ºC, there was a decrease of 6 MPa at 7 days, with a slight increase to 51MPa at 28 days. Similar results were reported by other authors (Bakharev, J.G. Sanjayan, et al. 1999; Chi et al. 2012), where they obtained better final resistance for the AAS cured at 23ºC than those cured at elevated temperatures.

In AAS system, similarly to OPC, when a thermal curing is applied, the reaction rate is increased and hydrated products do not have time to diffuse efficiently and remain close to the anhydrous slag particles. This creates a heterogeneous microstructure with more interstitial space. Moreover, the denser CSH gel near the slag particles may hinder further hydration acting as a barrier for the diffusion (Bakharev, J.G. Sanjayan, et al. 1999). Consequently, like for OPC, the porosity will increase and thus the compressive strength is lower when the system is cured at elevated temperatures as results showed. As for OPC, when mortar cubes were heated at 80ºC during the first 24 hours, they experienced a loss in compressive strength at 7 days of 6MPa. These results are also in accordance with those obtained by other authors (Fernández-jiménez et al. 1999), where heated specimens at 45ºC during the first 24 hours experimented a loss of compressive strength at 7 days, and compressive strength continued increasing with a normal tendency afterwards.

Regarding the AAFA (**figure 4.1c**), as it was expected, the compressive strength for mortar cubes cured at normal temperature (23ºC) did not achieve a high compressive strength, because of the particularity of these systems that need a thermal curing in order to accelerate the hardening process (Palomo, Grutzeck, et al. 1999). The mortar cubes cured at normal temperature, of 23ºC, reach 14 MPa at 28 days. When we heat at 35ºC during the first 24 hours, the compressive strength after the 1st day reaches 7 MPa, and 17 MPa at 28 days. But when we heat during the first 24 hours at 80ºC, the compressive strength is improved, obtaining all its performance after the 1st day (34 MPa). This compressive strength decreases slightly after 7 days, and then keeps constant up to 28 days.

In this case, when FA is used as a precursor of AAM, a different hydration process than those occurred in OPC and AAS takes place. In these systems, thermal curing at elevated temperatures is sometimes necessary (depending on its composition and physical properties) for a good dissolution of all the FA components. If a bad dissolution takes place, the reaction rate as well as the hydration degree will be low and leave high anhydrous FA particles and more porous microstructure. This is evident in the results, where mortar cubes cured at 23ºC and 35ºC (firsts 24 hours) had less strength than those cured at 80ºC. This behavior is also evident in other precursors for AAMs, as the metakaolin (Muñiz-Villarreal et al. 2011; Bing-hui et al. 2014). When a thermal curing of 80ºC is applied, the compressive strength is increased after the 1st day, and then decreases slightly and keeps constant. These results are in the line with studies done by other authors (Bakharev 2005b) who found a maximum of compressive strength after thermal curing at elevated temperatures (75 and 95ºC) that then decreased slightly to maintain a constant value. They also argue that this behavior is mostly due to the conditions of curing, and can be avoided by restricting the thermal curing time.

4.2 Dimensional stability in water

Figure 4.2a and b shows the length change of the OPC, AAS and AAFA mortar bars stored in water during 7 days when they were subjected to thermal curing during the first 24 hours at 35 and 80ºC. As it can be observed, the dimensions of the OPC bars heated at 35ºC (**figure 4.2a**) remained practically constant until 7 days, showing a negligible shrinkage. The AAS bars, after 1 day experimented an expansion up to 0.02%. The AAFA, contrary to the other, experimented a rapid expansion at 15 min of 0.05%. After 7 days, the expansion of all the specimens kept practically constant during time.

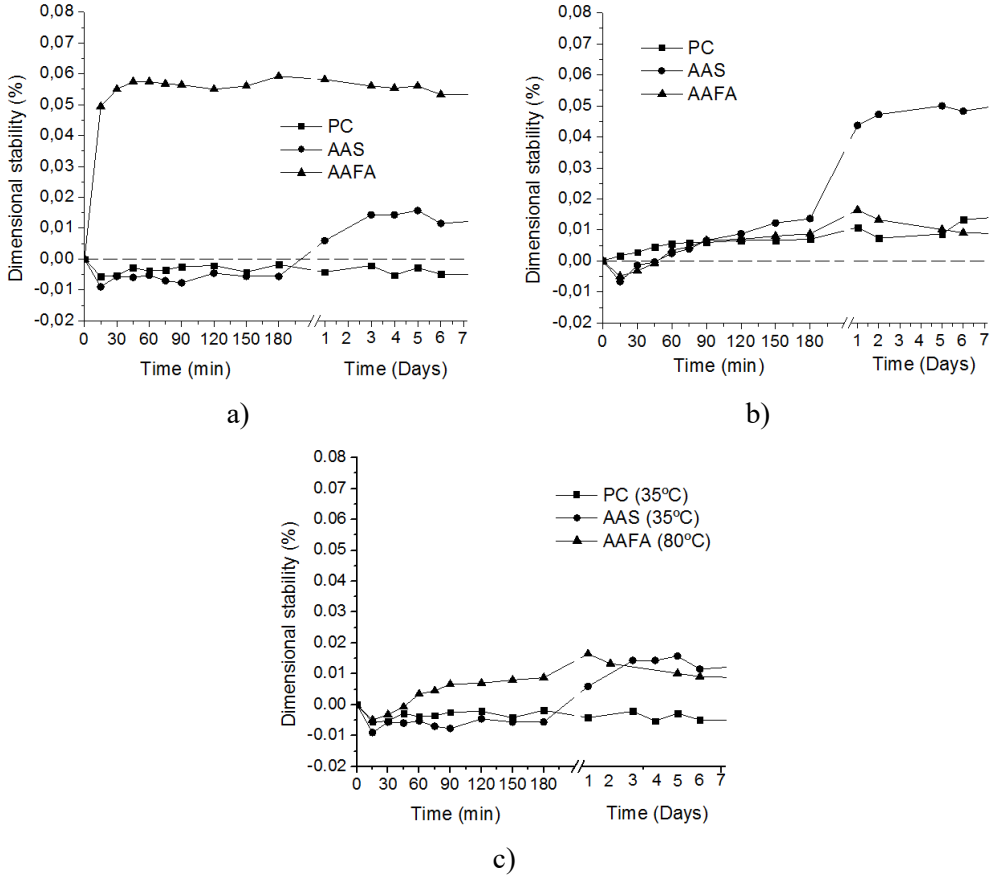

Figure 4.2 Dimensional stability of OPC, AAS and AAFA mortar bars submerged in water during time: a) Curing procedure 35ºC (24h) + 23ºC, b) 80ºC (24h) + 23ºC, c) Comparison of OPC and AAS cured at 35ºC with FA cured at 80ºC.

OPC bars heated at 80ºC (**figure 4.2b**) experimented an expansion of 0.01% the 1st day, remaining practically constant until 7 days. The AAS bars experimented a high expansion the 1st day of 0.045%, and then slightly increasing to 0.05% up to 7 days. The AAFA bars experimented an expansion of 0.01% that kept practically constant during time. As occurred with the bars cured at 35ºC, after 7 days the expansion kept practically constant during time.

In OPC system when the bars were cured at 80ºC and, in AAS system when the bars were cured at 35ºC and 80ºC, an expansion was observed at 7 days. This behavior can be related to the total porosity of the microstructure, as explained in **chapter 4.1**. Therefore, this expansion is attributed to the water absorption by the total porosity. As the mortar bars are cured at elevated temperature, the total porosity is higher and thus the water uptake is higher, resulting in higher expansion.

In AAFA system, another behavior is observed. When the bars are heated at 35ºC, there is an expansion that is not observed when cured at 80ºC. This is consequence of the special thermal curing of the AAFA that requires energy in order to accelerate the hydration rate and thus the improvement of the microstructure properties. As explained in **chapter 4.1**, at 35ºC the total porosity is higher than that at 80ºC (corroborated by the compressive strength results) resulting in higher water absorption and thus higher expansion.

Comparing each system with its better curing temperature (**figure 4.1c**) (for OPC and AAS 35ºC and for AAFA 80ºC), it can be seen similar behavior despite minor differences. Thus, it can be concluded that each systems needs its curing conditions in order to have similar behaviors.

4.3 Sulfate resistance

4.3.1 Expansion results

Figure 4.3, 4.4 and 4.5 shows the sulfate expansion results for the OPC, AAS and AAFA mortar bars respectively. The influence of the sodium sulfate concentration (2, 5 and 8 wt%), and the curing temperature during the first 24h on the results is reported up to 1 year. Note that after the special curing temperature during the first 24h at 35ºC and 80ºC the test was conducted until the end at 23ºC.

In **figure 4.3a** it can be observed the expansion curves when all the OPC bars have been stored at 23ºC. In this case, the bars were put in the sulfate solutions after 2 days, because the compressive strength after the 1st day was below than 20 MPa required by the standard ASTM C1012 (14.5 MPa at 1 day, 22.2 MPa at 2 days). In all the sulfate concentrations, the bars exceeded the limit compliance specified in the ACI 201.2R-08 (*Guide to durable concrete*) for Class 2 exposure, of 0.05% at 6 months and 0.10% at one year. In the **table 4.1**, it can be observed the exact date when the test failed in each case. The expansion was higher and faster with higher sulfate solution concentration.

Figure 4.3b shows the OPC bars expansion when the curing temperature was 35ºC during the first 24h (conditions described at the standard ASTM C1012). In this case, also all the bars exceeded the limit compliance at 6 months and 1 year, except the bars exposed at 2wt% of sulfate concentration, that passed the test at 6 months, but failed at 1 year. However, even if the test failed too, results were better

compared to the bars exposed all the time at 23ºC (**figure 4.3a**). Also, there was a correlation between the sulfate concentration and the expansion, where thee expansion increases with the increase of the sulfate solution concentration.

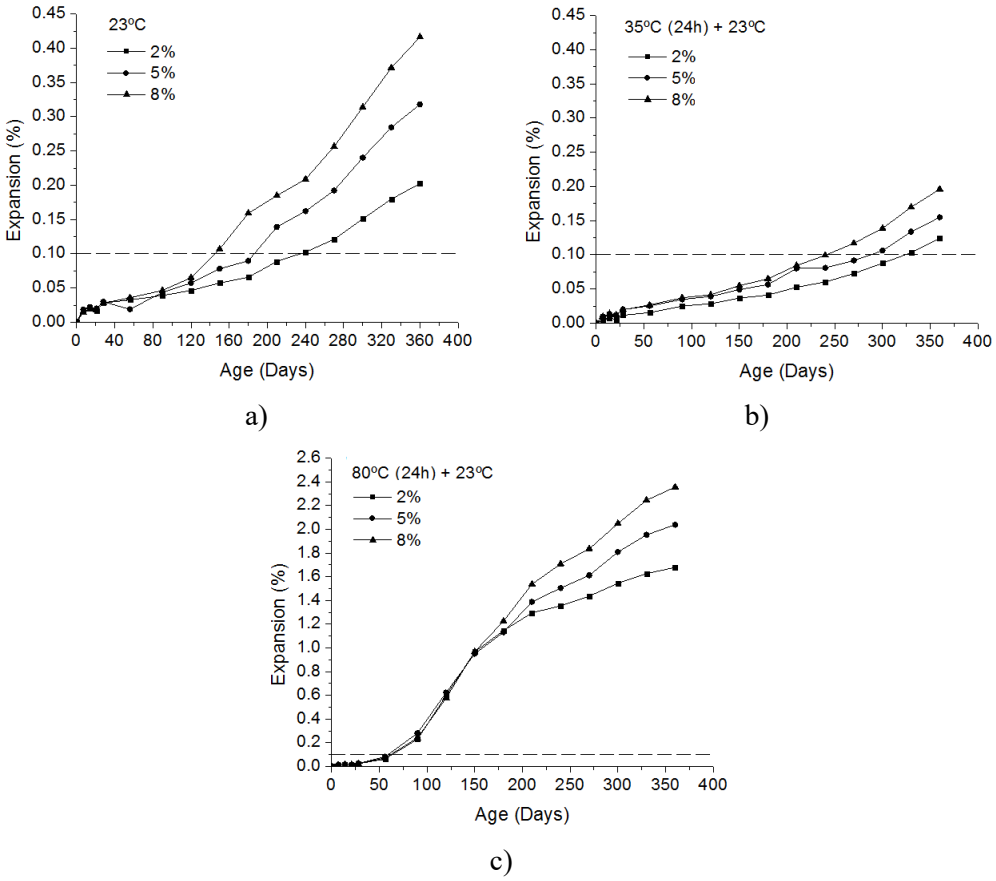

Figure 4.3 Sulfate resistance for OPC bars (ASTM C1012) at 2, 5 and 8% of sulfate concentrations. a) Curing temperature for first 24h of 23ºC. b) 35ºC. c) 80ºC, followed by a normal temperature conditioning at 23ºC.

Figure 4.3c shows the OPC bars expansion when the curing temperature was 80ºC during the first 24h. In this case, with an unusual curing conditions for this system, the bars experimented a fast and high expansion after 50 days. This expansion was practically the same for all the sulfate concentrations up to 150 days, when the bars subjected to higher sulfate concentration started to expand more. All the bars exceeded the limit compliance at 1 year after 60 days.

Figure 4.4a shows the sulfate expansion results for the AAS mortar bars when all the bars have been at 23ºC. As it can be observed, there were no expansion in none of the sulfate concentrations, and it

was found that the sulfate concentration had no influence on the results. **Figure 4.4b** shows the sulfate expansion results for the AAS mortar bars when the curing temperature was 35ºC during the first 24h.

Table 4.1. Expansion of OPC mortar bars at 6 and 12 months

	6 months			12 months		
Na_2SO_4 wt%	2	5	8	2	5	8
23ºC	0.07	0.09	0.16	0.20	0.32	0.42
35ºC (24h) + 23ºC	0.04	0.06	0.07	0.12	0.16	0.20
80ºC (24h) + 23ºC	1.14	1.13	1.22	1.68	2.04	2.36
Limit compliance*	< 0.05%			< 0.10%		

* According ACI 201.2R-08 for Class 2

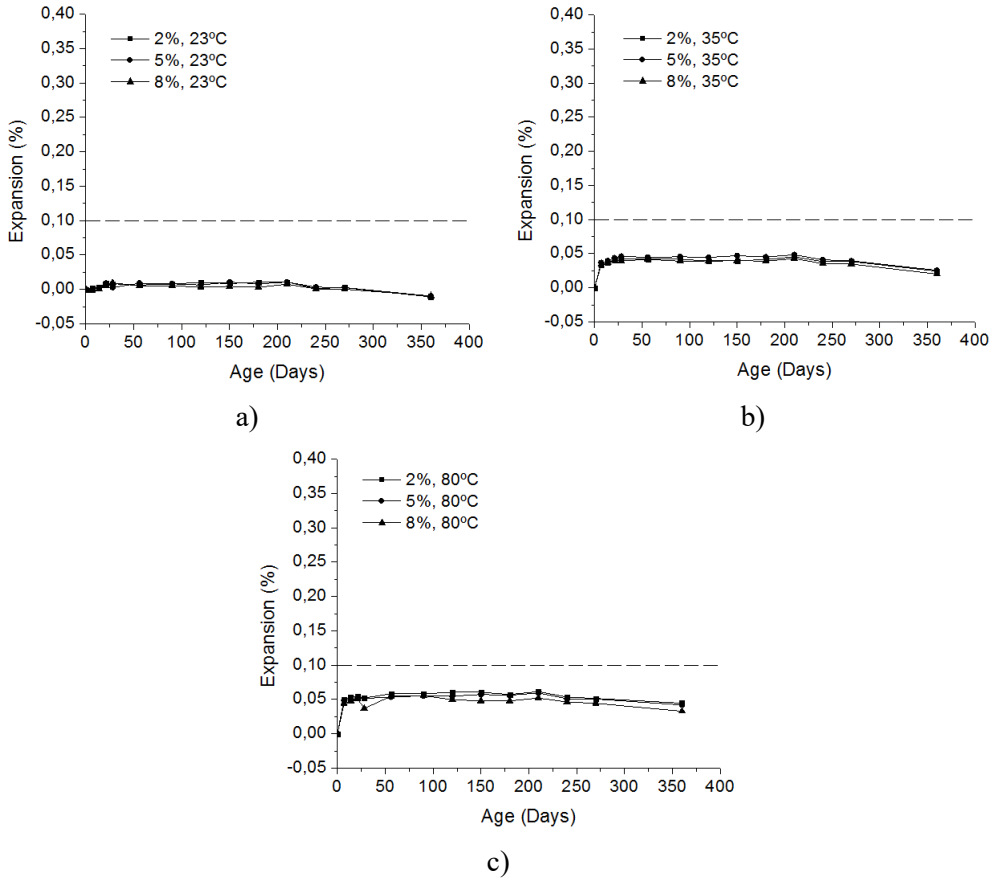

Figure 4.4 Sulfate resistance for AAS bars (ASTM C1012) at 2, 5 and 8% of sulfate concentrations. a) Curing temperature for first 24h of 23ºC. b) 35ºC. c) 80ºC.

In this case, a rapid expansion after the first week of immersion was observed, but afterwards the expansion is kept constant and showed the same tendency like the bars exposed all the time at 23ºC (**figure 4.4a**). This behavior correlates well with the results of dimensional stability test, where the bars

exposed only to tap water experimented a similar expansion at 7 days than the bars exposed to sulfates. Then, this expansion is attributed to the water absorption of the bars, and not to sulfate attack. **Figure 4.4c** shows the sulfate expansion results for the AAS mortar bars when the curing temperature was 80ºC during the first 24h. As it happened with the bars cured at 35ºC, a rapid expansion occurred after the first week of immersion that kept constant afterwards. This expansion correlates well too with the results of dimensional stability test, and it is attributed as well to the water absorption.

Figure 4.5a, b and c shows the sulfate expansion results for the AAFA mortar bars when they were cured at 23, 35 and 80ºC respectively. For the bars cured at 23 and 35ºC, the test was started after 28 days of curing, even if the compressive strength did not achieve the 20 MPa required at the standard ASTM C1012 (14 MPa and 18 MPa at 28 days respectively) (see **figure 4.1c**). Because of the slow hardening reactions for this FA at normal curing temperatures, it would have been necessary to attend too much time to get 20MPa and thus start the test (mostly for those cured at 23ºC). Consequently, it was decided to start the test after 28 days as the goal of this test is rather to study the influence of the test parameters, and it was thought interesting to see the influence of the compressive strength. All of these bars were stored in a moist chamber (100 %RH) at 23ºC until tested. As it can be observed, there was not any expansion for all the conditions, and it was found that the sulfate concentration had not influence on the results. Instead, a little shrinkage during time was observed for all the bars in all the conditions.

4.3.2 Mineralogical characterization by means of X-ray diffraction

XRD experiments were performed on samples after 1 year exposed to sulfate solutions. For each system, a piece of one bar for each sulfate concentration and each curing temperature was taken to analysis.

Figure 4.6a, b and c provides the XRD spectra for the OPC specimens when curing temperatures were 23, 35 and 80ºC respectively. It can be observed that the peaks found are the same in all the cases, with different intensity depending on the curing temperature. Those peaks are: Q, quartz; X, C-S-H gel; P, portlandite; E, ettringite and G, gypsum.

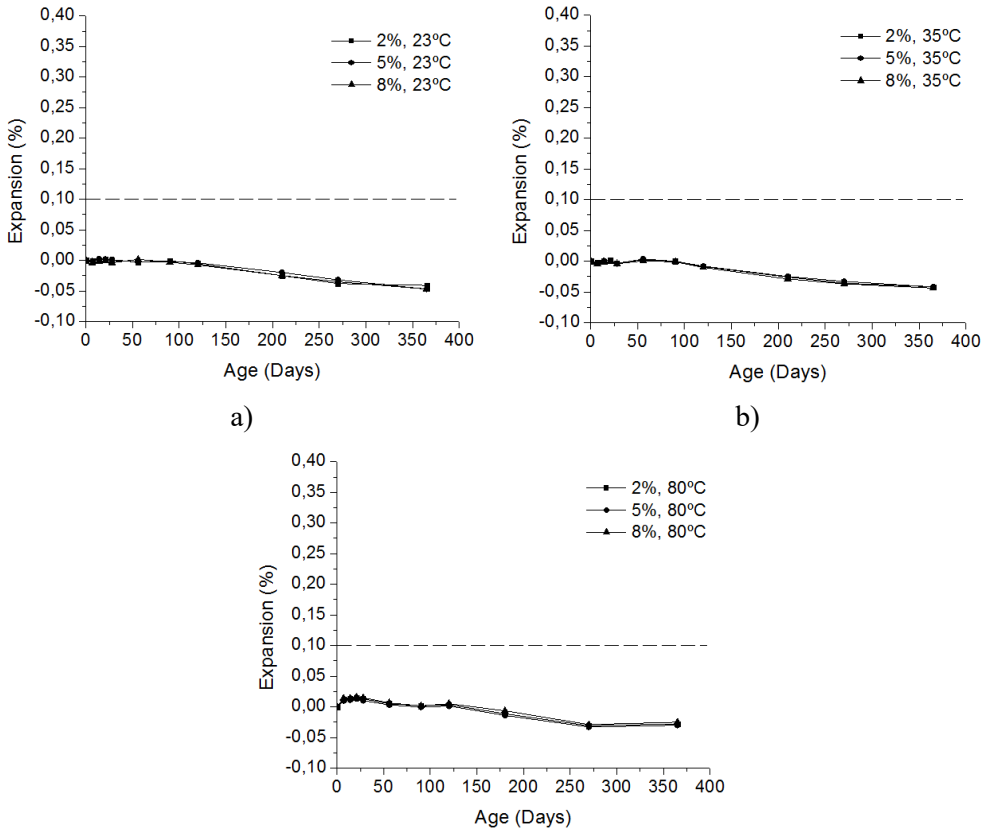

Figure 4.5 Sulfate resistance for AAFA bars (ASTM C1012) at 2, 5 and 8% of sulfate concentrations. a) Curing temperature for first 24h of 23ºC. b) 35ºC. c) 80ºC.

In the case of the OPC bars cured the whole time at 23ºC (**figure 4.6a**), the intensity of the main peak of portlandite (2θ = 18.0) decreased slightly when the sulfate concentration in the solution was higher, meanwhile the other portlandite peaks kept practically constant. At the same time, the intensity of the main peak of the ettringite (2θ = 9.1) increased slightly with the sulfate concentration. The intensity of the main peak of gypsum observed in the 2θ = 11.6 increased too when higher was the sulfate concentration, keeping very close when the sulfate concentrations were 5 and 8wt%. These results are in line with the fact that when more sulfates are available in the solution, more of them will react with the portlandite present in the OPC mortar, as it is noted by a decreasing of the intensity of the portlandite peaks. Therefore, the portlandite reacts with the sulfates to form in a first step gypsum, also found in the analysis, that finally will convert to ettringite (Eglinton 2003). Both gypsum and ettringite are found to increase with the sulfate concentration, with the consequent decrease of the portlandite. The ettringite and gypsum are thus responsible of the expansion observed in the **figure 4.3a**. The region attributed to the C-S-H gel (2θ = 29.0) was practically the same in the 3 cases, indicating the stability of the gel in these conditions. The huge peaks of quartz observed in all the conditions are due to the sand used for

the confection of the mortar specimens. These peaks of quartz are not illustrated completely because of rescaling the figure to better differentiate the important peaks. Therefore, this rescaling is applied in all the XRD figures.

When the OPC bars were cured during the first 24 hours at 35ºC (**figure 4.6b**), there is not a clear evolution of the peak intensity with the sulfate concentration. Regarding the peaks of gypsum and ettringite, they seem to keep constant with the sulfate concentration. For the portlandite, the main peak intensity increased with 5% of sulfates, but decreased at 8% to the minimum value. With a normal behavior, when more sulfates are present in the solution, more will be able to react with the portlandite, so the peak intensity of portlandite expected at 5% should be lower for 2% (as it happens with 8% of sulfates). Nevertheless, the intensity of the XRD peaks should be carefully taken for quantifying the compounds. The ettringite and gypsum are therefore responsible of the expansion observed in **figure 4.3b**. In the case of the CSH gel (X), the intensity of the peak is kept constant in every case. Compared to the bars cured at 23ºC all the time, the peaks of the portlandite, gypsum and ettringite had lower intensity in this case (35ºC). Lower quantity of the gypsum and ettringite will result in lower expansion, as it is corroborated by the expansion results shown in **figure 4.3a and b**, where the bars cured at 35ºC the first 24 hours got lower expansion than the bars cured the whole time at 23ºC in every sulfate concentration.

When the OPC bars were cured during the first 24 hours at 80ºC (**figure 4.6c**), as for 35ºC (**figure 4.6b**), there was not a clear evolution of the peak intensity with the sulfate concentration. It was observed that the intensity of the main peak of portlandite, gypsum and ettringite was practically the same for 2% and 8% of sulfate concentration, while for 5% was lower. Regarding the expansion (**figure 4.3c**), there is a clear difference with the sulfate concentration, with more expansion with higher sulfate concentration. Compared to the bars cured at 23ºC and 35ºC, the main peak of the portlandite had lower intensity in this case, while the main peak of gypsum and ettringite were higher. This is in line with the expansion results (**figure 4.3a, b and c**), where the bars cured at 80ºC during the first 24 hours suffered a much higher expansion than those cured at 23 and 35ºC, attributed to a higher formation of gypsum and delayed ettringite.

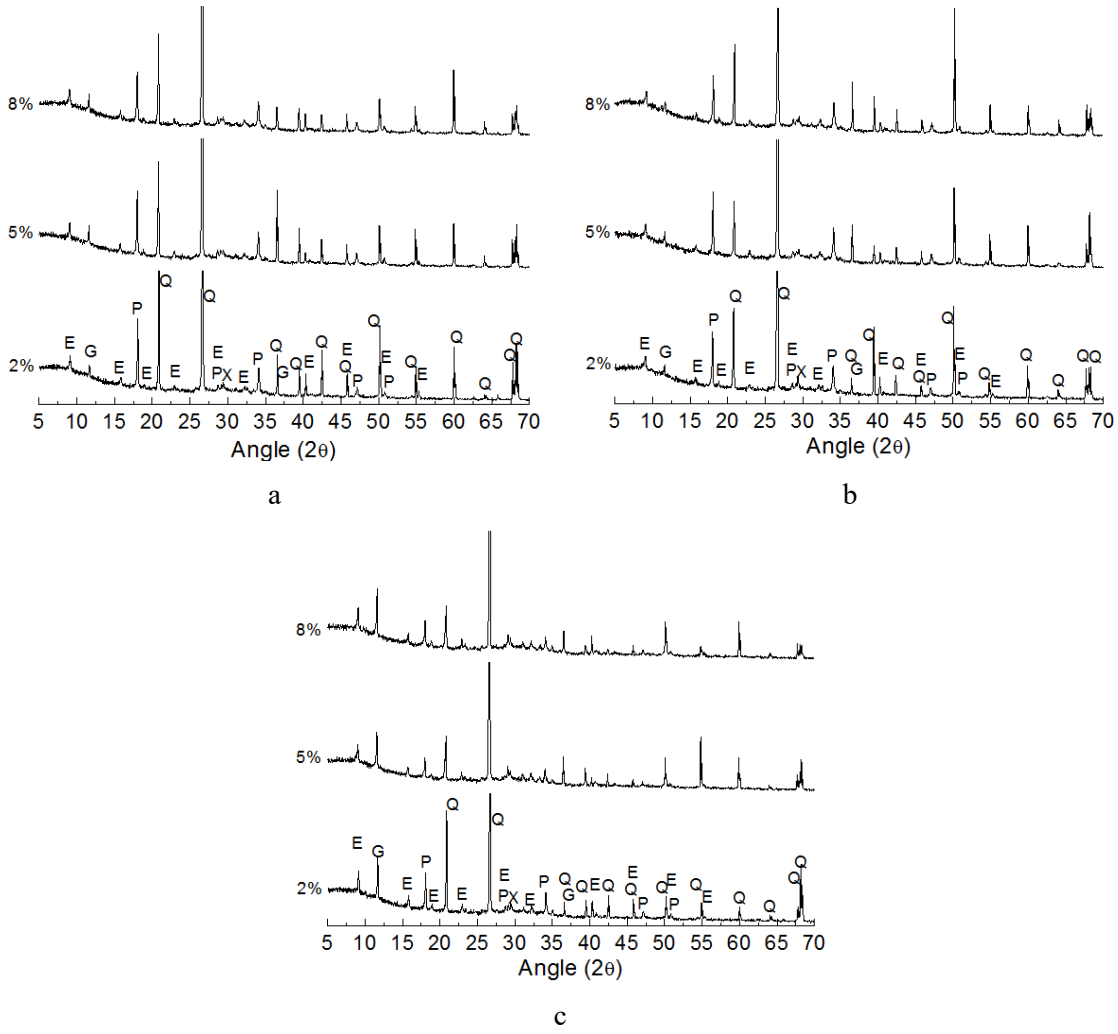

Figure 4.6 XRD patterns for OPC mortar bars exposed at different sodium sulfates dissolutions (2, 5, and 8wt%) after 1 year of exposition. a) curing temperature during the first 24h: 23ºC; b) 35ºC; c) 80ºC. Peaks: E, ettringite; G, gypsum; P, portlandite; Q, quartz; X, C-S-H gel

Figure 4.7a, b and c provides the XRD spectra for the AAS specimens when curing temperature was 23, 35 and 80ºC respectively. In this case, the peaks found where quartz (Q), C-(A)-S-H gel (X) and hydrotalcite (HT). This compounds are in accordance with the findings of other studies for AAS at normal curing conditions (Wang & Scrivener 1995; Puertas et al. 2002; Gruskovnjak et al. 2006). No other peaks of crystalline products due to sulfate attack were found, in accordance with the expansion results shown in **figure 4.4a, b and c**. The intensities of the main peak of C-(A)-S-H gel (2θ = 29.3) and hydrotalcite (2θ = 11.3) are practically the same in all the cases, indicating its stability to sodium sulfate attack. The peaks of quartz varies depending on the sampling process, and it os due to the sand used in the confection of the mortars. Similar results were obtained by other authors in similar attack conditions (Komljenović et al. 2013).

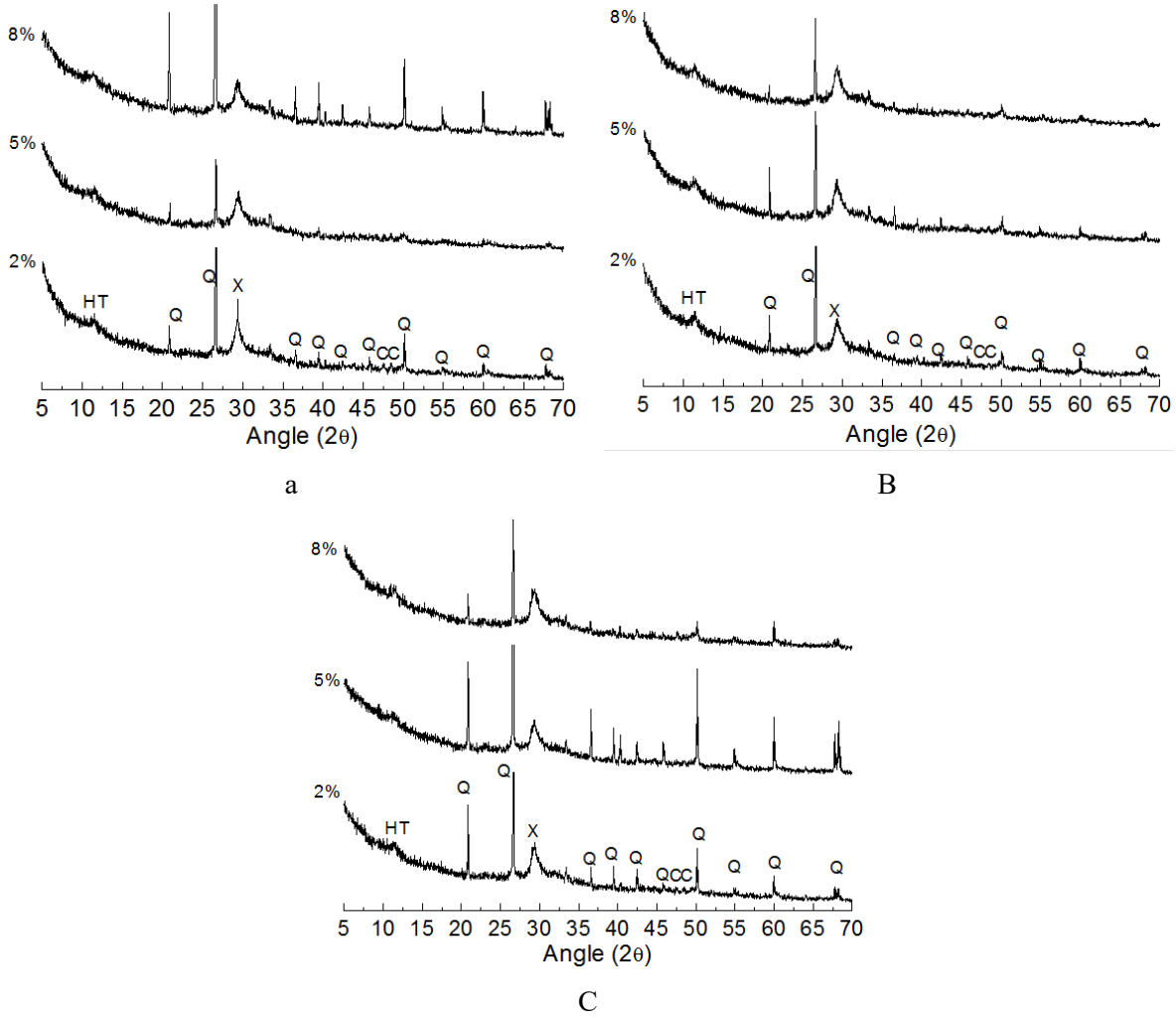

Figure 4.7 XRD patterns for AAS mortar bars exposed at different sulfates dissolutions (2, 5, and 8wt%) after 1 year of exposition. a) curing temperature during the first 24h: 23ºC; b) 35ºC; c) 80ºC. Peaks: Q, quartz; X, C-(A)-S-H gel; HT, hydrotalcite; C, calcite.

Figure 4.8a, b and c provides the XRD spectra for the AAFA specimens when curing temperature were 23, 35 and 80ºC respectively. In this case, as it happened with the AAS specimens, no peaks of the presence of new crystalline products due to the sulfate attack were found. The peaks found were mostly the crystalline phases of the unhydrated FA (M, mullite; N, magnetite) (see Chapter 3.2.1.3) plus the quartz due to the sand used for the confection of the mortar.

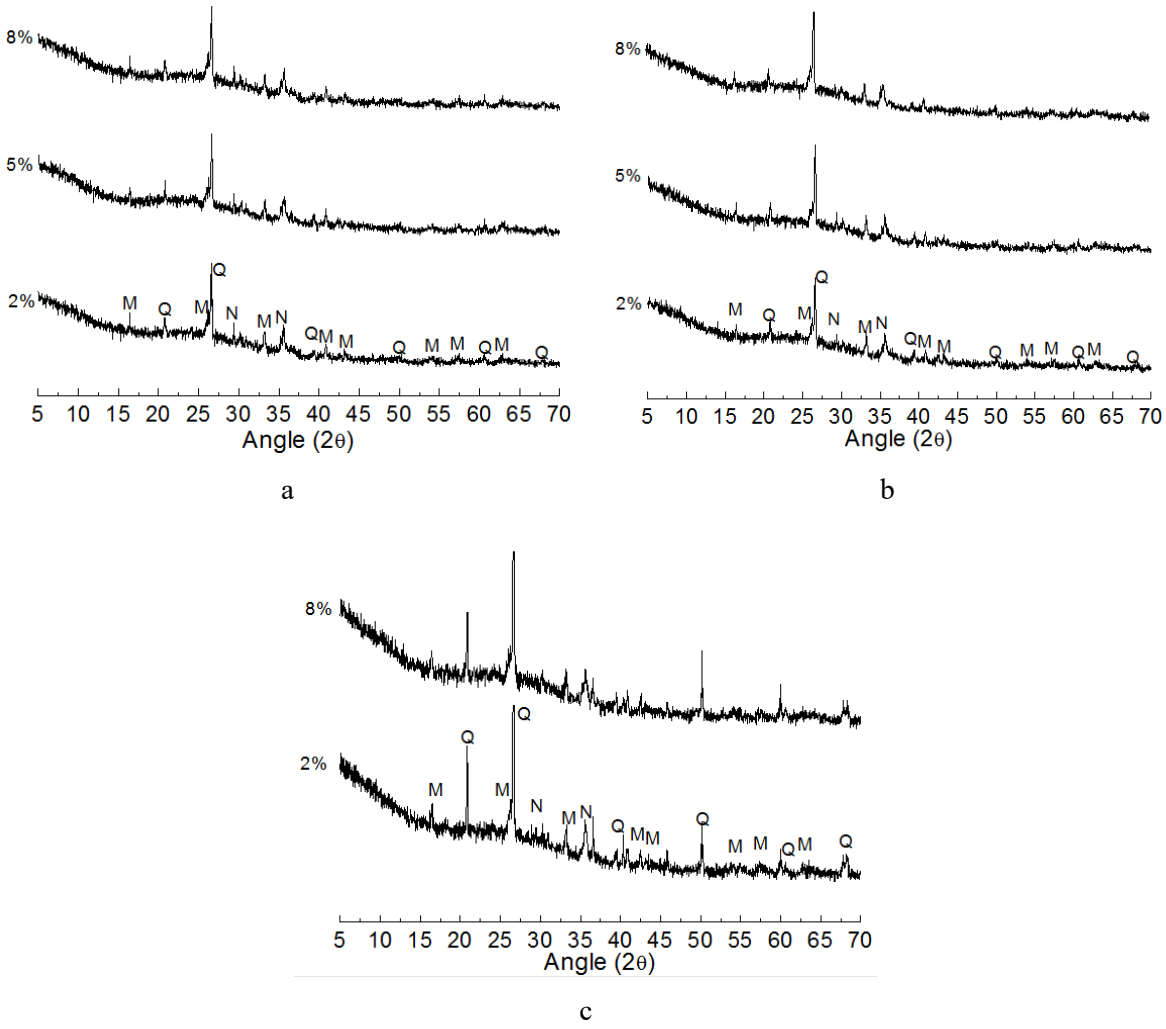

Figure 4.8 XRD patterns for AAFA mortar bars exposed at different sulfates dissolutions (2, 5, and 8wt%) after 1 year of exposition. a) curing temperature during the first 24h: 23ºC; b) 35ºC; c) 80ºC. Peaks: Q, quartz; M, mullite; N, magnetite.

4.3.3 Microstructural analysis by means of SEM-BSE

SEM-BSE experiments were performed on samples after 1 year exposed to sulfate solutions. For each system, a piece of one bar exposed only to 5% of sulfate concentration and each curing temperature was taken to analysis.

Figure 4.9a, b and c provides SEM-BSE images for the OPC specimens when curing temperature was 23, 35 and 80ºC respectively. As it can be observed in each image, ettringite crystals are found and it isresponsible of the expansion. In the images of the bars cured at 23ºC and 35ºC (**figure 4.9a and b**), the presence of fine crystals and deposits of ettringite, located always near the aggregates or in the regions among the aggregates, are observed. For OPC bars cured at 80ºC in **figure 4.9c**, it can be observed huge deposits of ettringite. In this case, all the region is practically led by delayed ettringite,

finding huge agglomerations of these crystals. Consequently, this bars were found to have much higher expansion than the bars cured at 23 and 35ºC. This huge formation of delayed ettringite is related to the elevated temperature used in this case, 80ºC, as explained in chapter 4.3.1.

Figure 4.10a, b and c provides SEM-BSE images for the AAS specimens when curing temperature was 23, 35 and 80ºC respectively. In this case, as shown in the XRD spectra (**figure 4.7a, b and c**), no anomalous compound was found. In the images, it can be observed the presence of anhydrous slag particles, and some fine cracking, probably due to the shrinkage that these systems suffer (Bakharev, J. G. Sanjayan, et al. 1999; Collins & Sanjayan 1999; Palacios & Puertas 2007; Bakharev, J.G. Sanjayan, et al. 1999; Wang et al. 1994). It can be noted in these images that for the specimens cured at 35 ºC and 80ºC, a black region appears to surround the aggregates, whereas for the specimen cured at 23ºC, this is not observed. This black region is in fact related to the porosity. As it can be observed, there is a discontinuity between the aggregates and the paste probably due to a desiccation during the heat treatment. This porosity can be also responsible of the expansion due to water absorption as explained before in chapter 4.2.

Figure 4.11a, b and c provides SEM-BSE images spectra for the AAFA specimens when curing temperature was 23, 35 and 80ºC respectively. No anomalous compound was found in the micrographs related to the sodium sulfate attack. In every case, the EDX spectra obtained showed the elements of the sodium aluminosilicate gel (N-A-S-H), typical hydration product of these systems: Si, Al and Na (Fernández-Jiménez et al. 2005; Palomo, Grutzeck, et al. 1999). Anhydrous FA particles (plenospheres, spheres) and white particles related to mullite/magnetite present in the original FA are also observed. Observing this images, it can also be deduced a relative hydration degree in terms of anhydrous FA particles (spheres) observed. When the curing temperature was 23 and 35ºC (**figure 4.11a and b**), the quantity of anhydrous FA particles was higher in comparison to the curing at 80ºC. Thus, in this particular system, it is demonstrated the heat curing at elevated temperatures dissolve all the necessary elements present in the FA [ref]. **Table 4.2** shows the atomic ratios of the paste regions for each image. The atomic ratios are an average of a minimum of 5 points of the image (1.00k of scale). It can be observed that the Si/Al ratio is decreased as the curing temperature during the first 24 hours increases. This means that more aluminum is dissolved and hence fixed at the structure of the N-A-S-H gel. It is also observed that the Na/Al ratio is constant when curing temperature is 23 and 35ºC, and then decreases for 80ºC. This is also an evidence of the increase of the aluminum content in the structure at elevated temperatures. Therefore, the atomic ratios also corroborate the higher solubility of the elements at elevated curing temperatures.

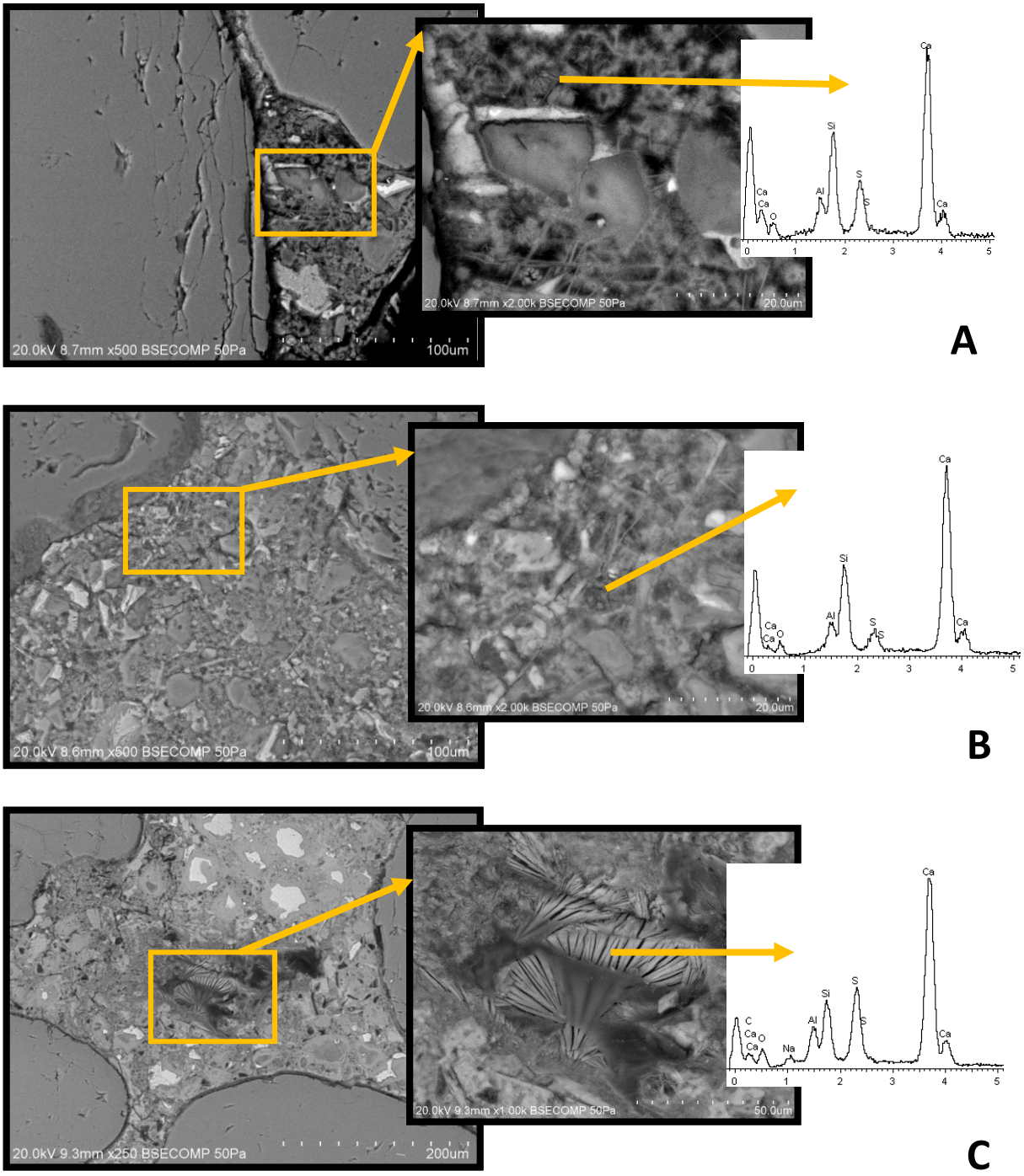

Figure 4.9 SEM-BSE images for OPC mortar bars exposed to 5% of sulfate concentration after 1 year of exposition. a) Curing temperature during the first 24h: 23ºC; b) 35ºC; c) 80ºC.

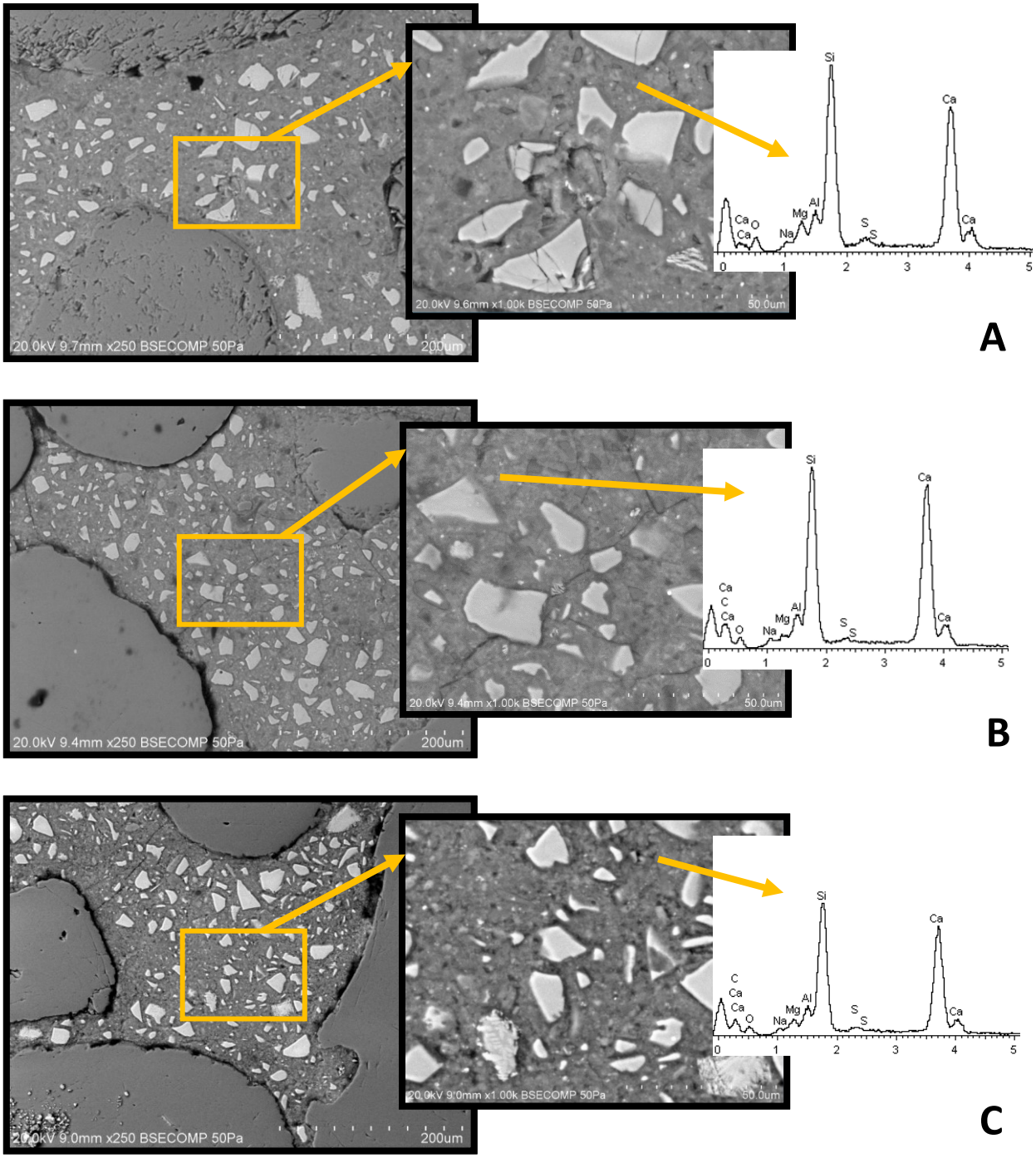

Figure 4.10. SEM-BSE images for AAS mortar bars exposed to 5% of sulfate concentration after 1 year of exposition. a) Curing temperature during the first 24h: 23ºC; b) 35ºC; c) 80ºC.

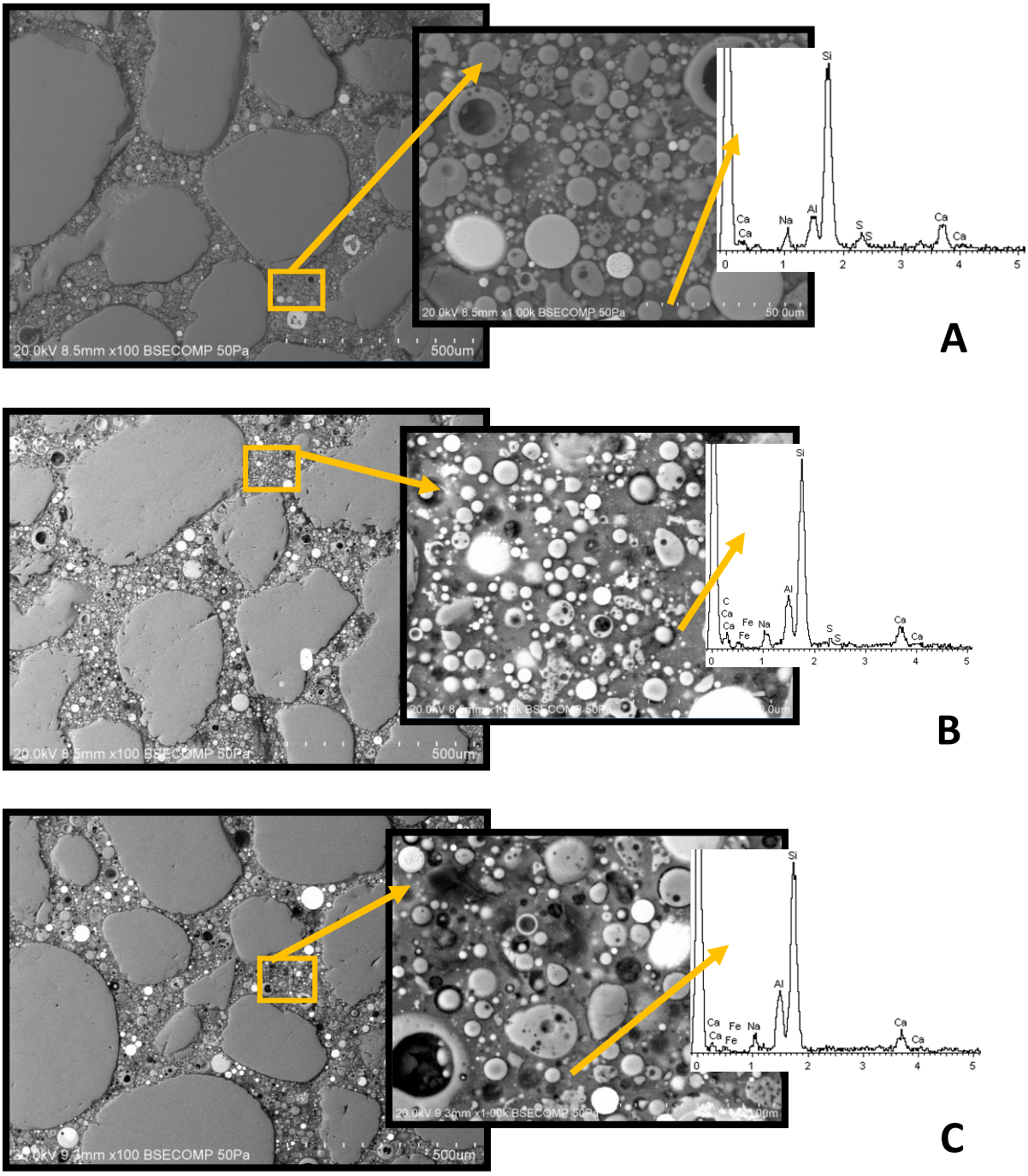

Figure 4.11. SEM-BSE images for AAFA mortar bars exposed to 5% of sulfate concentration after 1 year of exposition. a) Curing temperature during the first 24h: 23ºC; b) 35ºC; c) 80ºC.

Table 4.2 Atomic ratios obtained by the EDX analysis of the AAFA mortars exposed during 12 months to 5wt% sodium sulfate solution. A) Curing temperature during the first 24 hours of 23ºC, b) 35ºC, c) 80ºC.

Curing Temperature	$\frac{Si}{Al}$	$\frac{SiO_2}{Al_2O_3}$	$\frac{Na}{Al}$	$\frac{Na_2O}{Al_2O_3}$
23ºC	5.22	10.44	0.54	0.54
35ºC	4.07	8.15	0.53	0.53
80ºC	3.56	7.12	0.38	0.38

4.3.4 Discussion

The sulfate resistance of OPC, AAS and AAFA was investigated following of ASTM C1012 and modified ASTM C1012. The parameters of the test that have been investigated are the curing temperature during the first 24 hours (23, 35 and 80ºC) and the sodium sulfate concentration (2, 5 and 8wt%). Results showed the worst situation for OPC binder, finding very good results with AAS and AAFA binders.

It is well known that the external sulfates reacts with some components of the hydrated OPC paste (Eglinton 2003; CEB 1989). These reactions (**equation 4.1** to **4.4**) will lead to the formation of ettringite and to a lesser extent gypsum that can result in an increase of the solid volume, and thus leading to expansion and cracking.

$$Ca(OH)_2 + Na_2SO_4 \cdot 10H_2O \rightarrow CaSO_4 \cdot 2H_2O + 2NaOH + 8H_2O \quad (4.1)$$

$$4CaO \cdot Al_2O_3 \cdot 13H_2O + 3(CaSO_4 \cdot 2H_2O) + 14H_2O \rightarrow 3CaO \cdot Al_2O_3 \cdot 3CaSO_4 \cdot 32H_2O + Ca(OH)_2 \quad (4.2)$$

$$3CaO \cdot Al_2O_3 + 3(CaSO_4 \cdot 2H_2O) + 26H_2O \rightarrow 3CaO \cdot Al_2O_3 \cdot 3CaSO_4 \cdot 32H_2O \quad (4.3)$$

$$3CaO \cdot Al_2O_3 \cdot CaSO_4 \cdot 12H_2O + 2(CaSO_4 \cdot 2H_2O) + 16H_2O \rightarrow 3CaO \cdot Al_2O_3 \cdot 3CaSO_4 \cdot 32H_2O \quad (4.4)$$

As shown in the results (**figure 4.3**), OPC bars experimented expansion whichever conditions is applied (curing temperature and sulfate concentration). This was mainly due to the reaction of calcium hydroxide and calcium aluminate compounds with the sulfates (according to **equations 4.1** to **4.4**) to produce expansive compounds as gypsum and ettringite. XRD analysis performed after 12 months of exposure to sulfates confirmed the presence of gypsum and ettringite. Moreover, SEM-BSE performed in the same OPC samples showed the presence of crystals of ettringite in the regions near the aggregates. Precipitation of ettringite near the aggregates could be the consequence of a higher

concentration of portlandite in these regions (Odler 2003), which will react with sulfates to form gypsum, which will react with calcium aluminate compounds to form ettringite. Gypsum crystals were revealed by XRD analysis but difficult to detect by SEM.

Moreover, the expansion rate experimented by the bars cured at 23 and 35ºC was very slow considering that the OPC used is not considered as a sulfate resistant cement. The time elapsed by these bars to reach the limit compliance at 12 months of 0.1% varied depending on the sulfate concentration, as observed in the results. Hence, for OPC bars cured at 23ºC, the time to reach the limit compliance was 236, 186 and 143 days for 2, 5 and 8% of sulfate concentration respectively, and for the bars cured at 35ºC the time was of 325, 291 and 241 days respectively. The main parameter considering the susceptibility of a cement to react with sulfates is the C_3A content. Regarding its phase composition, calculated according to ASTM C150, this cement has 7.4% of C_3A phase. As specified in this standard, cement with less than 8% of C_3A, among other parameters, can be considered as a moderate sulfate resistant. This moderate quantity of C_3A could be the responsible of the slow expansion rate shown. Other studies found similar expansion rates when similar cements were used under the same sulfate test method conditions (Hossack & Thomas 2015; Schmidt et al. 2009).

One interesting aspect to mention is the better resistance of the OPC specimens treated at 35ºC during the first 24 hours than those cured at normal conditions (23ºC). This could be related to several factors. First is the total porosity. As observed in the **figure 4.1a**, the compressive strength of the OPC mortars heated at 35ºC is lower after 7 days. This higher porosity could be the responsible of the lesser expansion observed, because there is more space to the growth of ettringite crystals, and thus, the expansion stresses will be lower. Other factor could be related with the primary ettringite formed. At 35ºC, hydration rate is accelerated. At these conditions, primary ettringite formation could have been favored, and thus less anhydrous C_3A and less hydrate calcium aluminate hydrates (Afm and C_4AH_{13}) are formed. Less calcium aluminates compounds would result in less secondary ettringite, responsible of the expansion.

Another point to highlight is that the fast expansion of the OPC mortar bars cured at 80ºC was practically the same regardless the sulfate concentration until 150 days. However, at later ages, the expansion was higher when the sulfate concentration of the solution was higher, showing a direct influence of the sulfate concentration. Accordingly, there seem to be two differentiate effects. In a first stage, at early ages, it could occur an expansion due to an internal sulfate attack (ISA). This type of attack is favored in OPC systems when they have been subjected to high temperatures over 60-70ºC (Collepardi 2003; Tagnit-Hamou & Petrov 2004). At these conditions, primary ettringite normally produced during hydration and beneficially for the concrete is not formed or, if it is already formed and

decomposes to monosulfoaluminate. As a consequence, much more of the sulfates, not stabilized by the primary ettringite, will be either in the pore solution or incorporated in the CSH gel. In presence of high humidity and microcracks (also produced by the thermal curing), the sulfates normally adsorbed in the CSH gel can be released and produce again ettringite (thus called delayed-ettringite: DEF) with a subsequent expansion (Skalny et al. 1996; Collepardi 2003). This stage would be less affected by the external sulfate concentration. This stage is therefore responsible of the fast expansion experimented for this OPC bars. In a second stage, at later ages, the influence of an external sulfate source is manifested (external sulfate attack: ESA) and thus the reaction of external sulfates with the calcium and aluminum compounds of the cement paste will produce again ettringite, hence causing further expansion. In this second stage, the concentration of the external sulfates will have an important role, with more expansion when higher the sulfate concentration is.

In the case of AAS, different behaviors were observed depending on the curing temperature during the first 24 hours. For the bars cured at 23ºC, no expansion was observed due to sodium sulfate attack. XRD and SEM-BSE characterization of samples after 12 months of exposure to sodium sulfate solutions did not reveal any compound resulting on the sulfate interaction with the hydration products of AAS. For the bars cured at 35 and 80ºC, an initial expansion was observed that was then kept constant during all the test (higher for those cured at 80ºC). As for the bars cured at 23ºC, XRD and SEM-BSE, characterization did not show the presence of crystalline products to which attribute the expansion observed. Therefore, this expansion has been attributed to water absorption that bars suffer during the first week, as explained in **Chapter 4.2**. SEM-BSE revealed the apparition of black region surrounding the aggregates when the bars were thermally cured, showing an additional porosity. This porosity surrounding aggregates could have been produced during the heating of the bars caused by a desiccation of the paste. Thus, water uptake during saturation could be the responsible of the initial expansion during the first week. Once the specimen was saturated, expansion by water absorption stopped and the bar length kept stable during time.

In the three curing temperature regimes and the three sulfate concentrations, XRD analysis revealed the presence of typical hydration products for AAS systems, such as calcium aluminate hydrate gel (called C-A-S-H) and hydrotalcite (HT) (Wang & Scrivener 1995; Puertas et al. 2002; Gruskovnjak et al. 2006). These products are thus consequence of the hydration of the anhydrous slag with the activator, in this case, sodium silicate (Ms = 1.45). EDX analysis also confirm the presence of these hydration products. As it can be seen in the spectra of **figure 4.10**, independently of the curing temperature, the elements present are Si, Ca, Al, Mg, Na and S. These elements are thus represented in the C-A-S-H gel and in the hydrotalcite ($Mg_6Al_2CO_3(OH)_{16}\cdot 4(H_2O)$). Both compounds are intermixed and thus it is

difficult to differentiate by SEM-BSE. Si, Ca and Al are present in the main hydration product, the C-A-S-H gel. Al, otherwise, is also present in the hydrotalcite together with Mg. The extent on which the Al is present on the hydrotalcite or in the C-A-S-H gel is influenced by the Mg content (Ben Haha, Lothenbach, et al. 2011; Bernal et al. 2014). Thus, the excess of Al that is not incorporated to the hydrotalcite will be further incorporated in the C-S-H gel. The presence of Na in the matrix is still controversial, but it is believed to be absorbed in the C-A-S-H gel rather than incorporated to their structure (Wang 2000). Moreover, in the spectra, it can be observed the presence of S, probably present in the pore solution due to the ingress of sulfates.

According to the results obtained in this part of the work, it is evident that AAS system is resistant to the sodium sulfate attack. These results are in accordance with other works found in literature (Bakharev et al. 2002; Douglas et al. 1992; Puertas et al. 2002; Komljenović et al. 2013).

Although no attack form part of the sodium sulfate was found, this does not mean that AAS are sulfate resistant. As shown in other works (Bakharev et al. 2002; Ismail et al. 2012), sulfate attack on AAS pastes depends also of the cation. Therefore, it has been found deterioration by sulfate attack of AAS binders when they were exposed to magnesium sulfate. In this case, decalcification of the binder, gypsum formation, loss of mechanical performance and dimensional changes were found as a result of the magnesium sulfate attack of AAS. The degradation of the calcium silicate hydrate gels (as the C-A-S-H) was mainly attributed to the low solubility of magnesium hydroxide compounds (formed during the interaction of the magnesium sulfate with the gel) and the resulting low pH value (Ismail et al. 2012; Eglinton 2003).

In the case of AAFA, no expansion was observed independently of the curing temperature regime and the sulfate concentration. Although curing temperature showed to be an important aspect on the mechanical performance of these systems (see chapter 4.1), it seems that mechanical properties are not the most important aspect regarding the sulfate resistance but the chemical composition of the AAM precursor. The low Ca-content of the class F fly ash could be the reason which AAFA is highly resistant to sodium sulfate attack.

XRD analysis performed on samples after 12 months of sulfate exposure did not show the presence of new crystalline products other than those present initially in the FA (mullite and magnetite). SEM-BSE images neither revealed the formation of any crystalline product nor a degradation of the matrix. EDX analysis (for the three curing regimes) showed typical spectra of AAFA with sodium silicate as activator (Fernández-Jiménez & Palomo 2005), with Na, Al and Si as the main elements attributed to the formation of the N-A-S-H gel.

The results therefore showed very good resistance of AAFA to sodium sulfate attack, independently of the curing temperature regime and sulfate concentration. These results are in accordance with those found in literature (Škvára et al. 2005; Bakharev 2005a; Wallah & Rangan 2006; Fernandez-Jimenez et al. 2007b).

4.3.5 Conclusions

The conclusions of the sulfate attack test that have been obtained in this project are the following:

- In OPC systems, it was found that regarding the temperature during the first 24 hours (23, 35 and 80ºC) and regarding the sulfate concentration in the solution (2, 5 and 8wt%), all the bars exceeded the limit compliance established in the ACI201.2R-08 for class 2 of exposure to sulfates (0.5% of expansion at 6 months and 0.1% at 1 year). The only exception were the bars cured at 35ºC and exposed in 2 wt.% sulfate solution, which passed the test at 6 months but failed at 1 year. The expansion was attributed in all cases to a gypsum and ettringite formation, as demonstrated by XRD and SEM-BSE characterization of samples after 1 year of sulfate exposure.
- It was found less expansion for the OPC bars cured at 35ºC (as required in the standard) than those cured at 23ºC. This could be probably due to a higher porosity of the bars cured at 35ºC, as demonstrated by a lower compressive strength, which could buffer the effect of the stress caused by ettringite crystals growth and consequently produce less expansion. Else, XRD results showed less intensity of the expansion products for the bars cured at 35ºC (gypsum and ettringite), that could be related to a lower quantity of the expansion products. Thus, it would mean as well lower expansion.
- The OPC bars cured at 80ºC experimented a fast expansion from the beginning, exceeding the limit compliance at 1 year (0.1%) after 50 days of exposure in all cases. This has been attributed to a double effect: internal sulfate attack and external sulfate attack. The ISA will be a consequence of the curing temperature at 80ºC. At this temperature, primary ettringite that is formed during hardening process is not formed, and therefore, the sulfates normally stabilized in it will be internally available for further reaction with aluminates producing delayed ettringite, responsible of this huge expansion.
- In AAS system, it was observed that independently of the curing temperature and the sulfate concentration in the solution, the expansion of the bars were quite below the limit compliance.
- The curing temperature had an influence on the expansion results for AAS systems. It was found that higher curing temperatures resulted in higher initial expansion (after 7 days) that

was remained constant afterwards during time. This was attributed to a water absorption rather than a sulfate attack, as XRD and SEM-BSE characterization did not show any presence of crystalline peaks other than the normal hydration products (C-A-S-H gel and hydrotalcite). Else, SEM-BSE images showed that for bars cured at 35 and 80ºC there was large porosity surrounding the aggregates. Therefore, higher curing temperature results in higher porosity, then higher water absorption and higher initial expansion.

- Results show that sodium sulfate attack had no influence on the AAS microstructure, i.e. AAS system does not interact with the presence of sulfates when the source is sodium sulfate.

For AAFA systems, no expansion was observed in none of the conditions, showing a great resistance of these systems to sodium sulfate attack. Instead, some shrinkage during time was found. XRD and SEM-BSE characterization did not show any presence of crystalline products associated to sulfate attack, with the presence of a sodium aluminosilicate hydrate gel typical of these systems.

4.3.6 Applicability of the ASTM C1012 test method to AAM

The most important parameters evaluated in this test were the curing temperature as well as the sulfate concentration. Therefore, regarding the 3 systems studied, OPC, AAS and AAFA, it can be stated that:

- For the OPC system, it has been observed an improvement of the results when specimens are subjected to thermal curing at 35ºC during the first 24 hours, as described in the standard ASTM C1012. Consequently, it could be concluded that these conditions are favorable for the final performance.
- For the AAS system, a negative influence has been observed when specimens are subjected to thermal curing at 35 and 80ºC during the first 24 hours. Nevertheless, the expansion observed is attributed to a water absorption due to higher porosity rather than sodium sulfate attack.
- For the AAFA system, as there is not any interaction between sodium sulfate and the paste, it was not possible to observe the effect of the curing temperature.
- Sodium sulfate concentration had an important influence of the OPC system, as the severity of attack was increased with the sulfate concentration. For AAS and AAFA systems, the sodium sulfate seemed to have a negligible influence, as no difference was found between expansion curves of bars exposed to solutions with different sulfate concentrations.

As a final remark for this test, several recommendations are given for future standards including AAM:

- Curing regime (temperature and time) should not be a prescriptive parameter but selected according the precursor used to get the AAM. Curing temperature can be an important

parameter for the performance of the AAM systems, and thus will affect severely the performance against sulfate attack.

- Sulfate concentration, as in the ASTM C1012, should also be selected depending on the real conditions simulated.
- The expansion seemed to be an adequate indicator of sodium sulfate attack in OPC systems, because the expansion is caused by the calcium-sulfate products. Nevertheless, for AAM systems where calcium is less present, other indicators of the degree of attack should be analyzed, e.g. the compressive strength loss. Anyhow, microstructural characterization of samples after sulfate exposure should be carried out to confirm the stability of the binder.
- The achievement of 20 MPa required in the standard prior to start the test should not be a requirement. Due to the great variability of AAM systems, compressive strength should not be a requirement.

4.4 Acid resistance

4.4.1 Mass change

Figure 4.12a, b and c show the mass change results due to sulfuric acid attack over time for the OPC, AAS and AAFA mortar bars respectively. The influence due to sulfuric acid attack over time concentration (1, 3 and 5 wt%) and the curing time (7 and 28 days) on the results is reported until 196 days.

In the case of OPC mortars (**figure 4.12a**), the mass decreased significantly when the acid concentration increased. For 1% of concentration, the mass of mortars remained almost constant over time. Increasing the concentration up to 3% and 5% led to enhance the mass loss by 30% and 60% respectively after 56 days. Curing time did not affect sample behavior in acid medium, since no difference on the mass was noted between 7 and 28 days of curing prior to testing. After 140 days the sample with 5% sulfuric acid was completely deteriorated.

Figure 4.12b provides the mass change of AAS mortars. As observed with OPC mortars, for 1% of concentration, the mass of AAS mortars remained practically constant over time. Nevertheless, AAS samples yielded a mass gain with increasing acid concentration resulting in an expansion of specimens instead of the mass loss experimented by the OPC specimens. Actually, the increase of the concentration from 3% to 5% caused a mass gain of 7% and 15% respectively after 112 days of exposure. The curing time did not affect the sample behavior, as for OPC.

For AAFA mortars (**figure 4.12c**), the mass remained almost constant over time regardless of the acid concentration and the duration of exposure. Yet, a slight mass loss was observed when the acid concentration was increased with the maximum loss of 3.5% after 140 days of exposure in the 5% acid solution. As already observed with OPC and AAS mortars, curing time had no effect on the mass change.

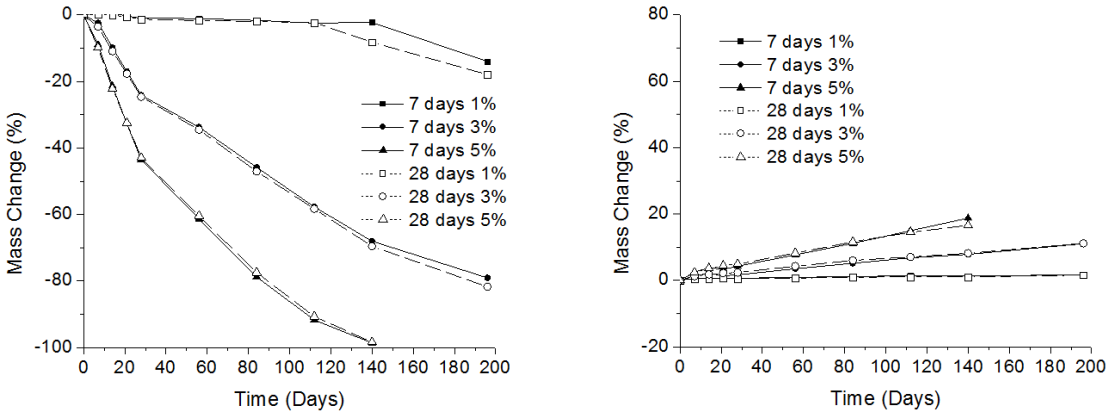

a) OPC b) AAS

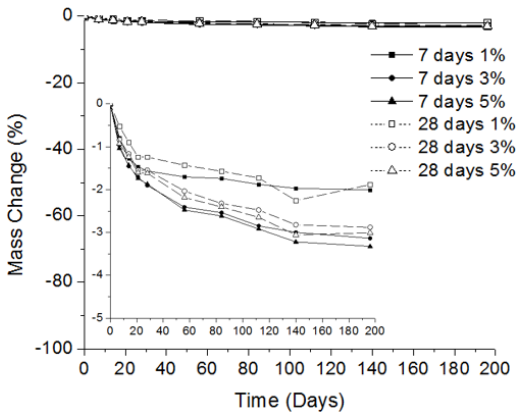

c) AAFA

Figure 4.12. Mass change of mortar cubes exposed to acid solutions with different concentration (1, 3 and 5wt%) and different curing time before exposure to acid (7 and 28 days). a) OPC, b) AAS, c) AAFA.

When exposed to sulfuric acid, the three systems present different behaviors. This difference depends on the precursor used.

4.4.2 Cross-sectional dimension change

Figure 4.13 provides the change of the cross-sectional dimension of specimens. Two measures per side of the cube were performed, with a total of 12 measures per cube. Results shown in **figure 4.13** is the average of these 12 measures for each specimen.

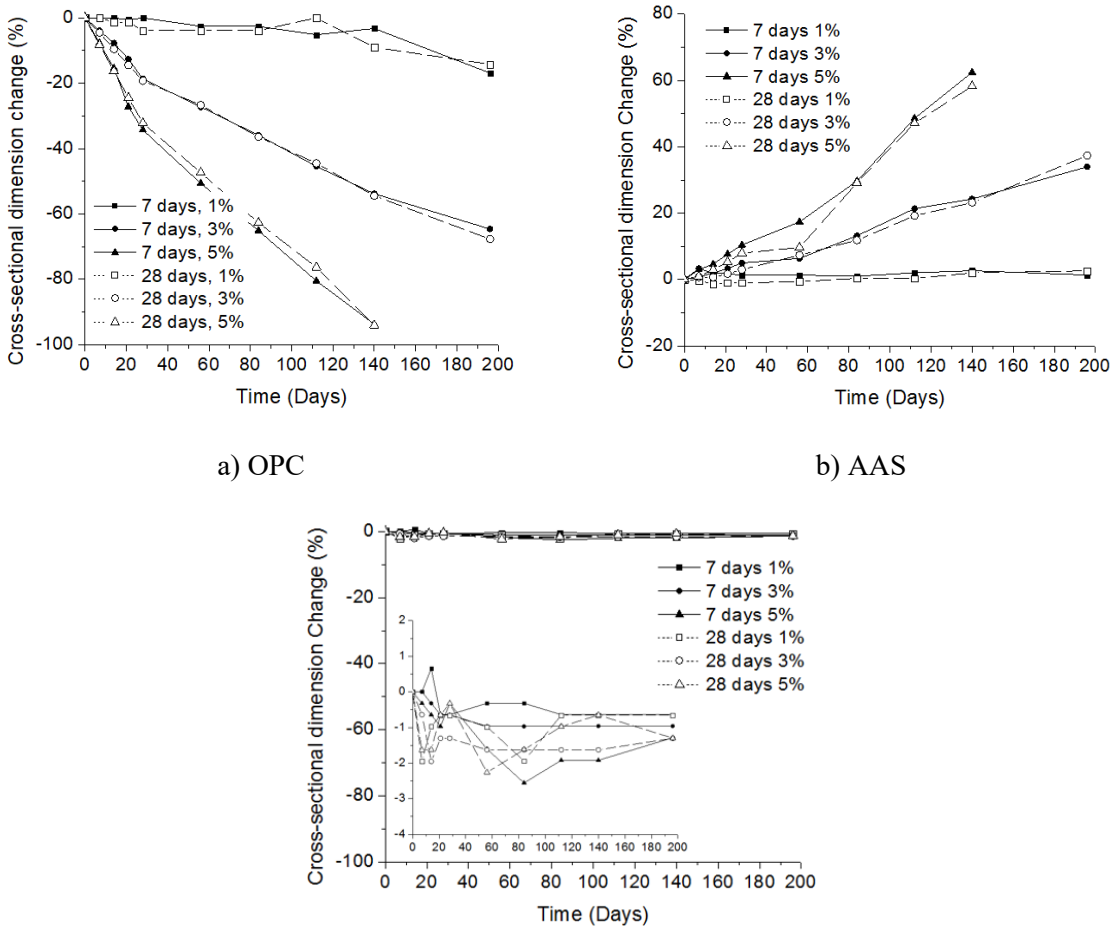

a) OPC

b) AAS

c) AAFA

Figure 4.13. Cross-sectional dimension change of mortar cubes exposed to acid solutions with different concentration (1, 3 and 5wt%) and different curing time before exposure to acid (7 and 28 days). a) OPC, b) BFS, c) FA.

OPC mortars (**figure 4.13a**) experimented a decrease of the dimensions that was in accordance with the mass loss observed in **figure 4.12a**. Consequently, for 1% of acid concentration the dimension was practically stable during time. Increasing the concentration to 3% and 5% result in a dimension loss of 34% and 61% respectively after 56 days of exposure.

Figure 4.13b provides changes in cross-sectional dimensions of AAS mortars. Similar tendency to the mass change was observed, but with higher order of magnitude. A 1% of acid concentration did not affect the cross-sectional dimension of the sample. While 3% and 5% of acid concentration allowed a significant expansion. For example, increasing the concentration to 3% and 5% leads to an increase of the dimension by 21% and 47% respectively after 112 days of exposure, i.e. almost 3 times the mass change. The expansion phenomenon is therefore more marked than mass change.

As in the case of mass change, the cross-sectional dimension remained almost constant with negligible variations for the AAFA mortars (**figure 4.13c**).

4.4.3 Visual appearance

Figure 4.14 exhibits the physical appearance of mortar specimens after 28 and 196 days of immersion in 1%, 3% and 5% sulfuric acid solution. Samples shown were cured during 7 days before acid exposure.

OPC samples showed severe deterioration resulting in a decrease of cube dimensions with increasing acid concentration and over time (**Figure 4.14a1 and a2**). OPC specimens exposed to the 5% acid solution were completely disintegrated after 196 days. The attack appeared to be an external phenomenon with a complete dissolution of the binders in layers into the acid solution, leaving an apparently healthy surface subjected to a new acid attack. The deterioration of OPC mortars is thus an erosion-like phenomenon. This deterioration is in line with both mass and cross sectional dimension changes observed with OPC mortars.

AAS mortars also showed severe deterioration over time especially in high acid concentration (3% and 5%) (**Figure 4.14b1 and b2**). The 1% acid solution had a negligible effect on AAS similar to OPC. The deterioration process of AAS cubes was completely different. In this case there was no erosion, but an expansion resulting in cracks which began on the cubes' edges and gradually extended along the diagonal towards the center of specimens. Therefore, the deterioration starts from the acid-exposed surface and progresses inward. This leads to the formation of six pyramid-like corroded fragments after 196 days of exposure in the case of 5% of concentration (**Figure 4.14b2**). Instead, an insoluble expansive product was formed, causing a mass gain and an increase in cube dimensions.

AAFA did not exhibit any noticeable change in appearance (**Figure 4.14c1&c2**) even in a high acid solution concentration (5%) and after prolonged time of exposure (196 days). This result is in accordance with the unchanged mass and dimension observed with AAFA mortars.

The poor acid resistance of the OPC (62.5% CaO) and AAS (42% CaO) mortars is related to their high calcium contents. Since the acid reacts with calcium-based components such as C-S-H and C-A-S-H in the cement and slag, respectively, to form calcium salts, it leads to specimen strength loss and quick deterioration (Bakharev et al. 2003). The insolubility of the corroded surface of the AAS mortar could be due to aluminum in the binder. The low Ca content in the AAFA mortar (4.5% CaO) could account for its apparent acid resistance.

a1) OPC after 28 days

a2): OPC after 196 days

b1) AAS after 28 days

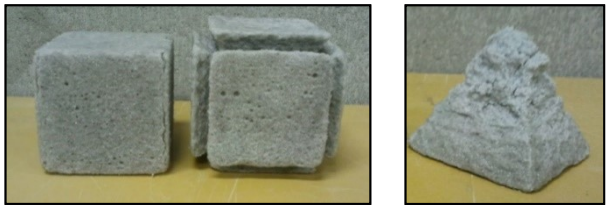

b2) AAS after 196 days

c1) AAFA after 28 days

c2) AAFA after 196 days

Figure 4.14 Visual appearance of mortars cured during 7 days after 28 and 196 days of exposure to sulfuric acid. In all the photos, first cube was immersed in 1wt% sulfuric acid solution, second cube was immersed in 3wt% and the third cube in 5wt%.

4.4.4 Compressive strength

The severe deterioration of OPC and AAS specimens subjected to acid solution did not allow their compressive strength characterization. Only AAFA mortars, which exhibited unaffected dimensions of the cubes by the acid, were submitted to compressive strength tests. **Figure 4.15a and b** provides the evolution of the compressive strength of the AAFA mortars cured during 7 and 28 days respectively, after 28, 56, 112 and 196 days of exposure to acid attack. The compressive strength gradually decreased

with the time of exposure, and the rate of strength loss increased with the acid concentration, especially at the first 28 days of acid exposure. AAFA specimens showed a strength loss of about 15% after 28 days of exposure in 1% solution. Increasing acid concentration to 3% and 5% allowed a strength loss of 33% and 45% respectively after 28 days of exposure. From 56 days of exposure onwards, however, the rate of strength loss slowed down with a compressive strength that evolved towards a constant value of around 11 MPa. This value, achieved rapidly with the high acid concentration, is likely due to residual strength after the complete corrosion of the specimens. The time of curing did not affect the compressive strength, as evidenced by the results for 28 days of curing being very close to those obtained with 7 days of curing.

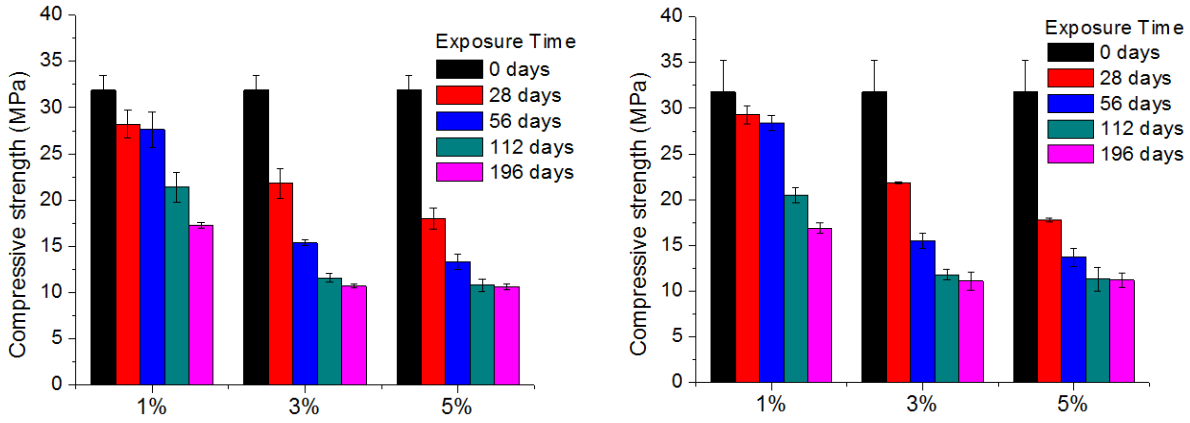

Figure 4.15 Compressive strength evolution of AAFA mortar cubes exposed to acid solutions with different concentration (1, 3 and 5wt%) and different curing time before exposure to acid, a) 7 and b) 28 days.

To better understand the attack process, the AAFA samples were split into halves. **Figure 4.16** provides the pictures of split samples, according to acid concentration, cured for 7 days after 56 days of exposure. The thickness of the corroded part (light gray) depends on the acid concentration, since this zone increased as the acid concentration increased, thereby reducing the non-corroded zone (dark gray). This reveals the gradual penetration of the acid solution into the sample, altering the binder and resulting in the observed strength loss. The decreased thickness of the healthy part of the specimens (internal dark gray zone) as the acid concentration increased is in line with the achievement of a residual value of compressive strength (11 MPa) when the samples have been completely corroded (i.e., disappearance of all dark gray zones).

These results suggest another type of deterioration in the AAFA mortar, even though no change was noted in terms of visual observation, mass, or cross-sectional dimensions. Although the acid mode of action is not the same than with the OPC and AAS systems, the deterioration was also initiated in the

acid-exposed surface and progressed inward. The corrosion product formed in this case was insoluble but not expansive, resulting in apparently healthy specimens after 196 days of exposure.

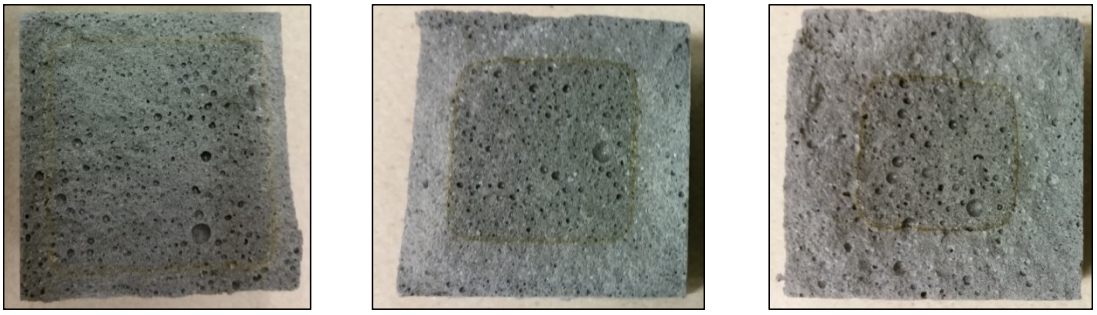

a b c

Figure 4.16 Split mortar cubes after 56 days of exposure to acid attack: a) half cube exposed at 1 wt.% of acid concentration; b) 3 wt.%; c) 5 wt.%

4.4.5 Mineralogical characterization by means of X-ray diffraction

XRD analysis was performed on samples after 28 days of exposure to the acid. **Figure 4.17** provides only the XRD spectra of specimens after 7 days of curing, as no difference was noted according to the curing time. Two measurements were taken for each sample: one for the acid-exposed surface, referred as EXT, and one for the unaffected internal region, referred as INT.

For OPC mortars (**figure 4.17a**), the internal surface seems unaffected by the acid regardless of the concentration used, since XRD patterns of "1% INT, 3% INT and 5% INT" show the presence of typical crystalline products of hydrated OPC namely portlandite (P) and ettringite (E). However, "1% EXT, 3% EXT and 5% EXT", which represent the external layer in contact with the 1%, 3% and 5% acid solutions respectively, showed the formation of gypsum (G). At the same time, no peaks for portlandite and ettringite were detected, suggesting the conversion of portlandite and ettringite into gypsum. This is in line with the statement of Attiogbe (Attiogbe & Rizkalla 1988) who assumed that gypsum formation is primarily due to the sulfate attack of portlandite. It was also demonstrated that ettringite is not stable in low-lime environments when the pH falls below 11.5-12 and could decompose to form gypsum (Allahverdi & Skvara 2000). The quartz phase (Q) observed in both cases is due to the sand used to make the mortars.

For AAS (**figure 4.17b**), the analysis of the internal region of mortars (1% INT, 3% INT and 5% INT) revealed also the presence of quartz from the sand and a broad pick around 29º-2θ corresponding to a poorly crystallized C-S-H gel (X) (Wang & Scrivener 1995; Sakulich et al. 2009). The internal surface seems not to be affected by the acid regardless of the concentration used, since the observed XRD

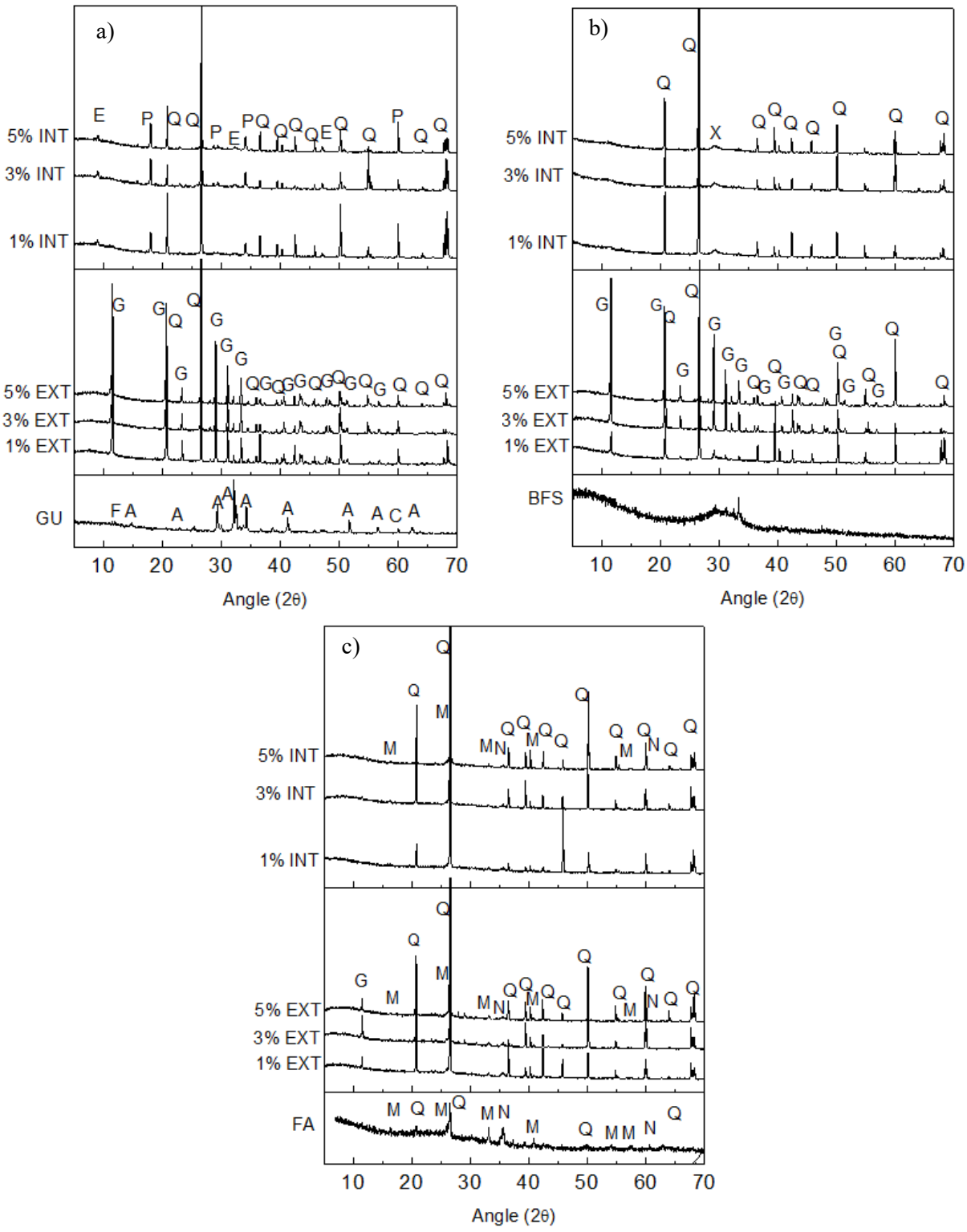

Figure 4.17 XRD patterns of the specimens after 28 days of exposure in the different acid solutions: a) OPC, b) AAS, c) AAFA. INT: unreacted core; EXT: corroded layer. Pics: Q, quartz; P, portlandite; E, ettringite; G, gypsum; X, C-S-H gel; M, mullite; N, magnetite.

patterns are typical of AAS mortar (Wang & Scrivener 1995; Sakulich et al. 2009). XRD analysis of external layer ("1% EXT, 3% EXT and 5% EXT") showed the presence of quartz due to the sand used and, as for OPC mortar, the formation of gypsum. In this case, the formed gypsum did not cause the spalling and disintegration of the corroded sections (**figure 4.14b2**) as it did in the OPC mortar (**figure 4.14a2**). Instead, the gypsum caused internal stresses that ultimately led to the expansion and cracking of the corroded layer (Allahverdi & Skvára 2005).

The FA is mainly composed of quartz (Q), mullite (M) and magnetite (N) along with an amorphous phase characterized by a broad region located at 20-30° 2θ. As in the case of OPC and AAS, both internal and external region after acid-exposure of AAFA mortars were characterized through XRD analysis and results are displayed in **figure 4.17c**. The internal region shows typical crystalline phases of AAFA mortar with the presence of mullite, magnetite, and quartz, suggesting that this region was not affected by the acid. In the case of external region, a small peak of gypsum was observed at about 11.8° 2θ, regardless of the concentration. The amount of gypsum did not appear to be enough to cause deterioration in the samples, as confirmed by their morphology (**figure 4.14c**).

4.4.6 Microstructural analysis by means of SEM-BSE

Microstructural analysis was performed on 7-day cured OPC, AAS and AAFA mortars after 28 days of exposure to the 5wt% sulfuric acid.

Figure 4.18 shows the micrograph and the elementary analysis (EDX) of the transition zone of OPC mortar showing both the external (left part) and internal (right part) regions. The EDX elementary analysis of a line (line scan) represented by an arrow crossing the analyzed sample revealed that the left region is a calcium- and sulfur-rich zone confirming the presence of gypsum as the resulting product of corrosion. In addition, the magnitude of the scan in this part is in the same order for both sulfur and calcium element (C:S = 1:1), which is in line with the gypsum composition ($CaSO_4 \cdot H_2O$). The presence of the peak corresponding to silicon element at about 75 μm is probably due to the scan of a quartz particle. The progression toward the right part induces an abrupt decline of sulfur element and an increase in silicon and calcium elements. This indicates that the right zone is not affected by the acid and is essentially composed of silicon and calcium—that is to say C-S-H gel with C/Si ration around 1.4-1.9.

Figure 4.19 shows the microstructural analysis of the transition zone of AAS for a 7-day cured sample after 28 days of exposure to the 5wt% sulfuric acid. Two clearly distinct regions can also be observed. The more porous zone on the right side corresponds to the corroded layer, and the denser part on the

left side represents the unaffected layer. EDX analysis of a line (line scan), represented by an arrow crossing the analyzed sample, revealed that the left region is rich in calcium and silicon element along

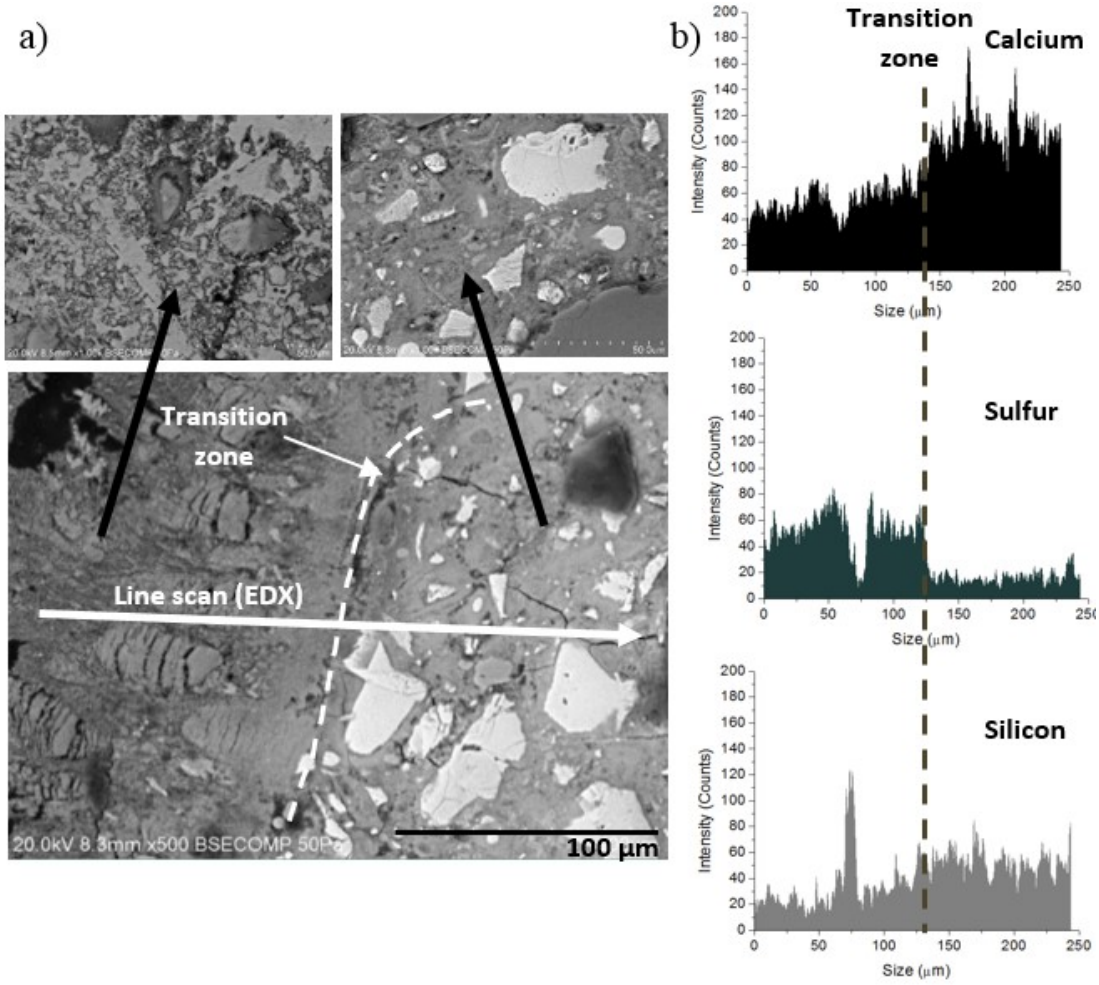

Figure 4.18 Microstructural analysis of OPC mortar after 28 days of exposure to 5% acid solution: a) SEM (BSE) image and b) EDX analysis (line scan)

with a non-negligible amount of aluminum, i.e. C-(A)-S-H gel with Ca/Si ratio of 0.6-1.0 different to those found in the OPC mortar, and typical for such systems (Wang & Scrivener 1995; Puertas et al. 2004; Pacheco-Torgal et al. 2008a). This confirms that the denser part (on the left) was not yet affected by the acid. The progression toward the right part induces a significant increase in sulfur, present in the same order of magnitude of calcium sustaining the presence of gypsum as the corrosion product.

Visual inspection, mass and cross-section dimension of AAFA mortars did not show any change after acid attack, regardless of the concentration. However, split samples showed a gradual ingress of the acid into specimens (**figure 4.16**) suggesting another sort of acid attack confirmed by a gradual strength loss (**figure 4.15**). To identify the nature of the corroded product formed, microstructural analysis was

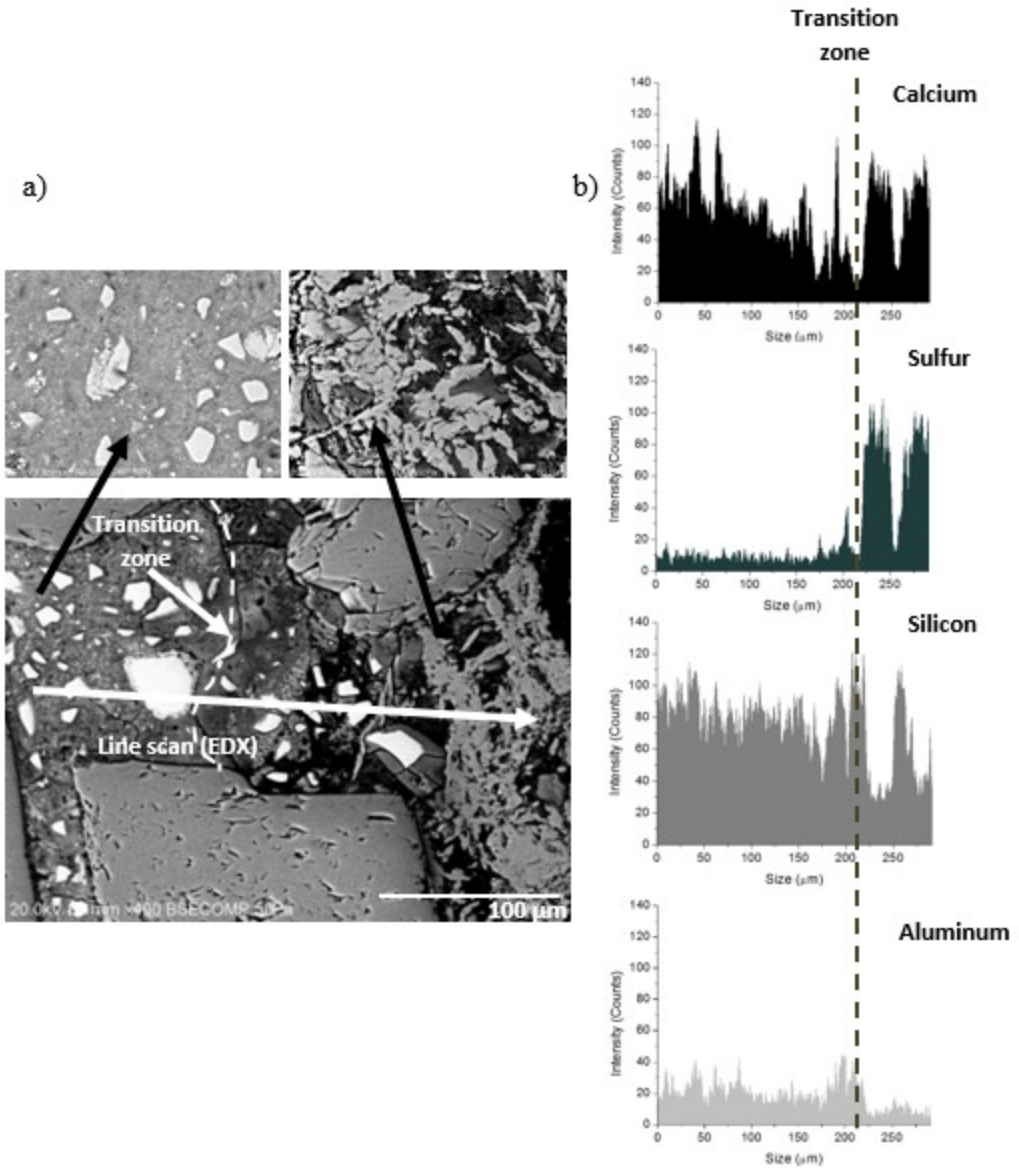

Figure 4.19 Microstructural analysis of AAS mortar after 28 days of exposure to 5% acid solution: a) SEM (BSE) image and b) EDX analysis (line scan)

performed on both the corroded external (**figure 4.20a**) and the unaffected internal (**figure 4.20b**) layers after 28 days of exposure to the 5 wt.% sulfuric acid. The results provided in **figure 4.20a** show that the unaffected internal region was composed of a typical sodium aluminosilicate gel (known as N-A-S-H) found in alkali-activated class F fly ash (Fernandez-Jimenez & Palomo 2003). Nevertheless, in the attacked region (**figure 4.20b**), the gel contained very low sodium and aluminum contents, suggesting a dealumination and dealkalinization of the gel in the presence of the acid. This finding is in agreement with that obtained by other authors (Bakharev 2005c; Allahverdi & Skvára 2005). The presence of sulfur indicates the formation of gypsum in low quantity and thus confirming XRD results.

The gypsum appeared to be preferentially deposited in air bubbles (**figure 4.21**), because they provide the best nucleation site, explaining the absence of crack and any expansion due to acid attack.

4.4.7 Discussion

The behavior of AAS and AAFA mortars subjected to sulfuric acid at concentrations varying from 1% to 5% was investigated over time and compared to that of an OPC mortar. The results show that the three systems behaved differently under acid attack, suggesting distinct deterioration mechanisms. Actually, the OPC mortar exhibited severe deterioration, resulting in a loss of mass and a decrease in cross-sectional dimensions culminating in the entire disintegration of the specimen subjected to 5% acid concentration after 196 days. Gypsum was determined to be the corrosion product. Therefore, the sulfuric acid attack of the OPC mortar is similar to sulfate attack on calcium-bearing compounds, such as portlandite, since the XRD investigations of the acid-exposed layer showed the formation of gypsum along with the disappearance of portlandite and ettringite peaks (**Figure 4.17a**). This finding was

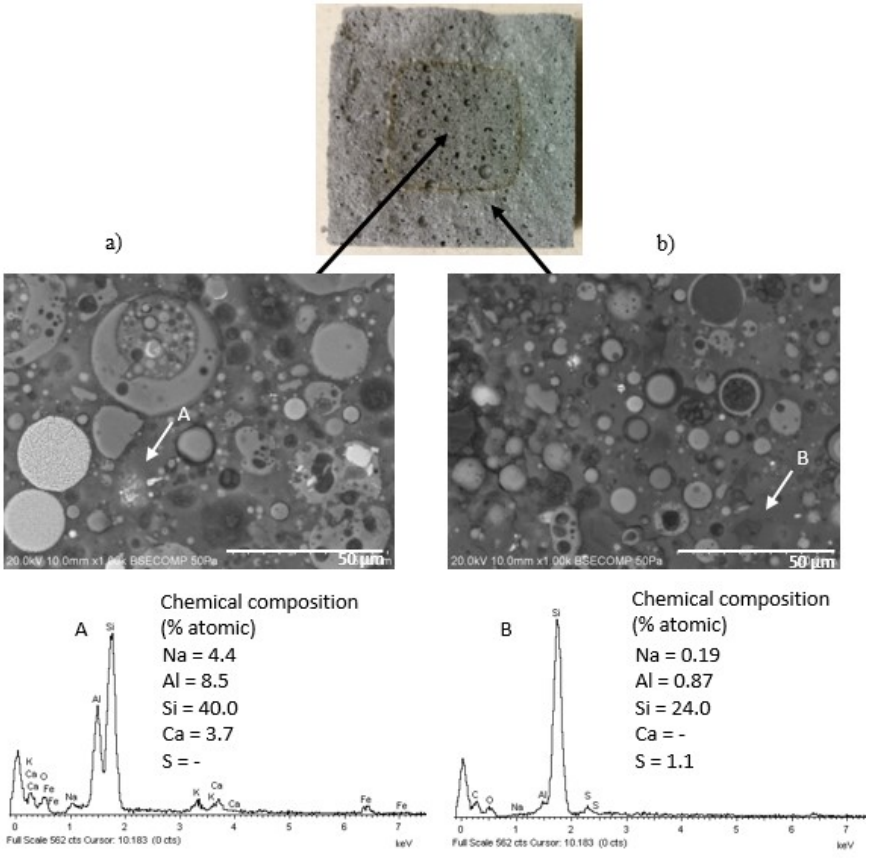

Figure 4.20 SEM (BSE) images and EDX analysis after 28 days of exposure to 5% acid solution for AAFA. a) internal region; b) external region.

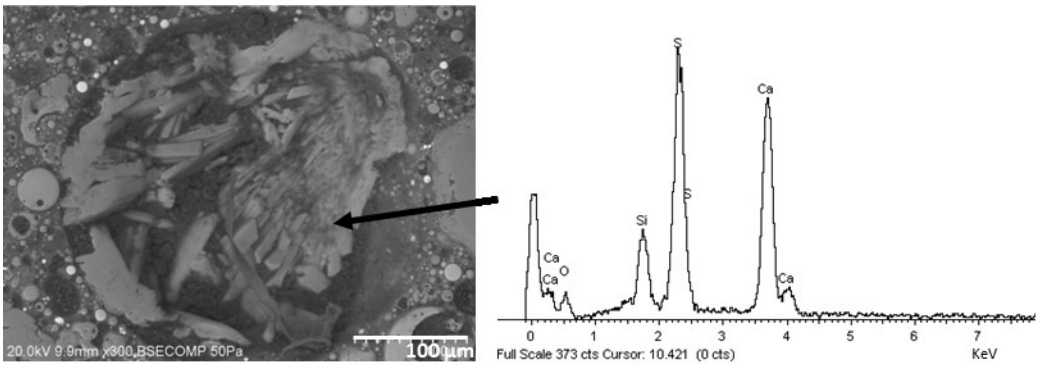

Figure 4.21 SEM (BSE) images and EDX analysis after 28 days of exposure to 5% acid solution for AAFA showing gypsum crystals in a pore.

confirmed by SEM observations, which revealed the presence of a large quantity of gypsum on the attacked layer (Figure 8). According to Attiogbe & Rizkalla (1988), sulfate attack is only one aspect of sulfuric acid attack on OPC concrete. The absence of ettringite in the attacked zone relates to the very low pH, favoring the formation of gypsum, which is more stable in low pH environments. Indeed, it has been demonstrated that ettringite is not stable in low-lime environments when the pH falls below 11.5 and could decompose to form gypsum (Allahverdi & Skvara 2000). The formation of gypsum resulted in the softening of the acid-exposed surface and the loss of both mass and cross-sectional dimensions, as was visually evident (**figure 4.14a1 and a2**). According to (Mehta 1983), long-term exposure to sulfate-bearing solutions causes significant concrete spalling and loss of strength due to the formation of gypsum (Santhanam et al. 2002). Moreover, SEM analysis of the acid-exposed layer showed no correlation between elemental silicon and calcium, suggesting the attack of C-S-H. Therefore, the disintegration of the corroded surface might also be attributed to the decalcification of calcium silicate hydrate through ion exchange between hydrogen from the acid solution and calcium from C-S-H, resulting in a soluble amorphous hydrogel (Cizer et al. 2011).

The corrosion process in an OPC system is an erosion-like phenomenon. **Figure 4.22** summarizes a four-step mechanism to account for this degradation. In step 1, the acid solution comes into contact with the surface of the specimen and initiates the attack through a process of ion exchange between H_3O^+ from the acid solution and Ca^{2+} mainly from portlandite present in the specimen. This induces a decrease in the local pH near the exposed surface, causing binder destabilization. Accordingly, as described in step 2, the C-S-H gel in the acid-exposed surface undergoes a type of calcium depletion known as decalcification phenomenon, inducing the formation of an amorphous silica hydrogel. The altered C-S-H becomes an unstable acid-soluble silica gel, softening the corroded layer. Meanwhile, Ca^{2+} ions diffusing towards the solution react with SO_4^{2-} ions in the acid solution and start forming gypsum crystals in the regions close to the surface. The formed expansive gypsum generates internal

stresses that propagate throughout the weaker part, which is, in this case, the corroded layer, resulting in its spalling, as shown in step 3. Finally, as described in step 4, this process allows the acid to attack the newly exposed surface until the sample deteriorates completely. This process is similar to the sulfate attack at elevated pH levels (Santhanam et al. 2003).

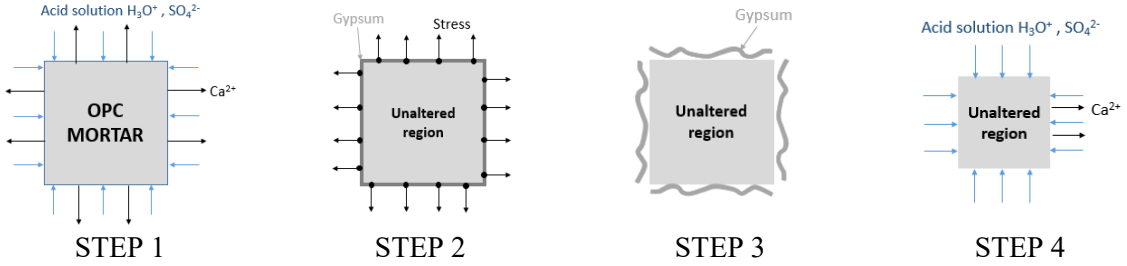

Figure 4.22 Proposed mechanism of sulfuric acid attack in OPC mortars

Moreover, due to the nature of the corrosion, the indicators used herein (change in mass change and cross-sectional dimensions) to assess the degree of the attack are assumed to be good indicators for OPC systems. In this case, the corroded product is separated from the mortar surface and dissolved into the solution. In addition, the results show that both the mass and cross-sectional dimensions varied on the same order of magnitude. Compressive strength is not recommended as an indicator for these systems due to the great loss in specimen dimensions, skewing measurements of this property.

The AAS mortar has the same corrosion product as the OPC mortar, since both the XRD and SEM characterizations revealed the formation of gypsum. That notwithstanding, the deterioration processes are completely different. Although the AAS mortar showed severe deterioration, the process was expressed through expansion phenomenon, resulting in a gain in mass and cross-sectional dimensions. The magnitude of the expansion was three times greater than that of the mass gain. The degree of deterioration depended strongly on the acid concentration and on exposure time, since the samples exposed to 5% acid showed severe degradation, particularly after 196 days. This culminated in the specimen splitting into pyramid-like pieces (**figure 4.14b2**). **Figure 4.23** summarizes a four-step reaction mechanism to account for the degradation of the AAS mortar. In step 1, the acid solution comes into contact with sample surfaces, lowering the local pH in the zone close to the mortar surface due to an ion-exchange process between H_3O^+ and Ca^{2+}. As in the case of the OPC mortar, this results in calcium depletion of the C-A-S-H gel. The ion-exchange reaction occurs along with an electrophilic attack of Si-O-Al bonds by acid protons, resulting in the formation of an imperfect highly siliceous framework in the exposed surface (Allahverdi & Skvára 2005) in accordance with the disappearance of the broad peak of C-A-S-H observed in the internal unaffected region (**figure 4.17b**). Meanwhile, the Ca^{2+} ions diffusing towards the acid solution react with SO_4^{2-} ions in the solution, resulting in the

deposition of gypsum crystals on the sample surface, as described in step 2. Unlike the acid-soluble altered C-S-H observed in the OPC mortar, the altered C-A-S-H in the AAS mortar was not soluble in the acid, allowing the corroded layer to remain on the mortar surface. This corroded layer could be expected to act as a protective layer, thereby inhibiting the corrosion process. Nevertheless, this layer was quite permeable and the ingress of the acid occurred without any impediment, causing the thickness of the corroded layer to increase. The expansive gypsum generated stresses propagating through the weaker altered zone, inducing cracks on the cube's edges diagonally, as shown in step 3. The progression of the acid solution penetrating the specimen over time caused the mortar to gradually deteriorate, expressed as a huge expansion phenomenon. Lastly, this resulted in the specimen splitting into pyramid-like pieces (as described in step 4) when the acid reached the entire inner mortar.

The difference between the degradation process in the AAS and OPC systems is probably due to the nature of calcium-bearing compounds formed in the AAS mortar, such as a low-calcium C-S-H gel (C-(A)-S-H), hydrotalcites, and C_4AH_{13} (Huanhai et al. 1993; Puertas et al. 2007; Bernal, de Gutiérrez, et al. 2011) which are different from the portlandite and ettringite in OPC.

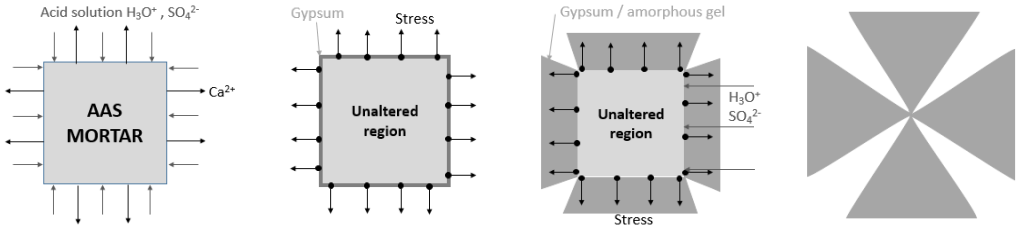

Figure. 4.23 Proposed mechanism of sulfuric acid attack in AAS mortars

Furthermore, according to the results, both the changes in mass and cross-sectional dimensions appear to be suitable indicators of the degree of acid attack both in AAS systems and OPC systems, even if the deterioration processes are different. The change in cross-sectional dimensions appears to be more indicative of attack severity, since the attack caused major sample expansion. As with OPC systems, compressive strength is not recommended as an indicator for AAS systems due to the significant expansion of specimen dimensions, which does not allow for adequate strength measurement.

The deterioration process in the AAFA mortar was quite different from that in the OPC and AAS systems. No deterioration was visually evident, neither were there any significant changes in specimen mass or dimensions, since only about 3.5% of mass loss was noted with the highest acid concentration (5%) after 112 days of exposure. Splitting the samples, however, indicated that the acid had penetrated the specimens, resulting in two distinct zones: a corroded zone (light gray) and an unaffected zone (dark

gray) (**Figure 4.16**). The thickness of the corroded layer strongly depends on the acid concentration and exposure time, since the 5% acid concentration evidenced the deepest corrosion. This is in line with the decrease in the compressive strength of acid-exposed samples (**Figure 4.15**). A residual value of compressive strength of 11 MPa was attained after long-term exposure, depending on the concentration, indicating complete corrosion of the specimens. XRD analysis revealed the presence of a very low gypsum content. No significant differences were observed between the crystalline phases of both the corroded and unaffected zones, suggesting that the acid preferentially attacked amorphous phases (Kovalchuk et al. 2008). Elementary chemical analysis through SEM characterization indicated Na and Al depletion in the region exposed to acid. The phenomenon, known as dealumination and dealkalinization, that induced a strength loss has been observed by other authors (Allahverdi & Skvára 2005; Allahverdi & Škvára 2005b; Bakharev 2005c). The depletion of Na and Al resulting in an amorphous silica-rich product could explain the slight mass loss (3.5%) observed with the 5% acid concentration after long-term exposure. In addition, the presence of a non-negligible amount of sulfur was observed in the corroded region with deposition of gypsum in air bubbles. That prevented any expansion or cracking, since air bubbles provide the best sites for nucleation (Santhanam et al. 2003). The calcium for the gypsum formation is probably due to a minor presence of calcium in the gel that is first depleted form the gel structure due to ion exchange with H_3O^+ from the acid. The presence of calcium in the gel is shown in the elemental analysis of **figure 4.20 a**.

Based on the results, changes in mass or cross-sectional dimensions or visual inspection are not suitable for characterizing the degree of acid attack in AAFA systems, since these parameters indicate that the sulfuric acid did not corrode the AAFA mortar. Conversely, compressive strength appears to be a better indicator of the degree of acid attack. Despite the acid effect, the fully corroded AAFA samples had a residual strength of about 11 MPa, suggesting that AAFA mortar develops better acid resistance than OPC and AAS systems.

4.4.8 Conclusions

The conclusions of the sulfuric acid attack test that have been obtained in this project are:

- The results reveal different processes of deterioration in the three systems, with the rate of corrosion increasing with increasing acid concentration and exposure time.
- The OPC samples exhibited mass loss and a decrease in specimen dimensions, ultimately culminating in their complete disintegration (in the case of the 5% acid concentration after 196 days of exposure).

- The AAS samples evidenced expansion with gains in both mass and dimensions, ultimately resulting in internal cracks and the splitting of the specimens into pyramid-like pieces (in the case of the 5% acid concentration after 196 days of exposure).
- Although the processes of deterioration in the OPC and AAS systems are different, gypsum was found to be the main corrosion product. The difference could probably be related to the nature of C-S-H gel in the OPC system, which is different from the C-(A)-S-H in the AAS system.
- As for the AAFA system, no changes were detected in terms of visual inspection or changes in mass and dimensions, suggesting that the material was able to withstand the acid attack. A decrease in compressive strength was, however, observed due to the progressive dealumination and dealkalization of N-A-S-H gel during acid penetration, indicating corrosion of the AAFA system.
- Despite the corrosion, the AAFA system developed a certain resistance, unlike the OPC and AAS systems, since the fully corroded AAFA specimens developed a residual strength of around 11MPa due to the silica-rich gel. This residual value was more rapidly reached as the acid concentration increased. It is important to note that curing time had no noticeable effect in any of the systems studied, with no differences observed at 7 and 28 days of curing after acid exposure.

4.4.9 Applicability of the test method to AAM

In this test, two parallel studies have been done. In one part, the influence of the indicators of the degree of attack have been analyzed, as the mass and cross-sectional change, visual inspection and compressive strength, as recommended in the standard ASTM C267. In the other part, the influence of the test conditions on the results has been studied, like the curing time before acid exposure and the acid concentration, in this case, sulfuric acid.

Therefore, regarding the 3 systems studied, OPC, AAS and AAFA, several conclusions can be found:

- Mass change, cross-sectional dimensions and visual appearance seemed to be good indicators of the degree of sulfuric acid attack for the OPC due to the nature of corrosion.
- As well as for OPC, mass change, cross-sectional dimensions and visual appearance are good indicators too, but cross-sectional showed to be more representative.
- The compressive strength test is not useful for OPC and AAS systems due to great variability of the dimensions of specimens.

- For AAFA, mass change, cross-sectional dimensions and visual appearance showed to be inadequate to measure the degree of attack. Conversely, compressive strength appears to be better indicator of the degree of acid attack.
- Curing time showed to be not influential on the results, as mortars in every system behave practically the same.
- The nature of corrosion of the AAM depends on the precursor used. Depending on the nature of corrosion, the adequate indicator of the degree of attack will be different.

To summarize, this work highlights certain gaps with applying standards, initially developed for OPC, to alkali-activated systems without any change. Due to the different deterioration processes, some of the indicators of the degree of attacks recommended by the ASTM C267 standard seems to be unsuitable for comparative studies between AAM systems. This brings out the necessity to develop new methods to replace conventional methods which are based on mass and cross-sectional dimension changes and sometimes on the compressive strength. Based on the work of Allahverdi and Škvára (Allahverdi & Škvára 2001a), some authors recommend the use of the corroded depth layer as indicator of the degree of attack (Lloyd et al. 2012; Bernal et al. 2012). Microstructural analysis and XRD characterization need also to be taken into account to assess the deterioration of AAM systems.

4.5 Alkali-Silica Reaction

For this test, two test methods have been analyzed for comparative reasons. The first method, ASTM C1260, is an accelerated method used in mortars where an aggressive environment is applied (see **chapter 3.5.4**), and the second method, ASTM C1293, is a less aggressive method used in concretes. In both tests, a reactive aggregate (Spratt) was used in order to induce the ASR.

4.5.1 Adaptation of the formulations according to the standards

In this test, it was necessary to adapt the formulations to the standard requirements in order to do comparative studies between different binders. Thus, binder content was 450g, water/solid was adjusted to 0.47 and sand/binder ratio was 2.25. Else, the solid part of the activator was taken in account as a binder. In the case of the AAFA formulation, water/solid ratio was kept unaltered (0.25), because increasing this ratio to 0.47 specified at the standard would have produced segregation in this system. Thus, the new formulations for the mortars according the ASTM C1260 are shown in **table 4.3**:

Table 4.3 Mortar formulations according to ASTM C1260

(g)	OPC	AAS	AAFA
Binder	450	393	465
w/s	0.47	0.47	0.25
SS	--	93.8	133.2
SH	--	29.6	40.7
HL	--	8	--
Sand 0 - 4.75	1012.5	1012.5	1012.5

In the case of the concretes, standard ASTM C1293 requires a minimum of alkali content of 1.25% Na_2O_{eq} for OPC-based binders, as explained in **chapter 3.5.4**. Thus, only OPC formulation, with a 0.8% of Na_2O_{eq}, had to be adjusted by adding dry NaOH powder to the mix water. The concrete formulations according to ASTM C1293 are shown in **table 4.4**:

Table 4.4 Concrete formulations according to ASTM C1293

(kg/m^3)	OPC	AAS	AAFA
Binder	400	400	465
w/s	0.45	0.45	0.25
SS	--	93.8	133.2
SH	2.3*	29.6	40.7
HL	--	8	--
Na_2O_{eq}	1.25	5.00	7.10
Sand 0 - 5	781	636	666
Spratt 4.75 - 9.5	356	356	356
Spratt 9.5 - 12.5	356	356	356
Spratt 12.5 - 19.0	358	358	358

*Added as dry powder and not as 50wt% solution

4.5.2 ASTM C1260 (Accelerated mortar-bar test method)

4.5.2.1 Length change

Figure 4.24 shows the expansion results of OPC, AAS and AAFA exposed to 1M NaOH solution at 80ºC during 28 days. For the test, a reactive aggregate usually employed for AAR tests has been used, sieved according the standard requirements, as explained in **chapter 3.5.4**.

It can be observed that the OPC mortar bars experimented a fast expansion after the 4th day, exceeding the limit compliance advisable by the standard of 0.1% at 14 days. Therefore, at 14 days the expansion is in the region above 0.2%, indicating "potential deleterious expansion" of OPC with this type of aggregate. Afterwards, the expansion continues linearly increasing.

In the case of AAS, the expansion experimented by the mortar bars lies in the region between 0.1% and 0.2% at 14 days, 0.138%. When this happens, as recommended in the standard, the aggregates could be reactive or not with the binder, therefore some extra test should be done to corroborate these results. However, at 28 days the expansion is closer to 0.2%, which indicates a potentially deleterious expansion.

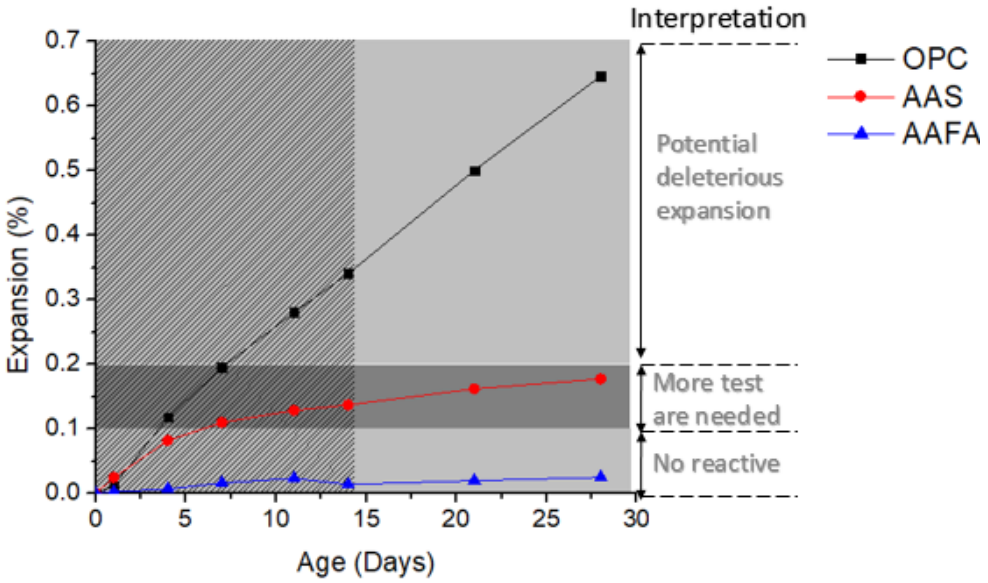

Figure 4.24 Expansion results for the OPC, AAS and AAFA systems with a reactive aggregate Spratt

Even if the AAS mortar bars exceeded the compliance limit of 0.1% at 14 days the expansion observed is 3 times less than those experimented by the OPC mortar bars. Therefore, AAS system can be considered better than OPC systems for preventing the ASR at the same conditions. This point will be seen later in the concrete test method.

Finally, in the AAFA system, the mortar bars were practically unaffected during time, even at 28 days. These systems are therefore very strong against ASR, even with high alkali content. The results are in accordance with other studies (Xie et al. 2003; García-Lodeiro, Palomo, et al. 2007; Kupwade-Patil & Allouche 2013) in which similar AAFA formulations behaved very well at the same conditions (ASTM C1260) with reactive aggregates.

4.5.2.2 Microstructural analysis by means of SEM-BSE

Microstructural analysis was performed by means of SEM-BSE analysis (**figure 4.25**) on OPC and AAS samples at the end of the test, i.e. after 28 days of exposure in 1M NaOH solution at 80ºC.

Regarding the OPC bars, it can be seen that aggregates have been seriously damaged (**figure 4.25 A**). We can observe a huge crack that traverses all the aggregate with some minor cracks. All the cracks are filled by a cracked gel, which composition is shown in the spectra obtained by EDX. This spectra shows that the gel inside the crack is mostly composed by Si, Ca and Na, then is a sodium and calcium silicate hydrate (Ca/Si = 0.59 and Na/Si = 0.27).

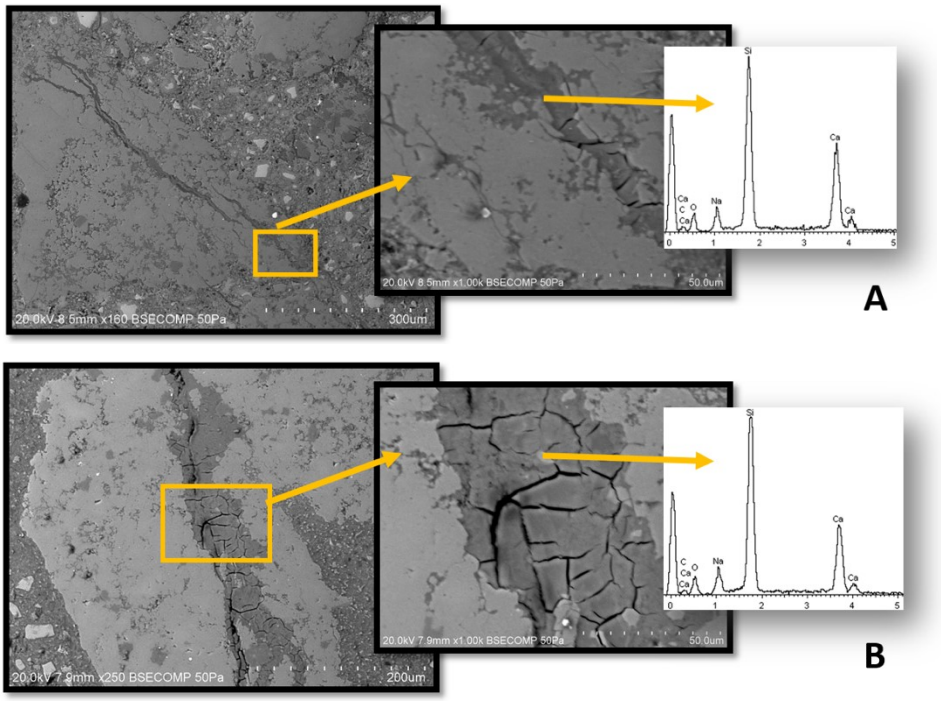

Figure 4.25 SEM-BSE images for OPC (A) and AAS (B) confectioned with the reactive aggregates after 28 days of exposure to 1M NaOH at 80ºC

Similarly to OPC samples, in AAS bars it can be found that aggregates are attacked too (**figure 4.25 B**), observing cracks crossing the aggregates filled by a cracked gel. The EDX analysis showed that the elemental composition was of Si, Ca and Na as well, with similar ratios to those found in OPC (Ca/Si

= 0.41 and Na/Si = 0.27). Thus, a sodium and calcium silicate hydrate is formed. In this case, the ratio Ca/Si was lower, indicating less Ca in the ASR gel.

4.5.2.3 Discussion

In this experiment, ASR was evaluated by means of the accelerated test method described in the ASTM C1260 standard on OPC, AAS and AAFA mortars. A reactive aggregate has been used for this purpose, a siliceous-dolomite limestone considered as highly reactive with alkalis (Spratt). The results obtained showed that the aggregate was susceptible to be attacked by the OPC as well as AAS, but not with the AAFA, under the test conditions (submerged in 1M NaOH at 80ºC).

The problems of OPC binder when mixed with aggregates that contains reactive silica are well known nowadays (Rajabipour et al. 2015; Lindgård et al. 2012), causing expansion by the reaction of the alkalis present in the pore solution of the binder with the reactive silica of the aggregate. The high pH in the pore solution (pH 13-13.5) is the responsible of the dissolution of the silica present in the aggregate. This silica, once dissolved, will then react with the alkalis of the pore solution to form an alkali-silica gel. This alkali-silica gel will furthermore adsorb water producing swelling and cracking of the aggregates and paste.

In this study, expansion results of OPC specimens are in accordance with literature. The fast expansion of the OPC bars has been confirmed by SEM-BSE/EDX analysis to be caused by the formation of an alkali-calcium silicate gel. These results are in accordance with other works in which authors found similar gel composition (Z. Shi et al. 2015).

As shown in the results, AAS expanded less than OPC. It can be seen from **figure 4.24** that the rate of expansion in AAS is lower, and tends to appease during time, which did not occur with OPC where expansion rate after 28 days kept constant. This agrees with Fernández-Jiménez (2002) results. These authors stated that more time is necessary in AAS systems to observe ASR due to the slow reaction rate. SEM-BSE/EDX analysis showed that an ASR gel was formed (between the aggregates). The gel was found to be composed in both cases by an alkali-calcium silicate gel. In the case of the OPC, the ASR gel had the following composition: Ca/Si = 0.59 and Na/Si = 0.27. In the case of AAS the ASR gel had a similar composition than that found in the OPC: Ca/Si = 0.41 and Na/Si = 0.27. Therefore, in both systems, an ASR gel is found with high content of Ca, higher than Na. Moreover, Ca was found to be higher in the ASR gel of the OPC than in the ASR gel of the AAS while alkali content was the same in both cases. It seems that Ca has replaced part of the alkalis in the ASR gel. This replacement of Na by Ca could be partly responsible of the continuous expansion of the OPC system. As stated by Wang & Gillott (1991), when Ca replaces Na in the ASR gel, alkalis released are available for further

reaction with silica to produce new expansive ASR gel. The source of Ca in the OPC system could come from the portlandite, that would decompose to balance the Ca ions in the pore solution as they are consumed in the ASR (Leemann et al. 2011; Rajabipour et al. 2015). In the case of AAS, Ca content is elevated too. However, in this case the Ca is present in more stable compounds such as C-A-S-H gel and hydrotalcites, which are not decomposed as easily as portlandite to further supply Ca to the pore solution.

Other causes can be attributed to the lower expansion observed in AAS systems compared to OPC systems by ASR. This is the case of the main hydration gel formed, C-A-S-H in the former and C-S-H in the latter. The C-A-S-H gel, with low Ca/Si ratio, has been found to bind more alkalis to their structure (Hong & Glasser 2002), thus less alkalis would be in the pore solution lowering the pH in it. Lower pH in the pore solution will have a positive effect reducing the dissolution of the reactive silica of the aggregates and thus the ASR gel produced. Therefore, although the alkalinity is maintained by the external NaOH solution, it can be a competition for the alkalis between the slag and the ASR (Fernández-Jiménez & Puertas 2002), inhibiting the effect of ASR. Other cause, as explained before, is that the lack of calcium hydroxide (portlandite) in AAS system decreases the concentration of calcium ions in the pore solution (Ichikawa 2009; Leemann et al. 2011). Calcium is thought to play an important role in the developing of expansive ASR gels (Rajabipour et al. 2015), although its influence is still controversy.

In some works, the effect of the pH evolution of the pore solution in the expansion of AAMs has been demonstrated (Pouhet & Cyr 2015; Z. Shi et al. 2015). In these works, the evolution of $[OH^-]$ in the pore solution of AAMs has been followed, concluding that the systems with less $[OH^-]$ tended to form less ASR gel and thus to expand less.

All of the reasons stated above about the lower expansion of AAS compared to OPC are in the same manner applicable to AAFA results. In these systems, no expansion was found. These results are in accordance with some other works (Xie et al. 2003; Kupwade-Patil & Allouche 2011; Kupwade-Patil & Allouche 2013; Fernandez-Jimenez et al. 2007a; García-Lodeiro, a. Palomo, et al. 2007), in which AAFA systems under similar conditions were found to have low expansion. The main reasons of the good behavior against ASR of AAFA system were already stated by Xie et al (2003): a) the low content of Ca allows to produce an ASR gel with low Ca-content, believed to be less expansive, b) there is more space to grow the ASR gel due to a higher porosity of these systems, c) reactivation of chemical reactions due to elevated temperatures and extra alkali supply by the NaOH solution that are favorable for this system, and d) autogenous shrinkage of AAFA systems that can compensate expansion due to ASR gel.

4.5.2.4 Conclusions

The following conclusions can be drawn from the results of ASR by means of the accelerated test method (ASTM C1260):

- It has been found potential deleterious expansion when reactive aggregate was used with OPC (expansion more than 0.2%).
- In the case of AAS, the expansion of bars after 14 days falls in the region between 0.1% and 0.2% of expansion. Thus, according standard, more test are needed to predict the potential reactivity of AAS.
- AAS has been found to be less susceptible to deterioration by ASR than OPC with 3-fold lower expansion. The low calcium content and the type of hydration products formed in AAS (C-A-S-H and hydrotalcites) seemed to be the primary reason of the lower expansion.
- The rate of expansion in AAS system was lower than in OPC, and tended to slow after 28 days of exposure. On the contrary, the expansion rate in OPC was constant during test.
- SEM-BSE/EDX results in OPC and AAS showed the apparition of a gel between the reactive aggregate, producing cracks. The gel was found to be an alkali-calcium silicate.
- AAFA didn't produce any expansion, showing very high resistance against ASR. The low-Ca content, higher porosity, autogenous shrinkage and the test conditions (that are favorable for this system) seem to be the primary causes of this.

4.5.3 ASTM C1293 (test method in concrete)

4.5.3.1 Length change

Figure 4.26 a, b and c shows the expansion of the OPC, AAS and AAFA concrete prisms exposed to 38ºC. In each figure four curves can be seen, representing different conditions in which the concrete bars were subjected. One set of bars were kept at 23ºC and 100% RH chamber all the test (represented as 23ºC in the figure). Other set of bars were cured according to ASTM C1293 standard (after demolding, the prisms were placed in a sealed container at 38ºC and 100% RH) (represented as 38ºC/1D in the figure). In the last conditions, the prisms were kept in a humidity chamber at 23ºC during 28 days and 90 days respectively prior to put them in a sealed container at 38ºC (represented as 38ºC/28D and 38ºC/90D respectively in the figure). In these special cases, the zero time is when the prisms are placed in the sealed container at 38ºC and 100% RH, and it has already an initial value showing the expansion that occurred during the period in the humidity chamber prior to place them at 38ºC.

For the OPC concrete prisms (**figure 4.26 a**) it can be observed that the expansion of the prisms kept the whole time in a humidity chamber at 23ºC is practically constant until 300 days. Instead, it is observed a shrinkage between 100 and 300 days. At 300 days, it seems that the prisms start to expand, although more data is needed to confirm that trend. The prisms that followed the standard conditions (38ºC/1D in the figure) experimented an expansion after 50 days, exceeding the limit compliance of the standard (0.04%) after 100 days. Afterwards, the expansion was practically constant until 360 days. For the prisms that were put in the sealed container at 38ºC after a 28 and 90 days period in a humidity chamber (38ºC/28D and 38ºC/90D in the figure), it can be observed that the expansion is lower than those put at 38ºC after demolding. The later the prisms were put at 38ºC, the lower the expansion was. Nevertheless, in both cases the limit compliance was exceeded.

In the case of the AAS concrete prisms (**figure 4.26 b**) none of the set of prisms exceeded the limit compliance after 360 days. Instead, it can be seen that all the sets of prisms suffered a shrinkage during the first 2 months approximately. The lowest shrinkage was found for the prisms kept in a humidity chamber at 23ºC all the time. After this age, the latter prisms still continued with a shrinkage trend. However, the prisms that were at 38ºC started to expand after the first two months. It can be seen that the prisms with higher expansion were the prisms put in the sealed container at 38ºC after demolding, with a total of 0.01%. Then it was found that the prisms kept during 90 days in a humidity chamber at 23ºC expanded again to kept around 0.00% (still in shrinkage values) and those kept during 28 days expanded to reach around -0.01% (again still in shrinkage values).

In the case of AAFA concrete prisms (**figure 4.26 c**) it can be seen a shrinkage during all the test (360 days), with some minor fluctuations. Two different periods can be observed. The first period around 60 to 100 days, in which all the prisms experimented a low shrinkage, and the second period afterwards in which there was a fast shrinkage. In all the conditions, the prisms seem to stabilize around 275 days. It has been found the same shrinkage for the prisms kept the whole time in a humidity chamber at 23ºC and for the prisms put in the sealed container at 38C after demolding. Hence, both set of prisms got -0.03% of expansion. For the other set of prisms, the shrinkage was the same, being of -0.04% of expansion.

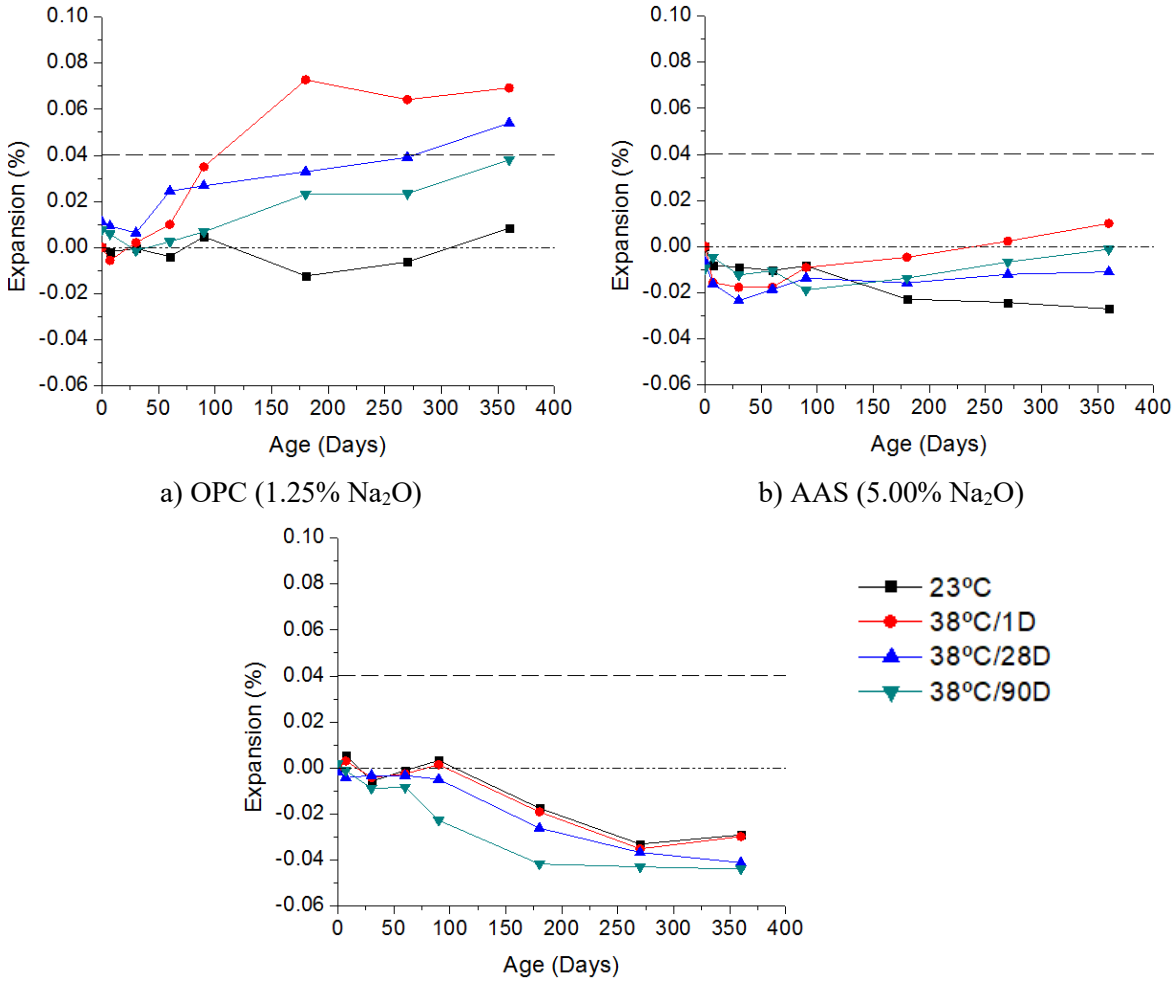

a) OPC (1.25% Na_2O)

b) AAS (5.00% Na_2O)

c) AAFA (7.00% Na_2O)

Figure 4.26 Expansion of OPC (a), AAS (b) and AAFA (c) concrete prisms exposed at different conditions: at 23ºC/100% RH all the time; at 38ºC/100%RH (ASTM C1293) after demolding, after 28 days and after 90 days at 23ºC/100% RH.

4.5.3.2 Mass change

The mass change of the same prisms used to follow the expansion was also measured. The results can be seen in **figure 4.27**. As in the case of the expansion, the zero value represents the point in which the prisms were placed at the test conditions, i.e. sealed container at 38ºC (less the set of prisms kept all the time at 23ºC).

In the case of the OPC concrete prisms (**figure 4.27 a**), all the set of prisms experimented an increase of the mass during time. The prisms that were kept in a humidity chamber at 23ºC the whole time experimented a higher increase. The prisms put in the sealed container at 38ºC after demolding experimented a more progressive increase of the mass, being quite similar to that obtained by the prisms in a humidity chamber after 360 days. In the case of the prisms kept during 28 and 90 days in a humidity

chamber, it can be seen that at 0 days (when the prims were put at 38C) the mass has already increased. This, as explained before, is the mass change of the prisms during the period in a humidity chamber. Thus, it can be seen that in both cases, the prisms suffered a mass loss at the beginning of the conditions in the sealed container at 38ºC. This is logic because at these new conditions the humidity is lower than that of the humidity chamber (contact with fog), and the prisms experienced an initial mass loss. Afterwards, there was an increase in both conditions.

In the case of AAS, all the sets of prisms experimented the same mass gain after 360 days. The mass gain was around 0.6-0.7%.

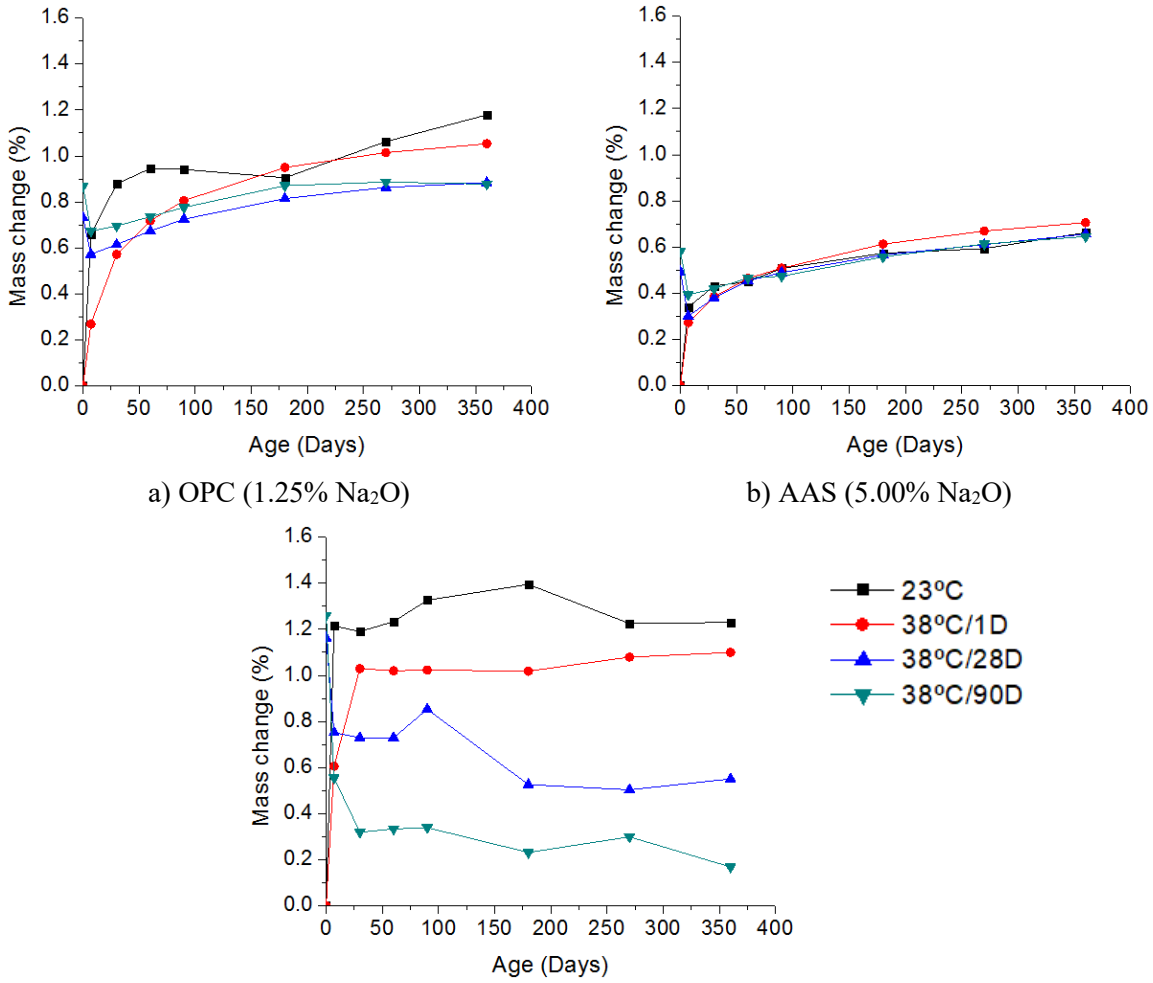

a) OPC (1.25% Na_2O)

b) AAS (5.00% Na_2O)

c) AAFA (7.00% Na_2O)

Figure 4.27 Mass change of OPC (a), AAS (b) and AAFA (c) concrete prisms exposed at different conditions: at 23ºC/100% RH the whole time; at 38ºC/100%RH (ASTM C1293) after demolding, after 28 days and after 90 days at 23ºC/100% RH.

Finally, for the AAFA concrete prisms, different behaviors can be observed, although in all the cases there was a mass gain. Thus in all the cases, the mass increased. These mass increases were produced

during the first two weeks, and afterwards remained practically constant. The prisms with higher mass increase were those kept the whole time in a humidity chamber at 23ºC, with 1.2%. The set of prisms that followed the ASTM C1293 standard conditions (38ºC after demolding), experimented a mass gain after 360 days close to the formers, with 1.0%. In the case of the set of prisms with a pre-conditioning period in a humidity chamber prior to expose at 38ºC conditions (38ºC/28D and 38ºC/90D in the figure), it is observed a mass loss during the first months in the sealed container at 38ºC, as observed with the OPC concrete prisms. As explained before, in the new conditions at 38ºC, the prisms have lost part of the initial humidity as these conditions are different to those in the humidity chamber. After the first month, it can be observed a mass loss trend in the case of the 38ºC/28D prisms that became constant after 200 days. For the 38ºC/90D prisms, the mass kept constant all the test after the first month.

4.5.3.3 Discussion

In this experiment, ASR was performed by means of the concrete bar test method described in the ASTM C1293 standard for OPC, AAS and AAFA. In this case, a siliceous-dolomite limestone, considered as highly reactive with alkalis (Spratt), has been used as the coarse aggregate. Normal silica sand, considered to be non-reactive, has been used as the fine aggregate of the concretes.

In this test, not only the susceptibility to ASR of different systems (with very big differences on the alkali content) have been studied but the test conditions in which the experiment was carried out too. Thus, the effect of the curing time prior to subject the concrete prisms to 38ºC (according to ASTM C1293 standard) has been also analyzed.

As shown in the results, the OPC concretes prisms have shown to exceed the standard limit compliance of 0.04% at 360 days in all the situations in which the prisms were subjected to 38ºC conditions. The prisms which were kept all time at 23ºC did not expand as fast as the others, as has been already demonstrated for OPC (Wigum et al. 2006). In this system, it has been found that temperature of the test conditions had a main role in the expansion rate and extent (Wigum et al. 2006). At ambient temperature, it has been found lower expansion rate, but higher expansion extent during years. In this study, it can be seen that after one year (the end of the test), the expansion is lower comparing with prisms subjected to 38ºC. Hence, the results of this test are in line with literature, showing a low expansion for the prisms kept at 23ºC after 1 year.

Similar trend was observed for AAS. But in this case, none of the studied concrete prisms exceeded the compliance limit of 0.04%. For this system, it was found that the prisms kept at normal temperature all time, i.e. 23ºC, experimented a shrinkage rather than an expansion. It can be seen that at the end of the test according to standard, one year, the prisms continued to shrink. It has already been found in other

studies that AAS systems have tendency to shrink, even in humidity conditions (Duran Atiş et al. 2009; Chi et al. 2012; Ye & Radlinska 2016). In the other cases studies, in which prisms were subjected to 38ºC, it was found that as the prisms were kept longer at 23ºC prior to place them at 38ºC, the expansion at 1 year was lower. However, prisms cured during 90 days at 23ºC got higher expansion than those cured during 28 days at the same conditions. This could be due to the higher shrinkage that this prisms suffered during the first month at 38ºC in the sealed container. It has to be pointed out that there is a direct effect of changing the conditions of the prisms from the humidity chamber at 23ºC to the sealed container. This change can produce a partial desiccation of the samples prior to stabilize to the new conditions, producing this shrinkage. This effect was also observed in a lesser extent in the OPC prisms.

According to this results, it is shown again, as it was found in the OPC system, that the curing time at normal temperature prior to subject the prisms at 38ºC is beneficial in terms of the expansion extent observed at one year. This demonstrate that following the ASTM C1293 standard procedure, higher expansion would be observed at one year. This will confirm that alkalis in pore solution continue to be fixed in the structure with curing time, decreasing the allowable alkalis to participate in the ASR. However, the same time as alkalis are fixed to the structure during time, the natural shrinkage of these systems would balance the effect of the expansion by ASR.

Finally, in the case of the AAFA system, different behavior that those found in the OPC and AAS was observed. For this system, it was not found any sign of expansion but a high shrinkage. Despite the test conditions used (in terms of curing time and temperature), in all cases it was found similar shrinkage trend and extent. In the case of the prisms that were subjected to 38ºC after a period in humidity conditions, the shrinkage extent was little higher.

An interesting point to note comparing the three systems is that, as happened in the accelerated ASR test method in mortar (**section 4.5.2**), the OPC concrete prisms got the highest expansion despite its lowest alkali content (1.25% of Na_2O_{eq} comparing to 5.00% of AAS and 7.10% of AAFA). Furthermore, in the case of AAFA, there was a shrinkage instead, that stabilize after 200 days.

4.5.3.4 Conclusions

The following conclusions can be drawn from the results of ASR by means of the concrete bar test method (ASTM C1293):

- OPC concrete prisms experimented higher expansion than the AAS and AAFA concretes prisms, despite the higher alkali content of the last.

- OPC concrete prisms got the higher expansion when they were subjected to 38ºC after demolding (ASTM C1293 procedure). Keeping the prisms in humidity conditions at 23ºC showed to be beneficial for the expansion extent after 1 year.
- AAS concrete prisms passed the test in all the curing regimes studied. The worst condition was when the prisms were subjected to 38ºC after demolding and the best when the prisms were kept all time at 23ºC. However, it was found shrinkage in all cases at the beginning of the test, and during all the test for the prisms kept all time at 23ºC. This shrinkage could be partly responsible of the lower expansion of AAS comparing to OPC.
- AAS concretes cured longer at 23ºC before being subjected to 38ºC showed to have lower expansion than the prisms that were exposed at this temperature after demolding. This could be due to a higher fixation of alkalis in the microstructure, and thus, less free alkalis are allowed to participate in the ASR.
- AAFA concretes showed in all the cases a shrinkage instead an expansion. Thus, this systems are very favorable for preventing ASR.

4.5.4 Applicability of the ASR test methods to AAM

From the results obtained in both test methods (accelerated mortar-bar test method and concrete test) the following recommendations are given:

- There is a correlation in both test methods for AAMs. For both AAM systems studied (AAS and AAFA) it has been found similar conclusions.
- Shrinkage could compensate the real expansion due to ASR in AAS and AAFA, thus obtaining misleading results. In the case of AAFA, this factor is higher, as the expansion due to ASR is considered as negligible.
- The test conditions of the ASTM C1260, where samples are immersed in an alkaline solution at 80ºC, could be favorable in some extent due to an extra supply of alkalis for the hydration/geopolymerization reactions. Thus, it could be a competition by the ASR and the normal hardening reactions for the alkalis. This effect could take place too in the concrete test, where the alkalis in pore solution could be participating in both reactions.

4.6 Freeze-thaw resistance

4.6.1 Fresh and hardened concrete properties

In this particular test, as one of the parameters to study is the influence of the air content of the AAM concretes on the freeze-thaw resistance, an air-entrainer agent (AEA) have been employed, as described in chapter 3.5.5. Therefore, as a new admixture is introduced in the concrete formulations, the fresh and hardened properties of the concretes are different. Thus, the effect of the AEA on the fresh properties are shown in **table 4.5**:

Table 4.5 Fresh properties of the concretes with and without AEA

	OPC		AAS			AAFA		
AEA[1]	0	60	0	60	120	0	60	120
Air (%)	1.5	4.9	1.6	3.6	7	2.1	1.1	1.3
Wk[2] (cm)	7.5	8.5	22	20.5	24	24	24	24

1: mL AEA/100kg of binder

2: Wk: workablity

In OPC, the addition of 60 ml of AEA each 100 kg of binder considerably increased the air content, from 1.5% of air without addition to 4.9% with AEA. This air content is a priori very good value, as the recommended air content for concretes exposed to F-T environments are around 4.5 to 7.5% depending on the severity of exposure, according to ACI 201.2R-08. The workability of the concretes are not affected by the AEA addition.

For the AAS concretes, as it is not still well understood how the AEA will behave in the presence of high alkaline system, an extra AEA addition has been evaluated, in this case it was 120 mL AEA/100kg of binder. The results showed a progressive increase of the air entrained as the AEA added increased. However, this increase was lower than those experimented by the OPC concretes. Considering the F-T behavior of AAS systems like OPC systems, we could consider that the AEA dosage necessary to be in the range of the ACI 201.2R-08 recommendations (4.5-7.5%) should be more than 60mL/100kg of binder. This consideration will be answered in the following points. Regarding the workability, it is observed that up to 60 ml of AEA is practically constant, and then increases.

In the case of AAFA concretes, different behavior of those observed for OPC and AAS is obtained. The air content without addition of AEA initially was of 2.1%. When a 60 ml/100kg of binder was added, the air content decreased up to 1.1%. Something similar happened with the addition of 120 ml of AEA, with an air content of 1.3%. However, it has to be pointed that the viscosity of the AAFA

concrete mixtures was too high, and thus the air content measurement method could be ineffective. The method used in this project was the pressure method type B, according to ASTM C231. It is possible that the pressure applied by the sealed air chamber (see standard for more details) cannot effectively be diffused by the fresh mixture due to the high viscosity and thus may record wrong values. Moreover, workability showed to be constant independently of the AEA added.

In **table 4.6** it can be observed the air content measured in hardened conditions after 28 days of curing, according to the standard ASTM C457 (modified point test). It can also be observed the specific surface (α), defined as the surface area per unit volume of voids, and their spacing factor (L), defined as the largest distance from anywhere in the cement paste to an air void.

Table 4.6 Hardened properties of the concretes with and without AEA

	OPC		AAS			AAFA		
AEA[1]	0	60	0	60	120	0	60	120
Air[2] (%)	1.0	4.3	0.8	1.3	2.1	1.4	N.A.[5]	N.A.
α[2,3] (1/mm)	4.5	27.3	8.3	15.1	19.9	16.8	N.A.	N.A.
L[2,4] (μm)	2231	202	1475	662	395	535	N.A.	N.A.

1: mL AEA/100kg of binder

2: According ASTM C457 (modified point test)

3: α, specific surface

4: L, spacing factor

5: N.A. Not available

For every case, it is observed that the air content measured in hardened conditions is always lower than what is measured in fresh condition. For OPC system, the difference is negligible, but in the case of AAS, the difference was more marked. These results are in accordance with those obtained by Douglas et al. (1992). The authors state that it is relatively easy to introduce air in the concrete, but the air-voids generated in the mixing are probably unstable because of a poor air-voids system found in hardened conditions compared to fresh conditions. Regarding the spacing factor and the specific surface parameters, the ACI 201.2R-08 indicates that the generally accepted maximum spacing factor value for concrete with good resistance to freezing and thawing is a maximum of 200 μm, and the generally accepted value of specific surface for resistance to freezing and thawing is a minimum of 25 mm^2/mm^3. Therefore, the OPC without AEA was out of this specifications, being 4.5 of specific surface and 2231 of spacing factor. Nevertheless, when we add 60 mL/100kg of binder, both spacing factor and specific surface are very close to the specifications. For AAS concretes, in all the cases, the spacing factor and the specific surface were out of the specifications. However, the addition of an AEA improves the

value, getting closer to the specifications when the AEA content was 120 mL/100kg of binder. In the case of AAFA, the only analyzed concrete was without AEA addition, and the results were also out of the specifications.

Although the ACI recommendations of specific surface and spacing factor are not met by the AAMs systems, it should be evaluated if this recommended values are also valid for them. This will be evaluated in the next points.

In order to see how AEA affected the mechanical properties, compressive strength was tested in OPC and AAS concretes. Results are shown in **figure 4.28**. It can be seen that for OPC, the compressive strength decreases by 41% after the 1st day when 60mL of AEA/100kg was added to the binder. This compressive strength is in line with the higher volume of pores entrained when AEA was used. Afterwards, at 7, 28 and 90 days, the compressive strength is reduced by around 23% when AEA was added the AEA. This could suggest a refinement of the pores during time. In the case of AAS, the strength reduction after the 1st day was not as high than in OPC when 60mL of AEA/100kg was added to the binder. In both the AAS and OPC cases, the strength is reduced by 4%. At later ages, strength reduction increased in the range of 8-13%. When 120mL of AEA/100kg was added to the binder, the strength was reduced by 10% at one day, and at later ages, it was reduced in the range of 16-18%.

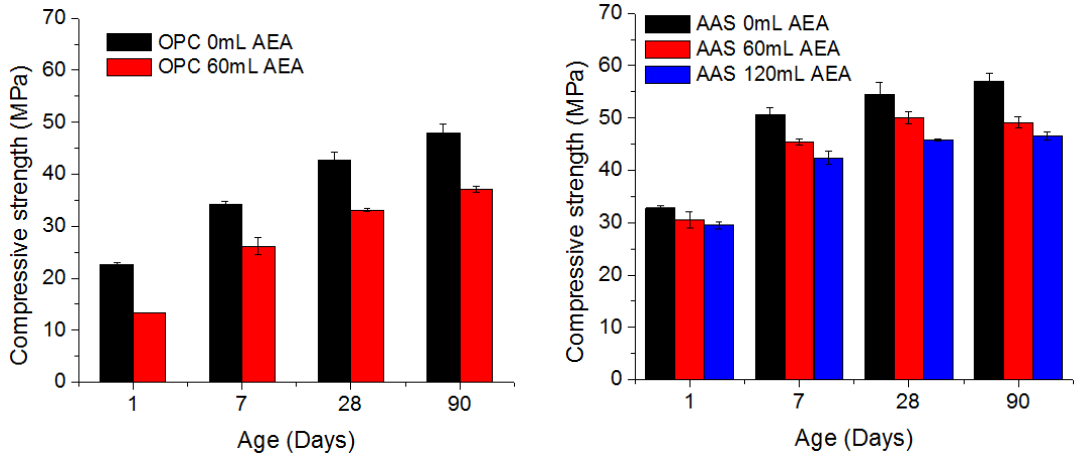

a) OPC b) AAS

Figure 4.28 Compressive strength evolution in function of the AEA agent added

4.6.2 Relative dynamic modulus of elasticity (RDME)

The relative dynamic modulus of elasticity (RDME) has been calculated according to the standard ASTM C666 by measuring the fundamental transverse frequency of the concrete prisms. Therefore, the RDME is calculated as follows:

$$p_c = (n_1^2 n^2) x 100 \quad (4.5)$$

where:

p_c is the RDME, after c cycles of freezing and thawing, in percent
n is the fundamental transverse frequency at 0 cycles of freezing and thawing
n_1 is the fundamental transverse frequency at c cycles of freezing and thawing

This equation, as pointed in the standard, is based on the assumption that the mass and dimension of the specimens are constant during the test. According to the standard, when RDME falls below 60% of the original, the test is failed, or when the length change exceeds 0.10% of expansion.

With RDME, the standard propose to calculate the durability factor (D_F) as follows:

$$\mathrm{DF} = \mathrm{PN}M \quad (4.6)$$

where:

DF, is the durability factor,
P, is the RDME at N cycles, %
N, I the number of cycles at which P reaches the specified minimum value for discontinuing the test or the specified number of cycles at which the exposure is to be terminated, whichever is less,
M, is the specified number of cycles at which the exposure is to be terminated

Figure 4.29 A and B show the F-T resistance of OPC concrete prisms without AEA and with AEA respectively, in terms of RDME. In each figure, it can be observed the influence of the curing time (7, 14 and 28 days) before starting the F-T cycles on the results. Moreover, figures are accompanied by a photo of the aspect of the prisms at the end of the test (only prisms cured during 14 days are shown). When OPC concrete was confectioned without an AEA (1.5% of air) (**figure 4.29 A**) RDME decreased with the F-T cycles up to destruction of the prisms after 100 cycles. It is observed an influence of the curing time before starting the F-T cycles on the RDME loss rate. Longer the prisms were cured, the faster was the decrease of RDME. It has to be pointed out that in all the cases, RDME felt below 60% before 300 cycles. There, the F-T tests could have been stopped. In this case, it was decided to continue the test until a total destruction of the sample. Nevertheless, during this period, the mass of the samples changed considerably (as shown later in chapter 4.6.4), so RDME calculations should only be taken for comparative purposes.

When OPC concrete was confectioned with an AEA dosage of 60mL/100kg of binder (4.9% of air) (**figure 4.29 B**), RDME remained practically invariable during time regardless the curing conditions. This put in evidence the importance of adding an AEA in this kind of systems in order to increase the total volume of voids, and thus their frost resistance. With this dosage, we got 4.9% of air voids that demonstrated to be very good to resist in an effective manner to the F-T environments.

A) No AEA

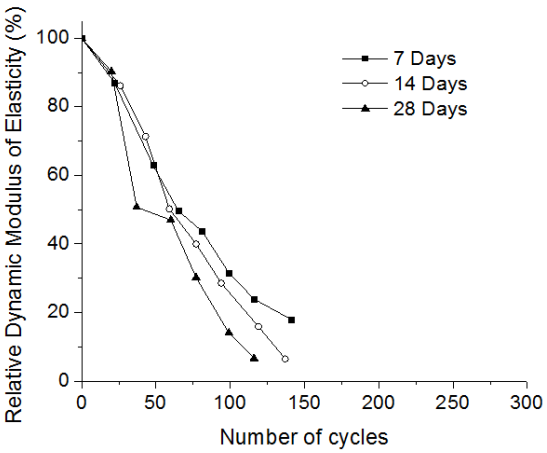

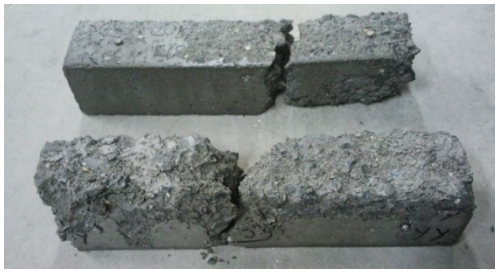

OPC prisms without AEA (14 days curing) after 140 F-T cycles

B) 60mL AEA/100kg binder

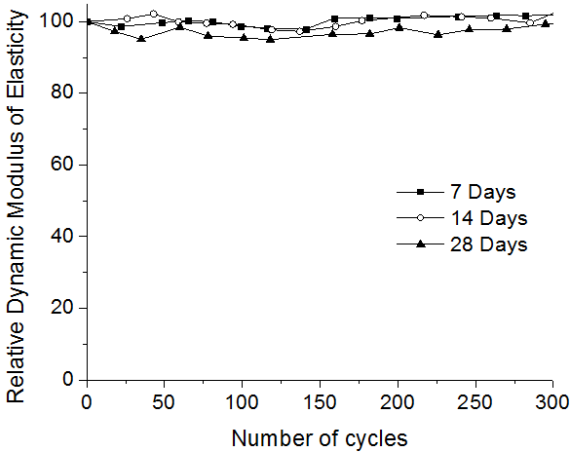

OPC prisms with AEA (14 days curing) after 300 F-T cycles

Figure 4.29 Relative dynamic modulus of elasticity of OPC concretes exposed to F-T cycles at different curing times: A, without AEA; B, with 60mL of AEA/100kg of binder

Observing the pictures of the OPC samples at the end of the test, we can see the difference between introducing an AEA or not in OPC concretes. When an AEA was not introduced (**figure 4.29 A**), the prisms were broken into two halves, with a noticeable loss of mass in all the faces of the prisms. On

the contrary, with an AEA (**figure 4.29 B**) the prisms kept practically intact during all the test, just with a small loss of the skin in certain regions of the surface.

Figure 4.30 A, B and C shows the F-T resistance of AAS concrete prisms without AEA, with AEA and with extra AEA respectively, in terms of RDME, and when concretes were subjected to different curing times (7, 14 and 28 days). When concrete was confectioned without an AEA (1.6% of air) (**figure 4.30 A**), RDME remained practically invariable regardless the curing time up to 100 cycles. At this point, RDME started to continuously decrease up to 91%, 84% and 63% after 300 cycles when the prisms were cured during 7, 14 and 28 days respectively. In every case, the test was passed, as RDME was above 60% at 300 cycles as recommended in the standard ASTM C666. It was found that the best results were also for 7 days of curing time, as happened in OPC concretes. The addition of a dosage of 60mL of AEA/100kg of binder (3.6% of air) (**figure 4.30 B**) increased the final resistance for every case. In this case, RDME remained practically constant up to 210 cycles, more time compared to the 100 cycles that the RDME kept constant without air. In the case of the prisms cured during 7 days, RDME stayed practically constant until the end of the test, 300 cycles. However, for the prisms cured at 14 and 28 days, after 210 cycles, RDME decreased up to 88% and 80% respectively. Final RDME for these prisms are higher than the obtained without air at the same conditions (84% and 63%). Thus, AEA seems to be effective in improving the frost resistance. Finally, with the addition of an extra AEA, with a dosage of 120mL of AEA/100kg of binder (7.0% of air) (**figure 4.30 C**), different behaviors were observed depending on the curing time. For the prisms cured at 7 days, RDME increased over 100% at the end of the test, what it would mean that the mechanical properties were still increasing during the F-T cycles. For those cured during 14 days, RDME kept practically constant up to 250 cycles, and decreased up to 91% afterwards. Compared to the prisms with 60mL of AEA/100kg of binder, there is a slight improvement of the resistance. And for the prisms cured at 28 days, RDME slightly decreased during the first 235 cycles up to 90% and decreased up to 77% afterwards, showing less resistance than when the AEA was of 60mL (80%), although the results were quite similar.

Observing the photos, no great differences can be visually appreciated between the prisms without AEA, with 60ml and with 120mL/100kg of binder. It is appreciable in all cases a loss of the skin of the prisms, which is more noticed for the prisms without AEA.

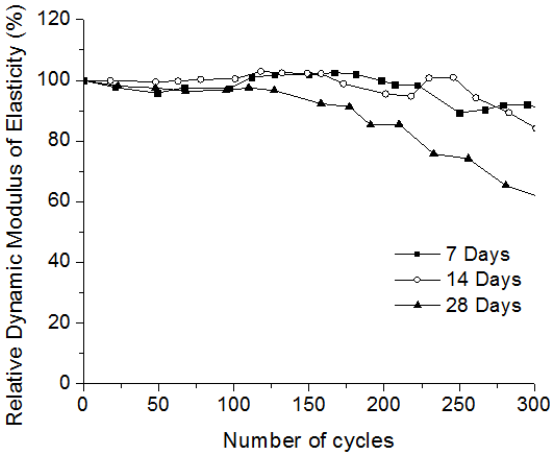

A) No AEA

AAS prisms without AEA (14 days curing) after 300 F-T cycles

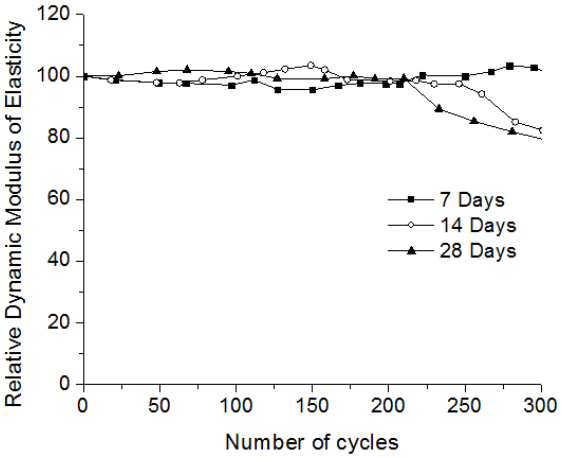

B) 60mL AEA/100kg binder

AAS prisms with AEA (14 days curing) after 300 F-T cycles

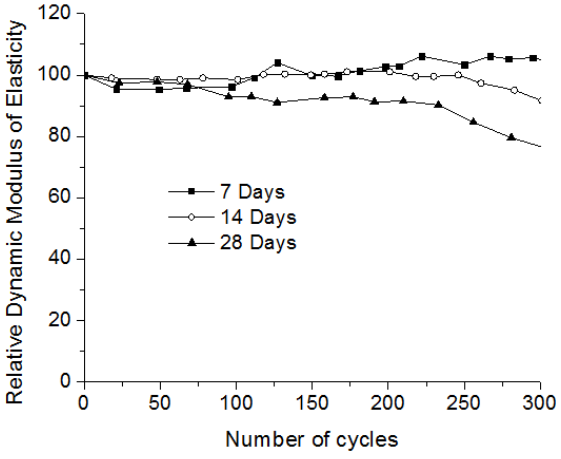

C) 120mL AEA/100kg binder

AAS prisms with extra AEA (14 days curing) after 300 F-T cycles

Figure 4.30 Relative dynamic modulus of elasticity of AAS concretes exposed to F-T cycles at different curing times: A, without AEA; B, with 60mL of AEA/100kg of binder; C, with 120mL of AEA/100kg of binder

Finally, **figure 4.31** shows the F-T resistance of AAFA concrete prisms without AEA, with AEA and with extra AEA respectively. In these systems, particular results were found. As the prisms were destroyed before 20 F-T cycles, RDME could not be measured. Despite the addition of AEA, the resistance was not improved. As it was shown in **table 4.5**, the addition of AEA did not increase the air content but decreased it. Consequently, this particular formulation, as it was designed, had very bad F-T resistance, and the type of AEA used, based on sulfate hydrocarbons, proved to be not effective.

A) No AEA

AAFA prisms without AEA (14 days curing) after 22 F-T cycles

B) 60mL AEA/100kg binder

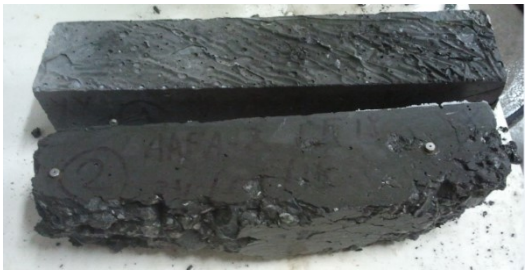

AAFA prisms with AEA (14 days curing) after 22 F-T cycles

C) 120mL AEA/100kg binder

AAFA prisms with extra AEA (14 days curing) after 22 F-T cycles

Figure 4.31 Relative dynamic modulus of elasticity of AAFA concretes exposed to F-T cycles at different curing times: A, without AEA; B, with 60mL of AEA/100kg of binder; C, with 120mL of AEA/100kg of binder

Table 4.7 shows the durability factors (DF) calculated by **equation 4.6** by means of RDME results. This factor represents the real resistance of the concrete compared to a maximum of 100% at 300 cycles. The great differences between OPC and AAS concretes without AEA can be observed. AAS prisms had very good results whereas OPC prisms were completely destroyed. Nevertheless, with the addition of the AEA, OPC concrete resistance was improved with a DF of more than 100, indicating very good resistance. Instead, the improvement in AAS was more progressive, requiring more AEA dosage to get

around of 100 of DF. In the case of AAFA concretes, DF could not be calculated because of the fast failure of the prisms.

Table 4.7 Durability factors of OPC, AAS and AAFA concrete prisms whit different curing times

		OPC		AAS			AAFA		
AEA		**0**	**60**	**0**	**60**	**120**	**0**	**60**	**120**
DF	7 days	9	102	90		104			
	14 days	3	103	84		92		N.C.	
	28 days	2	99	60	78	74			

N.C.: It was not possible to calculate due to rapid failure

4.6.3 Length change

Figure 4.32 shows the length change of OPC concrete prisms exposed to F-T cycles at different curing times, with and without AEA addition. When concretes were confectioned without AEA addition (**figure 4.32 A**), it could be observed a rapid and exponential expansion of the prisms. The expansion limit allowable by the standard, 0.10%, was exceeded after 39 cycles for the prisms cured at 7 and 14 days, and at 31 cycles for those cured at 28 days. As it happened with the loss of RDME, the worst situation was obtained for the prisms cured during a longer time: 28 days. On the other hand, when AEA was added with a dosage of 60mL/100kg of binder (**figure 4.32 B**), the length was constant and practically negligible.

Comparing length change and the RDME failure criteria, results showed that with length change as an indicator of the degree of attack, the test failed earlier. For instance, test failed at 39, 39 and 31 cycles for the prisms cured at 7, 14 and 28 days, when length change was used as indicator, whereas test failed at 52, 52 and 35 cycles respectively according RDME results. In this particular case, the differences are not noteworthy, as they are not big differences, and in all the cases the test failed rapidly.

Figure 4.33 shows the length change of AAS concrete prisms exposed to F-T cycles at different curing times, without, with and with an extra AEA addition. For the concretes without AEA (**figure 4.33 A**), the length kept practically invariable up to 100 cycles. This value is in accordance with RDME results, were RDME kept invariable too during this period. Afterwards, it is observed an expansion of all the prisms, more marked when higher was the curing time. According to the specifications of the standard ASTM C666, test failed at 262, 280 and 222 cycles for the prisms cured at 7, 14 and 28 days respectively, as the length change was superior to 0.10%. According to RDME failure criteria (**figure**

4.30 A), the test succeed in every curing conditions, as RDME was at 300 cycles more than 60%. Therefore, in this case, there is a contradiction depending on the criterion used to evaluate the results.

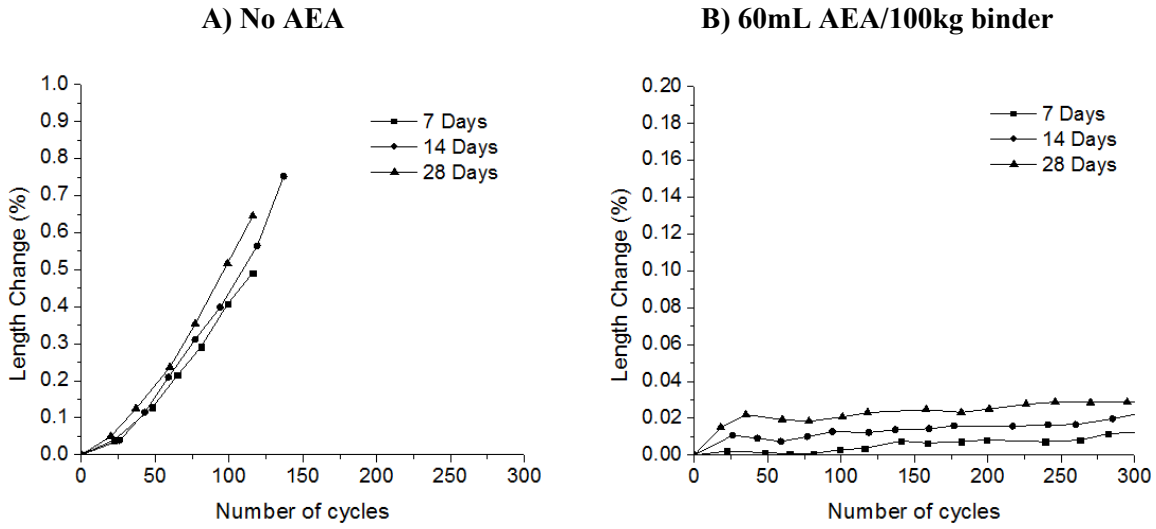

Figure 4.32 Length change of OPC concretes exposed to F-T cycles at different curing times: A, without AEA; B, with 60mL of AEA/100kg of binder

When a dosage of 60mL AEA/100kg of binder was added to the AAS concrete (**figure 4.33 B**), the length remained practically invariable up to 100 cycles, as for the concrete without AEA. Nevertheless, in this case, after 100 cycles the length increased softly until 300 cycles, up to 0.04, 0.11 and 0.11% when prisms were cured during 7, 14 and 28 days respectively. In all the cases, length change was lower than that of the prisms without AEA, in line with the better RDME results. According to the failure criteria of the standard, only the prisms cured during 7 days passed the test meanwhile the rest was slightly superior to the limit expansion of 0.10%. Compared to RDME failure criteria (**figure 4.30 B**), where the prisms very well succeed the test, we find again different predictions depending on the indicator of the degree of damage used (unless for the prisms cured at 7 days where both indicators were in accordance).

When the dosage of AEA to the concrete was of 120mL AEA/100kg of binder (**figure 4.33 C**), the length increased very slowly during F-T cycles. At the end of the test, the measured expansion for the prisms cured at 7, 14 and 28 days was of 0.031 0.04 and 0.05% respectively. Therefore, the test was passed in all the curing conditions. These result thus agree with RDME results (**figure 4.30 C**). It is noted that the expansions are much lower than in the other cases (without AEA and with 60mL/100kg of binder). Thus, although RDME showed that an extra dose of 60mL of AEA/100kg of binder did not improve too much the results, length change stability was highly improved.

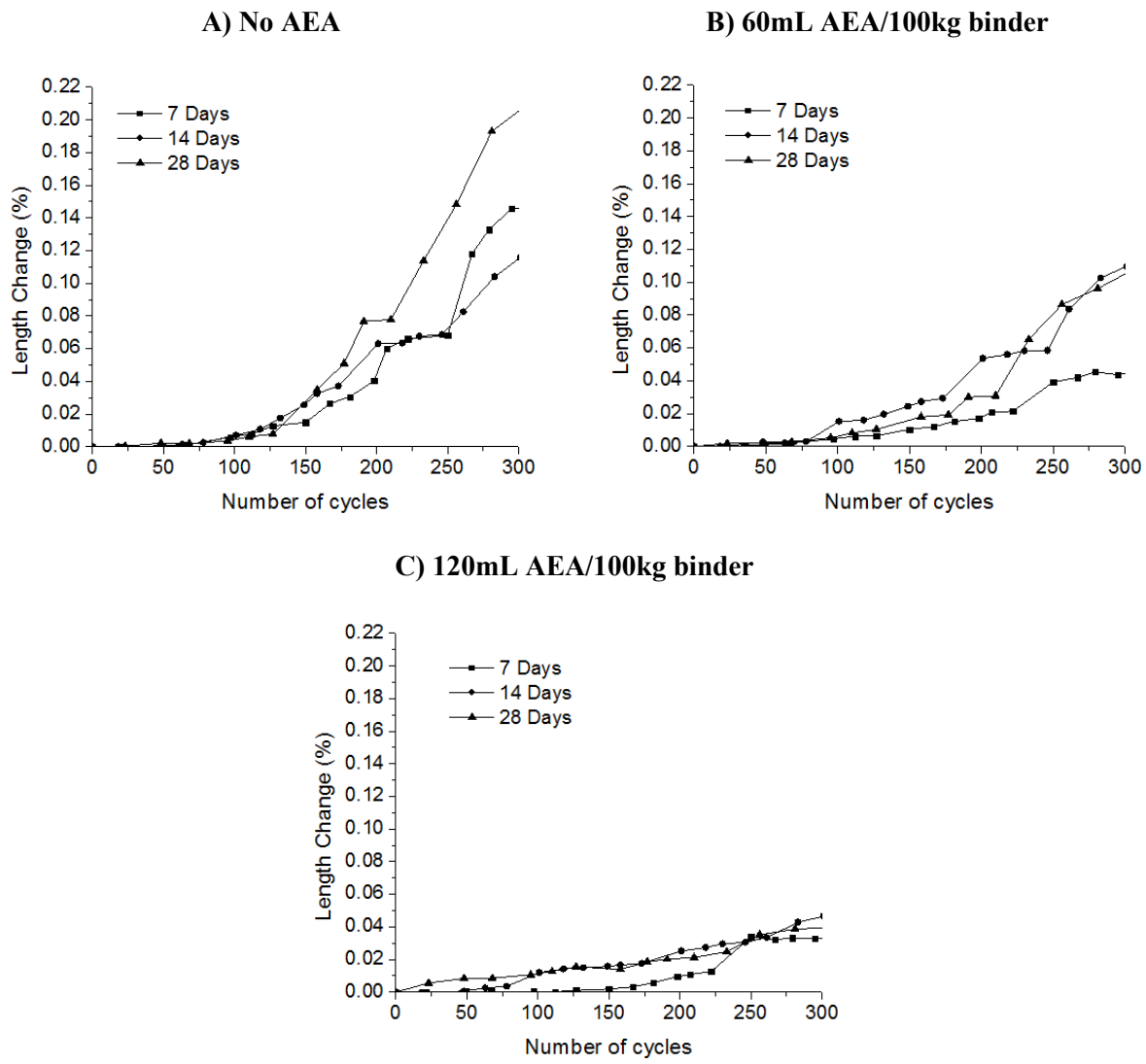

Figure 4.33 Length change of AAS concretes exposed to F-T cycles at different curing times: A, without AEA; B, with 60mL of AEA/100kg of binder; C, with 120mL of AEA/100kg of binder

4.6.4 Mass change

Figure 4.34 shows the mass change of OPC concrete prisms exposed to F-T cycles at different curing times, without and with AEA addition. When concretes were confectioned without AEA addition (**figure 4.34 A**), the mass continuously increased until 81, 95 and 60 cycles for the prisms cured at 7, 14 and 28 days respectively. Afterwards, the mass experimented a big loss, becoming lower than the initial mass. The initial increase of the mass is due to the increase of water in the system. As F-T cycles elapse, the concrete prisms experimented changes in its interior, where new cracks appear as shown by RDME results. This new cracks would lead to more water infiltration, thus increasing the mass of the prisms. The rapid mass loss experimented at certain point is due to a scaling of the prisms surface, as it

can be observed in the photos of the final aspect of the prisms in **figure 4.29A**. When concretes were confectioned with 60mL AEA/100kg of binder, it was found an initial mass gain for prisms cured at 7 and 14 days that then slightly decreased with time. On the contrary, prisms cured during 28 days experimented a mass loss after 100 cycles up to -1%.

Compared to RDME results, it is observed than even when the RDME was below 60%, the prisms were still gaining mass to a certain point in which the mass dropped fast. This point has been associated to the point where scaling of the prisms surface started. Therefore, when cracking occur, the prisms have their mass increased until the scaling starts.

Mass change is not considered by the standard as a failure criterion, nevertheless it can give us practical information, like the point where scaling starts.

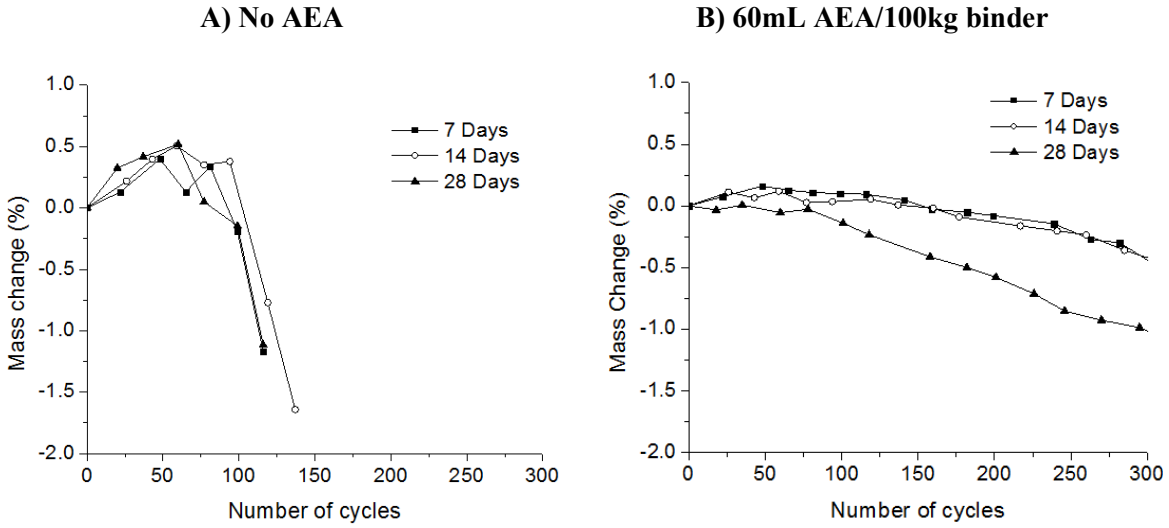

Figure 4.34 Mass change of OPC concretes exposed to F-T cycles at different curing times: A, without AEA; B, with 60mL of AEA/100kg of binder

Figure 4.35 shows the mass change of AAS concrete prisms exposed to F-T cycles at different curing times, without, with and with an extra AEA addition. For the concretes without AEA (**figure 4.35 A**), the mass decreased slowly during time. The mass loss becomes however more pronounced when higher was the curing time. In any case, there was not an increase of the mass as it was observed in OPC prisms without air. The mass loss is also attributed to a scaling of the prisms. As it was observed in the photo **figure 4.30A**, there is some appreciable scaling of the skin of the prisms cured at 14 days at the end of the test, responsible of the mass loss experimented.

When a dosage of 60mL AEA/100kg of binder was added to the AAS concrete (**figure 4.35 B**), a similar trend was observed to the concrete prisms without air, but giving better results. In this case,

there was a progressively decrease of the mass with the F-T cycles, to a maximum value of -0.5% for the 28 days cured prisms. With the addition of a certain quantity of air, the differences with the prisms cured at different times were less marked.

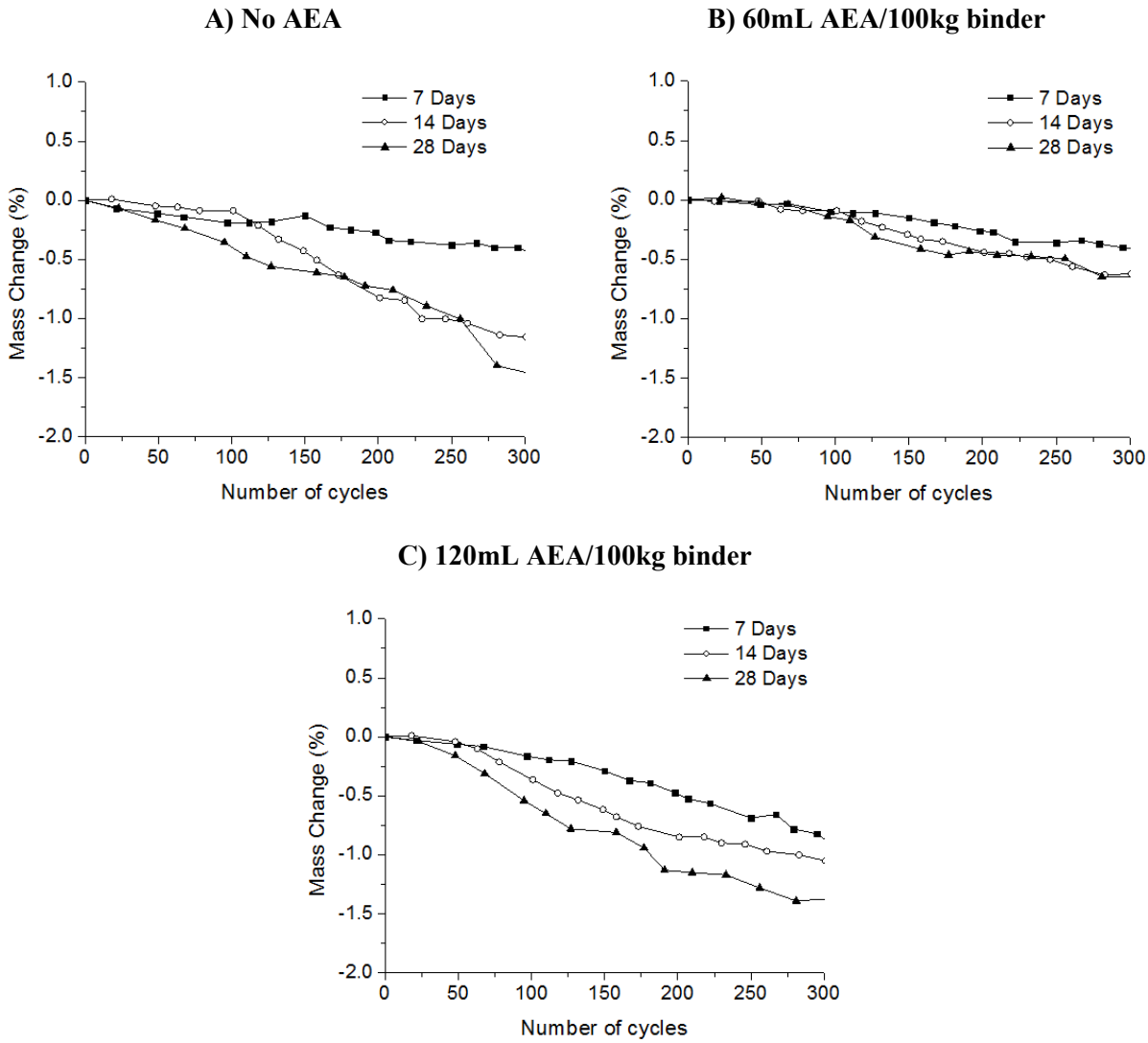

Figure 4.35 Mass change of AAS concretes exposed to F-T cycles at different curing times: A, without AEA; B, with 60mL of AEA/100kg of binder; C, with 120mL of AEA/100kg of binder

When a dosage of 120mL AEA/100kg of binder was added to the AAS concrete (**figure 4.35 C**), different behavior is observed. Contrary to the expected better results with a higher AEA dosage, in this case, the mass loss was higher than the mass loss of the prisms with 60mL of AEA/100kg of binder, and similar to the prisms without AEA. Once again, the best results are observed for the prisms cured at 7 days and the worst ones, for the prisms cured at 28 days.

4.6.5 Discussion

The evaluation of OPC, AAS and AAFA to F-T cycles has been carried out by means of ASTM C666. In order to see how some parameters can affect the results, curing time before exposition of concretes to F-T cycles and the effect of an AEA have been evaluated.

Some of the main aspects to consider when designing concretes to be exposed to frost conditions are the air void system -in terms of total air content-, the spacing factor and the specific surface. According to ACI 201.2R-08, based on extended literature review, these values should be around 5-8% (depending on the aggressiveness) for the air content, lower than 200μm for the spacing factor and higher than 25 mm^2/mm^3 for the specific surface. Looking the results, this was confirmed by the OPC concretes, in which concretes without AEA, that did not accomplish the ACI 201.2R-08 specifications, soon failed the F-T test, and concrete with AEA that accomplished the specifications performed very well. On the contrary in AAS concretes, these specifications showed to be ineffective. As shown in the results, none of the AAS concretes met the specifications, therefore, following this criteria, this concretes should have had very low frost resistance. However this did not happen. All AAS performed well in frost conditions. Similar results were obtained by Douglas et al. (1992), in which the authors found very good frost resistance of AAS concretes even though the air void system didn't meet the specifications. Therefore, in AAS systems, not only the air void system seems to be important in the frost resistance, but other factors could be involved. This will be discussed later.

It has been shown in the results the different effectiveness of the AEA used, in this case based on liquid hydrocarbons, in OPC, AAS and AAFA concretes. In AAS, it was necessary a higher dosage of AEA in order to obtain the same quantity of air in the concrete. Even so, this AEA showed to be effective, as the air content measured in fresh conditions showed an increase when the AEA dosage increased. However, the air content measured in hardened conditions after 28 days of curing time showed very different values. The air content in hardened conditions was highly reduced in AAS concretes, whereas for OPC decreased slightly. This suggests, as already stated by Douglas et al. (1992) that the air voids generated during the mixing, and measured immediately after mixing, are unstable in this highly alkaline systems. However, not all the air-voids generated by the AEA were eliminated, like the air content in hardened conditions for concretes with AEA increased compared to the concrete without AEA. This was also confirmed by the compressive strength reduction observed in the AAS concretes with AEA, higher when higher was the AEA dosage. The compressive strength reduction by the effect of the AEA addition was lower in AAS concretes than for OPC concretes, according the air content observed in hardened conditions. In the case of AAFA, a pessimum effect of the AEA was observed. In this case, the addition of the AEA did not improve the air content, instead, it was observed a decrease.

However, as stated in chapter 4.6.1, the air content measurement method failed due to the high viscosity of the AAFA concrete mixtures. Therefore interpretation of these results should be taken with care.

Results therefore demonstrate the fact that the typical AEA used and designed for OPC-based binders (based on liquid hydrocarbons) do not introduce extra air with the same efficacy for AAMs. In the work done by Gifford & Gillott (1996), the authors stated that a typical liquid hydrocarbon-based AEA was not effective for AAS concrete mixtures. Instead, authors found more effective to use an AEA typical used for high-alkali cements based on surface active agents. Nevertheless, the dosage of the latter was still higher than for OPC concretes.

As it was expected, the introduction of an AEA in OPC concretes highly favors the resistance to frost conditions. This is well known to be due to better stabilization of air bubbles by the AEA that gives an extra space to water to accumulate, and thus relieving the stress created by the ice to the concrete pore walls (CEB 1989). One important aspect to point out in the results is the fact that for the OPC concretes without AEA, when the frost conditions were started at later curing times, the frost damage rate was higher. On the contrary, this fact was not observed in OPC with AEA, where there was not practically any differences between the results. This loss of frost resistance at higher curing time could be due to several factors. First factor is the concrete saturation degree at the time the test starts. This will be higher at higher curing times, so the water content inside the pores will be higher. Therefore, as the F-T cycles elapse, the damage of the concrete will occur at a faster rate when higher is the saturation of the concrete. Second factor is that at higher curing time, pore connectivity will be lower, so water entrapped in the pore structure during curing will nt be able to diffuse as effectively to the free space when ice is growing in a pore. Thus, the hydraulic pressure generated for the unfrozen water will not be released and will expand causing tensile stresses in the surroundings. This was not the case of OPC concrete with AEA, where the air bubbles seemed to relief that hydraulic pressure regardless the curing time of the concretes.

In AAS systems, as explained before, it has been observed to have very good frost resistance, in accordance with that found in literature (Douglas et al. 1992; Gifford & Gillott 1996b; Fu et al. 2011). It has been observed that the addition of certain quantity of AEA helped to improve the F-T resistance of the concretes, however, not at the same efficacy as for OPC concretes. AAS concretes without AEA showed to have very good resistance, although the percentage of air voids in the system was very low (1.6%). The same conditions for OPC concretes showed to be detrimental, and the concrete prisms were quickly destroyed. The better results of AAS concretes compared to OPC concretes without air could be due to several factors. First one is the lower w/c ratio, 0.45 for AAS concrete and 0.49 for OPC concrete. It is well known that higher w/c ratios will induce a coarser microstructure and thus more

water will diffuse to concrete bulk (CEB 1989). However, this differences in w/c ratios are not sufficient to explain those differences in the frost behavior. Hence, other factor could be related to the pore structure. In AAS concretes pore sizes are lower (Collins & Sanjayan 2000) and the pores are less interconnected than the OPC one (Song et al. 2000; Provis et al. 2012). Thus, a decrease of pores size will lead to less freezable water in the pore at a given temperature since a lower temperature is necessary for ice to grow in smaller pores (CEB 1989). Else, the low connectivity of the pores will prevent further introduction of new water into the system. Moreover, another factor affecting the results could be also related to the pore solution composition. The alkalis of the pore solution could play a role. In a highly alkali pore solution, the temperature to form the ice will be lower, and thus, less ice will be formed at the same pore size conditions (Gifford & Gillott 1996b). It has been found that more alkalis are present in pore solution of AAS concretes than in OPC concretes (Gruskovnjak et al. 2006). Therefore, it could be expected that alkalis in the pore solution favors the frost resistance.

The increase of the dosage of the AEA, passing from 0 to 60 mL and 120 mL by 100kg of binder, seems to improve the time where the RDME remained unaffected. This time passes from 100 cycles when there was no AEA to 210 and 230 cycles for 60 and 120 ml of AEA respectively. This is mainly due to the fact that, increasing the AEA dosage, the total air voids are increased (as shown in the results), and thus more time is required to fill all this voids with water. According to theory (CEB 1989), artificial voids introduced by the AEA are defined as quasi-closed pores, what it means that they are not connected to the natural pore structure. Thus, at the beginning of the test, these artificial air pores are empty (even in the case of saturated concrete). As F-T cycles elapse, these artificial air pores, by diffusion processes, are filled with water and give enough place to grow. These diffusion processes are to some extent irreversible, and consequently, the filling with water of these artificial pores will increase with cycles. At certain age, these pores will be completely filled and thus damaged by the frost (CEB 1989). This behavior is observed in the results, where the time were RDME kept practically constant was higher when higher was the air content, that is to say, when higher was the AEA dosage. However, it has to be pointed out that although there was a very loss of RDME for AAS concrete with the higher dosage of AEA (120mL), it can be concluded that AAS concretes performed very well at these conditions.

It is also observed that the F-T resistance decreases when the concrete prisms are more mature. As explained before, this fact could be due to the concrete saturation degree and the pore structure.

Contrary to the good results obtained in AAS concretes, AAFA concretes do not well performed under F-T cycles, with severe destruction of the prisms in a few cycles. These results are contradictory with those found in literature, in which very good frost resistance was found in AAFA (Rostami & Brendley

2003; Škvára et al. 2005; Sun & Wu 2013), even without AEA, that showed not to be essential in these systems. Probably this bad F-T resistance of AAFA concretes was due to an elevated porosity. In fact, curing regime of the former works were not the same of the one followed in this project. It is possible that curing at 80ºC during the first 24 hours has produced a lot of harmful porosity for the frost resistance. Other possibility could have been the concrete casting method into the molds. In this case, with a very highly viscous concrete, it was compacted by rods, and maybe some of the large air bubbles produced during mixing could have not been eliminated by this compaction method. Compaction by vibration could have eliminated this problem, although it has not been tested. Complementary information would be thus necessary to verify the porosity.

Mass change was another studied parameter, although is not used as indicator of the degree of attack. It has been seen that in OPC concrete without air, mass increased until a certain point, in which mass dropped rapidly. This point could be related to a fast scaling of the surface due to an increase of internal cracks near the surface. The continuous formation of cracks inside the bulk due to the F-T cycles effect would lead to the destruction of the surface in a given moment, until the prisms were broken into two halves, as observed in the photos of **figure 4.29A**. When AEA was added to OPC concrete, mass loss decreased slightly during time. This is attributed to a loss of the concrete skin. In the case of AAS concretes, similar mass loss was observed regardless the AEA dose to those obtained for AEA OPC concrete. In this concrete, there was a progressive mass loss during F-T cycles, also attributed to a loss of the concrete skin.

Regarding the indicators of the degree of attack, ASTM C666 specifies the RDME and length change as the test failure criteria. In the case of OPC, both indicators were in good agreement, despite of the minor differences, since the test failed approximately in similar amount of F-T cycles. However, regarding the AAS concretes, some differences were found. When AAS was confectioned without AEA, according to length change failure criteria, the test failed. But with RDME failure criteria, the test passed. For concretes with 60 mL of AEA/100kg of binder these differences are still observed. The only case in which both indicators agreed was when concretes were confectioned with the higher dose of AEA (120mL). Whichever of both indicators is a more realistic measure, it is clear that both have to be used as a complementary to the other.

4.6.6 Conclusion

According to the results obtained, the following conclusions are found:

- In every system (OPC and AAS), it has been observed that performance of the prisms to F-T cycles was lower when curing time was increased from 7 to 14 and 28 days.

- AEA addition had not the same influence for AAS as in OPC. In OPC, AEA was more efficient to introduce extra voids to the concrete. However, AAS performed very well with low quantity of air voids, contrary to what happens with OPC.
- Spacing factor and specific surface recommended values seem not to be applicable in the same way for AAS than for OPC concretes. Therefore, these recommendations should be revised for AAM concretes.
- AAFA showed to have very bad frost resistance probably due to a high porosity.

4.6.7 Applicability of the test methods to AAM

In this test, standard ASTM C666 has been evaluated to know if it is applicable to AAM. Curing conditions have been modified in terms of curing time of the prisms before starting the test. Moreover, the influence of using an AEA to modify the air voids systems has been also observed.

From results obtained in this test, the following recommendations are given:

- Curing time prior starting the test has been found to affect the results. Longer curing times negatively affected the results, although the differences did not affect the final conclusion. Therefore, curing time could be stablished at 14 days.
- Regarding the operation conditions (F-T cycles frequency, thaw and freeze points, etc.), no modifications have been found necessaries according to our results.

4.7 Permeability

4.7.1 Results

Permeability was measured in OPC and AAS by means of two test methods: rapid chloride penetrability test (RCPT) as described in ASTM C1202 standard, and bulk resistivity (BR) by means of a Giatec RCON2 resistivity meter (see chapter 3.5.7).

Results are shown in **table 4.8**. It can be seen that for OPC concretes, the charge passed due to chloride ion decrease with time as expected due to a refinement of pores as measure as hydration reaction evolves. At the same time, resistivity of electrical current to flow across the bulk of the specimen (cylinders of Ø100x200mm) slightly increases during time, also indicating a decrease of pores in the concrete.

In the case of AAS concretes, similar behavior can be seen. In this case, although the initial alkali content is higher than the OPC concrete (5wt% and 0.8% Na_2O respectively), charge passed at early

ages is much lower (11438 and 3682 coulombs for OPC and AAS respectively at 3 days). Regarding the resistivity of AAS, it can be seen that as the time passes, resistivity increases much more rapidly than for OPC.

Table 4.8 Charge passed and BR with time

Age (Days)	Charge passed (Coulombs) ASTM C1202		Bulk resistivity (kΩ·cm) Giatec RCON2	
	OPC	AAS	OPC	AAS
3	11438	3682	3.6	11.9
7	7847	2330	4.4	18.1
28	4853	2219	6.4	19.6
90	3272	1511	7.5	21.6

4.7.2 Relationships between RCPT, BR and compressive strength

In the **figure 4.36**, it can be seen the relationship between the two methods used to determine the chloride ion penetrability: the RCPT and BR methods. In this figure, shaded regions represent the different combinations according to charge passed (ASTM C1202) and bulk resistivity results (see **table 4.9** for permeability classes). Hence, darker regions mean higher chloride ion penetrability. According to these classifications, a good relationship between RCPT and BR results should follow a power tendency ($y = ax^b$).

In the case of OPC, it can be seen a correlation between both methods. As seen in the figure, the results follow a power tendency, which showed to have the best coefficient of determination ($R^2 = 0.9840$). At 3, 7 and 28 days, RPCT results are in the region classified as high chloride ion penetrability and BR results are as well in the region classified as very high or high corrosion risk, thus finding an equivalence. However, at 90 days, RCPT results are in the region of moderate chloride ion penetrability whereas BR results are still in high corrosion risk. Therefore, at 90 days, it is found a poor correlation between the chloride ion penetrability predictions in both methods.

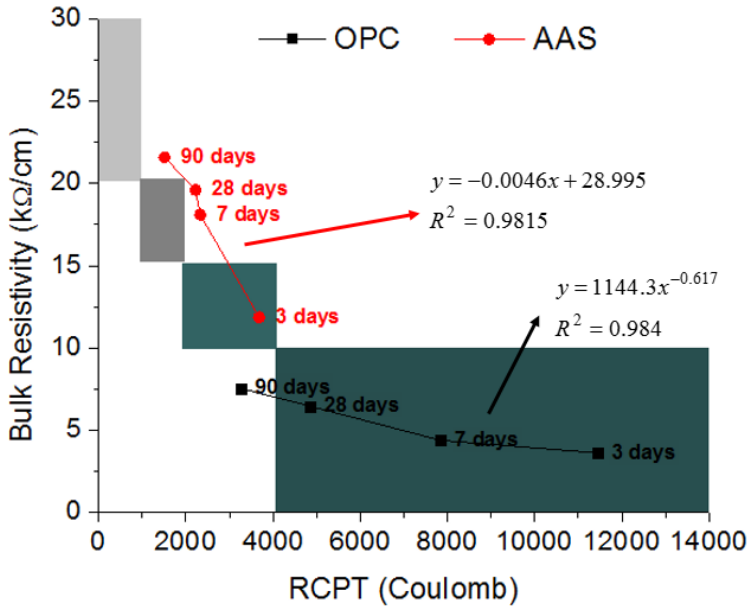

Figure 4.36 Relationship between RCPT and bulk resistivity measurements

Table 4.9 Classification of permeability results by means of ASTM C1202 and bulk resistivity (bulk resistivity based on literature review)

Chloride ion penetrability based on charge passed [1]		**Surface resistivity [2]**	
Charge passed (coulombs)	**Chloride ion penetrability**	**Resistivity (kΩ·cm)**	**Corrosion risk**
		<5	Very high
>4000	High	5-10	High
2000-4000	Moderate	10-20	Moderate to Low
1000-2000	Low	>20	Negligible
100-1000	Very low		
<100	Negligible		

1 Classification from ASTM C1202

2 Classification from: Song & Saraswathy (2007), (Bungey et al. 2006)

In the case of AAS, it was found a correlation at 3 days but not at later ages. In this case, it can be seen that the relationship fitted the best to a linear tendency with a coefficient of determination of R^2 = 0.9815, contrary to that found to fit best in OPC, a power tendency. For instance, at 3 days RCPT results are classified as moderate chloride ion penetrability, close to the region of high chloride ion penetrability, whereas BR results are classified as well as moderate corrosion risk. At 7 days, higher differences are observed between the two methods, as in RCPT results are in the region of moderate

chloride ion penetrability and BR results are now in the region of low corrosion risk, close to negligible corrosion risk. At 28 and 90 days, similar behavior to what was observed at 7 days occurs. For AAS system, it seems that both classifications do not predict the same permeability, therefore finding discrepancies.

Both test methods, RCPT or BR, have been compared to compressive strength. Hence, in the **figure 4.37,** it can be seen the relationship between RCPT and compressive strength of concretes. It can be seen that for OPC concrete, RCPT results follow a logarithmic tendency with the compressive strength with a very good coefficient of determination (R^2 = 0.9906). A linear tendency was found for AAS, with a lower coefficient of determination (R^2 = 0.9462). The different trends of the curves are normal considering the different compressive strengths of both concretes. Thus, at certain point, it is necessary to increase much more the compressive strength to decrease the RCPT value, as shown for AAS concrete. It is important to note that joining both curves (OPC and AAS), all points follow the same tendency (logarithmic with R^2 = 0.9841). It can be seen that compressive strength of AAS concrete at 3 days (44.4 MPa) is similar to that of OPC concrete at 90 days (around 46.0 MPa), and that the passed charge was similar too (3682 and 3272 for AAS and OPC concretes respectively).

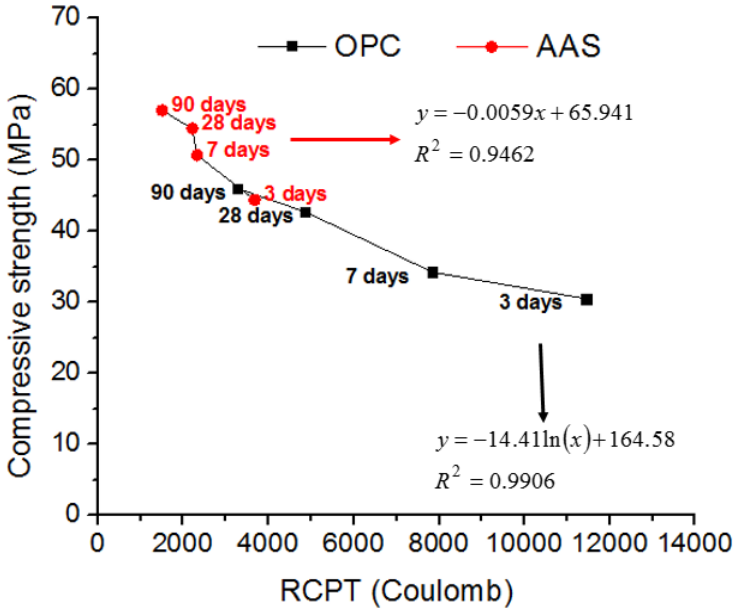

Figure 4.37 Relationship between RCPT and compressive strength

In the same way, BR was compared to compressive strength in the **figure 4.38.** Now, in both cases it has been found that the tendency fitted the best to linear relationship, better in the case of OPC (R^2 = 0.9974). Contrary to RCPT, a similarity of compressive strength and BR between OPC and AAS concretes was not found, since for the same compressive strength grade, BR is much higher for AAS

than for OPC. This puts in evidence that RCPT values in AAS could have been overestimated due to the presence of alkalis in pore solution, thus, increasing the measured charge passed.

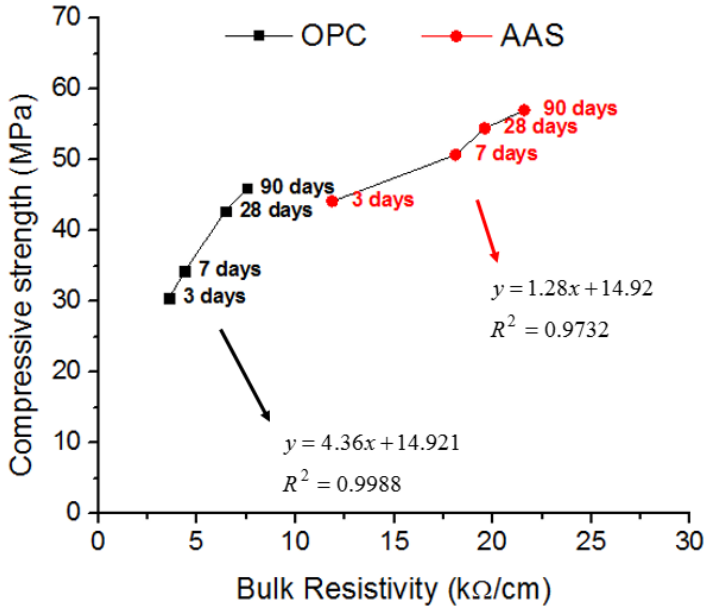

Figure 4.38 Relationship between bulk resistivity and compressive strength

4.7.3 Discussion

The main objective of this test was to observe if results given by rapid chloride penetrability test (as per ASTM C1202) were in accordance with results given by bulk resistivity (using a two electrode resistivity meter) for AAMs, by means of AAS. This has been carried out by comparing the classifications given in **table 4.9** for both methods. Else, OPC formulation is used as a comparative purposes.

Before starting to get conclusions about the results, it is important to mention the provenance of each classification, since results could be differently interpreted using other classifications, especially for BR. It is well known that both classifications have been developed for OPC-based binders. The RCPT method was intended to be a substitute of the chloride ponding test (such as AASHTO T259 and ASTM C1543), because of the necessity to get results in a shorter period of time. Thus, RCPT classification was obtained comparing the RCPT results of various types of concrete which was obtained with the chloride ponding test (Whiting 1981). This classification has therefore widely been accepted for concrete quality purposes. Nevertheless, RCPT method has been considered to have poor correlation with chloride ponding test (Pfeifer et al. 1994), particularly for blended cements, together with a great variability and poor correlation.

Regarding electrical resistivity, several classifications can be found in literature (Hornbostel et al. 2013). Electrical resistivity is receiving increasing attention in order to get fast predictions of the corrosion rate. Several factors can affect the threshold values, such as the experimental setup (two electrode, four electrode, DC/AC, etc.), corrosion rate technique used in which resistivity values are compared, the exposure conditions and the material used (Hornbostel et al. 2013). Thus, depending on the study conditions, different classifications have been obtained. According to this, it is supposed that a new scale should be validated to predict permeability for AAMs, comparing electrical resistivity with other methods as chloride diffusion, water permeability, compression strength, corrosion rate, etc. The classification finally adopted in this project (Song & Saraswathy 2007; Bungey et al. 2006) has been found to be the most realistic considering the results obtained. A similar classification was recently obtained by Sengul (2014) by experimental relationship between chloride diffusivity test method (NT Build 492) and electrical resistivity (two-electrode method with AC and ASTM C1760).

Different behavior has been found for OPC and AAS concretes in terms of the relationship between RCPT and BR. RCPT results were lower for AAS at any age than those for OPC. Accordingly, BR results were higher for AAS at any age than for OPC. These results showed that AAS was less permeable than OPC. It has to be said that w/s ratio for AAS concretes was lower than that for OPC concretes (0.45 and 0.49 for AAS and OPC respectively). Thus, an improvement of AAS results is expected to happen. However, differences are too high to be attributed only to the lower w/s ratio. This will be confirmed observing the relationship between both permeability methods with compressive strength.

Regarding the RCPT values, one can expect to find very high charge passed values for AAS, as alkalis in pore solution are high at early ages (Gruskovnjak et al. 2006). It is well known that in both techniques, based on electrical conductivity, the results will be affected not only by pore structure but also by pore solution chemistry. Thus, pore solution with higher ions concentration will conduct as well the charge together with the chloride ions, overestimating the results. However, what is found is far to be like that. Charge passed in AAS concrete at early age is three times lower than that measured in OPC concrete. One factor is the lower w/s ratio, as explained before, but other factor could be the pore connectivity. Pore connectivity of AAS is known to be lower than OPC (Song et al. 2000; Provis et al. 2012), thus more tortuosity is found by electrical current to pass through the bulk concrete. Hence, the lower pore connectivity of AAS could be the main factor regarding the lower RCPT results obtained. Similar results were obtained in BR test method, with higher resistivity for AAS.

Observing the relationship between RCPT and BR methods, it can be found a good correlation between results obtained in each method for OPC concretes at the ages of 3, 7 and 28 days, according to the

classifications of **table 4.9**. However, at 90 days, some differences were found. In the case of AAS, it was found a good correlation at 3 days, but some differences were found at 7, 28 and 90 days. This clearly shows that the RCPT method could misread the real behavior of AAMs, although other tests would be necessary to confirm this hypothesis. For this reason, both tests have been compared to compressive strength values, which depends on the pore structure.

Comparing RCPT results with compressive strength, it can be found a relationship for both systems: a linear trend for AAS and a logarithmic trend for OPC. In both cases, the higher the compressive strength, the lower the charge passed. This evidenced that at higher compressive strength the passed charge has more difficulties to pass through the concrete due to lower porosity of the system. The most important thing to note here is that when joining all the values obtained with OPC and AAS concretes, a common relationship has been found, following a logarithmic trend. Thus, although compressive strength grade for both systems is not the same at similar age, it could be concluded that there is a relationship of both systems between RCPT and compressive strength.

In the case of BR, it has been also found a relationship with the compressive strength, following in both cases a linear trend. It can be noted a difference in the BR for both systems at the same compressive strength grade, being higher for AAS. According to the results obtained by RCPT method, it could be expected to get the same BR at the same compressive strength grade. However, this does not occur. This different relationship between both systems with the compressive strength could also explain why the classifications for RCPT and BR used in this project do not predict the same behavior (**table 4.9**). This could be due to two factors: pore connectivity and pore solution chemistry. As explained before, pore connectivity in AAS systems is lower than in OPC one, and thus electrical current will have more impediments to flow through the bulk concrete. Thus, at the same pore structure and connectivity and similar pore solution chemistry, results should be similar for the same compressive strength grade (in both tests). AAS and OPC are known to differ in both pore structure and connectivity and pore solution chemistry, thus results are expected to differ. Why in the case of RCPT method results are similar for both systems at the same compressive strength is explained by the pore solution chemistry? It is possible that with the RCPT method, the values measured for AAS concretes are higher than the actual ones because of the influence of the pore solution chemistry. Thus, alkalis in pore solution of AAS concretes could have transported the current and therefore increased the passed charge. Else, test conditions in RCPT with a high voltage DC (60V) applied during long time (6 hours) could have also increased the temperature of pore solution, with elevated concentration of ions (alkalis, OH^-), that would have induced a higher ion mobility and thus more passed charges. Instead, BR test method used in this project uses an AC current that affects less the pore solution of concretes, and thus avoiding heating of the

sample. Else, the duration of this test is very short, of few seconds. Furthermore, DC measurements (as RCPT) have already been not recommended even for OPC systems due to electrode polarization effects (Polder 2001). It is therefore expected that results obtained in BR are more realistic than results obtained in RCPT.

4.7.4 Conclusion

Regarding the results obtained in this test, it can be concluded the following:

- It was found that AAS concrete was less permeable than OPC concrete in both electrical test methods, RCPT and BR.
- For OPC concrete, it was found a relationship between RCPT and BR at 3, 7 and 28 days. However, a 90 days, results differed.
- For AAS, only at 3 days, it was found a relationship between RCPT and BR. At 7, 28 and 90 results were not in accordance.
- The strength-RCPT/BR relationship indicates that electrical results are not affected only by the pore structure (which gives the strength) or pore solution chemistry (that can affect the passed charge) but also by the pore connectivity. Although pore structure and pore connectivity have not been measured, the different electrical results obtained in both methods at the same strength could be an indicator of that.

4.7.5 Applicability of test methods to AAMs

In this test, two electrical-based test methods used to predict permeability have been compared. The first one, the RCPT is the most used nowadays, however, it is put in doubt due to the problems stated before. The second one, BR, is receiving special attention in order to replace the former. BR is considered to be more realistic.

From results obtained in this test, the following recommendations are given:

- RCPT method has been found to overestimate results in AAS.
- BR test method used in this project seems to be a very good technique predicting the permeability of AAMs (based on AAS results).
- A new classification should be obtained in BR test method for AAMs in order to predict the permeability of concretes. This classification should be based comparing results with other methods such as water permeability,

4.8 Alkali leaching

This test was conducted in order to evaluate the alkali leaching in AAMs when they are exposed in water conditions. In this case, as the activator used are based on Na as alkali metal, Na leaching will be evaluated. The Na content was measured with an ICP-Ms instrument, as explained in **chapter 3.6.7**.

4.8.1 Results

Figure 4.39 shows the Na leaching of AAS and AAFA mortar bars when they were immersed in distilled water at different curing times such as after demolding, 7 and 28 days. During this curing time, all the mortar bars were kept at 23ºC and 95%RH, avoiding direct contact of the bars with the water mist of the chamber. This will prevent initial leaching of the bars. Test duration of the test was 28 days, changing the distilled water every week (4 seven-day cycles) to increase driving forces (see **chapter 3.5.8**).

It can be seen in the figure that in both systems, AAS and AAFA, there is a high Na leaching after the first week, being a little higher for AAFA mortar bars. The same tendency was found in both cases, finding a deceleration of Na leaching rate during time. This is mainly attributed to an equilibrium of the Na between the distilled water and the pore solution of the binders. After the second week, the Na leaching was drastically reduced in both systems, and kept the same tendency afterwards.

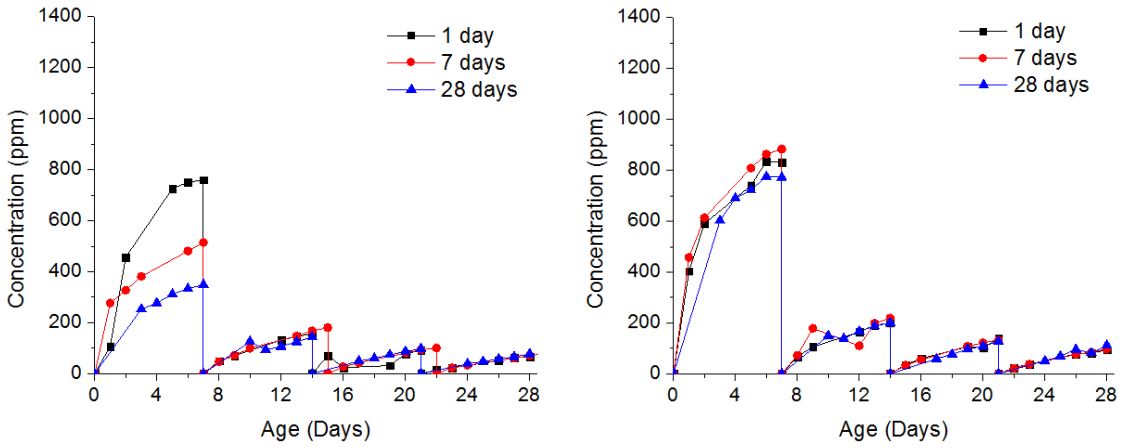

a) AAS b) AAFA

Figure 4.39 Sodium leaching of AAS (a) and AAFA (b) mortars when submerged in distilled water

Regarding AAS mortar bars, it can be observed that when longer was the curing time prior to put the bars in distilled water, the Na leaching during the first week was lower. This could be due to a higher fixation of alkalis in the structure at later ages, thus less alkalis are present in the pore solution. After the second week, no differences were observed regarding the initial curing time. On the contrary, for

AAFA mortar bars, it was not found the same behavior, with practically the same Na leaching regarding the curing time. For this system, the special curing procedure could be the reason. In this case, mortar bars were heated at 80ºC during the first 24 hours in order to accelerate the hardening mechanisms. Therefore, all the alkalis to be fixed at the structure could have been fixed in this period and no differences were found after 28 days of dry curing at normal temperature.

In the **figure 4.40a and b**, it can be seen the accumulate Na leached in all tests. Looking these figures, it could be concluded that in AAS, the total Na leached is lower. However, AAFA has higher alkali content in the initial mix. Considering the initial alkali content in the mix, it has been calculated the degree of alkalis leached (**figure 4.41**). Thus, in **figure 4.41** it can be seen that the degree of alkali leached is quite similar for both systems, with 3.5% of Na leached. It is interesting, as mentioned before, the significant reduction of the alkali leached in AAS when the bars are cured longer in controlled conditions (23ºC, 95%RH, with no direct contact with fog). In contrast, for AAFA, te leached alkali is practically constant, no matter the curing time studied (7 and 28 days).

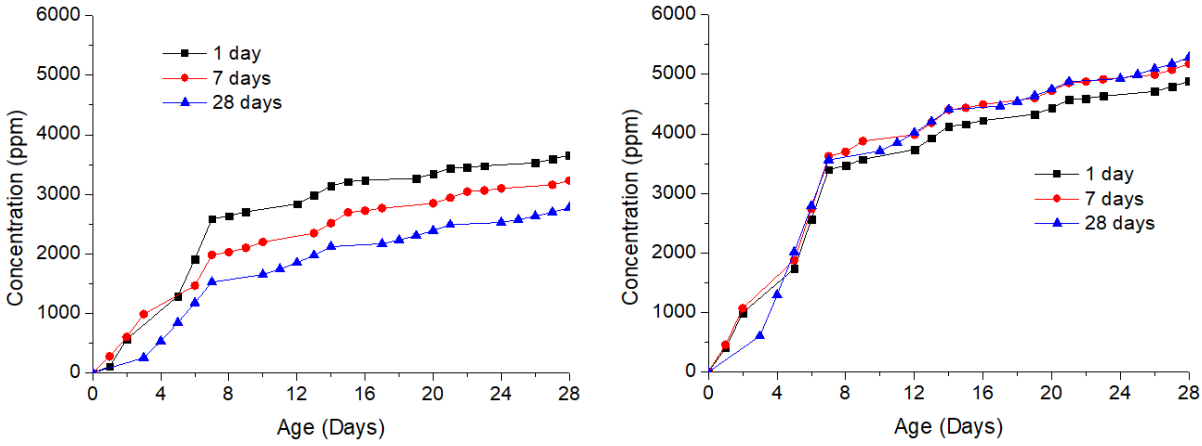

Figure 4.40 Sodium leaching accumulate of AAS (a) and AAFA (b) mortars when submerged in distilled water

4.8.2 Discussion

In this test, Na-leaching of AAMs exposed to distilled water has been analyzed. Although distilled water is rarely used as a curing procedure, it has been used in order to accelerate the driving forces.

As it has been observed in the results, both systems start with a high initial Na leaching, higher in the case of AAFA. The leached Na is a consequence of a disequilibrium of Na content between the distilled water and the binder pore solution. The leaching rate is fast at the beginning of the exposition to distilled water, and it decreases with time. This could be related to two factors. First, the alkalis of the outer layer of the bars could be readily dissolved in the distilled water, quickly increasing the Na on it at early

ages. The alkalis in the deeper zones will be more difficult to be dissolved, thus decreasing the dissolution rate with time. Second, the decrease could be also associated to an equilibrium point in which Na content in the distilled water is close to the pore solution one. Once the medium (distilled water) was changed (start of the second cycle), the equilibrium is displaced to the medium side, and again Na leaching is observed. This time, however, the concentration of the Na leachate is fourfold lower than in the first cycle. Every passed cycle, the Na leaching decreases more.

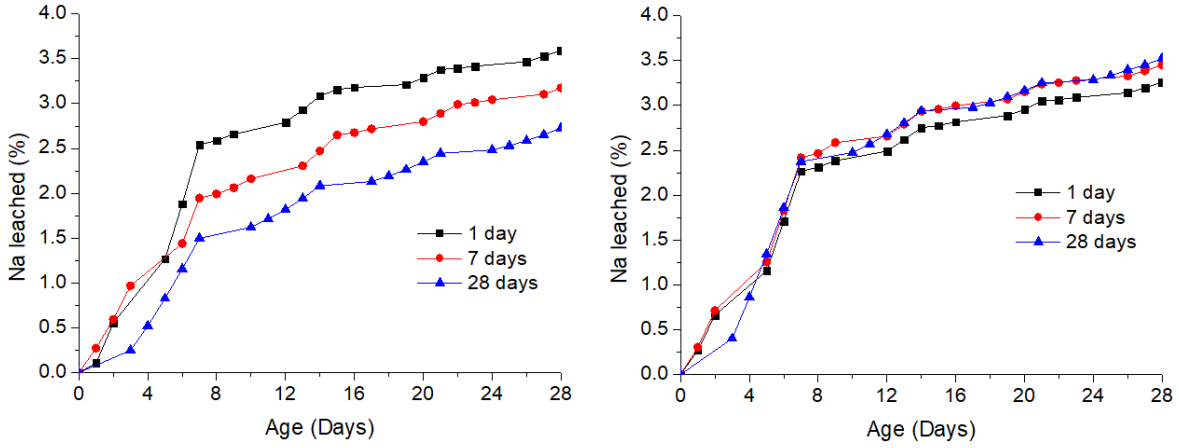

Figure 4.41 Degree of sodium leached regarding the initial sodium content in the mix.(a) AAS, and (b) AAFA

Na leaching has been considered to be due to a concentration gradient of Na between the binder pore solution and distilled water. However, it could also be due to an extraction of part of the alkalis already bound to the binder structure. It is not possible to distinguish by the test method used in this project if part of the Na leachates are due to a release of the bounded Na in the gel structure.

Regarding the curing time before exposure to distilled water, different behavior was found between AAS and AAFA. In the case of AAS, it was found lower Na leaching when specimens were cured for longer periods in a humidity chamber (avoiding direct contact of specimens with fog). This curing procedure of specimens before exposure to distilled water was used to prevent any Na leaching in the humidity chamber. Thus, higher curing times showed to improve the Na incorporation to the binder structure. These results were in accordance with the findings of Puertas et al. (2004), in which the authors found a decrease of the Na content of the pore solution during time. Nevertheless, it could be another explanation to the lower Na leaching. This would be related to the pore structure. It is well known that total pores in AAS are reduced during time, as well as the pore connectivity. Therefore, diffusion of alkalis from pore solution to distilled water will be hindered at higher curing times (Lloyd et al. 2010).

It is important to note that regarding the precursor used (BFS or FA) to produce the binder, the degree of Na leached has been found the same (3.5%).

In the case of AAFA, curing time showed any effect on the Na leaching. In these systems, this behavior could be due to two reasons. First, Na could be incorporated to the structure mainly at the heating period (i.e. 80ºC during the first 24h). As the reaction kinetics at normal temperature are known to be slow, further Na incorporation to the structure will therefore be slow. Thus, after 28 days of curing time, it is probable that pore solution has not changed significantly. Second, by the same reason, the refinement of the pore structure in AAFA is very slow after the heating period (Ma et al. 2013). Thus, alkalis in pore solution will not be restricted during time because of a refining of pore structure.

The results reflect very well the problems that can cause the curing in tap water, which could create a concentration gradient of Na between water and binder pore solution, and thus allowing Na to leach. For instance, curing in aqueous solutions is the case of most durability test methods. Although in most test the aqueous solution is not pure water, immerse AAMs specimens in it can induce Na leaching from pore solution and thus reduce the performance. Therefore, a good curing procedure before starting the test is required to improve the performance of AAMs, unless in high-Ca AAMs such as AAS. Curing in dry conditions, or in chamber at elevated RH (around 90%), may be advantageous in terms of Na leaching. In fact, the latter conditions have already been used in AAMs (Bernal, de Gutiérrez, et al. 2011). Alkali leaching could therefore be non-favorable for the further development of the AAMs binders. Other possible curing conditions could be evaluated, as water containing certain quantity of Na (e.g. NaOH solution) to keep stable Na content of the binder pore solution. This is in fact the technique used in OPC binders, in which these specimens are immersed in lime saturated water in order to prevent lime leaching from the binder and thus, reducing the performance.

Moreover, alkalis in pore solution are responsible in maintaining the pH of the binder. In reinforced concrete, this is important in terms of passivating the steel from corrosion. Therefore, alkalis leaching of concretes exposed to water conditions could have a great impact on the durability of the concrete structures.

4.8.3 Conclusion

According to the results, the following can be concluded:

- Na leaching was found in AAS and AAFA when immersed in distilled water. Thus, curing in water of AAMs could decrease its performance at later ages due to Na leaching.

- Na leaching is attributed to the free alkalis that are in the pore solution. The gradient of concentration of Na between the pore solution and distilled water push Na ions to move to the distilled water.
- Na leaching rate is very fast when specimens are first introduced in water. As exposure time elapses, leaching rate tends to appease. This is because an equilibrium point of Na is reached between binder pore solution and distilled water.
- Na leaching of AAS and AAFA practically occurs during the first contact of specimens with distilled water, attributed to the dissolution of the alkalis of the outer layers. When distilled water was changed by new one, Na leaching was fourfold lower than at the first contact, and tended to decrease in each subsequent change of fresh distilled water. This is because alkalis in the deeper layers are more difficult to dissolve.
- In AAS, it was found a reduction of Na leaching when specimens were cured for longer periods in a humidity chamber in which specimens were not in direct contact with water. This would indicate that more Na would be fixed in the binder structure, and thus, better performance.
- In the case of AAFA, no differences on Na leaching were found in specimens cured at different periods (up to 28 days). It is possible that all Na that was not fixed in the binder structure during the heating period (80ºC during the first 24h) took a longer time to be incorporated in it afterwards.

CHAPTER 5. Durability of a novel alkali-activated material based on glass powder/metakaolin

In this chapter, durability of three alkali-activated formulations based on the system glass powder-metakaolin (AAGP) has been analyzed, using the existing durability test methods but applying the recommendation given in **chapter 4**.

The three formulations have been obtained from a related project developed in the concrete research group of the "Université de Sherbrooke". The name of this project is: "*Élaboration de nouveaux liants minéraux pour la formulation de bétons écologiques et durables* », conducted by Ana Balaguer Pascual (Balaguer Pascual 2014). The formulations are described in **chapter 3.3.1**.

Therefore, compressive strength and durability results are shown next.

5.1 Compressive strength

The compressive strength results of AAGP mortars cubes are shown in **Figure 5.1**. The influence of replacing glass powder (GP) by metakaolin (Mk) in the binder on the compressive strength can be observed. Therefore, the systems with 95% of GP and 5% of Mk (95GP in figure), 85% of GP and 15% of Mk (85GP in figure) and 70% of GP and 30% of Mk (70GP in figure) have been analyzed. It can be observed the best compressive strength results for the system with 95% of GP, where compressive strength at 28 days was of 31 MPa. When Mk content was increased to 15% and 30%, the compressive strength at 28 days was lower, being 23 and 26 MPa respectively.

According to compressive strength results, the replacement of higher quantities of GP by Mk in the binder leads to a decrease of the compressive strength. Small differences were found between 15 and 30% of Mk replacement at later ages, getting higher compressive strength the system with 30% of Mk. This reduction in compressive strength when Mk content increases in the binder is related to the reaction products formed, as it will be discussed in latter sections. When the GP content is higher, a sodium silicate gel is favored, whereas when the Mk content is more present, a coexistence of a sodium silicate gel with sodium aluminosilicate gel appears. The sodium silicate gel is shown to have better compressive strength, as evidenced in other works (Redden & Neithalath 2014).

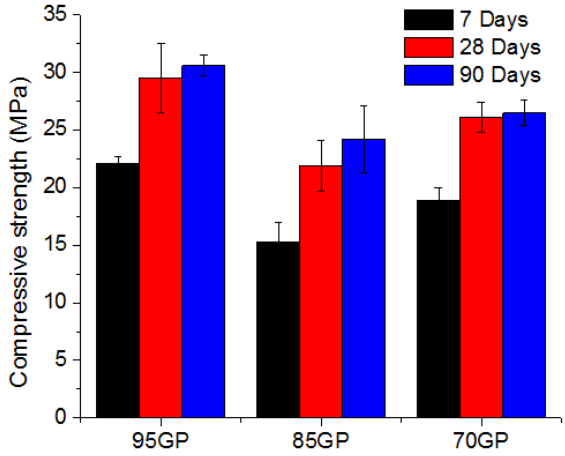

Figure 5.1 Compressive strength of AAGP mortar cubes

5.2 Stability in water

5.2.1 Description of the test

In this test, AAGP mortar bars, prepared according to the procedure described in **chapter 3.3.2.1**, have been immersed in tap water in order to see their stability under aqueous solutions. For that purpose, length and mass change of the mortar bars have been followed during 45 days.

In this case, specimens were immersed in tap water after 28 days of curing in dry conditions, i.e. 23ºC and 56% RH. Longer curing time was found effective to fix more alkalis in the binder (chapter 4.7) and thus increasing the performance of the binder. This is also confirmed in later sections (see **chapter 5.3**) where alkali leaching in distilled water decreases at longer curing times.

5.2.2 Results

Figure 5.2 shows the length change (dimensional stability) and the mass change of AAGP mortar bars stored in tap water during 45 days. Regarding the length change (**figure 5.2 A**), an expansion during time is observed in all the systems, 95GP, 85GP and 70GP. This expansion is much higher for the system with 95% of GP and 5% of Mk, getting an expansion of 0.25% at 45 days. In this case, bars experimented a rapid expansion during the first 14 days that stabilizes afterwards. When the Mk content was increased to 15%Mk (85GP) and 30%Mk (70GP), the expansion decreased considerably up to 0.09% and 0.04% at 45 days respectively. In both cases, the maximum expansion was achieved after the first week, and then remained constant during time. None of the bars suffered an important expansion during the first 180 minutes.

Regarding the mass change (**figure 5.2 B**), different behaviors were observed. For the 95GP bars, there was an increase of the mass of 1% during the first 180 minutes that then remained constant until 7 days. Afterwards, the mass started to decrease to a negative value at 45 days, indicating a lower mass than the one before exposition to water. On the other hand, 85GP and 70GP bars experimented an increase of the mass around 1% during 180 minutes as well. Nevertheless, in these cases, the mass continuously incremented during the first 7 days up to 3.5 and 4.9% for 85GP and 70GP respectively. Afterwards, 85GP bars started to decrease their mass and for 70GP bars, the mass seemed to stabilize around 4.9%.

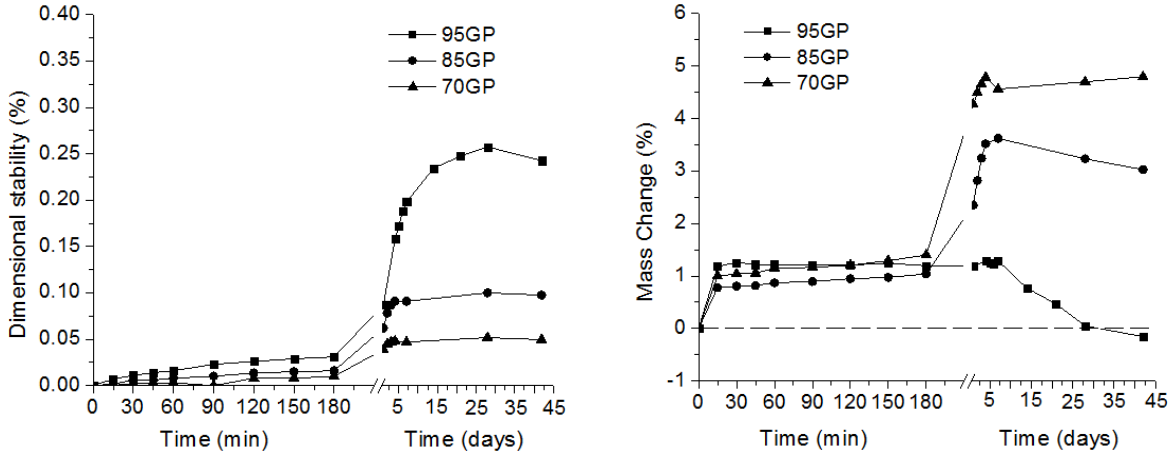

a) b)

Figure 5.2. Dimensional stability (a) and mass change (b) of AAGP mortars bars submerged in tap water during time

5.2.3 Discussion

The immersion of AAGP mortar bars in water has shown an expansion during time. This expansion reached its maximum after 7 days of immersion, and then remained constant up to 45 days. In the case of the bars manufactured with the higher content of GP (95GP), it is observed that after 28 days, expansion decreased slightly. As it can be observed, Mk content in the binder improves the dimensional stability of the bars in water, as the expansion was lower when higher was the Mk content. In the case of 5% of Mk (95GP), the expansion was the highest with 0.26%. The replacement of 15% of GP with Mk helped to stabilize the dimensions of the bars in water, decreasing the expansion more than a half (0.10%). Moreover, the replacement of 30% of GP with Mk decreased even more the expansion to 0.05%.

The expansion observed in every case is attributed to the water absorption by the system. When the mortar pores become saturated, an internal pore water pressure is generated resulting in a deformation.

Thus, higher expansion is related to higher water absorption. With the increase of the replacement of GP by Mk, the microstructure could be more refined in terms of porosity, and thus less water is penetrated, originating less expansion. Nevertheless, results show that the 70GP increased more in mass than 85GP bars and 95GP bars, although 70GP bars had the lowest expansion. This results indicate that not only water absorption is occurring but a mix of several effect. Hence, it could be also an influence of the leaching of ions from the paste and pore solution to the tap water. The leaching from the paste could be due to a disintegration of the sodium silicate gel formed in presence of water. It has been already reported the lack of hydrolytic stability of alkali silicate gels (Dimas et al. 2009). In a first step, sodium can be leached out according to **equation 5.1**, increasing the alkalinity of the solution. Afterwards, as alkalinity of the medium increases, dissociation of silica gel could take place according to **equations 5.2** and **5.3** (Jantzen & Plodinec 1984). Therefore, a mass loss could take place by a sodium and silica dissolution. On the other hand, the leaching of alkalis from the pore solution could be originated by the concentration gradient. The alkalis in the pore solution will diffuse to tap water and thus contributing to the mass loss. Summarizing, in 95GP bars two opposite effects could take place: a mass gain by the water absorption, and a mass loss by the leaching of ions (from both gradient concentration and disintegration of the gel).

$$\equiv Si-O-Na+H_2O \rightarrow \equiv Si-OH-H+Na^+ + OH^- \quad (5.1)$$

$$\equiv Si-O-Si\equiv +OH^- \rightarrow \equiv Si-OH+\equiv SI-O^- \quad (5.2)$$

$$\equiv Si-OH+OH^- \rightarrow \equiv Si-O^- + H_2O \quad (5.3)$$

The introduction of Al to the binder is known to have a positive effect on the stability in water of the formed gel (Redden & Neithalath 2014; Dimas et al. 2009; Giannopoulou & Panias 2010), as the gel formed in presence of Al converts the sodium silicate gel into a sodium aluminosilicate gel (N-A-S-H). This happens because Al^{3+} ions replace Si^{4+}. In order to balance the charge in the structure by the replacement of Si^{4+} with Al^{3+}, Na^+ is incorporated. Thus, increasing Mk in the binder will incorporate more Al to the gel structure and there will be higher binding of Na ions. Consequently, there will be less alkalis in the pore solution. Else, as the N-A-S-H formed gel is more stable in water, leaching of Na and Si from the paste will be lower. Hence, 70GP would experiment less leaching of ions than 85GP and the latter less than 95GP. This is confirmed in the following section by the alkali leaching test (**chapter 5.3**). The mass loss of the 95GP mortar bars can be therefore attributed to a disintegration of the sodium silicate gel by a lack of hydrolytic stability.

5.2.4 Conclusion

The results of this test showed that there is an expansion of all the AAGP systems when exposed to tap water during 45 days. As the Mk content increases, it has been shown that the dimensional stability is higher, getting the lowest expansion (0.05%). This expansion has been attributed to a water absorption. Thus, when Mk content increases, the microstructure of the paste could be more refined, with less porosity. By this principle, mass change of the system with higher Mk content should be the lowest, but it is the system with highest increment of the mass instead. This showed that water absorption is not the only effect which affects the mass change but a mix of it with other effects: leaching of alkalis and silica due to an instability of the sodium silicate gel in water and a leaching of alkalis of the pore solution by concentration gradient.

Finally, Mk has shown to be beneficial for the water stability of the AAGP systems.

5.3 Leaching test: Sodium ions

5.3.1 Results

In order to see how alkalis, in this case Na, are fixed to the structure or can be leached, two mortar bars of each system have been stored in distilled water during 28 days. Each week, distilled water was renewed. The Na content was measured with an ICP instrument, as explained in **chapter 3.6.7**.

Figure 5.3 shows the sodium leached from the mortar bars to the distilled water during time, when curing time was 1, 7 and 28 days. During the curing time (7 and 28 days), the bars were kept in dry conditions at 23ºC and 56%RH.

Results showed that regardless of the curing time there was a rapid leaching of Na^+ ions to the distilled water during the first 7 days (first cycle). Comparing with other AAMs, as AAS and AAFA (see **chapter 4.8**), the leaching during the first week was between 3-4 times higher in AAGP systems. In the subsequent 7-day cycles, an attenuation of the Na^+ ions leachate during cycles was observed. At the end of each cycle, an attenuation of the concentration was also observed, indicating that the chemical equilibrium between the pore solution of the mortar and the distilled water was close. Moreover, the curing time had an influence in the Na leaching. When bars were exposed to distilled water at higher curing times, the Na leachate was lower. Nevertheless, this differences are mostly marked at early exposure times (first cycle).

It was also observed an influence of the Mk content. When Mk content increased the Na leaching at every age was lower.

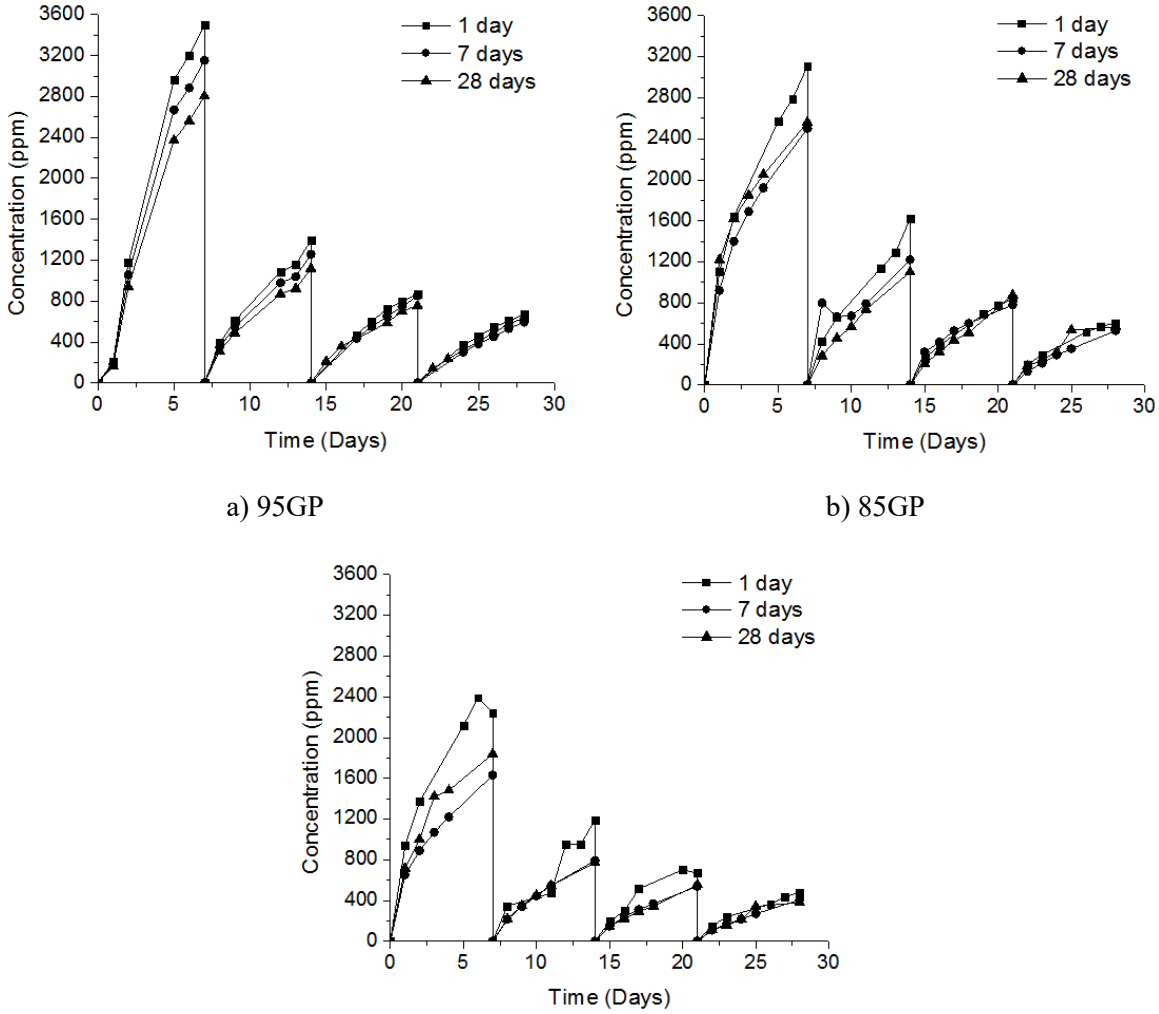

a) 95GP

b) 85GP

c) 70GP

Figure 5.3. "Na" leaching of bars exposed in distilled water during 4 weeks

5.3.2 Discussion

In this test, three AAGP systems have been submerged in distilled water and the Na-leaching has been periodically analyzed.

Regardless of the Mk content in the binder, it was found a rapid Na leaching when AAGP bars were immersed in distilled water. This leaching was found to be 3-4 times higher than those experimented by others AAMs, such as AAS and AAFA studied in **chapter 4.8**. As for these systems, the Na-leaching is mainly attributed to a dissolution of Na of the pore solution by the distilled water driven by a concentration gradient. The highest Na-leaching in AAGP compared to AAS and AAFA could be associated to the initial alkali content of each system, being 3-4 times higher in AAGP systems. As exposition time in distilled water increases, it was observed that the leaching rate decreases. This could

be associated to two effects. First, as Na concentration increases in the distilled water, an equilibrium between distilled water and the binder pore solution could be close, and the driving force could be decreased. The second effect could be related to the disposition of alkalis in the binder. Alkalis in the outer layers would be easier to dissolve than those of the inner layers. Thus, as time elapses, alkalis of the inner layers would be more difficult to dissolve, decreasing as well the dissolution rate.

One interesting fact to point is that when Mk content increased in the binder, the alkalis leaching was reduced notably, even though it was still high compared with AAS and AAFA results. This could be due to several reasons. First, the alkalis of the initial materials are lower as Mk content increases, since the Mk are mostly free of alkalis. Thus, less initial quantity of Na is present in the binder when higher is the GP replacement by the Mk. Second, as shown by the dimensional stability, the total porosity could be lower when higher is the Mk content, thus alkali diffusion would be more restricted. Other reason could be explained by the gel structure formed. The ratios of SiO_2/Na_2O and Na_2O/Al_3O_2 in the binder are important to obtain a sodium silicate gel with good hydrolytic and mechanical properties (Dimas et al. 2009). When the presence of Al is not significant, a sodium silicate gel will be favored. Dimas et al. (2009) reported that the sodium silicate gels are more stable as the SiO_2/Na_2O ratio increases, having good stability when this ratio is over 4.4. However, in later sections of this chapter (**chapter 5.4.3**), it has been found that the sodium silicate gels have an important presence of Al. In another work, it has been found that the hydrolytic stability of the sodium silicate gels is affected by the content of Al and Na (Giannopoulou & Panias 2010). Thus, systems with low content of Al and high content of Na have been found to be less stable. In our systems, it has been found a higher amount of Al in the gel when Mk (Si/Al ratio of 21.83, 10.68 and 6.46 for 95GP, 85GP and 70 GP respectively, see **table 5.1**), thus proportioning higher stability. Although Na content is similarly increased, the Al will play a more important role on the hydrolytic stability, since the increase of Na content is associated with charge balancing of the negative charge when Si^{4+} is replaced by Al^{3+} rather than network modifying agent. The sodium silicate gel with lower Al content has, therefore, tendency to disintegrate in presence of water, by means of a leaching of Na and Si ions.

Moreover, SEM results of **chapter 5.5.5**, where AAGP systems were exposed to tap water, evidence the formation of an Al-richer sodium silicate gel (N-A-S-H) when higher is the Mk content.

Summarizing, as the bars are put in contact with an external solution, the alkalis of the sodium silicate gel will pass to solution by the instability of this gel, and the alkalis present in the pore solution will diffuse to the external solution by a concentration gradient. This could be responsible for the mass loss experimented by 95GP bars observed in **figure 5.2 b**.

5.3.3 Conclusion

The results of this test showed that:

- There is a high alkali leaching when AAGP systems are immersed in distilled water, mainly attributed to a concentration gradient between pore solution and distilled water.
- As Mk content increases, the alkali leaching decreases because of a higher incorporation of alkalis when higher is the Al content: formation of a sodium aluminosilicate gel.
- In all the three AAGP systems studied, when the bars are kept in dry conditions for more time before exposure to distilled water, a decrease of alkalis leaching is observed, attributed to a higher incorporation of alkalis in the structure with time.

5.4 Sulfate resistance

Sulfate resistance test was conducted following the standard ASTM C1012, with some modifications done after the recommendations given in **chapter 4.3.5**. These modifications have been the following:

- The curing temperature used for all the AAGP systems has been 60ºC during 2 days (see **chapter 3.3.2.1**). Afterwards, mortar bars were demolded and stored during 28 days in 23ºC and 56%RH chamber until test.
- Prior to exposition to sulfate solutions, all bars were submerged in tap water during 15 min (in order to reduce the influence due to water absorption).
- The source of sulfate was sodium sulfate, with a concentration of 5wt%.

5.4.1 Expansion results

Figure 5.4 shows the sulfate resistance test for the three AAGP systems studied, with 95, 85 and 70% of GP in the binder, the rest being replaced by Mk. As it can be seen in the figure, there is an initial expansion during the first 14 days whatever the GP or Mk content was. The largest expansion was observed for the system with 95% of GP and 5% of Mk (95GP), with 0.20% of expansion after 14 days. When Mk content was increased to 15% (85GP) and to 30% (70GP), the expansion decreased to 0.10 and 0.05% respectively. After 14 days, the expansion in every case remained practically constant during time, especially for 85GP and 70GP systems. Regarding 95GP, a progressive shrinkage during time was observed.

It seems that there is no expansion of the bars due to sodium sulfate attack with AAGP, in the proportions of GP and Mk studied here. The behavior observed during exposure to 5% of sodium sulfate solution is quite similar to that obtained when bars were exposed to tap water (**figure 5.2a**). For

example, 95GP had an expansion of 0.24% after 40 days in tap water, and an expansion of 0.21% in sodium sulfate solution. For 85GP and 70GP, the results are practically the same in both conditions, of 0.10% and 0.055 respectively. Therefore, as explained in that section (**chapter 5.2**) the expansion is attributed to water absorption by the system.

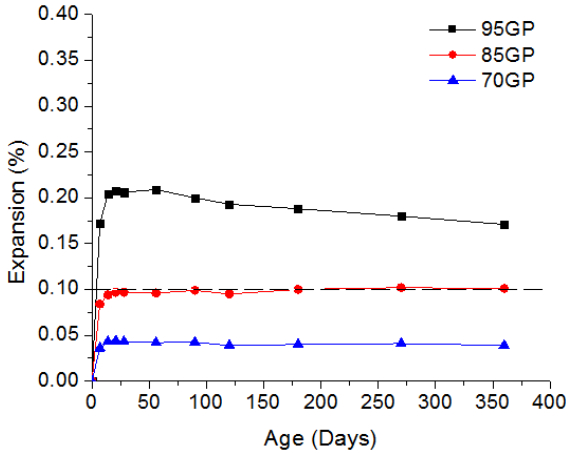

Figure 5.4 Sulfate resistance for AAGP bars exposed at 5% of sulfate concentration during 1 year

a) 95GP

b) 85GP

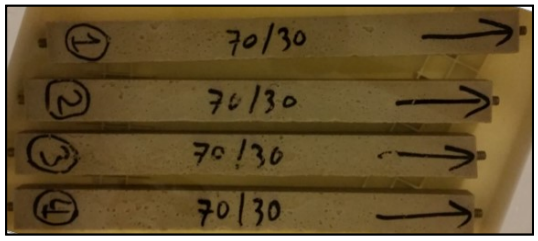

c) 70GP

Figure 5.5 Visual aspect of AAGP bars after 28 days of exposure to 5% sodium sulfate solution. a) 95GP, b) 85GP, and c) 70GP.

The progressive shrinkage observed in 95GP mortar bars after 50 days could be due to the disintegration of the sodium silicate gel when exposed to humidity (Dimas et al. 2009; Redden & Neithalath 2014), as explained in former sections.

It has to be pointed out a white gel observed in the surface of the 95GP bars, and to a lesser extent in the 85GP bars. This white gel is attributed to the precipitation of sodium silicate gel in the surface. Details of its formation will be discussed in discussion.

5.4.2 Mineralogical characterization by means of X-ray diffraction

XRD experiments were performed on samples at the end of test, i.e. after 1 year exposed to 5% sodium sulfate solutions. For each system, a piece of one mortar bar was taken to analysis.

Figure 5.6 provides the XRD spectra for the AAGP specimens. No crystalline products from the reaction of sulfates with the components of the binder were found in any of the three cases. For the 95GP and 85GP, the only crystalline phase observed was quartz (Q), attributed mainly to the sand used to prepare the mortars.

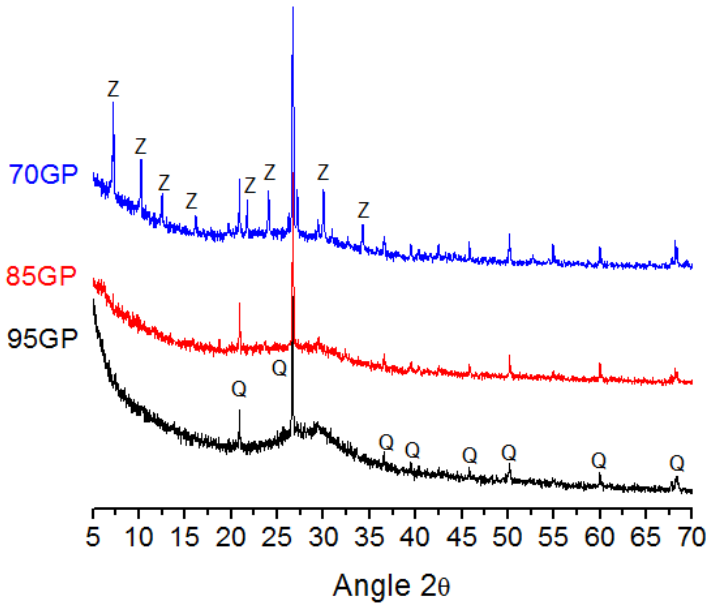

Figure 5.6 X-ray diffraction spectra for AAGP systems after 12 months of exposure to 5wt% sulfate solution

In the case of 70GP, it was found another crystalline product else than quartz, a zeolite (Z). The zeolite formed in this case was the so called Zeolite A, with a Si/Al ratio of 1 ($Na_{96}Al_{96}Si_{96}O_{384}\cdot 216H_2O$). This kind of zeolite has been already reported in alkali activation of metakaolin (Fernández-Jiménez, Palomo, et al. 2008; Fernández-Jiménez, Monzó, et al. 2008; Palomo et al. 2014).

5.4.3 Microstructural analysis by means of SEM-BSE

Figure 5.7 provides the SEM-BSE (EDX) analysis of the different AAGP mortar bars after 12 months exposed to 5wt% sulfate solution. No presence of new crystalline products from the reaction of the binder with sodium sulfate were found in any of the three cases, as shown by XRD. In the case of 95GP (**figure 5.7 A**), we can see the presence of cracks connecting the aggregates (magnification x100). If we observe the image with higher magnification (x1000), it can be seen a heterogeneous microstructure of the paste, with most of the gel surrounding the anhydrous glass powders in form of rims. This rims, similarly to OPC systems when a thermal curing is applied (Lothenbach et al. 2007), could be due to a denser gel formed during the heating period. Afterwards, gel formation is not well distributed in the phase, thus originating high porosity. The EDX analysis showed that the formed gel was predominantly composed by Si, Ca, Na, and Al. This suggests that the gel formed in this case could be a C-S-H gel, but in this case with very low Ca/Si ratios (average of several points of the image = 0.26 see **table 5.1**). The presence of Na in the gel, and to a lesser extent of Al, could be explained by an incorporation of these elements in the C-S-H due mainly to the low Ca/Si ratio (Stade 1989; Hong & Glasser 1999; Hong & Glasser 2002). Thus, the new gel will be represented in some way like C-N-(A)-S-H, in which Ca will be more present than Na (Ca/Na ratio of 2.58). A similar gel ((N-C)-A-S-H) has already been found to exist in hybrid alkali-activated cements (García-Lodeiro et al. 2010; García-Lodeiro et al. 2013), where Ca has partially replaced the alkalis of N-A-S-H gel. On the other hand, the gel could be a mix of a C-S-H gel (with low Ca/Si ratio) and a separated sodium silicate gel (N-S-H), both with traces of Al. In the work of Cyr et al. (2012), a similar situation was reported using 100% of GP as a binder, in which a co-existence of a C-S-H gel (with low Ca/Si ratio) and a sodium aluminosilicate gel (N-A-S-H) was proposed. In another work (Ravikumar & Neithalath 2012), in which slag was alkali-activated, it was found that higher alkalinity (higher Na_2O/slag) resulted in the formation of an additional silica-rich gel. In our case, the alkalinity is increased as the Mk decreases, thus higher silica-rich gel could be expected to form in 95GP. The formed sodium silicate gel could incorporate the Al in the structure or well adsorb it in the gel surface (Stone et al. 1993). Depending on the Al content this sodium silicate gel will convert to sodium aluminosilicate gel (commonly named as N-A-S-H gel). More tests are needed to well identify the type of gels formed.

In the case of 85GP (**figure 5.7 B**), it can be seen that the presence of cracks has been considerably reduced. This means that the increase of Mk improves the cohesiveness of the paste with aggregates, as already reported by Balaguer Pascual (2014). In the image with higher magnification (x1000), it can be also seen a heterogeneous microstructure of the paste, with the gel surrounding the anhydrous glass powders in form of rims. Regarding the EDX spectrum, it is observed again the same compounds than

for 95GP samples, Si, Ca, Na and Al, but in this case the peak intensities are different. It can be observed that the presence of Al is considerably increased, but still in less concentration than Ca and Na. Comparing the elemental ratios with those obtained for 95GP samples, shown in **table 5.1**, it can be seen that: 1) the Ca/Si decreased from 0.26 to 0.14, indicating a reduction of Ca in the gel; 2) the Si/Al decreased from 21.83 to 10.68, indicating a significant increase of the incorporation of Al in the gel; 3) and that Si/Na decreased as well. This results suggest that gel is being enriched by Al, meaning the formation a sort of a sodium aluminosilicate gel ((N-C)-A-S-H), in which Ca has replaced part of the Na in the structure (Ca/Na ratio 0.93). However, despite the increase of the Al content in the structure, it is still lower than Ca and Na. On the other hand, C-S-H gel could co-exist with the N-A-S-H gel but with lower amount of Ca than in 95GP.

Finally, for the 70GP system (**figure 5.7 C**), it can be observed the best homogeneity of the three systems studied, with no presence of cracks. Regarding the EDX spectrum, the same elements were found again: Si, Al, Na and Ca. As happened in 85GP sample, the Al is in higher concentration than the Ca and Na, suggesting again the formation of an aluminosilicate gel with an important presence of Na, and in a lower extent of Ca ((C)-N-A-S-H). The Ca/Si ratio continues to decrease as the Mk content is higher in the binder, what is reasonable as the Ca is only provided to the system by the GP. Therefore, by the same reason Al is increased. The increase of Al in the gel structure will support the higher incorporation of Na, by a charge compensation in the substitution of Si^{4+} by Al^{3+}.

Table 5.1 Atomic ratios for AAGP mortars bars exposed to 5% of sulfate concentration after 1 year of exposition

	Ca/Si	Si/Al	Si/Na
95GP + 5Mk	0.26 ± 0.08	21.83 ± 7.60	9.94 ± 4.39
85GP + 15Mk	0.14 ± 0.02	10.68 ± 3.13	6.64 ± 1.55
70GP + 30 Mk	0.11 ± 0.02	6.46 ± 2.56	5.88 ± 1.53

5.4.4 Discussion

In this section, three AAGP formulations to sodium sulfate attack were subjected. As shown by the expansion results, it seems that these systems are stable to sulfates (when the source is sodium sulfate) regardless of the Mk. As observed in **figure 5.4**, expansion remained practically constant in time after

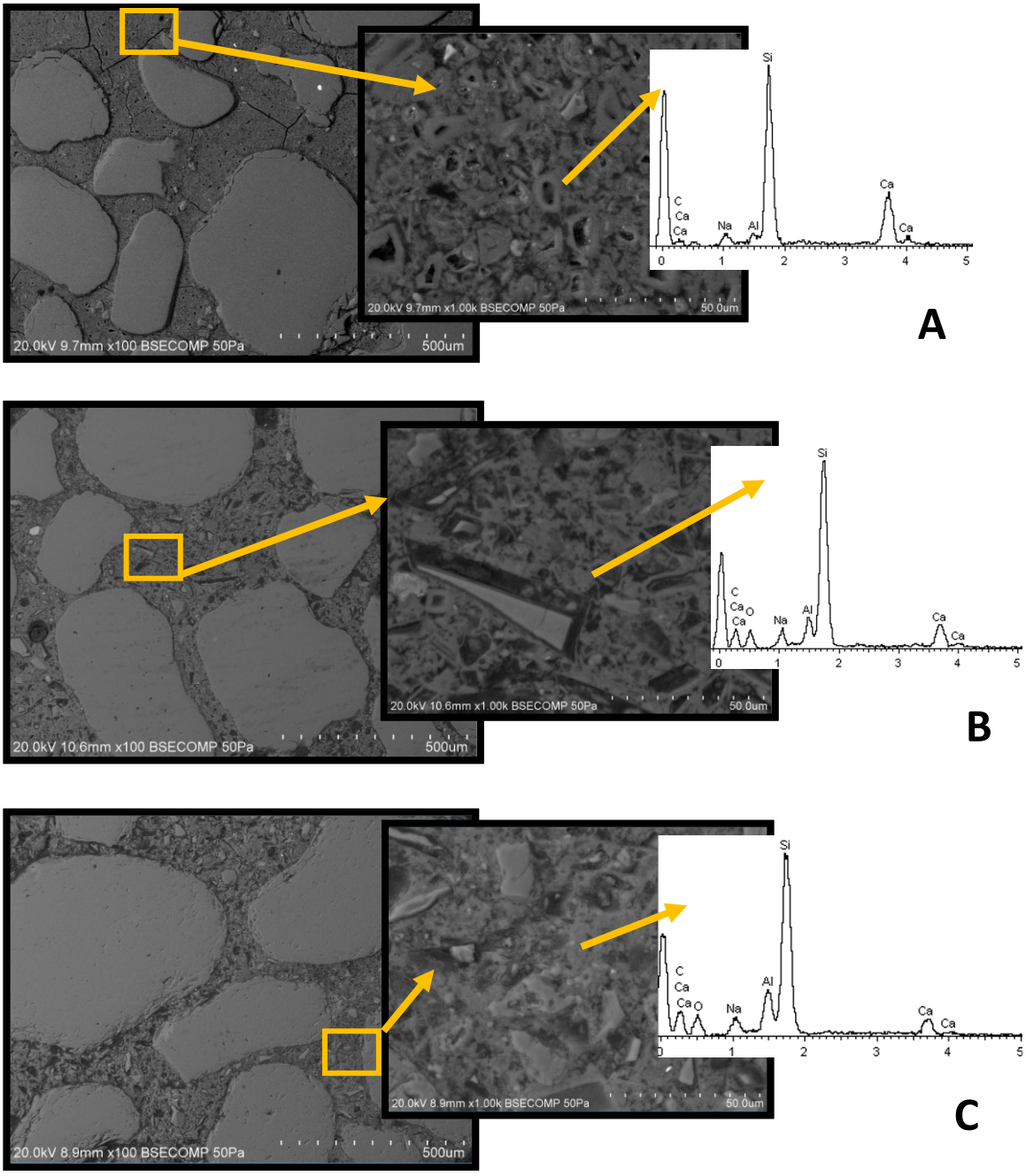

Figure 5.7 SEM-BSE images for AAGP mortars bars exposed to 5% of sulfate concentration after 1 year of exposition. A) 95GP; B) 85GP; C) 70GP.

2 weeks of exposition, although there was an initial expansion during the first 2 weeks. This initial expansion, however, has been attributed to the water absorption. Despite samples were pre-saturated during 15 min in tap water before starting the test, it does not seem to be sufficient for complete saturation, as samples are dry cured until the test (23ºC and 56%RH). Consequently, when samples are immersed in sulfate solution after the pre-saturation period, they continue to absorb water, thus creating

an internally pressure on the pore walls causing expansion. By the results, it is clear that 95GP is more porous, and the water absorption is higher, originating the highest expansion. As Mk content increases, the porosity seems to decrease, thus less water absorption and expansion is observed. Moreover, for 95GP samples, it is observed a shrinkage during time after 50 days of exposure that continued until the end of the test. This shrinkage was not observed in samples when Mk is increased to 15 and 30%.

The higher porosity of 95GP is also reflected in the SEM-BSE images, in which higher heterogeneity of the microstructure as Mk decreases can be seen. Moreover, a lot of cracks connecting the aggregates, and all along the sample, can be observed in this system. These cracks (in 95GP), however, are due to the weak cohesiveness between the paste and the aggregates (Balaguer Pascual 2014), probably caused by the shrinkage of the paste, and not to the sulfate attack. In fact, this high quantity of cracks could be responsible for the expansion experimented by the mortar bars after the first week. As explained before, the expansion was attributed to a water absorption (in this case sulfate solution). Thus, the cracks would have contributed to increase this water absorption.

Neither XRD nor SEM-BSE revealed the presence of crystalline products due to sulfate attack. Instead, the only system which showed crystalline phases (other than quartz from the sand) due to the alkali-activation was the one with the highest Mk content (30%, 70GP). In this system, the apparition of new peaks characterized as type A zeolites, with a Si/Al ratio of 1 ($Na_{96}Al_{96}Si_{96}O_{384}\cdot 216H_2O$) can be observed. These zeolites, already reported to form in systems with Mk (Fernández-Jiménez, Palomo, et al. 2008; Fernández-Jiménez, Monzó, et al. 2008; Palomo et al. 2014), are thus stable at the test conditions, and not affected by the sulfates.

Regarding the type of gel formed in each case, SEM-BSE (EDX) revealed different situations depending of the Al content (or Mk content). Although the type or types of gels formed in each one cannot be confirmed, it can be seen that the elemental characterization is different. Thus, for 95GP system, with the lower content of Mk, there was two possibilities. The first one would be a gel composed by C-S-H with low Ca/Si in which Na and to a lesser extent Al are incorporated. Thus, the gel will be represented as N-(A)-C-S-H, and the content of Ca will be higher than the Na one. The second possibility would be the coexistence of a C-S-H gel with low Ca/Si and a sodium silicate gel (N-S-H), in which Al could be incorporated in both gels.

In the case of 85GP, it has been shown that the formed gel is enriched by Al and Na, and analogously the Ca is decreased. Thus, the new formed gel will be somewhat like (N-C)-A-S-H, where Ca has replaced the sodium in the structure. On the other hand, another possibility could take place, like the co-existence of a C-S-H gel with low Ca/Si with a N-A-S-H gel.

When Mk content is increased to 30%, the same trend about the concentration of Al, Na and Ca than in 85GP is observed. Thus, Al and Na continue to increase in the gel, and Ca decreases. In this case, it is possible that the final gel obtained will be a sodium aluminosilicate hydrate with some Ca replacing Na ((C)-N-A-S-H). Ca, this time, will be in lower concentration than the Na as well as the Al.

An important aspect to remark is the white gel observed in the surface of the 95GP bars, and to a lesser extent in the 85GP bars (**figure 5.5**). As explained in former sections (**chapter 5.2**), due to an elevated leaching of sodium from the bars, pH of the solution raises quickly. At these conditions, the sodium silicate hydrate gel formed in the case of 95GP (N-(A)-S-H), formed together with the C-S-H gel, could be decomposed liberating silica ($Si\text{-}O^-$) to the solution (see **chapter 5.3**). This silica may therefore react with the Na ions of the solution (that would have been increased by the Na leaching), re-precipitating a sodium silicate on the surface (as well as on the bottom of the container).

Finally, it could be stated that AAGP are sulfate resistant when the metal cation accompanying the sulfate is Na.

5.4.5 Conclusions

From the results of the sulfate resistance test, it can be concluded that:

- AAGP, regardless of the Mk content, are sulfate resistant when the source of sulfates is the sodium sulfate.
- The fast expansion observed during the first 2 weeks is attributed to a water absorption rather than to sulfate attack, since after 2 weeks the expansion remained constant until 1 year.
- XRD showed no crystalline products associated to the sulfate attack. Instead, type A zeolite was found in the system with 30% of Mk.
- SEM-BSE (EDX) showed different types of formed gel, regarding the Mk content. Increasing the Mk will favor the formation of a sodium aluminosilicate gel, richer in Al.

5.5 Acid resistance

Acid resistance test was conducted following the standard ASTM C267, with some modifications done after the recommendations given in **chapter 4.4.7**. These modifications were:

- Specimens were cured during 28 days in dry conditions (23ºC and 56%RH) before exposure to acid solutions.
- Prior to exposition to acid solutions, all specimens were submerged in tap water during 15 min.
- Test was enlarged up to 196 days.

The indicators of the degree of attack were the same of the standard ASTM C267, since in this test we are going to do comparative studies between the same systems: glass powder/metakaolin. Thus, mass and cross-sectional dimension change, visual appearance and compressive strength have been measured during time. Microstructural analysis has been done as a complementary result to better understand the degradation process by means of X-ray diffraction and Secondary Electron Microscope.

The acid used was the same than in **chapter 4.5**, sulfuric acid at different concentrations: 3 and 5wt%.

5.5.1 Mass and cross-sectional dimension change

Figure 5.8 shows the mass and cross-sectional dimension change of the different AAGP mortar cubes exposed to 3 and 5% of sulfuric acid solutions during 196 days. It can be observed that the mass change was not very high in any case comparing to other systems such as OPC and AAS (see **chapter 4.5.1**). The results are more similar to those obtained with AAFA system. Despite the low mass change, there are different behaviors depending on the quantity of GP and Mk in the binder. When Mk content was 5% (95GP), there was a slight mass gain during first two weeks. Afterwards, the mass decreased until 150 days, when it remained stabilized around -1.8, 2.4 and 7.1% for 1, 3 and 5% of sulfuric acid concentration respectively. This increase of the mass at the beginning of the test is attributed to the saturation of the sample. Even though a pre-saturation period of the cubes was done during 15 min in tap water, this showed to be not sufficient as the mass increased slightly during the first 2 weeks. In the case of 5% of GP, as there were to opposite effects, the saturation and the disintegration of the sample (see **figure 5.9 a1**), the mass gain during the first 2 weeks was lower than the one for 1 and 3% of concentration. When Mk was 15 and 30% (85GP and 70GP respectively), the mass increased slightly during the first 2 weeks, and few differences were observed between the different acid concentrations. After 2 weeks, the mass remained practically constant. Again, this augmentation of the mass is attributed to the saturation of the sample. In these latter systems, contrary to 95GP, there were no mass loss at any time, indicating a priori a very good sulfuric acid resistance.

With regard to the cross-sectional dimension change (**figure 5.8b**), it is observed that the dimensions were not affected too much. The worst case was for 95GP mortar cubes, were dimensions expanded up to 5% at 196 days when exposed to 3 and 5% of acid solution. In this case, contrary to what it is observed when there is a mass loss, specimens did not reduce their dimension, but expanded. This is, therefore, a particular case. When Mk was 15 and 30% (85GP and 70GP respectively), the dimensions of the cubes remained practically constant during time, finding the worst situation for 85GP at 3%, experimenting a reduction of the dimensions of 3%.

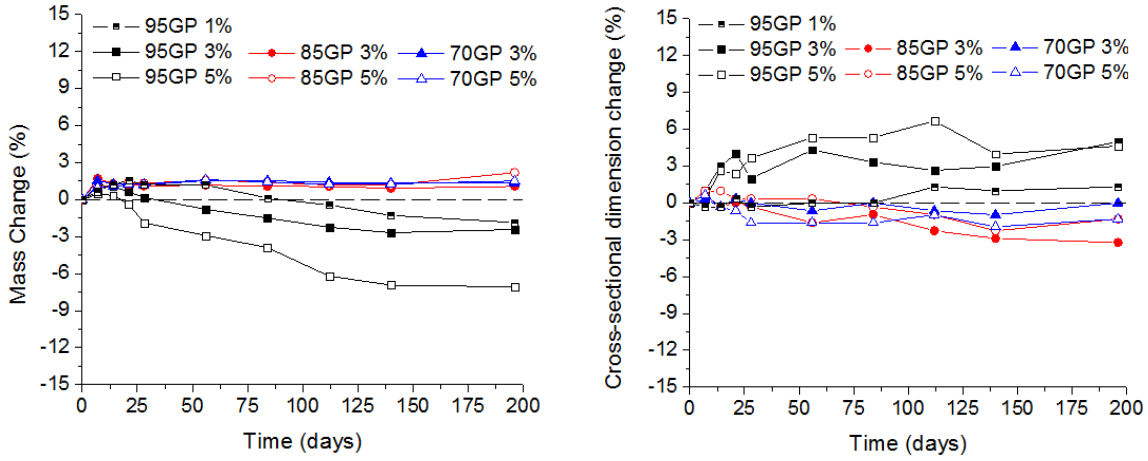

a) b)

Figure 5.8 Mass and cross-sectional dimension change of AAGP mortar cubes exposed to sulfuric acid at 3 and 5% of concentration during 196 days

5.5.2 Visual appearance

Figure 5.9 presents some photos of the visual appearance of the AAGP mortar cubes after 28 and 196 days of exposure to 3 and 5% acid solution. In the case of 95GP (**figure 5.9 a1 and a2**), it can be observed that there is a disintegration of the cubes. It can be observed a softening of the specimens' surface, with the emergence of cracks in all the axes. For cubes exposed to 1%, this was not observed, nevertheless, in these cubes it was found a white gel on the surface after the first weeks (**figure 5.10**). This white gel was not observed any more after 2 weeks. After 196 days, the cubes in all the acid conditions experimented an expansion and a severe deterioration of the surface. Therefore, the attack seems to start at the surface exposed to acid and then progress inward, similarly to what happened with AAS systems (see **chapter 4.4.3**). However, in this case, the further attack in inner layers did not cause severe expansion but a softening of the outer layers.

When Mk content in the binder was increased to 15% and 30% (**figure 5.9 b1, b2, c1 and c2**), it was observed that the cubes did not show any symptom of disintegration and softening of the surface. Since then the cubes were practically the same after 28 and 196 days of exposure to acid, whatever the acid concentration.

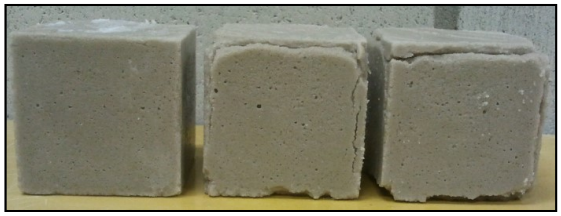

a1) 95GP after 28 days

a2): 95GP after 196 days

b1) 85GP after 28 days

b2) 85GP after 196 days

c1) 70GP after 28 days

c2) 70GP after 196 days

Figure 5.9 Visual appearance of AAGP mortars cured during 7 days after 28 and 196 days of exposure to sulfuric acid. In 95GP photos, first cube was immersed in 1wt% sulfuric acid solution, second cube was immersed in 3wt% and the third cube in 5wt%. For 85GP and 70GP photos, first cube was immersed in 3wt% sulfuric acid solution and the second cube was immersed in 5wt%.

Figure 5.10 White gel formed at the surface of 95GP cubes after 1 week of exposure to 1% of sulfuric acid solution

5.5.3 Compressive strength

The compressive strength test was only done for the 85GP and 70GP systems, because the dimension remained stable during acid attack, unlike the 95GP, where there was a deterioration of the surface.

Moreover, in order to have a more realistic comparison of the effect of the acid exposition on the compressive strength, a parallel study was done immersing cubes in tap water during the same time. In these systems, it has been found (**chapter 5.3**) that water exposure could produce changes in the gel structure, even if there was not any appreciable change in the visual inspection. Therefore, compressive strength change due to exposure to sulfuric acid attack will be compared for cubes exposed to tap water and cubes kept in dry curing (23ºC and 56%RH). As explained before, the test was started after 28 days of curing in dry conditions. Thus, all cubes were subjected to the different conditions after 28 days, i.e. some of the cubes were exposed to acid solutions, other to tap water (TW) and some of them kept in dry conditions.

Figure 5.11a shows the compressive strength evolution of 85GP mortar cubes exposed at the different conditions mentioned before. It can be observed that after exposition to acid solutions and tap water during 28 days, the compressive strength decreased in every case, meanwhile the cubes exposed in dry conditions kept gaining strength up to 90 days. The worst situation was found for the cubes exposed to tap water (TW in figure), with a compressive strength loss of 35.6%. For the cubes exposed to acid solutions, compressive strength loss was lower than that of the cubes kept in tap water, being of 10.1 and 28.3% for 3 and 5% of acid concentration respectively. Thus, the more concentrated was the acid solution, the higher was the compressive strength loss. As the exposition to different mediums continued, it was found a recovery of the compressive strength during time, but never reaching the initial value before exposition and the compressive strength of the cubes in dry conditions. The compressive strength remained practically stable from 90 days of exposition whichever the medium.

For the 70GP mortar cubes (**figure 5.11b**), similar trends were observed, but in this case, the compressive strength was higher in every case. Again the worst situation was found for the cubes exposed to tap water, with a compressive strength loss of 26.4% after 28 days of exposition. For the cubes exposed to acid solutions, compressive strength loss was 8.0 and 23.4% for 3 and 5% of acid concentration respectively. The same trend measured in 85GP was also found with the acid concentration, with more compressive strength loss when higher the acid concentration was. After 56 days of exposition, cubes exposed to 5% acid solution experimented a compressive strength gain, contrary to the cubes exposed to 3% that continued decreasing. Afterwards, compressive strength continued falling during exposition time in both acid solutions, although it seemed to stabilize in the case of the cubes exposed to 5% acid concentration. For the cubes in tap water, it was observed similar trend to the 85GP cubes in TW. Hence, after the initial compressive strength reduction, there was a recuperation than remained stable after 90 days of exposure.

For 70GP samples, it has been observed that there is not a clear tendency of compressive strength evolution depending on the acid concentration. However, it has to be pointed out that, when samples are damaged or degraded, there is a non-uniformity of the sample (with a strong unaffected core and weaker outer affected region), thus producing variability between replicates. This is observed in the high standard deviation of some points of the figures.

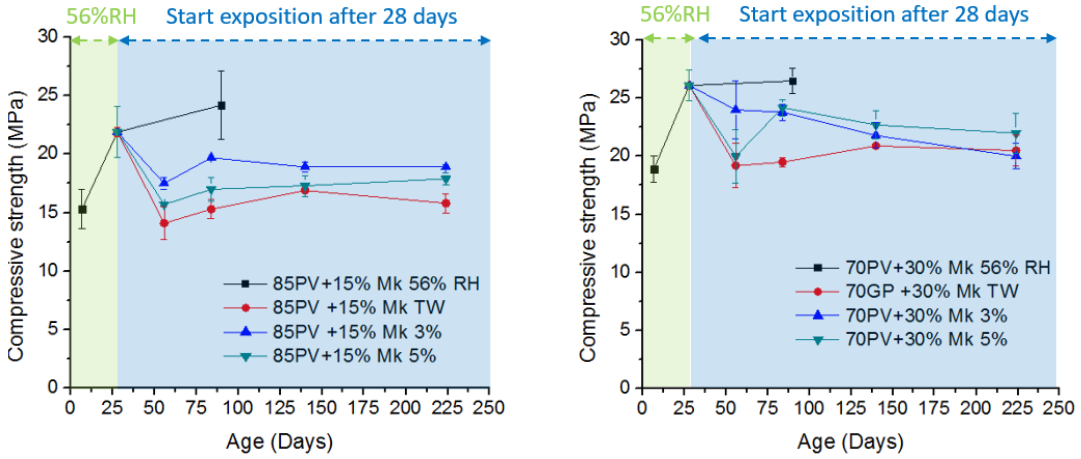

a) 85GP b) 70GP

Figure 5.11 Compressive strength of AAGP mortar cubes at different exposure conditions: 56% RH, tap water (TW), and 3 and 5% acid solution. Temperature during test was always 23ºC.

In all of the systems, after 28 days of exposition, compressive strength decreased, and then, at 56 days of exposition, compressive strength increased again. Afterwards, depending on the system, compressive strength continued to fall or to stabilize. To better understand this loss of compressive strength, samples were split into two parts, and one of them then sprayed with a phenolphthalein solution, as shown in **figure 5.12**. Phenolphthalein allows us to see the loss of alkalinity by the effect of the acid. As it can be seen in the figure, it can be observed two regions for the cubes exposed to acids, differentiated by the different color. An outer region, darker, and an internal region, clearer. The depth of the darker region increases during time of exposition to acid and acid concentration, and at certain age it is expected to occupy the entire cube body. In the case of the cubes exposed to tap water, no different regions were observed. When we sprayed with phenolphthalein cubes exposed in tap water, we observed that the pH is kept above 8. However, for those exposed to acids, it can be seen a loss of alkalinity of the outer layer, affecting both regions (darker and part of the clearer).

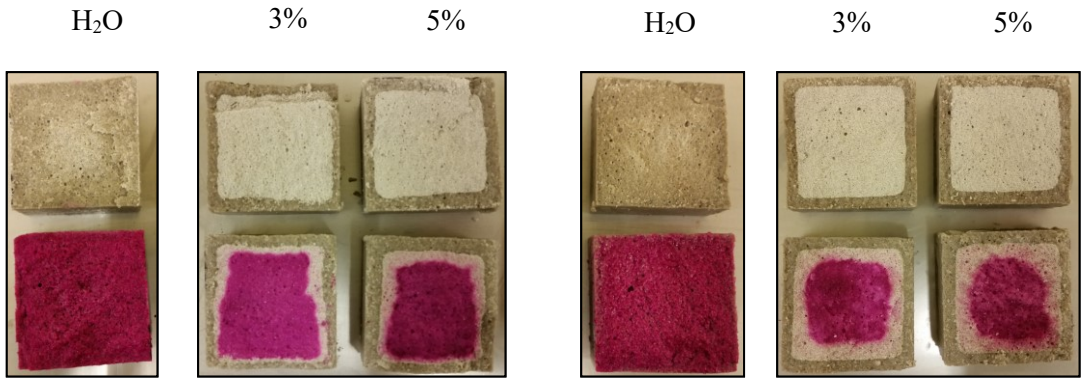

Figure 5.12 Split mortar cubes after 28 days of exposure to tap water and acid solutions (1, 3 and 5%). One half is shown just after splitting (above half) and the other was sprayed with phenolphthalein solution (below half). a) 95GP mortar cubes, b) 85GP and c) 70GP.

5.5.4 Mineralogical characterization by means of X-ray diffraction

XRD experiments were performed on samples after 28 days of exposure to the acid solutions and tap water, to characterize crystalline compounds in the system. In order to distinct the two regions observed in the **figure 5.12**, samples from each region have been analyzed. In the case of the inner region, sample was taken form the core who showed high basicity with the phenolphthalein test.

Figure 5.13 shows the X-ray patterns for the 95GP specimens. As it can be seen in the figure, there is not any difference between the inner region of the cubes exposed in acid solutions (1, 3 and 5% INT spectra) and the sample exposed to tap water (TW). In these spectra, there is a broad halo between 18-40º 2θ and centered at 29.4º 2θ. Comparing to the anhydrous GP spectra, it can be observed that the maximum of the halo has shifted to a higher 2θ values, indicating the formation of an amorphous reaction product. No trace of crystalline phases are observed other than the quartz (Q) (present in the initial materials and in the sand of the mortars), like zeolites that could be formed because of the reaction of Mk. Regarding the spectra of the outer layer of the cubes (1, 3 and 5% EXT spectra), the surface exposed to acid solutions, there are several changes. The most noticeable is the apparition of new peaks of gypsum (G) all around the spectra, whatever the acid concentration is. The formation of gypsum can be responsible for the expansion and surface softening of the mortar cubes observed in former section (see **chapter 5.5.2**). Other observation in the spectra is that the center of the halo has been shifted to lower values, at 23º 2θ, similar to the halo observed in anhydrous GP. This could be consequence of the disintegration of the amorphous gel. The peaks of quartz are also observed.

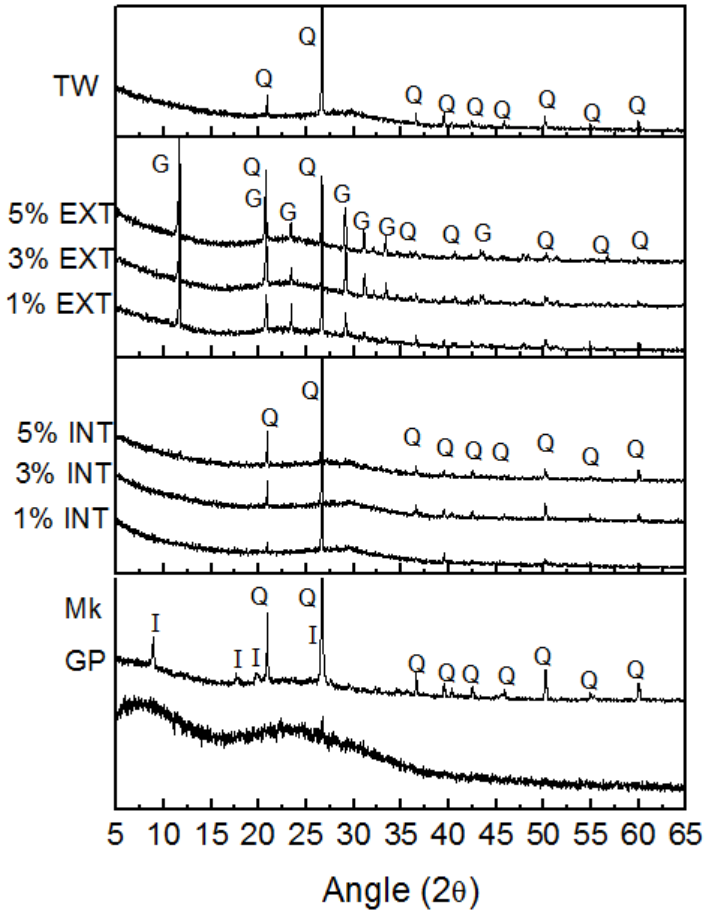

Figure 5.13 X-ray patterns of 95GP specimens after 28 days of exposure to acid solutions and tap water. INT: inner core; EXT: outer layer. Pics: Q, quartz; I, illite; G, gypsum.

Figure 5.14 shows the X-ray patterns for the 85GP specimens. Noteworthy differences between the spectra of the samples exposed to the different solutions can be seen. For the sample exposed to tap water, it can again be observed a halo between 18º and 40º 2θ, but now centered at lower 2θ values, at 27º. This halo, as happened with 95GP, has shifted to a higher 2θ values comparing to the halo of anhydrous GP, indicating a reaction and formation of a new gel. In this spectra, zeolitic crystalline phases (Z) can be observed. The zeolite formed in this case was the so called type A Zeolite, with a Si/Al ratio of 1 ($Na_{96}Al_{96}Si_{96}O_{384}\cdot 216H_2O$). This kind of zeolite has been already reported in alkali activation of metakaolin (Fernández-Jiménez, Palomo, et al. 2008; Fernández-Jiménez, Monzó, et al. 2008; Palomo et al. 2014). Other crystalline phase observed is due to the quartz, present in the initial materials as in the sand used to manufacture the mortar.

When the cubes are exposed to acid solutions, different spectra are obtained. For the inner region of the cubes (1, 3 and 5% INT), the spectra found are very similar to the spectra found for 95GP at the same

conditions, and are different from the spectrum of the sample immersed in tap water. In this case, the center of the halo is centered at 29º 2θ, as for 95GP spectra. No appreciable traces of zeolites are observed, as observed in the sample exposed to tap water. In regards with the spectra of the surface exposed to acid solutions (1, 3 and 5% EXT), it can be observed again the formation of crystalline peaks characterized as gypsum (G). Moreover, the center of the main halo observed for the inner regions has been displaced to lower values, close to those of anhydrous GP.

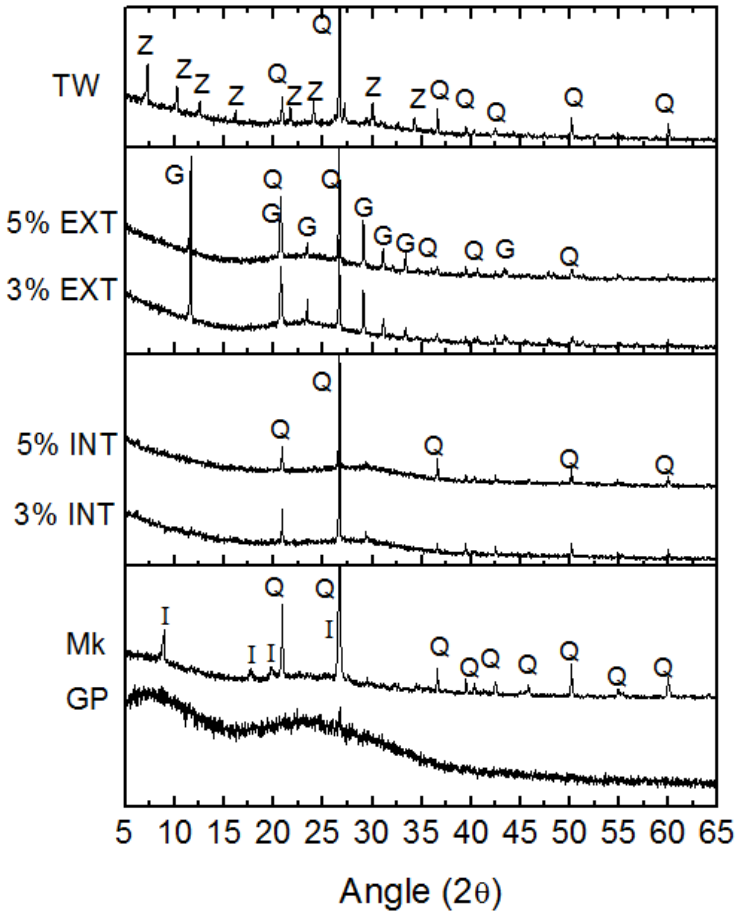

Figure 5.14 X-ray patterns of 85GP specimens after 28 days of exposure to acid solutions and tap water. INT: inner core; EXT: outer layer. Pics: Q, quartz; I, illite; G, gypsum; Z, zeolite type A.

Figure 5.15 shows the X-ray patterns for the 70GP specimens. In the case of the sample exposed to tap water (spectrum TW), the same peaks observed for 85GP sample exposed at the same conditions can be seen. Therefore, the peaks due to formation of zeolite type A, and those due to quartz, can be observed. Regarding the spectra of the inner region of the cubes exposed to acid solutions (1, 3 and 5% INT), exactly the same spectra can be observed, whatever the acid concentration. For the surface exposed to acid solutions (1, 3 and 5% EXT), it can be observed that the peaks due to type A zeolite

disappear in presence of the acid. Instead, the peaks attributed to the formation of gypsum appear again. The observed halo in the region between 17º and 30º 2θ seems to be broader than before, and centered at 27º 2θ.

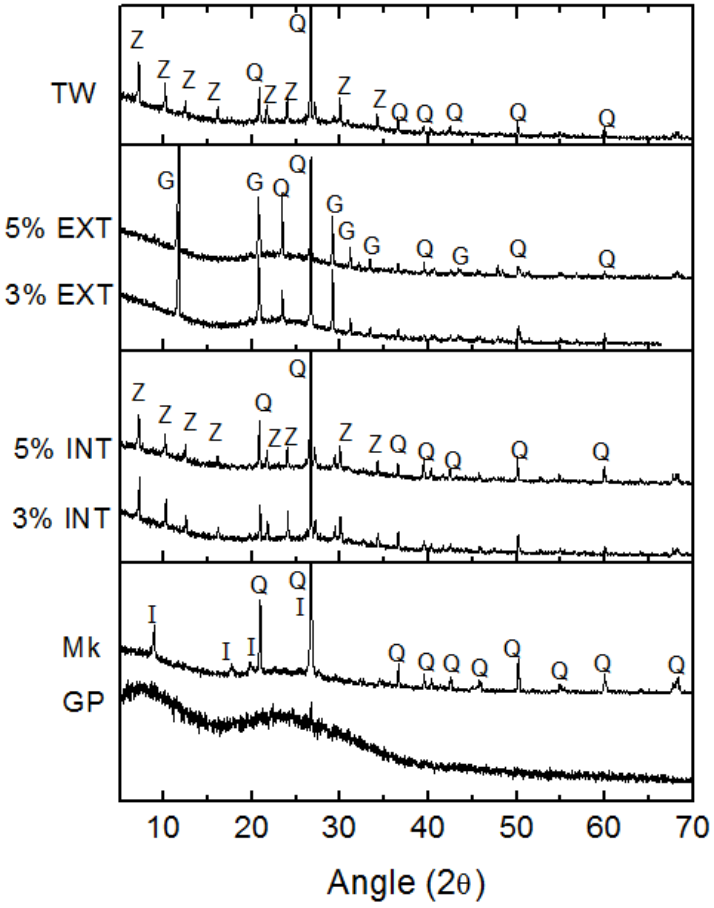

Figure 5.15 X-ray patterns of 70GP specimens after 28 days of exposure to acid solutions and tap water. INT: inner core; EXT: outer layer. Pics: Q, quartz; I, illite; G, gypsum; Z, zeolite type A.

5.5.5 Microstructural analysis by means of SEM-BSE

A microstructural analysis was performed on samples after 28 days of exposure to 5% acid solution, as well as in tap water. Again, as for XRD analysis, two parts of the cubes exposed to acid solutions were analyzed. One of them corresponds to the part exposed to acid solution and the other from the inner part of the cube, not in direct contact with the acid solution. Those parts are well differentiated visually in the photos of **figure 5.12**, with a darker color for the acid-exposed surface, and clearer color for the inner part. In the case of the inner part, samples were again taken from the core, which the phenolphthalein test showed high basicity.

Figure 5.16 shows the SEM-BSE images for the 95GP, as well as the EDX spectra. In the image of **figure 5.16 A**, it can be seen the sample after 28 days exposed to tap water. It is observed a heterogeneous phase, as it was found in the mortars exposed to sulfates (**chapter 5.4.3**), with most of the gel surrounding the anhydrous glass powders in form of rims. No signs of crystalline phases are observed, in accordance with the XRD results. The EDX spectrum of two points of the image shows a gel predominantly composed with Si, Ca, and Na, with traces of Al and Mg. This suggests, as already stated in **chapter 5.4.3**, that the formed gel could be a C-S-H gel, with very low Ca/Si ratios (average of several points of the image = 0.20, see **table 5.2**). This C-S-H gel, however, has a non-negligible content of Na, present practically in the same order than the Ca (Ca/Na ratio of 1.29). So the final formed gel could be a sodium calcium silicate hydrate, N-C-(A)-S-H, with traces of Al. On the other hand, the gel could be a mix of a C-S-H gel (with low Ca/Si ratio) and a sodium silicate gel (N-(A)-S-H) with traces of Al.

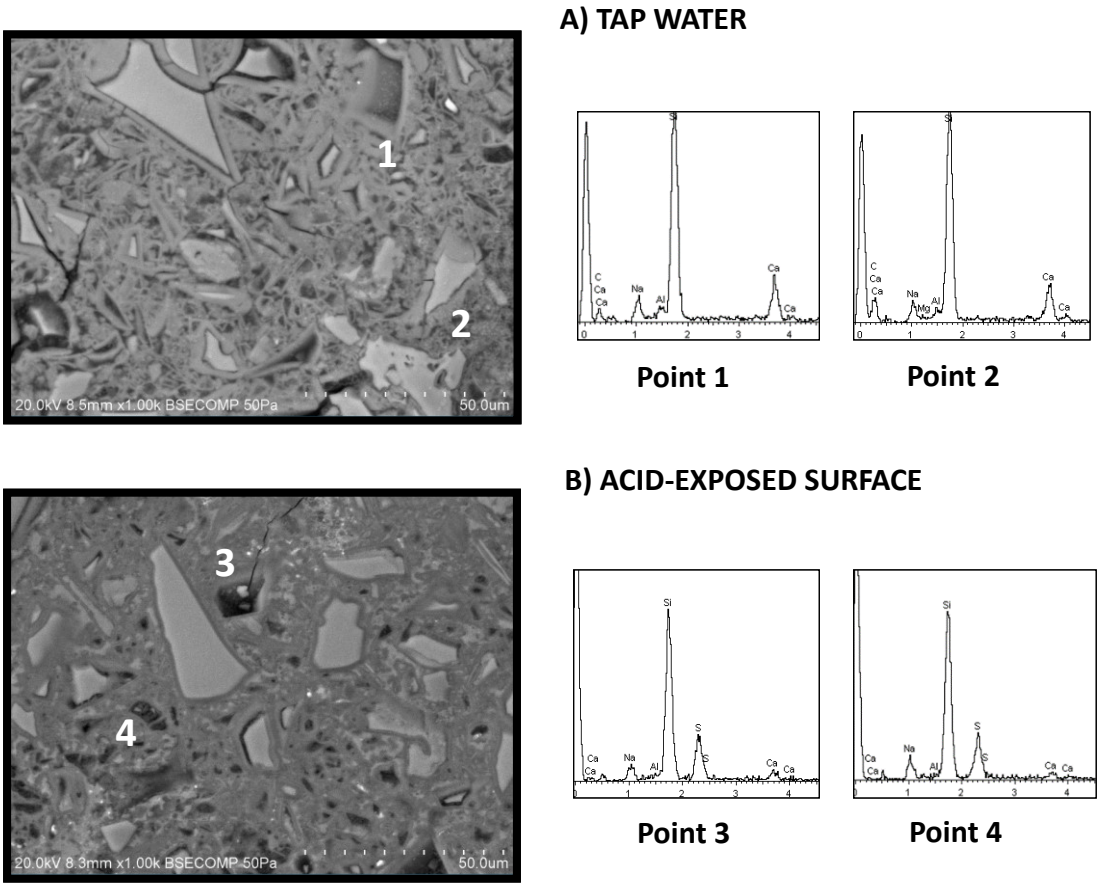

Figure 5.16a SEM (BSE) images and EDX analysis of 95GP mortar cubes after 28 days of exposure to tap water and 5% acid solution. a) Tap water, b) Face-exposed to acid solution (EXT)

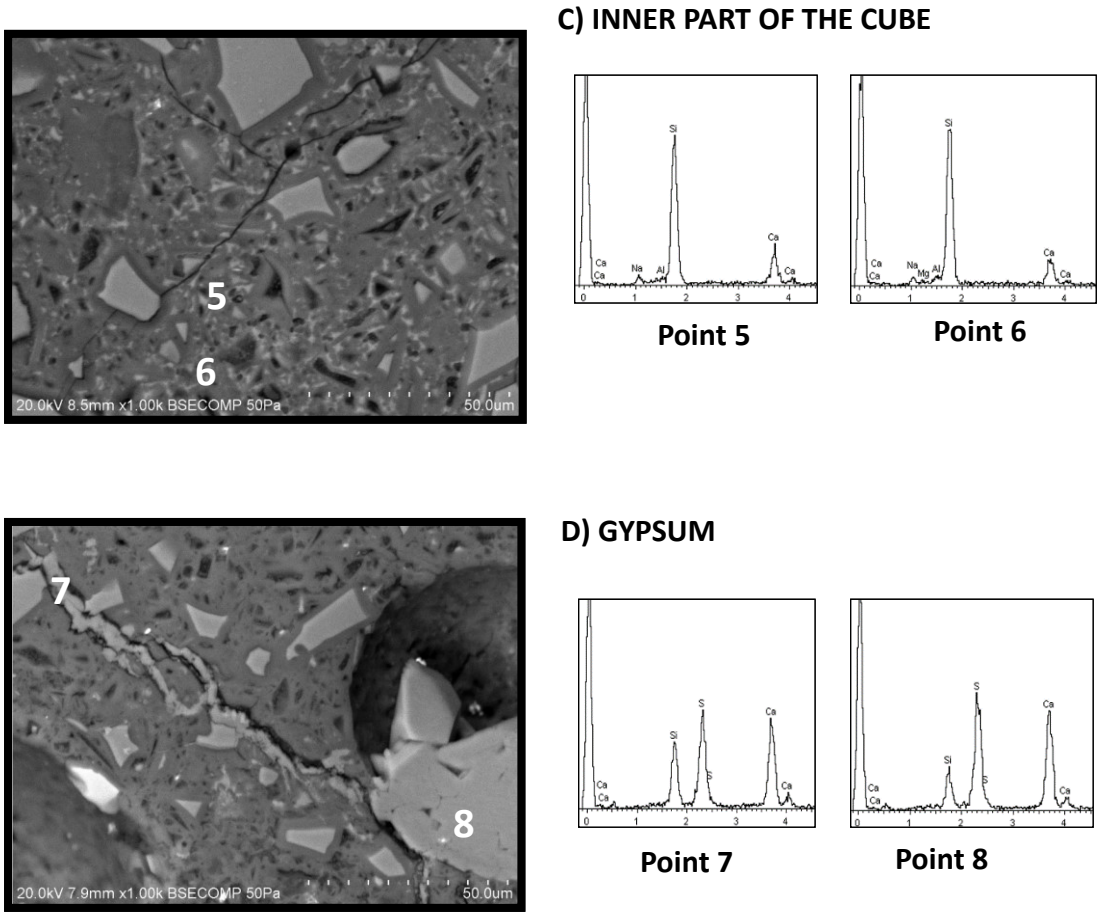

Figure 5.16b SEM (BSE) images and EDX analysis of 95GP mortar cubes after 28 days of exposure to tap water and 5% acid solution. c) Inner part not exposed to acid solution (INT), d) Gypsum formed in the face-exposed to acid solution

In **figure 5.16 B and C**, the SEM images for the acid-exposed surface and the inner part of the 95GP mortar cubes can be respectively seen, as well as the EDX spectra. For the inner part of the cube (**figure 5.16 C**), it is found better homogeneity of the phase gel than that found in the water-exposed cubes. It cannot be appreciated any presence of crystalline phases, in accordance with XRD results. Regarding the EDX spectra, we find similarities with those obtained with water-exposed cubes, mostly composed by Ca, Na and Si, with traces of Al and Mg. In this case, it has to be pointed out that the presence of Ca and Na is lower than the one in the water-exposed cubes, as the Ca/Si ratio is decreased from 0.20 to 0.15 and the Si/Na ratio is increased twice, whereas the Si/Al is maintained (see **table 5.2**). Despite this difference, gel composition is still considered the same, suggesting as before the formation of a N-C-(A)-S-H gel, or a mix of a C-S-H gel and a sodium silicate gel (N-(A)-S-H) with traces of Al. For the acid-exposed surface (**figure 5.16 B**), it can be observed better homogeneity of the phase, but still with high porosity present. The rims formed around the anhydrous GP particles can be also observed.

In the EDX spectra, representing two points of the image, there are noticeable changes in the elemental composition comparing to those found at the inner parts of the cube (**figure 5.16 C**), or with the water-exposed samples (**figure 5.16 A**). First, it is found the presence of sulfur (S) in much higher quantities than Al, Ca and Na. Moreover, the quantity of Ca found is lower than the parts not affected by the acid. Regarding the Ca/Si ratio of the **table 5.2**, it can be observed that theratio is decreased slightly from 0.15 of the inner part to 0.12, thus suggesting a decalcification of the gel. Moreover, the Si/Al ratio has been increased to very high values (in some points Al is negligible), indicating a dealumination process too. On the contrary, the Si/Na ratio decreases comparing to the inner part, showing an increment of the Na in the gel. Gypsum crystals were also found (**figure 5.16 D**), in accordance with XRD results. This gypsum has been found in several parts of the acid-exposed surface analyzed, always located in the large voids of the pore structure. The EDX analysis showed a chemical composition mostly of Ca and S, with atomic Ca/S ratio near to 1 that fits very well with the chemical formula of gypsum ($CaSO_4$).

Figure 5.17 shows the SEM-BSE images for the 85GP, as well as the EDX spectra. In the image of **figure 5.17 A**, it can be seen the sample after 28 days exposed to tap water. It can be seen again a heterogeneous phase distribution with high porosity. It cannot be appreciated any form of crystalline phases, although the XRD showed the formation of type A Zeolite. Nevertheless, this zeolite was not found for the inner parts of the cubes when exposed to acid solution. The EDX spectrum showed again the same compounds than for 95GP samples, Si, Ca, Na and Al. But in this case the peak intensities are different, as already pointed out in the sulfate attack test. Thus, in this case the Al is higher than Ca and Na. The results suggest again an enrichment of Al, indicating the formation of a sodium aluminosilicate gel (N-A-S-H or a (N-(C)-A-S-H). However, another possibility could occur, with C-S-H gel (with lower Ca/Si ration than in 95GP) co-existing with the N-A-S-H gel.

In **figure 5.17 B and C**, the SEM images for the acid-exposed surface and the inner part of the 85GP mortar cubes can be respectively seen, as well as the EDX spectra. For the inner part of the cube (**figure 5.17 C**), it is also observed a heterogeneous phase distribution and high porosity. Else, it is identified the formation of rims around the anhydrous GP particles. Regarding the EDX spectra, similar peaks of those obtained for water-exposed sample are observed, with the Al peak intensity similar to those of Na and Ca. This suggests that the formed gel is probably a N-A-S-H gel, or else a (N-C)-A-S-H. Also, it could be a mix of a N-A-S-H gel and N-C-S-H. For the acid-exposed surface (**figure 5.17 B**), again a heterogeneous phase distribution with high porosity is found. The EDX spectra obtained are similar to those found in 95GP at the same conditions, with small amounts of Al and Ca, and with an important presence of S. The Ca/Si ratio again is decreased, from 0.21 to 0.04, and the Si/Al is increased considerably, from 13.08 to 82.03, suggesting a decalcification and dealumination of the gel. Moreover,

in this case, the Si/Na is increased from 9.03 to 28.61, indicating also a dealkalinization of the gel. Therefore, the final gel after the acid attack could be a silicate gel with some traces of Na and Ca. As in the 95GP system, gypsum crystals were found, as shown in **figure 5.17 D**.

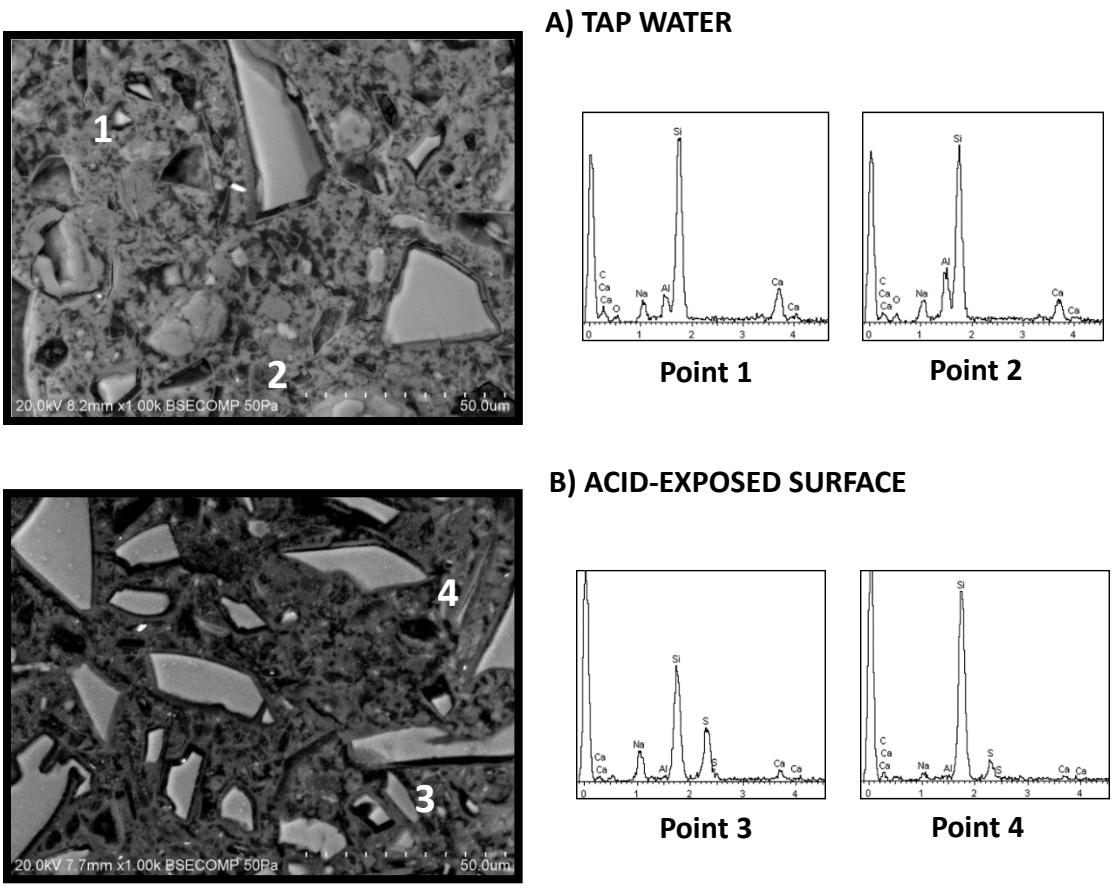

Figure 5.17a SEM (BSE) images and EDX analysis of 85GP mortar cubes after 28 days of exposure to tap water and 5% acid solution. a) Tap water, b) Face-exposed to acid solution (EXT)

Figure 5.18 shows the SEM-BSE images for the 70GP, as well as the EDX spectra. In the image of **figure 5.18 A**, it can be seen the sample after 28 days exposed to tap water. In this case, it is observed better homogeneity than the 95GP and 85GP samples exposed at the same conditions. Although XRD clearly showed the presence of type A zeolite, it cannot be observed any presence of crystals by this technique with polished surfaces in BSE mode. Regarding the EDX spectrum, the same elements were found again: Si, Al, Na and Ca. Thus, as stated in **chapter 5.4.3**, the formed gel could be an aluminosilicate hydrate gel with an important presence of Na (in higher concentration than Ca), (C)-N-A-S-H.

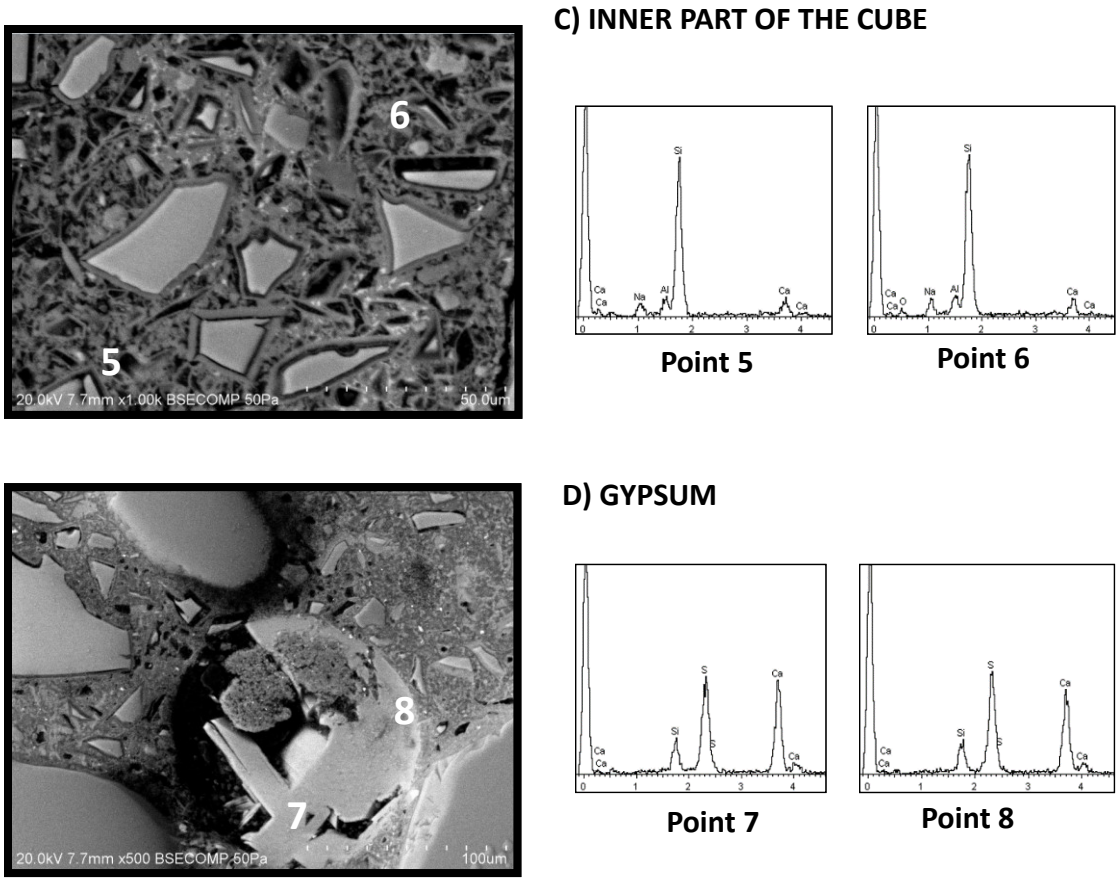

Figure 5.17b SEM (BSE) images and EDX analysis of 85GP mortar cubes after 28 days of exposure to tap water and 5% acid solution. c) inner part not exposed to acid solution (INT), d) Gypsum formed in the face-exposed to acid solution

In **figure 5.18 B and C**, the SEM images for the acid-exposed surface and the inner part of the 85GP mortar cubes can be respectively seen, as well as the EDX spectra. For the inner part of the cube (**figure 5.18 C**), similar phase distributions and EDX spectrum to those obtained in the water-exposed sample is observed. For the acid-exposed surface (**figure 5.17 B**), similar homogeneity to the inner part is observed. Comparing the EDX spectrum, it can be observed again that the Al and Na are practically negligible, while Ca is decreased. In this case, Ca loss is not as marked as in 85GP sample. Again, the EDX analysis show a dealumination as well as a dealkalinization of the gel. Gypsum crystals were also found (**figure 5.18 D**), in accordance with XRD results. As well as in 85GP sample, final gel after acid attack could be a silicate gel with some traces of Na and Ca.

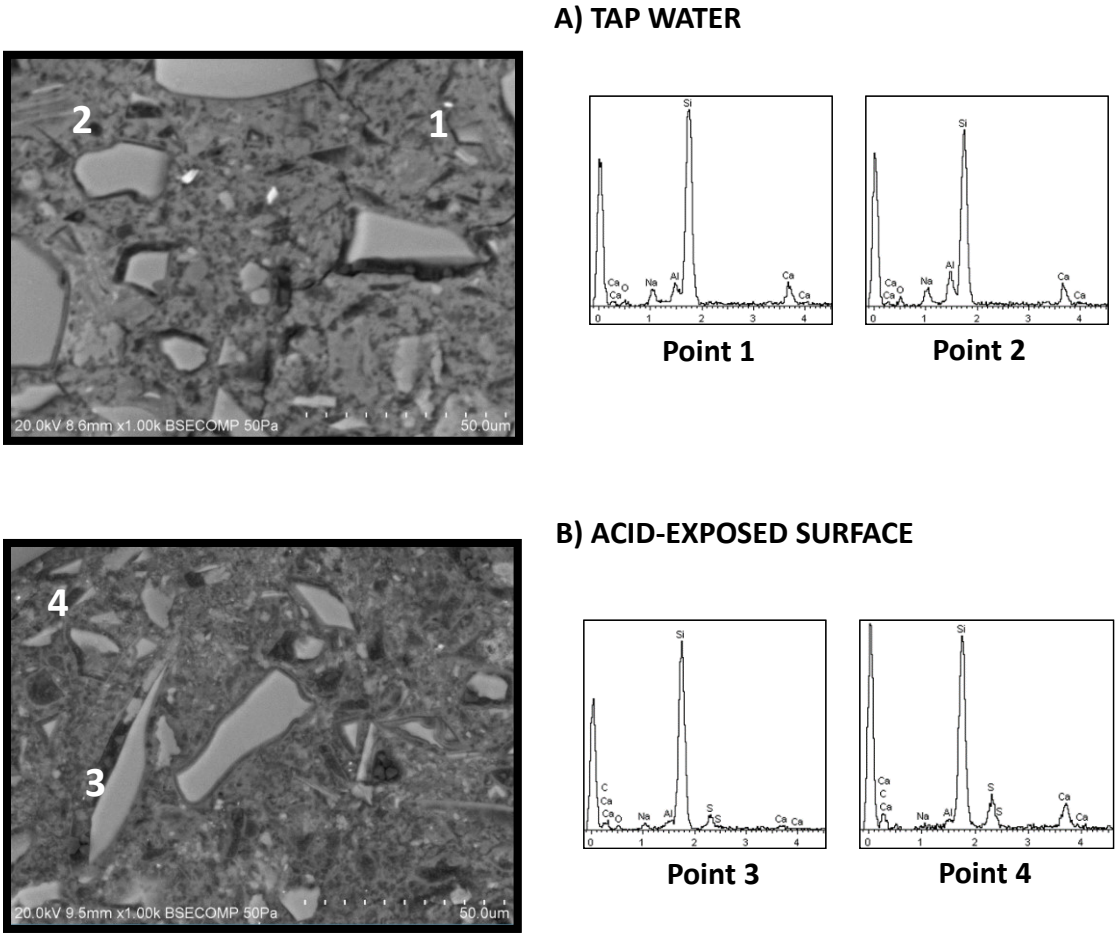

Figure 5.18a SEM (BSE) images and EDX analysis of 70GP mortar cubes after 28 days of exposure to tap water and 5% acid solution. a) Tap water, b) Face-exposed to acid solution (EXT)

Finally, in the table 5.12, the elemental atomic ratios of the images can be seen. Each value is an average of 15 points of the image focused on the paste. Anhydrous particles and aggregates were not taken into account for the average.

5.5.6 Discussion

The results demonstrate again the importance of Mk content in the binder to improve their durability. In this case, increasing the Mk up to 15% was good enough to keep the mass and cross-sectional dimension practically constant during time. When Mk content was of 5%, the mass decreased slightly during time to stabilize around 150 days. Despite this mass loss, it could be suggested a good acid sulfuric resistance. Although there is a mass loss, it was found an increase of the cross-sectional

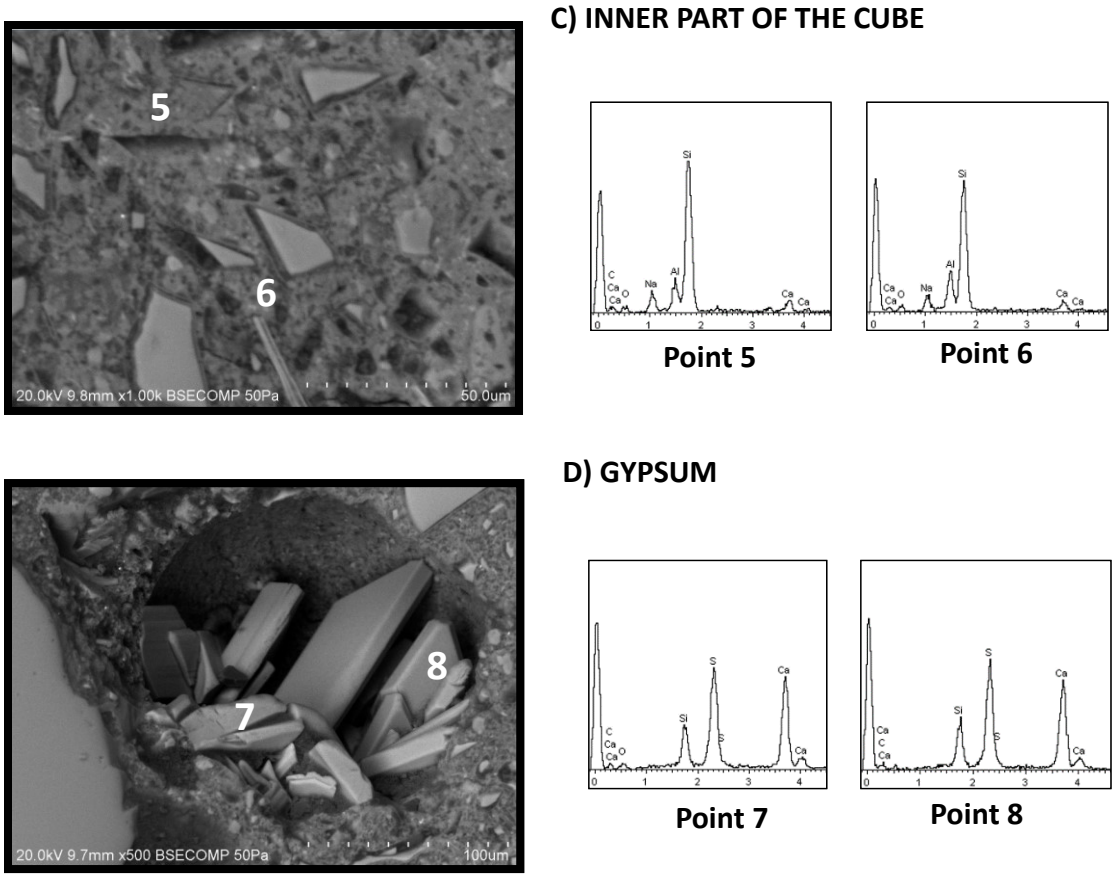

Figure 5.18b SEM (BSE) images and EDX analysis of 70GP mortar cubes after 28 days of exposure to tap water and 5% acid solution. c) Inner part not exposed to acid solution (INT), d) Gypsum formed in the face-exposed to acid solution

Table 5.2 Average elemental ratios obtained by EDX analysis of 95GP, 85GP and 70GP samples

		95GP	85GP	70GP
Ca/Si	H_2O	0.20 ± 0.02	0.15 ± 0.02	0.11 ± 0.05
	EXT	0.12 ± 0.04	0.04 ± 0.03	0.11 ± 0.07
	INT	0.15 ± 0.06	0.21 ± 0.12	0.13 ± 0.08
Si/Al	H_2O	25.78 ± 6.86	6.49 ± 2.16	6.23 ± 2.17
	EXT	81.33 ± 59.05	82.03 ± 25.84	38.13 ± 17.56
	INT	25.56 ± 6.09	13.08 ± 4.94	7.21 ± 2.61
Si/Na	H_2O	6.45 ± 0.81	6.01 ± 0.93	8.51 ± 2.89
	EXT	6.15 ± 2.11	28.61 ± 12.21	38.25 ± 17.39
	INT	14.71 ± 2.41	9.03 ± 1.82	7.94 ± 2.55
Ca/S	Gypsum-EXT	1.03 ± 0.10	1.07 ± 0.11	1.02 ± 0.07

dimension, i.e. an expansion. This system showed to be like AAS system (**chapter 4.4**), although the expansion was much lower. Again, we found a mass loss accompanied by an expansion. In this case, the visual inspection showed us a deterioration of the sample by means of surface softening and edge cracking. It has to be pointed out that the handling of these samples during measurements could have affected the mass, because part of the soft surface of the cubes could have been scaled, thus contributing to the mass loss. When Mk content was 15 and 30%, a notably improvement of the durability was observed, in terms of mass and cross-sectional dimension change. However, in both systems, the compressive strength reduction when these samples were immersed in acid solutions (even in tap water) showed that something was internally happening. This was visually confirmed when some cubes were split into two halves, and sprayed with phenolphthalein (**figure 5.12**). The cubes exposed to acid solutions showed that the acid-exposed regions were different in color than the inner regions (**figure 5.12**), and that the depth of this color modification was higher when higher was the acid concentration. This suggests a deterioration mechanism similar to that experimented by AAFA systems. Thus, it seems that there is a conversion of the gel. Despite this gel conversion affects the mechanical properties, once the sample is completely corroded, it has a residual strength that confers it an acid resistance. It can be seen that in the worst case the compressive strength reduction was 23.4% (70GP in 3% acid solution) after 196 days of exposure.

The better durability observed when Mk content increase is attributed to the formed gel. As shown by SEM-BSE (EDX) analysis, with 5% of Mk, the formed gel may be a mix of a low Ca/Si (0.15-0.20) calcium silicate hydrate gel (C-(A)-S-H) with a sodium silicate hydrate gel (N-(A)-S-H), both with some traces of Al. The Al could be placed in both C-S-H and N-S-H gel. However, the elemental analysis does not provide sufficient distinction between these two gels. These results are thus in accordance with what it was observed in the sulfate resistance test (**chapter 5.4**). The formation of calcium silicate hydrate could be due to the Ca content of the GP (12%). Nevertheless, this C-S-H gel is different to those found in OPC-based binders as the Ca/Si is very low (0.15-0.20). The latter gel, N-(A)-S-H, could be responsible for the instability of the samples when exposed to humidity (Dimas et al. 2009; Redden & Neithalath 2014). Dimas et al. (2009) reported that Al content of the initial materials played an important role on the hydrolytic stability of the resulting gel. Thus, depending on the incorporation of Al, it is suggested that the formed gel will move from N-S-H → N-(A)-S-H → N-A-S-H, improving its durability. It has been found that the incorporation of Al to the sodium silicate gels improve their hydrolytic stability (Giannopoulou & Panias 2010). Therefore, the stability (and durability) of this gel will depend on if the final gel is moved to a N-A-S-H gel.

This was confirmed by the addition of more Mk in the mix (15 and 30%). In this case, SEM-BSE showed that the elemental composition (EDX) changed, as the aluminum and sodium content found is higher. As it can be seen in **table 5.2** (for the inner part of the cubes exposed to the acids, INT), the Si/Al ratio is decreased almost 2 times in the case of 85GP, and 3.5 times in the case of 70GP, indicating higher incorporation of Al in the gel. Similarly, the Si/Na ratio decreased by 1.6 and 1.9 times for 85GP and 70GP respectively, indicating higher incorporation of Na. Again, these results are in accordance with that found in the sulfate resistance test. Regarding the Ca/Si ratio, indicative of a C-S-H gel formation, it increased for 85GP and then decreased for 70GP. However, it has to be pointed out the great variability of the results that could lead to misreading interpretations. If we look the Ca/Si ratio of the cubes exposed to water (TW in **table 5.2**), and those found in sulfate resistance test (**table 5.1**), it can be found a clear tendency, decreasing the Ca/Si ratio as the Mk increases. These results clearly show that the formed gel evolves to a sodium aluminosilicate gel (N-A-S-H) as the Mk content increases, and that the extent of the C-S-H formed is lower due to the lower presence of Ca (attributed to a lower content of GP, the only source of Ca). On the other hand, as stated in former sections, another type of gel can be suggested. When Mk is increased, and therefore Al content, it could be formed a (C-N)-A-S-H gel, where Ca has replaced in some way the Na in the structure. In the case of 70GP, Ca and Na are in the same extent, as Ca/Na ratio is of 1.03. It has been reported that Ca can replace Na by ion exchange mechanism to give (C-N)-A-S-H until all Na is completely replaced (if sufficient Ca is available) (Garcia-Lodeiro et al. 2011). According to these authors, it seems that (N-C)-A-S-H gels (where Ca has replaced Na) are formed in the regions of $0<CaO/SiO_2<0.3$, $0.08<Al_2O_3/SiO_2<0.5$ and $0<Na_2O/Al_2O_3<1.85$ (Garcia-Lodeiro et al. 2011). For 70GP, the (N-C)-A-S-H gel meets this ranges, with CaO/SiO_2 of 0.13, Al_2O_3/SiO_2 of 0.28 and Na_2O/Al_2O_3 of 0.91.

Whatever the type of formed gel (mix of C-S-H and N-A-S-H, or (N-C)-A-S-H), it is clear that it plays a major role on its durability against sulfuric acid and its stability on water.

In the case of the acids, it is observed a rapid strength reduction (only for 85GP and 70GP) at 28 days, and a slight increase afterwards. For 95GP mortar cubes, a softening and cracking on the surface was observed. In this test, the samples have been exposed to high acidic conditions (pH of 1.1, 0.7 and 0.5 for 1, 3 and 5% solutions respectively). In this acidic conditions, silicic acid could be liberated from the silicate gel to the solution (Bakharev 2005c). This will disrupt the microstructure leading to a softening of the mortar, as shown in the visual inspection (**figure 5.9a**). When the solution becomes supersaturated with the silicic acid, it is produced a "solid" phase of amorphous silica (Bakharev 2005c). This silica solid phase appears in form of a white gel in the surface of the specimen, as it can be observed in the picture of **figure 5.10**, taken at the end of the first week during exposition.

Nevertheless, this gel was only observed for 95GP samples exposed to 1% acid solution, and was not observed in more concentrated solutions or with higher Mk contents. Moreover, in this conditions, it was not observed new gel apparition after two weeks. When Mk content was higher, the apparition of this white gel on the surface of the cubes was not observed indicating that the gel formed in these cases had better stability in acidic conditions.

The decrease of the strength is then attributed to a disintegration of the silica gel. The formed gel is disintegrated in the acid-exposed surface and the gel of the inner regions of the cubes is maintained similarly to the gel formed in water-exposed cubes. A degradation of the amorphous gel present after acid attack is observed by XRD analysis, and with more detail by SEM-BSE (EDX). In XRD, for the three systems, it is observed that for the acid-exposed surface, the center of the main halo (which represent an amorphous gel) is displaced to lower values comparing to the inner regions (unattacked), and close to those of the anhydrous GP. This indicates that the initial gel that is formed in normal conditions has been modified. This was also confirmed by SEM-BSE (EDX) results. In every case, it has been found the presence of sulfur, indicating the presence of the sulfuric acid in the region. In the inner regions, no presence of sulfur is detected, corroborating that these regions have not been attacked yet. Else, the elemental analysis of the inner regions and those exposed to tap water are similar (**table 5.2**). In the case of 95GP, it was notified a loss of Al and Ca in the acid-exposed surface, suggesting a dealumination and decalcification of the gel. Conversely, the Na was increased in the gel. The final gel obtained could be sodium silicate gel. For 85GP and 70GP, it is also observed a loss of Al, Ca, and this time also of Na. For these systems, it is occurring therefore a dealumination, dealkalinization and decalcification of the gel at the same time. The final gel produced could in this case be a silicate gel. Furthermore, the zeolite formed in 70GP (**figure 5.15**), is not observed any more in the corroded region (acid-exposed surface), indicating that this zeolite is decomposed by the action of the acid.

In tap water, it is also observed a reduction of the strength after 28 days of exposure. This phenomena has also been found in other works, in which specimens exposed to moist conditions experimented a mass loss (Balaguer-Pascual et al. 2014; Cyr et al. 2012; Redden & Neithalath 2014). As observed in **figure 5.11**, there is not further reduction of the strength at later ages but a moderate increase. This could probably be due to the fact, as explained in former sections (**equation 5.1-5.3**), that Na+ of sodium silicate gel could be unstable in contact with water, contributing to its leaching. The increase of the alkalinity in the tap water due to leaching could disintegrate the sodium silicate gel at early ages, decreasing the mechanical properties (Redden & Neithalath 2014). After 28 days test, the tap water was renewed and the alkalinity of the tap water is expected to be lower, and no further disintegration of the gel would occur. On the contrary, in acidic conditions, the Na^+ ions leaching will balance the pH, and

therefore, the disintegration of the silica gel by the effect of the alkalinity will be more restricted, being just affected by the acid action. Although it was pointed out that the gel formed in 85GP and 70GP was more stable than that formed in 95GP, it is probable that this gel (with also a high Na leaching as observed in **chapter 5.3**) is still affected by the rise of pH due to Na leaching. Thus, during the first contact with tap water, the rise of the alkalinity will affect the gel of the outer layers, decreasing its compressive strength after 28 days. Then, as Na leaching is reduced with time and tap water is renewed (after each compressive strength test), the alkalinity of the tap water will not be as high to affect the inner regions of the cubes. Consequently, reactions will follow a normal scheme in order to improve the performance with time, as the observed increase of the compressive strength with time for both in 85GP and 70GP.

In all the systems, it has been observed the formation of gypsum in the acid-exposed surface, i.e. the colored region observed in the photos of **figure 5.12**. The gypsum was found in the XRD analysis and also in the SEM-BSE. In the latter technique, it was observed that gypsum deposited preferentially in the free space (e.g. air bubbles, pores, cracks) and therefore the effect of crystal growth pressure would not affect the system. This was observed by the cross-sectional dimension, in which samples, especially 85GP and 70GP, did not change significantly. The formation of gypsum is caused by the reaction of Ca ions, from the decalcification of the gel at low pH, with the sulfates of the acid. The extent of the gypsum formation will be therefore limited by the presence of Ca. Decalcification could occur in the C-S-H gel that would co-exist with N-(A)-S-H gel, although the exact formed gel is difficult to know. Then, it is well known that C-S-H gel (formed in OPC-based binders) decalcifies at low pH.

As seen in this test, the increase of the Mk content in the binder improves the acid resistance. Despite the binder is attacked by the sulfuric acid, the final gel is relatively stable, as shown by the maintenance of the mass and cross-sectional dimensions. The mechanical performance of the corroded gel is lower, however, it could be said that these systems will behave better than other binders in which the sulfuric acid destroys completely the sample (OPC and AAS).

5.5.7 Conclusions

In this test, 3 formulations of GP with Mk (varying the proportions) have been tested against acid sulfuric attack. The following conclusions can be made from the results obtained:

- When the GP content in the binder is 95% (with 5% of metakaolin), the gel is unstable in the presence of acid solutions, resulting in a softening of the surface, mass loss and increase of the cross-dimensional section.

- When metakaolin is increased to 15 and 30%, the resulting gel becomes more acid resistant in terms of dimensional stability and mass. Nevertheless, SEM-BSE and XRD showed that there is a modification of the gel composition. This new gel, however, is still stable in the presence of acid although its mechanical properties are lower.
- Compressive strength results showed that the systems with 15% and 30% of metakaolin performed well against the acid solutions. Even though a decrease of the strength at 28 days of exposure is observed, it seems that afterwards compressive strength is maintained at that level, or very slowly reduced during time. This loss of compressive strength is related to a disintegration of the gel during time.
- When cubes were exposed to water, there was a higher reduction in the compressive strength at 28 days than that observed in the cubes exposed to acid solutions. Nevertheless, compressive strength slightly increased at later ages.
- GP contributes to the formation of a sodium silicate gel, whereas the addition of Mk induces an aluminum richer gel, thus forming a sodium aluminosilicate gel. The resulting gel due to the acid attack becomes more stable when Mk content is increased, and gives a residual strength after the attack.
- Whatever the Mk content in the system is, gypsum crystals were formed attributed to the reaction of the Ca ions with the sulfates of the acid solution. The Ca ions are liberated from the different gels formed by a decalcification due to the acid attack.

5.6 Alkali-silica reaction (ASR)

ASR test was conducted by means of the accelerated test method in mortars, following the ASTM C1260 standard. It has to be pointed out that this test method has only been used as a comparative purpose as the three formulations studied are done with the same materials, glass powder and metakaolin. On the other hand, recommendations concluded in the **chapter 4.5.4** should be taken into account, as it has not been stablished yet how the high temperature used by this method (80ºC) and the NaOH solution (1M) can affect the microstructure of the system. Therefore, test conditions were the same as indicated in the standard (see **chapter 3.5.4**). Else, test was conducted until 28 days instead of the 14 days prescribed at the standard.

5.6.1 Adaptation of the formulations according to the standards

The formulations described at the **chapter 3.3.1** have been adapted to the prescriptions given in the ASTM C1260 standard. The new w/b ratio have been adjusted to 0.47, and the sand/binder ratio to 2.25. The other parameters, as activator concentration and admixture content, were the same.

Therefore, the new formulations for this test are shown in **table 5.3**.

Table 5.3 Mix proportions of AAGP mortars for the AAR test

		Mortar (g)		
		95GP	**85GP**	**70GP**
Binder	GP	388	347	286
	Mk	20	61	122
w/s		0.47	0.47	0.47
SH		253	253	253
% Ad *		0	0.5	0.5
Graded sand		1013	1013	1013

*%Ad: % of admixture, in dry powder: Lignosulfonate (EUCON WR P)

5.6.2 Length change

Figure 5.19 shows the expansion results of AAGP mortar bars exposed to 1M NaOH solution at 80ºC during 28 days. For this test, the Spratt, a reactive aggregate usually employed for AAR tests have been used, sieved according to the standard, as explained in **chapter 3.5.4**.

As it can be observed in the figure, the 95GP mortar bars with the reactive aggregate (9GP in the figure), experimented a huge expansion after 7 days, exceeding the limit compliance of 0.1% at 14 days. Then the expansion increased linearly during time up to 1% at 28 days. According to the standard, results are in the region of "potential deleterious expansion".

When Mk content was of 15% (85GP), it was observed that the experimented expansion at 28 days is 3 times lower than in the bars done with 5% of MK (95GP), exceeding the limit compliance around 6 days. At 14 days, the bars felt in the region close to "potential deleterious expansion", which means that more tests should be done to confirm the reactivity of this binder with the aggregate. The expansion rate seems to appease during.

Finally, when Mk content was of 30% (70GP), it was observed that the expansion was still lower (around the half) than in 85GP bars at 28 days, exceeding the limit compliance at 12 days. Therefore, the expansion fell in the limit between the regions of "no reactive" and "more tests are needed". Even

at 28 days, the expansion values are still in the region of "more tests are needed", which means that further testing (as ASR in concretes) should be done to confirm if this system is reactive with the aggregates or not.

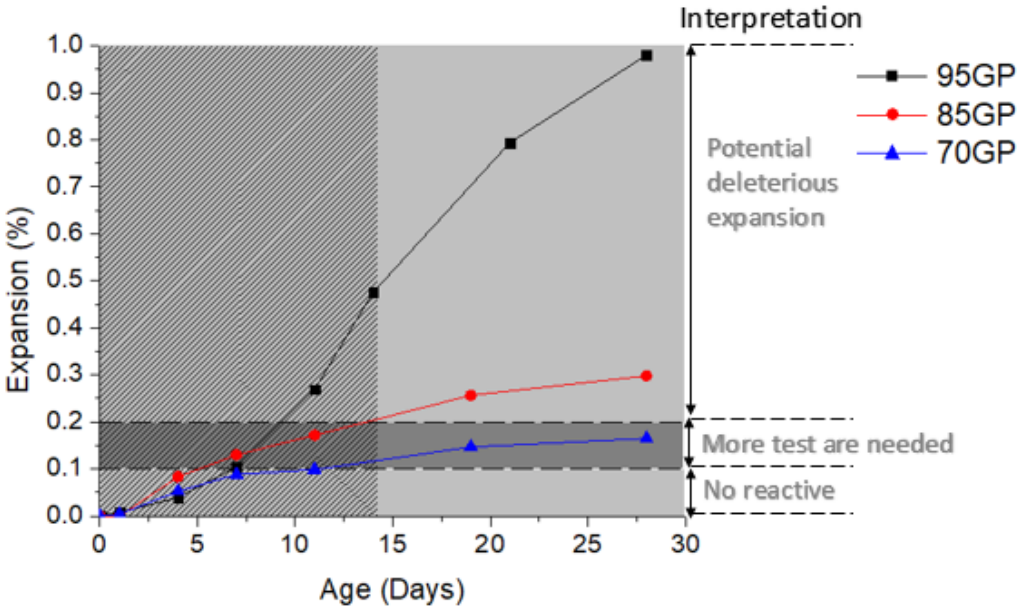

Figure 5.19 Expansion results for the AAGP systems with Spratt aggregate

The replacement of GP by Mk in the binder decreased the expansion due to ASR. Therefore, it seems that the gel formed when Mk is increased is better preventing the ASR.

5.6.3 Mass change

Figure 5.20 shows the mass change of the same AAGP mortar bars of the **figure 5.19**. It can be seen that practically all the systems experimented a mass loss during time. The results shown thus an expansion not accompanied by an increase of the mass.

5.6.4 Mineralogical characterization by means of X-ray diffraction

XRD experiments were performed on 85GP and 70GP samples after 28 days immersed in 1M NaOH solution at 80ºC, to characterize any change on the crystalline compounds of the systems. Results are shown in f**igure 5.21**. In the figure, any difference between the content of Mk (15 or 30%) can be observed. In the spectrum a serial of crystalline peaks attributed to the reactive aggregate (see **chapter 3.2.3**) and not to a new reaction product were observed. Thus, the peaks observed are mainly calcite, with traces of kaolinite, vaterite, ankerite and quartz.

In every spectra, a halo is observed around 25 and 35 degrees 2θ, corresponding to an amorphous gel. Furthermore, in the case of 70GP, it is remarkable to note that the type A zeolite normally found by XRD in normal curing conditions (see **chapter 5.4.2** and **chapter 5.5.4**) was not observed. This would confirm that the normal geopolymerization process of the systems is not the same when a temperature of 80ºC is maintained during long time.

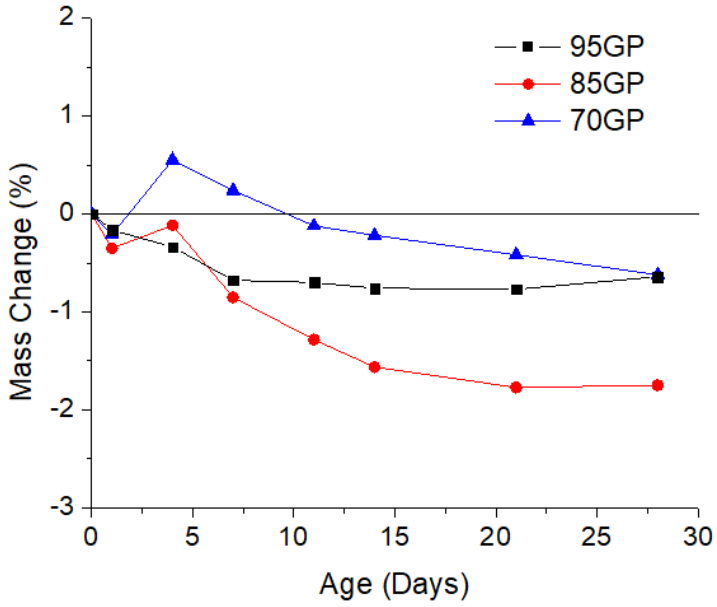

Figure 5.20 Mass change for the AAGP systems with Spratt aggregate

5.6.5 Microstructural analysis by means of SEM-BSE

Microstructural characterization was performed for all the systems by means of SEM-BSE (EDX) on the same samples after 28 days of exposure to 1M NaOH at 80ºC.

In **figure 5.22** exhibits 6 SEM micrographs of the 95GP mortar bars. As a reminder, the bars of this series experimented the highest expansion (close to 1% at 28 days). In image A, it can be seen a heterogeneous paste located in a region far from the aggregates. It seems like different gels have been formed, together with anhydrous GP and Mk particles. Hence, it can be observed a light grey gel, with small fissures, mostly located in the top center of the image. However, this texture is found in little traces all around the image. The other gel, darker in color, forms the rest of the paste. In the case of the light grey gel, the EDX spectrum showed that it is composed of Na, Ca and Si, and of a lower content of Al. The atomic percentage (excluding water, C, O and minor elements) of an average of 10 points of this gel showed a composition of 11.0% of Na, 61.0% of Si, 26.1% of Ca and 1.9% of Al (see 95GP A1, **table 5.4**). Similarly, the darker gel was composed of the same elements, with minor differences

on the atomic percentages: 14.1% of Na, 58.7% of Si, 24.1% of Ca and 3.1% of Al (see 95GP A2, **table 5.4**). In this case, Na and Al have increased at the expense of Si and Ca.

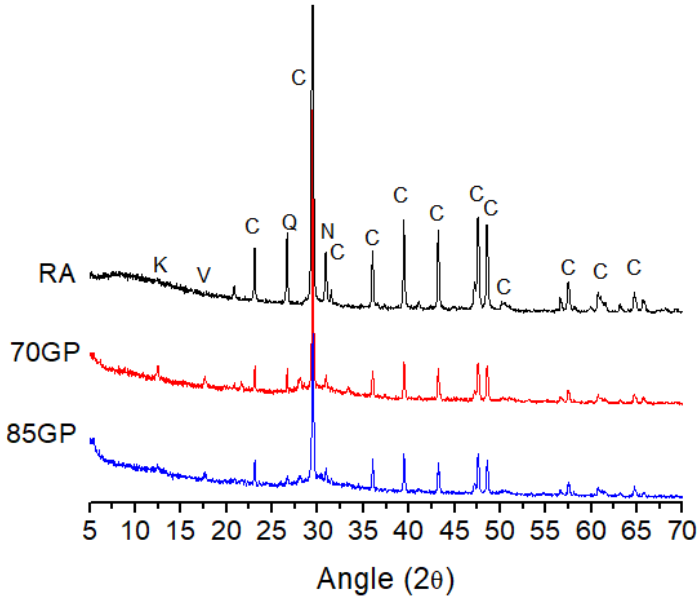

Figure 5.21 X-ray patterns of 85GP and 70GP specimens with Spratt aggregate after 28 days of exposition to 1M NaOH solution at 80ºC. Q, quartz; C, calcite; V, vaterite; K, kaolinite; N, Ankerite.

In image B of **figure 5.22**, it can be observed that the aggregates have been attacked, showing fissures and completely destroyed parts. Between the fissures, it is observed a gel filling this space. The EDX analysis showed that this gel contains Na, Si, Ca and Al, within an atomic percentage of 11.1%, 42.8%, 42.7% and 3.4% respectively (see 95GP B, **table 5.4**). In this case, the gel is very different to that found in the paste, increasing its Ca content at the same extent than Si (Ca/Si = 1). However, Na and Al contents are similar to those found in the paste. In this image, it can be observed huge cracks that are not filled by a gel. This cracks correlate well with those found in the SEM analysis of the acid and sulfate resistance test.

Moreover, it has been observed another product, normally found in air voids (image C of **figure 5.22**). In this case, the morphology of this product could be appreciated because it is located inside an air void, thus it was not affected by the sample polish process. As it can be seen, this product has rosette-type morphology. The EDX analysis showed that this product contains Na, Si, Ca, Al and K, similar to the other gels. However, the atomic percentages are very different in this case. Hence, the atomic percentage was: 12.9% of Na, 57.3% of Si, 13.4% of Ca and 14.3% of Al (see 95GP C, **table 5.4**). A new element was also found, K, with 2.0%. The differences between this new product and the other

types of gels observed in this sample were: 1) the Ca content is much lower than the other gels; 2) the Al content has increased to the same order than the Na; 3) a new element is present (K), with a non-negligible concentration.

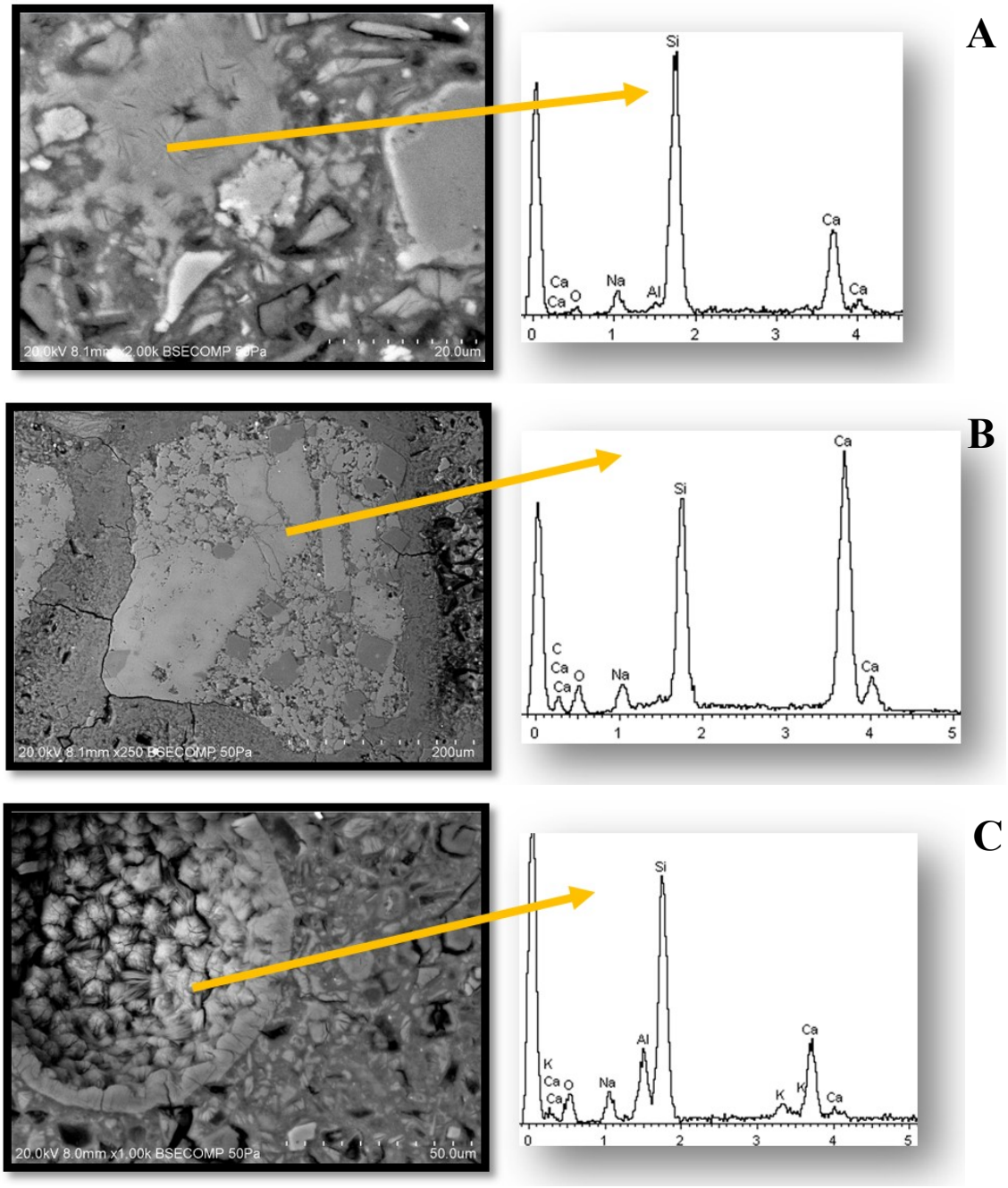

Figure 5.22 SEM (BSE) images and EDX analysis of 95GP specimens after 28 days of exposition to 1M NaOH solution at 80ºC. a) Fissured gel; b) Reactive aggregate with internal fissures filled with a gel; c) Rosette-like product in air voids.

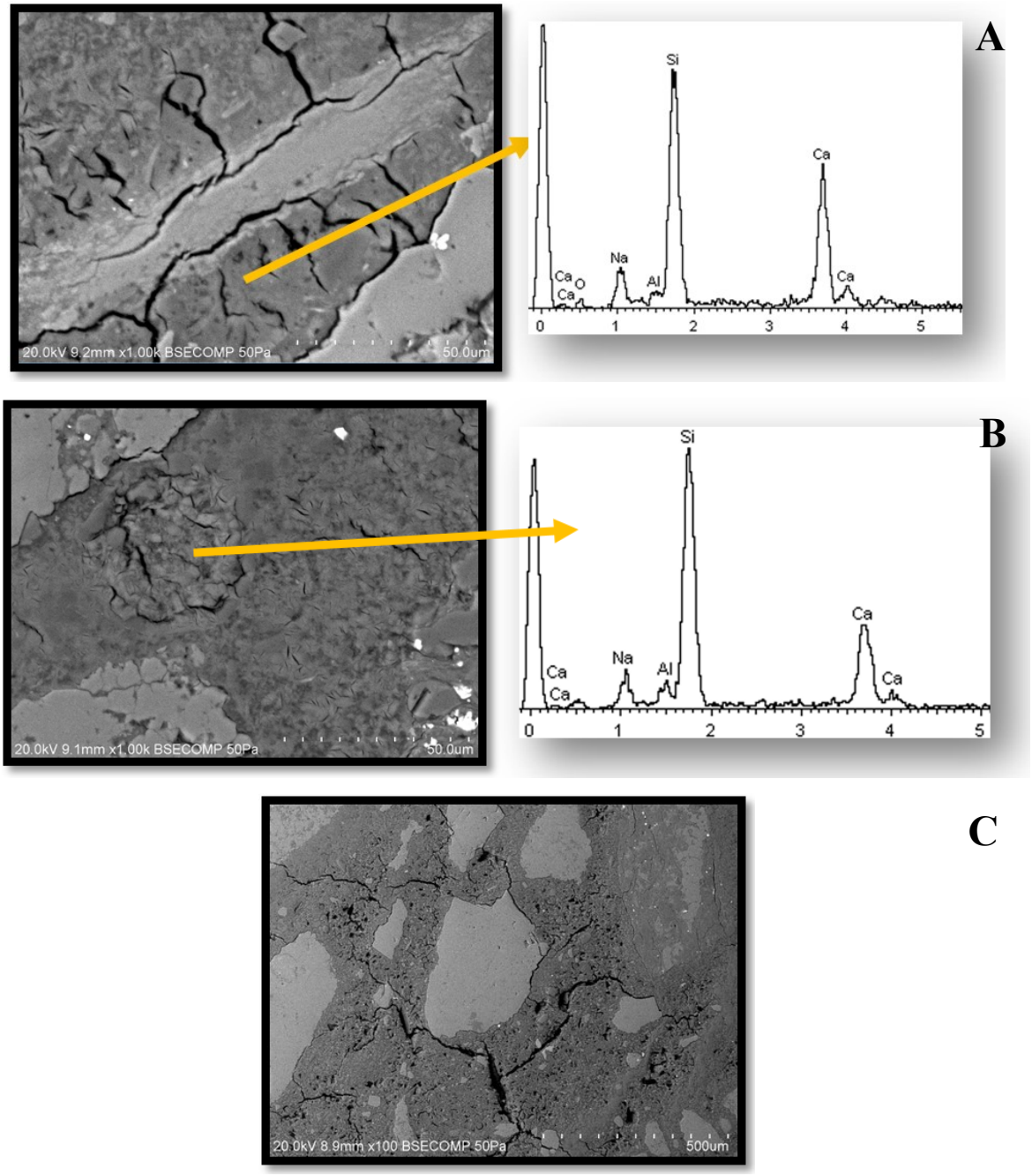

Figure 5.23 SEM (BSE) images and EDX analysis of 85GP specimens after 28 days of exposition to 1M NaOH solution at 80ºC. a) Cracked calcareous aggregate; b) Air-void filled with a gel; c) Attacked reactive aggregate at the top right

In **figure 5.23**, some SEM-BSE images for the 85GP mortar bars are presented. This series got much lower expansion that 95GP with the reactive aggregate (0.3% at 28 days). In the image A, it can be observed a small cracked calcareous aggregate, located in a region close to a reactive aggregate. The gel surrounding this aggregate also shows microcracking. The atomic percentage of this gel (average

of several points) was of 16.9% of Na, 55.2% of Si, 25.5% of Ca and 2.5% of Al (see 85GP A, **table 5.4**). This gel is rich in Ca, and its composition is similar to that found in 95GP with higher amount of Na. In the image B, it can be seen another region close to a reactive aggregate. On it, there is a region that seems an air-void filled with a new gel. This gel, which presents a lot of fissures, has the same composition that the surrounding gel, thus, no differences can be found between them. The EDX analysis showed that this gel contains 13.5% of Ca, 61.4% of Si, 20.5% of Ca and 3.2% of Al (see 85GP B, **table 5.4**). As it can be seen, this gel is very similar to that found in image A, but with smaller amount of Ca and Na. Finally in the image C, it can be seen a reactive aggregate that has been attacked (top right).

Table 5.4 Summary of the atomic percentages of the EDX analysis of the AAGP systems

		Atomic percentage						Atomic ratios		
		Na	Si	Ca	Al	K	Mg	Ca/Si	Na/Si	Al/Si
95GP	A 1	11.0	61.0	26.1	1.9	--	--	0.43	0.18	0.03
	A 2	14.1	58.7	24.1	3.1	--	--	0.41	0.24	0.05
	B	11.1	42.8	42.7	3.4	--	--	1.00	0.26	0.08
	C	12.9	57.3	13.4	14.3	2.0	--	0.23	0.22	0.25
85GP	A	16.9	55.2	25.5	2.5	--	--	0.46	0.31	0.05
	B	13.5	61.4	20.5	3.2	--	--	0.33	0.22	0.05
70GP	A	16.6	59.4	13.2	10.8	--	--	0.22	0.28	0.18
	B 1	19.9	63.7	10.5	1.6	--	4.6	0.16	0.31	0.03
	B 2	17.9	63.0	9.3	9.7	--	--	0.15	0.28	0.15

* All the atomic ratios are an average of 10 points

The **figure 5.24** shows SEM-BSE images for the 70GP mortar. This series got the lowest expansion, close to pass the test specifications (0.11 at 14 days). In the image A, we observed again a heterogeneous microstructure, with gels of different color intensities and anhydrous particles. As in the other cases, it was not possible to distinguish the gels by chemical composition. The average of the atomic percentage of the gels was: 16.6% Na, 59.4% Si, 13.2% Ca and 10.8% Al (see 70GP A, **table 5.4**). Compared to the gels of the other systems, it is observed that the Al content has increased. This could be attributed to the higher content of Mk in the mix, hence higher content of Al is present. In image B, it can be observed a gel inside of a crack, with different texture than the surroundings. In this case, the gel had different chemical composition than the rest, with 19.9% Na, 63.7% Si, 10.5% Ca, 1.6% Al and 4.6% Mg (see 70GP B1, **table 5.4**). In this gel, Mg is newly observed and it has an important content of Na. On the contrary, the Al content has decreased. On the other hand, the gel of the surroundings is free of

Mg, with a chemical composition of 17.9% Na, 63.0% Si, 9.3% Ca and 9.7% Al (see 70GP B2, **table 5.4**). The main changes in both gels are therefore the absence of Mg and an increment of Al content, while the other elements seem to be similar. Moreover, this gel is not so different to that found in image A. In the image C, with higher magnification, it can be appreciated the formation of a gel in small air-voids.

5.6.6 Discussion

In this section, ASR of AAGP systems with two types of aggregates were performed by means of the accelerated test method described at the ASTM C1260 standard.

The results have shown that the system with 95% of GP and 5% of Mk got a huge expansion when the mortar bars were manufactured with the reactive aggregate Spratt, exceeding the limit compliance of the standard after 9 days (0.1% at 14 days). The expansion rate continued to rise until the end of the test (28 days) with a total expansion of 1.0%. This expansion was higher of that experimented by the OPC system at the same age (0.65%, see **chapter 4.5.2.1**). However, OPC system failed the test before, at 4 days. This huge expansion leads to think that an expansive ASR gel has been produced. When the Mk content was increased to 15%, hence reducing the quantity of GP, the expansion decreased 3-fold. In the same tendency, by increasing the Mk up to 30%, the expansion decreased even more (5 times lower). This suggests that the Mk content has an important effect reducing the expansiveness of the gels formed. This aspect will be discussed later in this section.

Mass change has also given important information about the stability of the binder at the test conditions. The results showed a mass loss during the test in all the cases. When the alkali-silica reaction (ASR) takes place, a new alkali-silicate gel is produced in the matrix (Glasser 1992). This gel involves a water absorption, thus generating an increase of the mass and volume. The gel finally tends to swell and generate internal stresses that may result in a cracking. Regarding the results obtained, it can be seen that the expansion is not accompanied by an augmentation of the mass but a reduction. Thus, it is believed that a Na^+ leaching process is produced as well, responsible for the mass loss. As showed in previous sections, the studied AAGP systems have an important leaching of Na^+ ions. The leaching of Na^+ can take place not only by gradient concentration between pore solution and the external media, but also by hydrolysis of the gels at elevated pH, like the conditions of this test. As explained in **chapter 5.2.3**, the sodium silicate gel produced (with low Al content) can be partially disintegrated by a lack of hydrolytic stability of these gels. Thus, not only Na will be leached out but also silicates, contributing to the mass loss. Moreover, this hydrolysis process could have been accelerated by the high temperature used in this test (80ºC). Not only aggregates will be affected by the elevated pH but also the gel. To

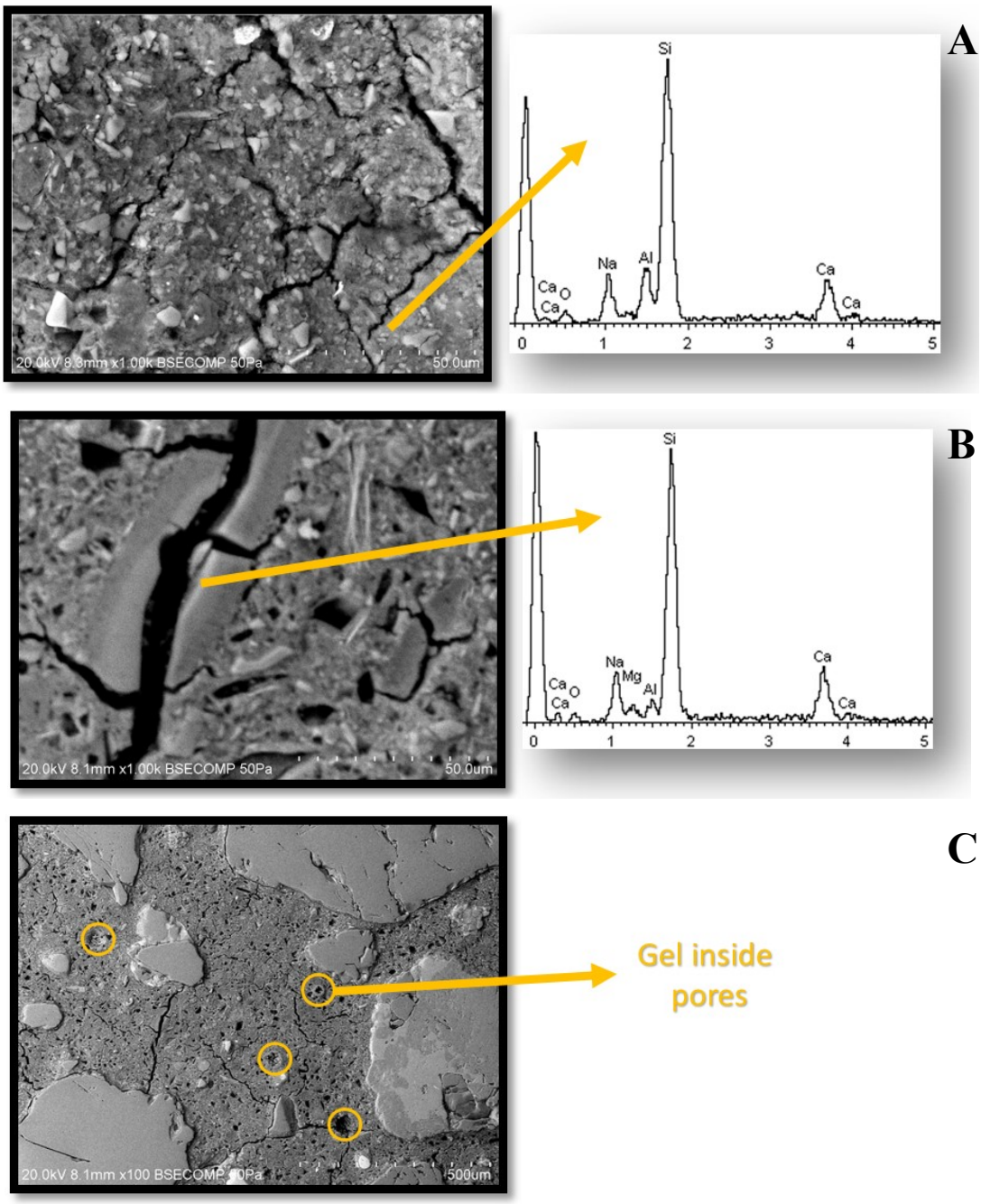

Figure 5.24 SEM (BSE) images and EDX analysis of 70GP specimens after 28 days of exposition to 1M NaOH solution at 80ºC. a) Paste; b) Gel inside a crack; c) Gel in small air-voids

sum it up, if a new gel is produced due to the ASR, there will be two opposite effects: an increase of the mass due to the new gel formed, and a decrease due to leaching. Final mass change will depend on which of the two factors has more influence. In all systems, it seems that leaching factor was imposed to the water uptake by the new ASR gel.

In order to better understand the products that are formed during the test, XRD and SEM-BSE (EDX) were performed. XRD analysis performed on the samples with 15% and 30% of Mk showed that an amorphous gel was formed. However, no differences between the amorphous gels found in the other tests were noted (as in tap water). An important aspect to point was the fact that for the systems with 30% of Mk (70GP), the peaks observed in tap water corresponding to the formation of type A zeolite were not present. This was an indication that the natural products normally found in real conditions for this system were not produced at the test conditions.

Regarding the chemical composition of the formed gels (showed in **table 5.4**), similar behaviors were found in every system. First, it is important to compare the chemical composition of the massive gels obtained during ASR test (i.e. those far from aggregates, voids or cracks) with that obtained in the previous tests (sulfate resistance (**table 5.1**), acid resistance and tap water (**table 5.2**)). Thus, it can be appreciated an increment of the Ca and Na content in the gel, while the Al content is quite similar. These differences on the chemical composition demonstrate that the gels normally formed in normal conditions are not produced in the same way as in the ASR test conditions. The higher amounts of Ca in the gels when the reactive aggregate Spratt was used, confirms also that aggregates have been attacked, dissolving not only the amorphous Si but also Ca ions. This Ca ions will subsequently diffuse to the matrix. It has been observed that the Ca content decreases in regions further from the aggregates. Thus, the higher Ca content was found in the gel inside a reactive aggregate (42.7%, see 95GP B in **table 5.4**), and then the gel surrounding the aggregates (25%, see 95GP A1-2 in **table 5.4**). Furthermore, the gel formed in the air-voids, in any system, was found to have the lowest Ca content (around 10%).

In the system with 95% of glass powder, it has been observed a new product that has precipitated in the air-voids with a singular morphology. This product shows a rosette-type morphology, as it can be clearly observed in the image of **figure 5.22 C**. The chemical composition of this product was: Si, Na, Ca, Al and K. Rosette-type morphology has already been observed to happen in air-voids during ASR test for OPC systems (Davies & Oberholster 1988). In the case of AAM, it has been observed a pseudo rosette-type in AAFA (García-Lodeiro, A. Palomo, et al. 2007) and also in AAS (Z. Shi et al. 2015; Fernández-Jiménez & Puertas 2002). As mentioned before, this product occurs normally in air-voids, so its contribution to the expansion will only play an important role when all the air-voids are filled. Therefore, the expansion may be mainly due to the massive gel.

Another important fact to mention is the gel found in the 70GP system. The SEM-BSE analysis revealed a smooth gel formed into a crack. The EDX showed that this gel, contrary to what it was observed in the other gels, had an important content of Mg (see 70GP B1 in **table 5.4**). Although Mg is already in the raw materials (GP), it is also present in the reactive aggregate, as shown by XRD (ankerite –

dolomite). Mg has been already found in a gel in the interface of the glass aggregates with a metakaolin geopolymer paste (Pouhet & Cyr 2015). However, the authors doubt if this compound was an ASR gel, or a product due to the reaction of the external glass layer with the surrounding environment rich in hydroxide and alkalis. In our case, this gel was found in a crack connecting two aggregates. The fissure observed in this gel could have been produced at the end of the test, when the specimen was prepared for analysis.

Even though during ASR test new gels are produced, the composition showed that they are not exactly the same than those found in OPC systems, with typical compositions around Ca/Si = 0.2 and Na/Si = 0.77. Thus, the gels observed have much less concentration of Na while the Ca content is similar.

The question arises why there are so much difference in the expansion when Mk was increased from 5% to 30%. This may be attributed to two facts: the presence of Ca and Al in the gels. In the case of Ca, there is still some controversy about its role in the formation of an expansive ASR. It is generally affirmed that without Ca the gels formed are less expansive (Rajabipour et al. 2015). According to these authors, Ca could act in two ways. First, as alkali recycling by means of an exchange process of alkalis by Ca in the gel. The substitution of alkalis by Ca will release new alkalis to the pore solution that would be able to react with the silica to form new expansive gel. This way of Ca interaction will have a minor effect in this test due to the 1M NaOH solution in which specimens are immersed, which will constantly supply alkalis. Second, the Ca will affect the properties of the gel and consequently its expansion. Therefore, from the results obtained in this work, the following statement can be made: higher is the Mk content (hence less Ca in the system), the lower the expansion of the prism will be.

However, not only the Ca content would have a direct influence on the expansion, as the differences in the Ca content are not enough to describe such a reduction in the expansion. Thus, another factor could be participating, as the Al content. The presence of Al has shown to play an important role on the aggressiveness of the test when OPC-based binders are tested. Although it seems that Al is beneficial to mitigate the effect of the ASR in OPC based binders, it is still a subject to study the exact role of this element (Rajabipour et al. 2015). Thus, it is thought that Al may act in two ways as well. First, it may reduce the dissolution of the amorphous silica of the aggregates (Chappex & Scrivener 2012; Leemann et al. 2015). Chappex & Scrivener (2012) concluded that the Al in pore solution is absorbed on the silica surface of the aggregates thus limiting its dissolution. A second possibility of the Al action is the reduction of the pH pore solution. This would be consequence of the substitution of Si by Al in the gel that would induce a higher binding alkalis capacity due to charge balancing phenomena. Thus, higher Al content will provide higher alkalis binding, and less alkalis will be in pore solution to form the expansive gels. Whichever of these possible effects of Al mitigating the ASR is predominant in our

systems, it is clear that when the Mk content is increased, higher incorporation of Al exists in the massive gel (see **table 5.4**).

To sum it up, this study shows that the replacement of GP by Mk up to 30% is beneficial for the performance of the binder, as it was found in the previous sections (water stability, acid resistance).

5.6.7 Conclusions

The followings conclusions can be made from the results obtained:

- As the Mk content increases from 5 to 30%, the expansion is decreased 5-fold.
- It was found a mass loss during test, higher when lower was the Mk content. This is attributed to a leaching of ions from the paste.
- XRD analysis showed that the type A zeoliteproduced during the geopolymerization process of the system with 30% of Mk was not formed at the test conditions, confirming that the products formed are therefore not the same.
- SEM-BSE (EDX) analysis revealed the apparition of different gels in all the systems. This gels were different to those found in normal curing conditions. Ca and Na were found to be higher in the ASR test.
- In the system with 95% of glass powder a new product formed in the air-voids has been observed. This product was found to have a rosette-type morphology.
- In the case of 70GP system, another type of gel was observed with Mg. The presence of Mg would be consequence of the decomposition of the ankerite present in this aggregate.

CHAPTER 6. General conclusions and Future research lines

6.1 General conclusion

The conclusions exposed in each section of the former chapters are summarized in this chapter, as well as the main contributions of this project.

6.1.1 Conclusions/recommendations of existing durability test methods for AAMs

In **chapter 4,** it has been shown the applicability of several durability test on AAMs, by using BFS and FA as a precursors. The durability tests analyzed have been the followings: dimensional stability in water, sodium sulfate resistance, acid sulfuric resistance, alkali-aggregate reaction, freeze-thaw reaction, permeability (by RCPT and Surface resistivity tests methods), and sodium leaching test. Some of these tests are standardized and others have been based on literature procedures. According to the findings exposed in **chapter 4**, the main conclusions are summarized next:

- ✓ In **chapter 4.2,** it is shown that the different systems studied (OPC, AAS and AAFA) need different curing conditions in order to have similar water stability, in terms of dimensional changes. Thus, AAFA have shown to be more stable when a thermal curing of 80ºC is applied during the first 24h, and OPC and AAS when they were cured at lower temperatures (35ºC).
- ✓ In **chapter 4.3,** it is shown that following the curing procedure described in the ASTM C1012 standard for sulfate resistance test there is an improvement of the OPC performance. This procedure requires to heat the samples at 35ºC during first 24h, to achieve a minimum compressive strength of 20MPa at 1 day in order to start the sulfate exposition. Contrary, for AAS a negative influence is observed, decreasing the performance when this curing procedure is used. In this system, the best performance is observed when the samples were cured at normal temperature (23ºC). Therefore, it is recommended by the results obtained that the curing temperature regime should not be imposed by the standard but by the nature of the precursor.
- ✓ In **chapter 4.4**, it is shown the applicability of the main measure parameters used to predict the degree of the acid attack in AAMs, as exposed in the ASTM C267 standard. These parameters are mass and cross-sectional change and compressive strength. From the results, it can be concluded that mass and cross-sectional change can reproduce the degree of attack for OPC and AAS, but no for AAFA. Contrary, the compressive strength is a good indicator for AAFA, but not for OPC and AAS due to its several dimensional changes. In the three systems, it is

recommended to do microstructural characterization (such as SEM). Other important aspect is that the different curing regimes evaluated (7 and 28 days in humidity chamber prior to start the test) had no influence on the results, probably due to the severity of the acid sulfuric.

- ✓ In **chapter 4.5**, two test methods usually used for ASR have been compared, the accelerated mortar-bar test method (ASTM C1260) and the concrete prism test method (ASTM C1293). The results showed that both methods are in good agreement. Nevertheless, the accelerated test method in mortar is not recommended because of the extra supply of alkalis and the high temperature that could improve in some manner the hardening reactions in AAMs. Concrete prims test method seems adequate.
- ✓ In **chapter 4.6**, the applicability of the freeze-thaw resistance test by means of the ASTM C666 in AAMs has been studied. The main parameter studied in this test was the curing time prior to start the frost cycles. According the results, it has been found a negative influence of a longer curing of the concrete bars prior to start the freeze-thaw cycles for OPC and AAS. Hence, this test has been found to be applicable as described at the standard for AAS.
- ✓ In **chapter 4.7**, two accelerated test methods based on electrical indicators of the permeability have been compared, the rapid chloride permeability test (RCPT) and the bulk resistivity test (BR). According to the findings in this point, it has been proved that the RCPT test overestimate the results in AAS (at low ages). Contrary, BR test is better predicting its permeability. This is attributed to the high alkali content of the pore solution in AAMs that have a negative influence on the RCPT, and a minor effect on the BR test. Moreover, it has been found no correlation between RCPT classification from ASTM C1202 standard and the BR classification (from literature). However, it is important to note the effect of the BR classification used to define the different permeability degrees. In that sense, it is concluded that more research should be done to well classify the different permeability degrees based on BR test method for AAMs.

6.1.2 Conclusions of AAS and AAFA durability properties

In this part, the main conclusions about the durability properties of the AAS and AAFA, showed in **chapter 4**, are summarized.

- ✓ In **chapter 4.1**, it has been shown the effect of heating the mortar cubes during the first 24h at 35ºC and 80ºC on the compressive strength development to. As shown by the results, heating only the AAFA has been found beneficial in terms of compressive strength development. In this system, is demonstrated the importance of the thermal activation on the development of its mechanical properties, on the contrary would be very slow. This is attribute to a faster

dissolution of the ionic species of the FA that will react to form the hardened products. In the case of AAS, it has been shown that the thermal curing is negative for the compressive strength development at later ages, as it happened with OPC. In both cases, this is attributed to the formation of a heterogeneous paste due to the acceleration of the hydration reactions.

- ✓ In **chapter 4.2**, it has been shown that the best curing regime for AAFA dimensional stability. In water, it is to heat at 80ºC during first 24h. Contrary for AAS, alower temperature curing (lower than 35ºC) is preferred.
- ✓ AAS have shown to resist very well to sodium sulfate solutions (**chapter 4.3**), regardless its sulfate concentration. The results showed that the expansion remained practically constant during all the test (1 year), and it was quite below the limit compliance of 0.1%. The same behavior was found for AAFA, with no interaction with the presence of sodium sulfate. Instead, this system showed a shrinkage during time. In both cases, the microstructural characterization, by means of XRD and SEM, did not showed any presence of new compounds due to the interaction of sulfates with the hydration products of the binders.
- ✓ AAS and AAFA showed different degradation mechanism due to sulfuric acid attack (**chapter 4.4**). These differences are due to the different nature of the hydration products: mainly C-A-S-H for AAS and N-A-S-H for AAFA. In the case of AAS, the presence of sulfuric acid showed to be detrimental, as the mortar samples tended to completely destroy. AAS mortar samples experimented an expansion during time due to the formation of expansive products during the attack. XRD and SEM showed the formation of a new product, gypsum, responsible of this expansion. For AAFA, the samples kept its dimensions during all the test, but compressive strength is reduced during time until a residual value. SEM results showed a conversion of the hydration products (dealkalinization and dealumination) due to the presence of the sulfuric acid, responsible of the reduction of the compressive strength. The residual compressive strength observed in this system is the point where all sample has been completely corroded by the acid.
- ✓ The high alkali content of AAS (5%) and AAFA (7%) showed to be not a problem in terms of ASR comparing with OPC (1.5%) (**chapter 4.5**). In both test methods (accelerated test in mortar and concrete prism test), AAS showed an expansion during time, however, below limit compliances. AAFA showed negligible expansion in the accelerated mortar test, and a shrinkage in the concrete test. In both systems, several phenomena could occur simultaneously: alkali consumption for ASR, alkali consumption for normal hardening reactions and an intrinsic shrinkage of the system. Final expansion will be the result of which of these factors is higher.

- ✓ The introduction of an AEA in AAS showed to be not as effective as in OPC for its frost resistance (**chapter 4.6**). The addition of air voids in AAS showed to improve its performance against freeze-thaw cycles. Howeverwithout extra air voids, the AAS concretes performed very well, complying with the limits compliances of the standard ASTM C666. This behavior is advantageous comparing with OPC concretes, where without the extra air voids the concretes bars were quickly destroyed. In the case of AAFA, it was found that the AEA used (based on hydrocarbons) was not effective at any dosage. AAFA concretes were very fast destroyed.
- ✓ AAS showed to have a very low permeability (**chapter 4.7**) regardless the test method used (RCPT and BR test). It has been found better relationship between compressive strength and BR test than with RCPT for AAS. For OPC, both test methods correlates well with compressive strength.
- ✓ Sodium is found to leach from AAS and AAFA mortar bars when they were exposed to distilled water. This leaching is attributed to the free alkalis in the pore solution. It is important to note that although both systems have different alkali content, the degree of sodium leached is practically the same. In the case of AAS, it was found that longer the mortar bars were put in distilled water, lower was the alkali leached. Contrary in AAFA, no influence was found in this aspect. This corroborates with the fact that while in AAS the alkalis continue to react and fix at longer time, in AAFA once the thermal curing is finished (80ºC during first 24h) the reaction of alkalis with the binder is very slow.

6.1.3 Conclusions of AAGP durability properties

This project analyzed for the first time the durability of a novel system based on glass powder/metakaolin mix by means of alkali-activation technology. Different composition of this binder have been studied, varying the content of glass powder and metakaolin in it. A summary of the conclusions obtained in the **chapter 5** is presented next:

- ✓ The system AAGP is able to reach up to 25 MPa after 90 days. The best compressive strength is obtained when metakaolin content is lower (5%). As metakaolin content is increased (up to 30wt%), compressive strength decrease.
- ✓ When metakaolin increases, the formed gel moves from a low-sodium silicate gel to a sodium aluminosilicate gel (**chapter 5.3 and 5.4**). Else, secondary products are obtained such as type A zeolites at higher dosages of metakaolin.

- ✓ When metakaolin content increases, the dimensional stability of the mortar bars is increased too. Thus, to add metakaolin to the glass powder will improve the dimensional stability of this systems when exposed to aqueous solutions.
- ✓ Metakaolin introduction helps to reduce the alkali leaching when exposed to distilled water (**chapter 5.2**), due to a higher incorporation of alkalis into the structure. The incorporation of alkalis is favored by the increase of aluminum in the gel replacing the silica. This aluminum incorporation fix alkalis in the structure in order to balance the charge.
- ✓ The alkali-activated glass powder/metakaolin system has high resistance to sodium sulfate regardless the metakaolin content. No changes on the microstructure have been observed by XRD and SEM characterization after 1 year of sodium sulfate exposition. By means of SEM-BSE (EDX) analysis the gel formed is proposed to be a mix of C-S-H gel with low Ca/Si ratio and a sodium silicate gel (N-S-H). The incorporation of metakaolin to the system moves the gel towards a sodium aluminosilicate gel (N-A-S-H).
- ✓ The incorporation of metakaolin helps to improve considerably the sulfuric acid resistance. Mineralogical and microstructural characterization (XRD and SEM) showed that the sodium aluminosilicate gel formed when metakaolin is the highest (30%) is more stable than the sodium silicate gel formed when metakaolin is the lowest (5%). Although the higher stability of the gel when metakaolin content is 30%, there is a conversion of the gel in the presence of the sulfuric acid to a silicate gel, i.e. dealumination and dealkalinization. This corrosion of the gel is responsible of a loss a compressive strength during the exposure to the acid sulfuric. As it happened with AAFA, there is a residual compressive strength when all the sample was corroded.
- ✓ The incorporation of metakaolin reduces 5-fold the expansion due to ASR, despite its high alkali content (16.8% Na_2O when 30% of metakaolin). Therefore, as shown in **chapter 4.5** for AAS and AAFA, elevated contents of alkalis in alkali-activated binders are not necessary to be negative for ASR.

6.2 General conclusion

In this work, two studies have been carried out. In the first study, the applicability of the durability test methods to AAMs have been conducted. This study has put in evidence the weaker points in each of the durability test studied, and hence recommendations for future standards are stated.

In the second part of the study, the durability of the alkali-activated glass powder/metakaolin has been analyzed for the first time. Alkali-activated glass powder have shown to require a minimum content of

aluminum in order to get a more stable gel. Aluminum was incorporated by the substitution of the glass powder by metakaolin. Thus, aluminum favors the formation of a sodium aluminosilicate gel instead of a sodium silicate gel.

6.3 Future research lines

From this research project, it is suggested the following research lines, as it is thought they are of special importance on the understanding of the applicability of the existing durability test methods to AAMs, as well as the improvement of the knowledge of glass powder as a construction material by means of alkali-activated technology. Thus, several research lines are proposed:

- ✓ Study of new curing procedures based on alkaline mediums for mechanical and durability tests.
- ✓ Study of new alkali-activated systems based on glass powder with other materials such as blast furnace slag, fly ash, and others.
- ✓ Study of the mechanical behavior in concretes of alkali-activated glass powder/metakaolin, as well as its durability.

References

Al-Dulaijan, S.U. et al., 1990. 29Si Magic-Angle-Spinning Nuclear Magnetic Resonance Study of Hydrated Cement Paste and Mortar. *Journal of the American Ceramic Society*, 73(3), pp.736–739.

Al-Otaibi, S., 2008. Durability of concrete incorporating GGBS activated by water-glass. *Construction and Building Materials*, 22(10), pp.2059–2067.

Ali, M.B., Saidur, R. & Hossain, M.S., 2011. A review on emission analysis in cement industries. *Renewable and Sustainable Energy Reviews*, 15(5), pp.2252–2261.

Allahverdi, A. & Skvara, F., 2000. Acidic corrosion of hydrated cement based materials. Part 1: Mechanism of the phenomenon. *Ceramics-Silikáty*, 44(4), pp.152–160.

Allahverdi, A. & Skvára, F., 2005. Sulfuric acid attack on hardened paste of geopolymer cements Part1. Mechanism of corrosion at relatively high concentrations. *Ceramics - Silikáty*, 49(4), pp.225–229.

Allahverdi, A. & Škvára, F., 2001a. Nitric acid attack on hardened paste of geopolymeric cements. Part 1. *Ceramics - Silikáty*, 45(3), pp.81–88.

Allahverdi, A. & Škvára, F., 2001b. Nitric acid attack on hardened paste of geopolymeric cements. Part 2. *Ceramics - Silikáty*, 45(4), pp.143–149.

Allahverdi, A. & Škvára, F., 2005a. Sulfuric acid attack on hardened paste of geopolymer cements. Part 1. Mechanism of corrosion at realtively high concentrations. *Ceramics - Silikáty*, 49(4), pp.225–229.

Allahverdi, A. & Škvára, F., 2005b. Sulfuric acid attack on hardened paste of geopolymer cements. Part 2. Corrosion mechanism at mild and realtively low concentrations. *Ceramics - Silikáty*, 50(1), pp.1–4.

Attiogbe, E.K. & Rizkalla, S.H., 1988. Response of concrete to sulfuric acid attack. *ACI Materials Journal*, 85(6), pp.481–488.

Aydın, S. & Baradan, B., 2012. Mechanical and microstructural properties of heat cured alkali-activated slag mortars. *Materials & Design*, 35, pp.374–383.

Bakharev, T., 2005a. Durability of geopolymer materials in sodium and magnesium sulfate solutions. *Cement and Concrete Research*, 35(6), pp.1233–1246.

Bakharev, T., 2005b. Geopolymeric materials prepared using Class F fly ash and elevated temperature curing. *Cement and Concrete Research*, 35(6), pp.1224–1232.

Bakharev, T., 2005c. Resistance of geopolymer materials to acid attack. *Cement and Concrete Research*, 35(4), pp.658–670.

Bakharev, T., Sanjayan, J.G. & Cheng, Y.-B., 1999. Alkali activation of Australian slag cements. *Cement and Concrete Research*, 29(1), pp.113–120.

Bakharev, T., Sanjayan, J.G. & Cheng, Y.-B., 1999. Effect of elevated temperature curing on properties of alkali-activated slag concrete. *Cement and Concrete Research*, 29(10), pp.1619–1625.

Bakharev, T., Sanjayan, J.G. & Cheng, Y.-B., 2001. Resistance of alkali-activated slag concrete to alkali–aggregate reaction. *Cement and Concrete Research*, 31(2), pp.331–334.

Bakharev, T., Sanjayan, J.G. & Cheng, Y.-B., 2002. Sulfate attack on alkali-activated slag concrete. *Cement and Concrete Research*, 32(2), pp.211–216.

Bakharev, T., Sanjayan, J.G. & Cheng, Y.B., 2003. Resistance of alkali-activated slag concrete to acid attack. *Cement and Concrete Research*, 33(10), pp.1607–1611.

Balaguer-Pascual, A., Tognonvi, M. & Tagnit-Hamou, A., 2014. Waste Glass Powder-Based Alkali-Activated Mortar. *Ijret.Org*, 3(13), pp.15–19.

Balaguer Pascual, A., 2014. *Élaboration de nouveaux liants mineraux pour la formulation de bétons ecologiques et durables*. Université de Sherbrooke.

Bernal, S.A., de Gutiérrez, R.M., et al., 2011. Effect of binder content on the performance of alkali-activated slag concretes. *Cement and Concrete Research*, 41(1), pp.1–8.

Bernal, S.A. et al., 2010. Effect of silicate modulus and metakaolin incorporation on the carbonation of alkali silicate-activated slags. *Cement and Concrete Research*, 40(6), pp.898–907.

Bernal, S.A., Provis, J.L., et al., 2011. Evolution of binder structure in sodium silicate-activated slag-metakaolin blends. *Cement and Concrete Composites*, 33(1), pp.46–54.

Bernal, S.A. et al., 2014. MgO content of slag controls phase evolution and structural changes induced by accelerated carbonation in alkali-activated binders. *Cement and Concrete Research*, 57, pp.33–43.

Bernal, S.A. et al., 2012. Performance of alkali-activated slag mortars exposed to acids. *Journal of Sustainable Cement-Based Materials*, 1(3), pp.138–151.

Bing-hui, M. et al., 2014. Effect of curing temperature on geopolymerization of metakaolin-based geopolymers. *Applied Clay Science*, 99, pp.144–148.

Bobirică, C. et al., 2015. Influence of waste glass on the microstructure and strength of inorganic polymers. *Ceramics International*, 41(10), pp.13638–13649.

Bondar, D. et al., 2012. Oxygen and Chloride Permeability of Alkali-Activated Natural Pozzolan Concrete. *ACI Materials Journal*, 109(1), pp.53–62.

Bungey, J.H., Millard, S.G. & Grantham, M.G., 2006. *Testing on concrete structures* 4th editio., Taylor&Francis.

Burciaga-Díaz, O. & Escalante-García, J.I., 2012. Strength and durability in acid media of alkali silicate-activated metakaolin geopolymers. *Journal of the American Ceramic Society*, 95(7), pp.2307–2313.

CEB, C. euro-international du beton, 1989. *Durable concrete structures - Design Guide* S. Rostman, ed.,

Chappex, T. & Scrivener, K.L., 2012. The influence of aluminium on the dissolution of amorphous silica and its relation to alkali silica reaction. *Cement and Concrete Research*, 42(12), pp.1645–1649.

Chi, M., 2012. Effects of dosage of alkali-activated solution and curing conditions on the properties and durability of alkali-activated slag concrete. *Construction and Building Materials*, 35, pp.240–245.

Chi, M., Chang, J. & Huang, R., 2012. Strength and Drying Shrinkage of Alkali-Activated Slag Paste and Mortar. *Advances in Civil Engineering*, 2012, pp.1–7.

Cizer, Ö. et al., 2011. Microstructural Changes in Self-Compacting Concrete by Sulphuric Acid Attack. In *13th International Congress on the Chemistry of Cement.* Madrid, pp. 1–7.

Collepardi, M., 2003. A state-of-the-art review on delayed ettringite attack on concrete. *Cement and Concrete Composites*, 25(4–5 SPEC), pp.401–407.

Collins, F. & Sanjayan, J.G., 2000. Effect of pore size distribution on drying shrinkage of alkali-activated slag concrete. *Cement and Concrete Research*, 30, pp.1401–1406.

Collins, F.G. & Sanjayan, J.G., 1999. Workability and mechanical properties of alkali activated slag concrete. *Cement and Concrete Research*, 29(3), pp.455–458.

Cyr, M., Idir, R. & Poinot, T., 2012. Properties of inorganic polymer (geopolymer) mortars made of glass cullet. *Journal of Materials Science*, 47(6), pp.2782–2797.

Damtoft, J.S. et al., 2008. Sustainable development and climate change initiatives. *Cement and Concrete Research*, 38(2), pp.115–127.

Davidovits, J., 1987. Ancient and modern concretes. What is the real difference? *Concrete International*, 9(12), pp.23–28.

Davidovits, J., 2008. *Geopolymer chemistry and their applications* 4th ed. J. Davidovits, ed., Saint-Quentin, France: Institut Geopolymère.

Davidovits, J., 1979. Synthesis of new high-temperature geo-polymers for reinfoced plastics/composites. In *PACTEC'79, Society of Plastics Engineers*. Brookfiel Center, USA, pp. 151–154.

Davidovits, J. & Davidovits, F., 2001. *The pyramids: An enigma solved* 2nd revise. J. Davidovits, ed., Saint-Quentin, France: Editions J. Davidovits.

Davies, G. & Oberholster, R.E., 1988. Alkali-silica reaction products and their development. *Cement and Concrete Research*, 18(4), pp.621–635.

Van Deventer, J.S.J., Provis, J.L. & Duxson, P., 2012. Technical and commercial progress in the adoption of geopolymer cement. *Minerals Engineering*, 29, pp.89–104.

Dimas, D., Giannopoulou, I. & Panias, D., 2009. Polymerization in sodium silicate solutions: A fundamental process in geopolymerization technology. *Journal of Materials Science*, 44(14), pp.3719–3730.

Douglas, E., Bilodeau, A. & Malhotra, V.M., 1992. Properties and Durability of Alkali-Activated Slag Concrete. *ACI Materials Journal*, 89(5), pp.509–516.

Duran Atiş, C. et al., 2009. Influence of activator on the strength and drying shrinkage of alkali-activated slag mortar. *Construction and Building Materials*, 23(1), pp.548–555.

Duxson, P., Fernández-Jiménez, A., et al., 2007. Geopolymer technology: the current state of the art. *Journal of Materials Science*, 42(9), pp.2917–2933.

Duxson, P., Provis, J.L., et al., 2007. The role of inorganic polymer technology in the development of 'green concrete.' *Cement and Concrete Research*, 37(12), pp.1590–1597.

Ecofys, 2009. *Methodology for the free allocation of emissions allowances in the EU ETS post 2012,*

Sector report for the glass industry,

Eglinton, M., 2003. *Resistance of concrete to destructive agencies* 4th ed. P. C. Hewlett, ed., Elsevier.

Elkhadiri, I., Palacios, M. & Puertas, F., 2009. Effect of curing temperature on cement hydration. *Ceramics - Silikaty*, 53(2), pp.65–75.

Federico, L.M. & Chidiac, S.E., 2009. Waste glass as a supplementary cementitious material in concrete - Critical review of treatment methods. *Cement and Concrete Composites*, 31(8), pp.606–610.

Fernández-Jiménez, A., Palomo, Á., et al., 2008. Alkaline Activation of Blends of Metakaolin and Calcium Aluminate. *Journal of the American Ceramic Society*, 91(4), pp.1231–1236.

Fernández-Jiménez, A., Monzó, M., et al., 2008. Alkaline activation of metakaolin–fly ash mixtures: Obtain of Zeoceramics and Zeocements. *Microporous and Mesoporous Materials*, 108(1–3), pp.41–49.

Fernández-Jiménez, A. et al., 2006. The role played by the reactive alumina content in the alkaline activation of fly ashes. *Microporous and Mesoporous Materials*, 91(1–3), pp.111–119.

Fernandez-Jimenez, A., García-Lodeiro, I. & Palomo, A., 2007a. Durability of alkali-activated fly ash cementitious materials. *Journal of Materials Science*, 42(9), pp.3055–3065.

Fernandez-Jimenez, A., García-Lodeiro, I. & Palomo, A., 2007b. Durability of alkali-activated fly ash cementitious materials. *Journal of Materials Science*, 42(9), pp.3055–3065.

Fernandez-Jimenez, A. & Palomo, A., 2004. Alkaline activation of fly ashes. Manufacture of concretes not containing Portland cement. In *International RILEM Conference on the use of recycling Materials in building and structures*. Barcelona, Spain, pp. 873–880.

Fernandez-Jimenez, A. & Palomo, A., 2003. Characterisation of fly ashes. Potential reactivity as alkaline cements. *Fuel*, 82(18), pp.2259–2265.

Fernandez-Jimenez, A. & Palomo, A., 2007. Factors affecting early compressive strength of alkali activated fly ash (OPC-free) concrete. *Materiales de Construcción*, 57(287), pp.7–22.

Fernández-Jiménez, A. & Palomo, A., 2005. Composition and microstructure of alkali activated fly ash binder: Effect of the activator. *Cement and Concrete Research*, 35(10), pp.1984–1992.

Fernández-Jiménez, A., Palomo, A. & Criado, M., 2005. Microstructure development of alkali-activated fly ash cement: a descriptive model. *Cement and Concrete Research*, 35(6), pp.1204–1209.

Fernández-jiménez, A., Palomo, J.G. & Puertas, F., 1999. Alkali-activated slag mortars. Mechanical strength behaviour. *Cement and Concrete Research*, 29, pp.1313–1321.

Fernández-Jiménez, A. & Puertas, F., 1997. Alkali-activated slag cements: Kinetics studies. *Cement and Concrete Research*, 27(3), pp.359–368.

Fernández-Jiménez, A. & Puertas, F., 2002. The alkali – silica reaction in alkali-activated granulated slag mortars with reactive aggregate. *Cement and Concrete Research*, 32, pp.1019–1024.

Fernández Jiménez, A.M., 2000. *Cementos de escorias activadas alcalinamente: influencia de las variables y modelización del proceso*. Universidad Autónoma de Madrid.

Fu, Y., Cai, L. & Yonggen, W., 2011. Freeze–thaw cycle test and damage mechanics models of alkali-activated slag concrete. *Construction and Building Materials*, 25(7), pp.3144–3148.

Gagné, L., 2010. Le verre - Fiches informatives.

Gao, X.X. et al., 2013. Behavior of metakaolin-based potassium geopolymers in acidic solutions. *Journal of Non-Crystalline Solids*, 380, pp.95–102.

Garcia-Lodeiro, I. et al., 2011. Compatibility studies between N-A-S-H and C-A-S-H gels. Study in the ternary diagram Na2O–CaO–Al2O3–SiO2–H2O. *Cement and Concrete Research*, 41(9), pp.923–931.

García-Lodeiro, I. et al., 2010. Effect of calcium additions on N-A-S-H cementitious gels. *Journal of the American Ceramic Society*, 93(7), pp.1934–1940.

García-Lodeiro, I., Fernández-Jiménez, a. & Palomo, a., 2013. Variation in hybrid cements over time. Alkaline activation of fly ash–portland cement blends. *Cement and Concrete Research*, 52, pp.112–122.

García-Lodeiro, I., Palomo, a. & Fernández-Jiménez, a., 2007. Alkali–aggregate reaction in activated fly ash systems. *Cement and Concrete Research*, 37(2), pp.175–183.

García-Lodeiro, I., Palomo, A. & Fernández-jiménez, A., 2007. Alkali – aggregate reaction in activated fly ash systems. *Cement and Concrete Research*, 37, pp.175–183.

Gartner, E., 2004. Industrially interesting approaches to “low-CO2” cements. *Cement and Concrete Research*, 34(9), pp.1489–1498.

Giannopoulou, I. & Panias, D., 2010. Hydrolytic stability of sodium silicate gels in the presence of aluminum. *Journal of Materials Science*, 45(19), pp.5370–5377.

Gifford, P.M. & Gillott, J.E., 1996a. Alkali-Silica reaction (ASR) and alkali-carbonate reaction (ACR) in activated blast furnace slag cement (ABFSC) concrete. *Cement and Concrete Research*, 26(1), pp.21–26.

Gifford, P.M. & Gillott, J.E., 1996b. Freeze-Thaw Durability of Activated Blast-Furnace Slag Cement Concrete. *ACI Materials Journal*, 93(3), pp.242–245.

Glasser, F.P., 1992. Chemistry of the alkali-aggregate reaction. In R. N. Swamy, ed. *The alkali-silica reaction in concrete*. Blackie and Son Ltd.

Glukhowsky, V.D., 1965. *Soil Silicates: Properties, Manufacturing technology and applications*. Doct. Tech. Sc. Degree Thesis, Civil Engineering Institute. Kiev, Ukraine.

Glukhowsky, V.D., 1959. *Soil Silicates*, Kiev, Ukraine: Gosstroi Publishers.

Gruskovnjak, A. et al., 2006. Hydration of alkali-activated slag: Comparison with ordinary Portland cement. *Advances in Cement Research*, 18(3), pp.119–128.

Habert, G., d'Espinose de Lacaillerie, J.B. & Roussel, N., 2011. An environmental evaluation of geopolymer based concrete production: reviewing current research trends. *Journal of Cleaner Production*, 19(11), pp.1229–1238.

Ben Haha, M., Le Saout, G., et al., 2011. Influence of activator type on hydration kinetics, hydrate assemblage and microstructural development of alkali activated blast-furnace slags. *Cement and Concrete Research*, 41(3), pp.301–310.

Ben Haha, M., Lothenbach, B., et al., 2011. Influence of slag chemistry on the hydration of alkali-activated blast-furnace slag - Part I: Effect of MgO. *Cement and Concrete Research*, 41(9), pp.955–963.

Hong, S.-Y. & Glasser, F.P., 1999. Alkali binding in cement pastes Part I. The C-S-H phase. *Cement and Concrete Research*, 29(12), pp.1893–1903.

Hong, S.-Y. & Glasser, F.P., 2002. Alkali sorption by C-S-H and C-A-S-H gels: Part II. Role of alumina. *Cement and Concrete Research*, 32(7), pp.1101–1111.

Hooton, R.D., 2008. Bridging the gap between research and standards. *Cement and Concrete Research*, 38(2), pp.247–258.

Hooton, R.D., 2015. Current developments and future needs in standards for cementitious materials. *Cement and Concrete Research*, 78, pp.165–177.

Hornbostel, K., Larsen, C.K. & Geiker, M.R., 2013. Relationship between concrete resistivity and corrosion rate - A literature review. *Cement and Concrete Composites*, 39, pp.60–72.

Hossack, A.M. & Thomas, M.D.A., 2015. Evaluation of the effect of tricalcium aluminate content on the severity of sulfate attack in Portland cement and Portland limestone cement mortars. *Cement and Concrete Composites*, 56, pp.115–120.

Huanhai, Z. et al., 1993. Kinetic study of hydration of alkali-activated slag. *Cement and Concrete Research*, 23, pp.1253–1258.

Ichikawa, T., 2009. Alkali-silica reaction, pessimum effects and pozzolanic effect. *Cement and Concrete Research*, 39(8), pp.716–726.

Ismail, I. et al., 2012. Microstructural changes in alkali activated fly ash/slag geopolymers with sulfate exposure. *Materials and Structures*, pp.361–373.

Jani, Y. & Hogland, W., 2014. Waste glass in the production of cement and concrete – A review. *Journal of Environmental Chemical Engineering*, 2(3), pp.1767–1775.

Jantzen, C.M. & Plodinec, M.J., 1984. Thermodynamic model of natural, medieval and nuclear waste glass durability. *Journal of Non-Crystalline Solids*, 67(1–3), pp.207–223.

Kim, M.S. et al., 2013. Use of CaO as an activator for producing a price-competitive non-cement structural binder using ground granulated blast furnace slag. *Cement and Concrete Research*, 54, pp.208–214.

Kjellsen, K.O., Detwiler, R.J. & Gjørv, O.E., 1991. Development of microstructures in plain cement pastes hydrated at different temperatures. *Cement and Concrete Research*, 21(1), pp.179–189.

Komljenović, M. et al., 2013. External sulfate attack on alkali-activated slag. *Construction and Building Materials*, 49, pp.31–39.

Komnitsas, K., Zaharaki, D. & Perdikatsis, V., 2009. Effect of synthesis parameters on the compressive strength of low-calcium ferronickel slag inorganic polymers. *Journal of Hazardous Materials*, 161(2–3), pp.760–768.

Komnitsas, K., Zaharaki, D. & Perdikatsis, V., 2007. Geopolymerisation of low calcium ferronickel slags. *Journal of Materials Science*, 42(9), pp.3073–3082.

Kovalchuk, G., Fernández-Jiménez, a. & Palomo, a., 2007. Alkali-activated fly ash: Effect of thermal curing conditions on mechanical and microstructural development – Part II. *Fuel*, 86(3), pp.315–

322.

Kovalchuk, G., Palomo, A. & Fernández-Jimenez, A., 2008. Alkali-activated fly ash. Relationship between mechanical strength gains and initial ash chemistry. *Materiales de Construcción*, 58(291), pp.35–52.

Krivenko, P., 1994. Alkaline cements. In *First Int. Conf. Alkaline Cements and Concretes*. Kiev, Ukraine, pp. 12–129.

Krivenko, P.V., 1992. Alkaline cements. In *Proceedings of the 9th international congress on the chemistry of cement, Vol.4*. New Dheli, pp. 482–488.

Krizan, D. & Zivanovic, B., 2002. Effects of dosage and modulus of water glass on early hydration of alkali–slag cements. *Cement and Concrete Research*, 32(8), pp.1181–1188.

Kühl, H., 1908. Slag cement and process of making the same. , p.2.

Kupwade-Patil, K. & Allouche, E., 2011. Effect of Alkali Silica Reaction (ASR) in Geopolymer Concrete. In *World of Coal Ash (WOCA) Conference*. Denver, USA.

Kupwade-Patil, K. & Allouche, E.N., 2013. Impact of Alkali Silica Reaction on Fly Ash Based Geopolymer Concrete. *Journal of Materials in Civil Engineering*, 25(January), pp.131–139.

Laldji, S. & Tagnit-Hamou, A., 2007. Glass frit for concrete structures: A new, alternative cementitious material. *Canadian Journal of Civil Engineering*, 34(7), pp.793–802.

Leemann, A. et al., 2011. Alkali-Silica reaction: The Influence of calcium on silica dissolution and the formation of reaction products. *Journal of the American Ceramic Society*, 94(4), pp.1243–1249.

Leemann, A. et al., 2015. ASR prevention — Effect of aluminum and lithium ions on the reaction products. *Cement and Concrete Research*, 76, pp.192–201.

Lindgård, J. et al., 2012. Alkali–silica reactions (ASR): Literature review on parameters influencing laboratory performance testing. *Cement and Concrete Research*, 42(2), pp.223–243.

Lloyd, R.R., Provis, J.L. & Van Deventer, J.S.J., 2012. Acid resistance of inorganic polymer binders. 1. Corrosion rate. *Materials and Structures*, 45(1–2), pp.1–14.

Lloyd, R.R., Provis, J.L. & Van Deventer, J.S.J., 2010. Pore solution composition and alkali diffusion in inorganic polymer cement. *Cement and Concrete Research*, 40(9), pp.1386–1392.

Lothenbach, B. et al., 2007. Effect of temperature on the pore solution, microstructure and hydration

products of Portland cement pastes. *Cement and Concrete Research*, 37(4), pp.483–491.

Ma, Y., Hu, J. & Ye, G., 2013. The pore structure and permeability of alkali activated fly ash. *Fuel*, 104, pp.771–780.

Mafalda Matos, A. & Sousa-Coutinho, J., 2012. Durability of mortar using waste glass powder as cement replacement. *Construction and Building Materials*, 36, pp.205–215.

Malhotra, V.M. & Mehta, P.K., 1996. Pozzolanic and cementitious materials. In *Advances in concrete technology*. New York: Gordon and Breach Publishers.

Maragkos, I., Giannopoulou, I.P. & Panias, D., 2009. Synthesis of ferronickel slag-based geopolymers. *Minerals Engineering*, 22(2), pp.196–203.

McLellan, B.C. et al., 2011. Costs and carbon emissions for geopolymer pastes in comparison to ordinary portland cement. *Journal of Cleaner Production*, 19(9–10), pp.1080–1090.

Mehta, P.K., 1983. Mechanism of sulfate attack on portland cement concrete — Another look. *Cement and Concrete Research*, 13(3), pp.401–406.

Mielich, O. & Ötll, C., 2004. Practical investigation of the sulfate resistance of concrete from construction units. *Otto-Graf-Journal*, 15, pp.135–132.

Muñiz-Villarreal, M.S. et al., 2011. The effect of temperature on the geopolymerization process of a metakaolin-based geopolymer. *Materials Letters*, 65(6), pp.995–998.

Nasvi, M.C.M., Ranjith, P.G., et al., 2014. Effect of temperature on permeability of geopolymer: A primary well sealant for carbon capture and storage wells. *Fuel*, 117, pp.354–363.

Nasvi, M.C.M., Ranjith, P.G. & Sanjayan, J., 2014. Effect of different mix compositions on apparent carbon dioxide (CO2) permeability of geopolymer: Suitability as well cement for CO2 sequestration wells. *Applied Energy*, 114, pp.939–948.

Odler, I., 2003. *Hydration, setting and hardening of portland cement* 4th ed. P. C. Hewlett, ed., Elsevier.

Pacheco-Torgal, F. et al. eds., 2015. *Handbook of Alkali-activated Cements, Mortars and Concretes*, Elsevier Ltd.

Pacheco-Torgal, F., Castro-Gomes, J. & Jalali, S., 2008a. Alkali-activated binders: A review Part 1. Historical background, terminology, reaction mechanisms and hydration products. *Construction and Building Materials*, 22(7), pp.1305–1314.

Pacheco-Torgal, F., Castro-Gomes, J. & Jalali, S., 2008b. Properties of tungsten mine waste geopolymeric binder. *Construction and Building Materials*, 22(1), pp.1201–1211.

Pacheco-Torgal, F., Castro-Gomes, J. & Jalali, S., 2009. Tungsten mine waste geopolymeric binder: Preliminary hydration products investigations. *Construction and Building Materials*, 23(1), pp.200–209.

Palacios, M. & Puertas, F., 2007. Effect of shrinkage-reducing admixtures on the properties of alkali-activated slag mortars and pastes. *Cement and Concrete Research*, 37(5), pp.691–702.

Palomo, A. et al., 2014. A review on alkaline activation : new analytical perspectives. *Materiales de Construcción*, 64(31), pp.1–23.

Palomo, A., Blanco-Varela, M.T., et al., 1999. Chemical stability of cementitious materials based on metakaolin. *Cement and Concrete Research*, 29(7), pp.997–1004.

Palomo, A., Alonso, S. & Fernandez-Jimenez, A., 2004. Alkaline Activation of Fly Ashes : NMR Study of the Reaction Products. *Journal of the American Ceramic Society*, 1145, pp.1141–1145.

Palomo, A., Grutzeck, M.W. & Blanco-Varela, M.T., 1999. Alkali-activated fly ashes A cement for the future. *Cement and Concrete Research*, 29, pp.1323–1329.

Passuello, A. et al., 2017. Evaluation of the potential improvement in the environmental footprint of geopolymers using waste-derived activators. *Journal of Cleaner Production*, 166, pp.680–689.

Pfeifer, D.W., McDonald, D.B. & Krauss, P.D., 1994. The rapid chloride permeability test and its relation to the 90-day chloride ponding test. *PCI Journal*, 39(1), pp.38–47.

Polder, R.B., 2001. Test methods for on site measurement of resistivity of concrete - a RILEM TC-154 technical recommendation. *Construction and Building Materials*, 15(2–3), pp.125–131.

Pouhet, R. & Cyr, M., 2015. Alkali–silica reaction in metakaolin-based geopolymer mortar. *Materials and Structures*, 48(3), pp.571–583.

Provis, J.L. et al., 2012. X-ray microtomography shows pore structure and tortuosity in alkali-activated binders. *Cement and Concrete Research*, 42(6), pp.855–864.

Provis, J.L. & van Deventer, J.S.J., 2009. *Geopolymer, structure, processing, properties and industrial applications* 1st ed. J. L. Provis & J. S. J. van Deventer, eds., Woodhead Publishing.

Provis, J.L. & van Deventer, J.S.J., 2013. *RILEM TC 224-AAM Alkali-Activated Materials: State of the art*,

Provis, J.L., Palomo, A. & SHI, C., 2015. Advances in understanding alkali-activated materials. *Cement and Concrete Research*, 78, pp.110–125.

Puertas, F. et al., 2009. Alkali-aggregate behaviour of alkali-activated slag mortars: Effect of aggregate type. *Cement and Concrete Composites*, 31(5), pp.277–284.

Puertas, F. et al., 2002. Alkaline cement mortars. Chemical resistance to sulfate and seawater attack. *Materiales de Construcción*, 52(267), pp.55–71.

Puertas, F., 1995. Cementos de escorias activadas alcalinamente: Situación actual y perspectivas de futuro. *Materiales de Construcción*, 45(239), pp.53–64.

Puertas, F., Fernández-Jiménez, A. & Blanco-Varela, M.T., 2004. Pore solution in alkali-activated slag cement pastes. Relation to the composition and structure of calcium silicate hydrate. *Cement and Concrete Research*, 34(1), pp.139–148.

Puertas, F., Palacios, M. & De Gutiérrez, R., 2007. Morteros de Escoria Activada Alcalinamente . Propiedades y Durabilidad. In *2° Congresso Nacional de Argamassas de Construcao*. Portugal.

Purdon, A., 1940. The action of alkalis on blast furnace slag. *J.Soc.Chem.Ind*, 56, pp.191–202.

Quantis, 2015. *Analyse environnementale du cycle de vie de projets de commercialisation du verre mixte récupéré via des centres de tri de matières recyclables au Québec - Mesurer la performance environnementale des filières de gestion de fin de vie du verre récupéré au* ,

Rajabipour, F. et al., 2015. Alkali–silica reaction: Current understanding of the reaction mechanisms and the knowledge gaps. *Cement and Concrete Research*, 76, pp.130–146.

Ravikumar, D. & Neithalath, N., 2012. Effects of activator characteristics on the reaction product formation in slag binders activated using alkali silicate powder and NaOH. *Cement and Concrete Composites*, 34(7), pp.809–818.

Recyc-Québec, 2015. *Le recyclage du verre au québec - Les chiffres, en bref*,

Redden, R. & Neithalath, N., 2014. Microstructure, strength, and moisture stability of alkali activated glass powder-based binders. *Cement and Concrete Composites*, 45, pp.46–56.

Rodríguez, E.D. et al., 2013. Geopolymers based on spent catalyst residue from a fluid catalytic cracking (FCC) process. *Fuel*, 109, pp.493–502.

Rostami, H. & Brendley, W., 2003. Alkali ash material: a novel fly ash-based cement. *Environmental science & technology*, 37(15), pp.3454–7.

Roy, D.M., 1999. Alkali-activated cements Opportunities and challenges. *Cement and Concrete Research*, 29(2), pp.249–254.

Saito, M. & Shukuya, M., 1996. Energy and material use in the production of insulating glass windows. *Solar Energy*, 58(4–6), pp.247–252.

Sakulich, A.R. et al., 2009. Mechanical and microstructural characterization of an alkali-activated slag/limestone fine aggregate concrete. *Construction and Building Materials*, 23(8), pp.2951–2957.

Santhanam, M., Cohen, M.D. & Olek, J., 2003. Mechanism of sulfate attack: a fresh look. Part 2. Proposed mechanisms. *Cement and Concrete Research*, 33(3), pp.341–346.

Santhanam, M., Cohen, M.D. & Olek, J., 2002. Mechanism of sulfate attack: A fresh look - Part 1; Summary of experimental results. *Cement and Concrete Research*, 32(6), pp.915–921.

Sata, V., Sathonsaowaphak, A. & Chindaprasirt, P., 2012. Resistance of lignite bottom ash geopolymer mortar to sulfate and sulfuric acid attack. *Cement and Concrete Composites*, 34(5), pp.700–708.

Schmidt, T. et al., 2009. Physical and microstructural aspects of sulfate attack on ordinary and limestone blended Portland cements. *Cement and Concrete Research*, 39(12), pp.1111–1121.

Schwarz, N., Cam, H. & Neithalath, N., 2008. Influence of a fine glass powder on the durability characteristics of concrete and its comparison to fly ash. *Cement and Concrete Composites*, 30(6), pp.486–496.

Schwarz, N. & Neithalath, N., 2008. Influence of a fine glass powder on cement hydration: Comparison to fly ash and modeling the degree of hydration. *Cement and Concrete Research*, 38, pp.429–436.

Sengul, O., 2014. Use of electrical resistivity as an indicator for durability. *Construction and Building Materials*, 73, pp.434–441. Available at: http://dx.doi.org/10.1016/j.conbuildmat.2014.09.077.

Shao, Y. et al., 2000. Studies on concrete containing ground waste glass. *Cement and Concrete Research*, 30(1), pp.91–100.

Shayan, A. & Xu, A., 2004. Value-added utilisation of waste glass in concrete. *Cement and Concrete Research*, 34(October 2002), pp.81–89.

Shi, C. et al., 2015. A review on alkali-aggregate reactions in alkali-activated mortars/concretes made with alkali-reactive aggregates. *Materials and Structures*, 48(3), pp.621–628.

Shi, C. et al., 2005. Characteristics and pozzolanic reactivity of glass powders. *Cement and Concrete*

Research, 35, pp.987–993.

Shi, C., 1996. Strength, pore structure and permeability of alkali-activated slag mortars. *Cement and Concrete Research*, 26(12), pp.1789–1799.

Shi, C., Fernández Jiménez, A. & Palomo, A., 2011. New cements for the 21st century: The pursuit of an alternative to Portland cement. *Cement and Concrete Research*, 41(7), pp.750–763.

Shi, C., Roy, D.M. & Krivenko, P., 2006. *Alkali-activated cements and concretes*, Taylor & Francis.

Shi, C. & Stegemann, J.A., 2000. Acid corrosion resistance of different cementing materials. *Cement and Concrete Research*, 30(5), pp.803–808.

Shi, C. & Zheng, K., 2007. A review on the use of waste glasses in the production of cement and concrete. *Resources, Conservation and Recycling*, 52, pp.234–247.

Shi, Z. et al., 2015. Comparison of alkali–silica reactions in alkali-activated slag and Portland cement mortars. *Materials and Structures*, 48(3), pp.743–751.

Skalny, J. et al., 1996. DEF: Una forma de ataque por sulfatos. *Materiales de Construcción*, 46(244), pp.5–29.

Škvára, F., Jílek, T. & Kpecký, L., 2005. Geopolymer materials based on fly ash. *Ceramics - Silikáty*, 49(3), pp.195–204.

Song, H. & Saraswathy, V., 2007. Corrosion Monitoring of Reinforced Concrete Structures - A Review. *International Journal of Electrochemical Science*, 2, pp.1–28.

Song, S. et al., 2000. Hydration of alkali-activated ground granulated blast furnace slag. *Journal of Materials Science*, 35, pp.249–257.

Stade, H., 1989. On the reaction of C-S-H (di, poly) with alkali hydroxides. *Cement and Concrete Research*, 19(5), pp.802–810.

Steinerova, M., 2011. Mechanical properties of geopolymer mortars in relation to their porous structure. *Ceramics - Silikaty*, 55(4), pp.362–372.

Stone, W.E.E. et al., 1993. Association of soluble aluminum ionic species with a Silica-Gel surface. A solid-state NMR study. *Journal of Physical Chemistry*, 97, pp.10127–10132.

Sukmak, P. et al., 2015. Sulfate Resistance of Clay-Portland Cement and Clay High-Calcium Fly Ash Geopolymer. *Journal of materials in civil enginnering*, 27(5), pp.1–11.

Sun, P. & Wu, H.C., 2013. Chemical and freeze-thaw resistance of fly ash-based inorganic mortars. *Fuel*, 111, pp.740–745.

Tagnit-Hamou, A. & Bengougam, A., 2012. The Use of Glass Powder as Supplementary Cementitious Material. *Concrete International*, (march), pp.56–61.

Tagnit-Hamou, A. & Petrov, N., 2004. A New Method for Evaluating the Risk of DEF. *Concrete and Aggregates*, 26(2), pp.1–6.

Tashima, M.M., Soriano, L., et al., 2012. Alkali activation of vitreous calcium aluminosilicate derived from glass fiber waste. *Journal of Sustainable Cement-Based Materials*, 1(3), pp.83–93.

Tashima, M.M., Soriano, L., Borrachero, M.V., et al., 2013. Effect of curing time on microstructure and mechanical strength development of alkali activated binders based on vitreous calcium aluminosilicate (VCAS). *Bulletin of Materials Science*, 36(2), pp.245–249.

Tashima, M.M., Akasaki, J.L., et al., 2012. New geopolymeric binder based on fluid catalytic cracking catalyst residue (FCC). *Materials Letters*, 80, pp.50–52.

Tashima, M.M., Soriano, L., Monzó, M., et al., 2013. Novel geopolymeric material cured at room temperature. *Advances in Applied Ceramics*, 112(4), pp.179–183.

Temuujin, J. & van Riessen, a, 2009. Effect of fly ash preliminary calcination on the properties of geopolymer. *Journal of hazardous materials*, 164(2–3), pp.634–9.

Thomas, J.J. et al., 2003. Effect of hydration temperature on the solubility behavior of Ca-, S-, Al-, and Si-bearing solid phases in Portland cement pastes. *Cement and Concrete Research*, 33(12), pp.2037–2047.

Thomas, M. et al., 2006. Test methods for evaluating preventive measures for controlling expansion due to alkali-silica reaction in concrete. *Cement and Concrete Research*, 36(10), pp.1842–1856.

Torrent, R.J., 1992. A two-chamber vacuum cell for measuring the coefficient of permeability to air of the concrete cover on site. *Materials and Structures*, 25(6), pp.358–365.

Torres-Carrasco, M. et al., 2015. Alkali activated slag cements using waste glass as alternative activators. Rheological behaviour. *Boletín de la Sociedad Española de Cerámica y Vidrio*, 54(2), pp.45–57.

Torres-Carrasco, M. & Puertas, F., 2015. Waste glass in the geopolymer preparation. Mechanical and microstructural characterisation. *Journal of Cleaner Production*, 90, pp.397–408.

Turner, L.K. & Collins, F.G., 2013. Carbon dioxide equivalent (CO2-e) emissions: A comparison between geopolymer and OPC cement concrete. *Construction and Building Materials*, 43, pp.125–130.

USGS, 2017. US geological Survey: Mineral commodity summaries: Cement. Available at: http://minerals.usgs.gov/minerals/pubs/commodity/cement/.

Wallah, S.E. & Rangan, B.V., 2006. *Low-calcium fly ash-based geoploymer concrete: Long-term properties*, Perth, Australia.

Wang, H. & Gillott, J.E., 1991. Mechanism of alkali-silica reaction and the significance of calcium hydroxide. *Cement and Concrete Research*, 21(4), pp.647–654.

Wang, S.-D. & Scrivener, K.L., 1995. Hydration products of alkali activated slag cement. *Cement and Concrete Research*, 25(3), pp.561–571.

Wang, S., Scrivener, K.L. & Pratt, P.L., 1994. Factors affecting the strength of alkali-activated slag. *Cement and Concrete Research*, 24(6), pp.1033–1043.

Wang, S.D., 2000. The role of sodium during the hydration of alkali-activated slag. *Advances in Cement Research*, 12(2), pp.65–69.

Whiting, D., 1981. *Rapid determination of the chloride permeability of concrete*, Whasington D.C.

Whiting, J., 1895. United States Patent ‘ Office ‘... , p.2.

Wigum, B.J. et al., 2006. *Report 2.1 - State of the art report: Key parameters influencing the alkali aggregate reaction*, Trondheim, Norway.

Winnefeld, F. et al., 2010. Assessment of phase formation in alkali activated low and high calcium fly ashes in building materials. *Construction and Building Materials*, 24(6), pp.1086–1093.

Xie, Z., Xiang, W. & Xi, Y., 2003. ASR Potentials of Glass Aggregates in Water-Glass Activated Fly Ash and Portland Cement Mortars. *Journal of Materials in Civil Engineering*, 15(February), pp.67–74.

Yang, K.-H., Song, J.-K. & Song, K.-I., 2013. Assessment of CO2 reduction of alkali-activated concrete. *Journal of Cleaner Production*, 39, pp.265–272.

Ye, H. & Radlinska, A., 2016. Shrinkage mechanisms of alkali-activated slag. *Cement and Concrete Research*, 88, pp.126–135.

You-zhi, C. et al., 2002. Alkali aggregate reaction in alkali slag cement mortars. *Journal of Wuhan University of Technology-Mater. Sci. Ed.*, 17(3), pp.60–62.

Zhang, S., 2015. *Waste Glass as Partial Binder Precursor and Fine Aggregate Replacement in Alkali Activated Slag / Fly ash System*. Delft University of Technology.

Zhang, Z., Yao, X. & Zhu, H., 2010. Potential application of geopolymers as protection coatings for marine concrete III. Field experiment. *Applied Clay Science*, 49, pp.1–6.

Zidol, A., 2009. *Optimisation de la finesse de la poudre de verre dans les systèmes cimentaires binaires*.

Zosin, A.P., Priimak, T.I. & Avsaragov, K.B., 1998. Geopolymer materials based on magnesia-iron slags for normalization and storage of radioactive wastes. *Atomic Energy*, 85(1), pp.510–514.